University of Southampton
Faculty of Engineering, Science and Mathematics
School of Electronics and Computer Science

Self-Concatenated Coding for Wireless Communication Systems

by

Muhammad Fasih Uddin Butt
BEng., MSc

A Doctoral thesis submitted in partial fulfilment of the requirements for the award of Doctor of Philosophy at the University of Southampton

June 2010

SUPERVISORS: *Professor Lajos Hanzo*
FREng, FIEEE, FIET, DSc
Chair of Telecommunications
and *Dr Soon Xin Ng*
PhD, SMIEEE, MIET
School of Electronics and Computer Science
University of Southampton
Southampton SO17 1BJ
United Kingdom

This thesis is dedicated to

my beloved parents (Rafi and Nilum), grandmothers
and parents-in-law
for their love and prayers
my lovely wife Ayesha
for her tremendous patience, love and care
and my adorable daughter Sarah
for making my days brighter with her smile and lovely actions
with all my heartfelt gratitude, appreciation and love ···

UNIVERSITY OF SOUTHAMPTON

ABSTRACT

FACULTY OF ENGINEERING, SCIENCE AND MATHEMATICS
SCHOOL OF ELECTRONICS AND COMPUTER SCIENCE

Doctor of Philosophy

Self-Concatenated Coding for Wireless Communication Systems

by

Muhammad Fasih Uddin Butt

In this thesis, we have explored self-concatenated coding schemes that are designed for transmission over Additive White Gaussian Noise (AWGN) and uncorrelated Rayleigh fading channels. We designed both the symbol-based Self-Concatenated Codes considered using Trellis Coded Modulation (SECTCM) and bit-based Self-Concatenated Convolutional Codes (SECCC) using a Recursive Systematic Convolutional (RSC) encoder as constituent codes, respectively. The design of these codes was carried out with the aid of Extrinsic Information Transfer (EXIT) charts. The EXIT chart based design has been found an efficient tool in finding the decoding convergence threshold of the constituent codes. Additionally, in order to recover the information loss imposed by employing binary rather than non-binary schemes, a soft-decision demapper was introduced in order to exchange extrinsic information with the SECCC decoder. To analyse this information exchange 3D-EXIT chart analysis was invoked for visualizing the extrinsic information exchange between the proposed Iteratively Decoding aided SECCC and soft-decision demapper (SECCC-ID). Some of the proposed SECTCM, SECCC and SECCC-ID schemes perform within about 1 dB from the AWGN and Rayleigh fading channels' capacity. A union bound analysis of SECCC codes was carried out to find the corresponding Bit Error Ratio (BER) floors. The union bound of SECCCs was derived for communications over both AWGN and uncorrelated Rayleigh fading channels, based on a novel interleaver concept. Application of SECCCs in both UltraWideBand (UWB) and state-of-the-art video-telephone schemes demonstrated its practical benefits.

In order to further exploit the benefits of the low complexity design offered by SECCCs we explored their application in a distributed coding scheme designed for cooperative communications, where iterative detection is employed by exchanging extrinsic information between the decoders of SECCC and RSC at the destination. In the first transmission period of cooperation, the relay receives the potentially

erroneous data and attempts to recover the information. The recovered information is then re-encoded at the relay using an RSC encoder. In the second transmission period this information is then retransmitted to the destination. The resultant symbols transmitted from the source and relay nodes can be viewed as the coded symbols of a three-component parallel-concatenated encoder. At the destination a Distributed Binary Self-Concatenated Coding scheme using Iterative Decoding (DSECCC-ID) was employed, where the two decoders (SECCC and RSC) exchange their extrinsic information. It was shown that the DSECCC-ID is a low-complexity scheme, yet capable of approaching the Discrete-input Continuous-output Memoryless Channels's (DCMC) capacity.

Finally, we considered coding schemes designed for two nodes communicating with each other with the aid of a relay node, where the relay receives information from the two nodes in the first transmission period. At the relay node we combine a powerful Superposition Coding (SPC) scheme with SECCC. It is assumed that decoding errors may be encountered at the relay node. The relay node then broadcasts this information in the second transmission period after re-encoding it, again, using a SECCC encoder. At the destination, the amalgamated block of Successive Interference Cancellation (SIC) scheme combined with SECCC then detects and decodes the signal either with or without the aid of *a priori* information. Our simulation results demonstrate that the proposed scheme is capable of reliably operating at a low BER for transmission over both AWGN and uncorrelated Rayleigh fading channels. We compare the proposed scheme's performance to a direct transmission link between the two sources having the same throughput.

Acknowledgements

First and foremost, I would like to express my sincere gratitude to my supervisors Professor Lajos Hanzo and Dr. Soon Xin Ng (Michael), for their exceptional supervision, insightful guidance and overall for their friendship. Their utmost kindness and encouragement have greatly benefited me and managed to cultivate in me the desire to be a good researcher through the enthusiasm and perseverance in research. I have learned greatly from them the urge to excel and look for solutions for each problem and also their attitude of conducting high quality research. I feel very privileged to work with such good researchers and excellent supervisors.

I am also grateful to Dr. Raja Ali Riaz, Dr. Mohammed El-Hajjar, Dr. Robert Maunder, Dr. Jos Akhtman and Dr. Rong Zhang for the numerous discussions I had with them and for their invaluable comments and suggestions. I also gratefully acknowledge all my former and present colleagues in the Communications Research Group for creating such a wonderful work environment and specially thank the Group secretary Mrs. Denise Harvey for her help in administrative matters.

The financial support of COMSATS Institute of Information Technology (CIIT), Islamabad, Pakistan under the auspices of the Higher Education Commission, Pakistan is gratefully acknowledged. I am also thankful for the financial support provided by EU Optimix Project and Dr. Wali Mohammad Trust during my last year of PhD. I am grateful to the School of Electronics and Computer Science for the excellent research facilities provided, and to the accommodation office for making our stay at the campus comfortable.

My stay in Southampton wouldn't nearly be as much enjoyable without my incredible friends, to whom I owe all of my good memories from this time. I thank each and every one of them for their trust and friendship.

Last but not least, I would like to dedicate this thesis to my family. My parents, grandmothers and parents-in-law, who have provided me with tremendous love, support, prayers and constant encouragement. The love, support and patience of my wife Ayesha has always been the greatest inspiration to me, and without that, it would not have been possible for me to complete this work.

To all these wonderful people, many thanks again.

DECLARATION OF AUTHORSHIP

I, **Muhammad Fasih Uddin Butt**,

declare that the thesis entitled

Self-Concatenated Coding in Wireless Communication Systems

and the work presented in the thesis are both my own, and have been generated by me as the result of my own original research. I confirm that:

- this work was done wholly or mainly while in candidature for a research degree at this University;
- where any part of this thesis has previously been submitted for a degree or any other qualification at this University or any other institution, this has been clearly stated;
- where I have consulted the published work of others, this is always clearly attributed;
- where I have quoted from the work of others, the source is always given. With the exception of such quotations, this thesis is entirely my own work;
- I have acknowledged all main sources of help;
- where the thesis is based on work done by myself jointly with others, I have made clear exactly what was done by others and what I have contributed myself;
- parts of this work have been published as: [1–9].

Signed: *Muhammad Fasih Uddin Butt*
Date: 23rd June 2010

List of Publications

Journal Papers:

1. **M. F. U. Butt**, R. A. Riaz, S. X. Ng and L. Hanzo, "Near-Capacity Iterative Decoding of Binary Self-Concatenated Codes Using Soft Decision Demapping and 3-D EXIT Charts", to appear in IEEE Transactions on Wireless Communications.

2. **M. F. U. Butt**, R. A. Riaz, S. X. Ng and L. Hanzo, "Distributed Self-Concatenated Coding for Cooperative Communications", to appear in IEEE Transactions on Vehicular Technology.

3. S. X. Ng, **M. F. U. Butt** and L. Hanzo, "On the Union Bounds of Self-Concatenated Convolutional Codes", IEEE Signal Processing Letters, vol. 16, pp. 754-757, September 2009.

4. R. A. Riaz, **M. F. U. Butt**, S. Chen and L. Hanzo, "Generic z-domain discrete-time transfer function estimation for ultra-wideband systems", IET Electronics Letters, Vol. 44, 2008, pp. 1491-1492.

5. R. A. Riaz, R. G. Maunder, **M. F. U. Butt**, S. X. Ng, S. Chen and L. Hanzo, "EXIT-Chart Aided 3-Stage Concatenated Ultra-WideBand Time-Hopping Spread-Spectrum Impulse Radio Design", in IEEE Transactions on Vehicular Technology, vol. 58, no. 9, pp. 5320-5324, 2009.

Conferences Papers:

1. **M. F. U. Butt**, S. X. Ng and L. Hanzo, "EXIT Chart Aided Design of Near-Capacity Self-Concatenated Trellis Coded Modulation Using Iterative Decoding", in Proceedings of the 67th IEEE Vehicular Technology Conference (VTC-2008 Spring), pp. 734-738, May 2008.

2. **M. F. U. Butt**, R. A. Riaz, S. X. Ng and L. Hanzo, "Near-Capacity Iteratively Decoded Binary Self-Concatenated Code Design Using EXIT Charts", in Proceedings of the IEEE Global Communications Conference, GLOBECOM '08, (New Orleans, USA), Nov/Dec 2008.

3. **M. F. U. Butt**, R. A. Riaz, S. X. Ng and L. Hanzo, "Distributed Self-Concatenated Codes for Low-Complexity Power-Efficient Cooperative Communication", in Proceedings of the IEEE Vehicular Technology Conference (VTC-2009 Fall), Anchorage, Alaska, September 2009.

4. R. A. Riaz, **M. F. U. Butt**, S. X. Ng, S. Chen and L. Hanzo, "Near-Capacity UWB Impulse Radio Using EXIT Chart Aided Self-Concatenated Codes", in Proceedings of the IEEE Vehicular Technology Conference (VTC-2009 Fall), Anchorage, Alaska.

5. R. A. Riaz, R. G. Maunder, **M. F. U. Butt**, S. X. Ng, S. Chen and L. Hanzo, "Three-Stage Concatenated Ultra-Wide bandwidth Time-Hopping Spread-Spectrum Impulse Radio using Iterative Detection", in Proceedings of the IEEE ICC'09, 14-18 June, Dresden, Germany, June 2009.

6. R. A. Riaz, **M. F. U. Butt**, S. Chen and L. Hanzo, "Optimized Irregular Variable Length Coding Design for Iteratively Decoded UltraWideBand Time-Hopping Spread-Spectrum Impulse Radio", in Proceedings of the IEEE Vehicular Technology Conference (VTC-2009 Spring), Spain, April 2009.

7. **M. F. U. Butt**, R. Zhang, S. X. Ng and L. Hanzo, "Superposition Coding Aided Bi-directional Relay Transmission Employing Iteratively Decoded Self-Concatenated Convolutional Codes", in Proceedings of the IEEE Vehicular Technology Conference (VTC-2010 Spring), Taipei, Taiwan, May 2010.

8. Nasruminallah, **M. F. U. Butt**, S. X. Ng and L. Hanzo, "H.264 Wireless Video Telephony Using Iteratively-Detected Binary Self-Concatenated Coding", in Proceedings of the IEEE Vehicular Technology Conference (VTC-2010 Spring), Taipei, Taiwan, May 2010.

Contents

List of Symbols

$A_{w,\delta}$: The two-dimensional Weight Enumerating Function.

b_k: The information symbol at instance k.

B_{Δ_H}: The distance spectrum of the code.

c_k: The coded symbol of the encoder at instance k.

C: The channel capacity in [bits/symbol].

$d^2(\mathbf{x}, \hat{\mathbf{x}})$: The squared *Euclidean distance* between the modulated symbol sequences $\mathbf{x}$ and $\hat{\mathbf{x}}$.

δ: The parity weight quantifying the number of erroneous parity bits in an encoded sequence.

$E(k)$: The expected value of k.

E_b: The bit energy.

E_s: The symbol energy.

f_D: The normalised Doppler frequency.

G: The entire code generator expressed in octal format.

G_{ab}: The power gain (or geometrical gain) between node a and b.

g_r: The feedback polynomial of a convolutional code.

g_i: The feed-forward polynomial of a convolutional code.

h: The channel's impulse response.

h_u: The gain of the resolvable multipath component.

I: The number of inner self-concatenated iterations.

$\mathbf{I}$: The identity matrix.

I_o: The number of outer decoding iterations between SPC and SECCC.

$I_A(\mathbf{b})$: The mutual information associated with the *a apriori* information of the bit stream $\mathbf{b}$.

$I_E(\mathbf{b})$: The mutual information associated with the *extrinsic* information of the bit stream $\mathbf{b}$.

$\mathbf{J}$: The overall system matrix.

K: The number of modulated layers.

$L(.)$: The LLR or Log-Likelihood Ratio.

$L^a(.)$: The *a priori* LLR values.

$L^e(.)$: The *extrinsic* LLR values.

$L^o(.)$: The *a posteriori* LLR values.

m: The number of bits in a modulated symbol.

m_r: The Nakagami fading parameter.

M: The number of constellation points of a multi-level modulation scheme, PSK or QAM.

n: The Additive White Gaussian noise.

N_0: The noise power spectral density.

O: The number of outer iterations between the demapper and the decoder.

P: The signal power.

$P_\pi^{N,w}$: The probability of occurrence for all the associated error events having w information bit errors, when employing a self-concatenated bit-interleaver having a length of N bits.

$\mathbf{P}$: The MMSE multiuser detector's weight vector.

P_b: The bit error probability.

$P(.)$: The symbol probability.

$P(A|B)$: The probability density function of variable A given variable B.

R: The overall coding rate.

R_1: The coding rate of SECCC encoder.

R_2: The puncturing rate of SECCC encoder.

$\mathbf{R}_b$: The covariance matrix of information symbols.

$\mathbf{R}_n$: The covariance matrix of the noise.

S: The number of coding states, which is equals to 2^{ν}, where ν is the code memory.

S_{ab}: The distance between nodes a and b

T_c: The time shift based on the TH code.

T_h: The small shift in the pulse position.

T_F: The frame duration.

T_{PP_n}: PPM-related shift in the pulse position.

V_{ξ}: The variance of ξ.

w: The information weight denoting the number of erroneous information bits in an encoded sequence.

x_k: The transmitted symbol at instance k.

y_k: The received symbol at instance k.

α: The path-loss exponent.

β: The set of indices t satisfying the condition of $x_t \neq \hat{x}_t$.

Δ_H: The effective Hamming distance.

$\mathcal{A}$: The cardinality of the set.

$\chi(i, b)$: The subset that contains all the phasors for which the position i of the phasor has the binary value b, $b \in \{0, 1\}$.

$\mu(.)$: The bit-symbol mapping function.

ν: The code memory.

π: The interleaver.

π^{-1}: The deinterleaver.

ϕ_u: The phase of the resolvable multipath component.

ρ: The layer-specific amplitude scaling factor.

ξ: The residual interference plus noise.

ϱ: The residual interference.

$\Psi(t)$: The OPSWF signalling pulse shape.

σ_n^2: The complex AWGN noise's variance.

θ: The layer-specific phase rotation parameter.

η: The bandwidth efficiency in [bits/sec/Hz].

γ: The SNR.

Λ: The threshold E_b/N_0 point.

ω: The channel capacity.

Chapter 1

Introduction

The need for high-rate wireless communication systems designed for supporting broadband wireless Internet and multimedia services has been growing over the past few years. However, the available radio spectrum is limited and the wireless channel is extremely hostile. Therefore, there is a demand for flexible and bandwidth-efficient transceivers [10, 11]. Shannon quantified the capacity of wireless communications systems in 1948 [12]. Advances in coding have made it feasible to approach Shannon's capacity limit for the case of a single-user system [13, 14]. Multiple-Input Multiple-Output (MIMO) communication systems create multiple wireless links by employing multiple transmit and receive antennas, hence they are capable of supporting high-integrity, high data rate communications [15]. However, MIMOs cannot be readily implemented in shirt-pocket-sized mobile stations (MS), which hence have a limited antenna spacing and impose correlation of the signals. Cooperative communications is capable of eliminating this correlation, while still achieving MIMO-like diversity gains for the system [16]. This is achieved by introducing a relay between the source and the destination with the aid of a completely independent path created by the relay. Coded cooperation [17] is potentially capable of flawlessly recovering the original source signal at the relays and then retransmitting it to the destination from reduced distance.

1.1 The Wireless Channel

The time-varying wireless channel imposes fundamental limitations on the attainable performance of wireless communication systems [18]. Wireless channels typically impose multi-path propagation [18], which is based on the fact that there are many

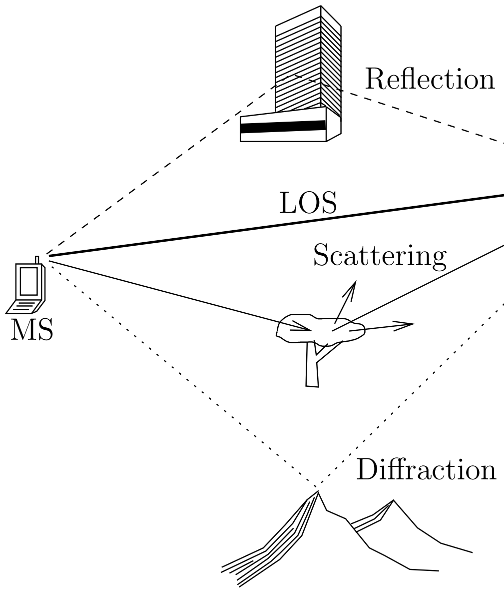

Figure 1.1: An example of different paths in a wireless channel

different paths between the transmitter and the receiver, as exemplified in Figure 1.1. The reflection, diffraction and scattering of the radio waves by objects in the environment give rise to additional radio propagation paths in addition to the direct Line Of Sight (LOS) path between the radio transmitter and receiver [18]:

- *Reflection* occurs due to the collision of a propagating electromagnetic (EM) wave from an object which has large dimensions when compared to the wavelength. Reflections occur from the surface of the earth, buildings and walls.

- *Diffraction* occurs, when a surface that has sharp irregularities obstructs the radio path between the transmitter and receiver. The secondary waves resulting from the obstructing objects give rise to the bending of waves around the obstacle, regardless of the presence or absence of a LOS path between the transmitter and receiver. At high frequencies, the nature of diffraction and reflection depends on the specific geometry of the obstructing objects, as well as on the amplitude, phase, and polarization of the incident wave at the point of diffraction.

- *Scattering* occurs, when the wave is dispersed by objects having dimensions that are small compared to the wavelength, and where the number of obstacles per unit volume is large. Scattered waves are produced by rough surfaces, small objects, or by other irregularities in the channel. In practice, foliage, street signs, rough walls and lamp posts might induce scattering in a mobile communications system.

Another phenomenon generating multipath propagation is constituted by *refraction* caused by the medium [19]. The result is that the destination receives different versions of the same transmitted signal, where these received versions experience different path loss and phase rotations [20].

There are two general aspects characterising a wireless channel. The first is referred to as large-scale fading that corresponds to the effect of the channel on the signal power over large distances, which is directly related to the path loss and shadow fading. The other aspect is the small-scale fading that is characteristic of the rapid fluctuation in the amplitude and phase of the signal. Again, the main mechanisms affecting the transmitted signal's propagation are reflection, diffraction and scattering, as shown in Figure 1.1. The direct path between the transmitter and receiver of Figure 1.1 is referred to as the LOS path, where the received signal propagating through the LOS path is typically the strongest signal. The transmitted signal can also be reflected by objects that are larger than its wavelength, before reaching the receiver. On the other hand, EM waves can also be diffracted by the sharp edges of objects having irregular surfaces. Finally, as shown in Figure 1.1, scattering results in several copies of the wave propagating in different directions. These factors result in the attenuation of the amplitude as well as the phase rotation of the signal, when the received signals are superimposed at the receiver [11]. Additionally, when the transmitter or receiver is moving, the resultant channel becomes a time varying channel, where the amplitude attenuation and phase rotation fluctuate with time. Other factors that influence the small-scale fading include the velocity of both the mobile as well as of the surrounding objects and the transmission bandwidth of the signal [18].

1.2 Channel Coding

Forward Error Correction (FEC) or **Channel Coding** in the context of digital communication has a history dating back to the middle of the twentieth century. In recent years, the field has been revolutionized by iterative detection aided codes, which are capable of approaching the theoretical limits of performance, namely the *channel capacity*. A typical Digital Communication System using error correction codes can be represented by the block diagram of Figure 1.2.

The *channel encoder* or simply *encoder* incorporates redundant information in the input stream in such a specific way so that the errors introduced by the channel

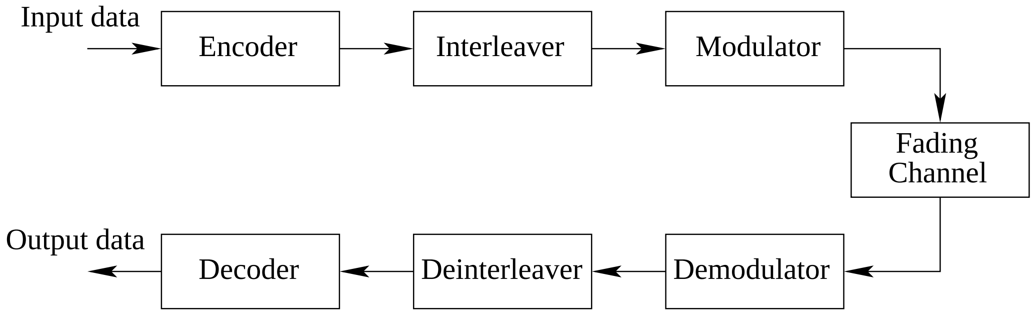

Figure 1.2: Block diagram of a digital communication system using channel coding

can be corrected. The *interleaver* is viewed broadly as a device that separates the successive coded symbols so as to arrange for having independent fading for each symbol (with the aid of the frequency- or time-domain separation of symbols) in the sequence. The *modulator* converts the symbol sequences emanating from the encoder into signals appropriate for transmission over the radio channel. The *channel* is the medium conveying the information. Examples of physical channels are telephone lines, Internet links, fiber-optic lines, microwave radio channels, high frequency radio channels, etc. Many channels require that the signals be sent as a continuous-time voltage, or an electromagnetic waveform in a specified frequency band. As signals travel through a channel they are corrupted. For example, a signal may have noise superimposed on it; it may also experience time delay or timing jitter, or suffer from attenuation which is proportional to the propagation distance and/or carrier offset; it may be reflected by objects in its path, resulting in constructive and/or destructive interference; it may also experience unintentional interference from other channels, or may be deliberately jammed. It may also be linearly distorted by the channel's response, resulting in interference among consecutive symbols. These sources of corruption may also occur simultaneously. For purposes of analysis, the channels are typically characterized by mathematical models, which are sufficiently accurate to be representative of the attributes of the actual channel, yet are also sufficiently abstract to facilitate tractable mathematical description. Most of our work in this treatise will assume having an Additive White Gaussian Noise (AWGN) and Rayleigh Fading channel. The *receiver* consists of a demodulator, whose output is deinterleaved and then fed to the channel decoder. The *demodulator* receives the signal from the channel and converts it into a sequence of discrete symbols, followed by a decoding step, in which decisions about the transmitted symbols are made at the *decoder*.

Owing to the redundancy introduced by the channel encoder, there are more symbols at the output of the encoder than at its input. Frequently, a channel encoder operates by processing a block of k input symbols and producing at its output a block of n symbols, with $n > k$. The rate of the channel encoder is specified as $R = k/n$ so that $R < 1$.

Different channels tend to have different information-carrying capabilities. For example, a dedicated fibre-optic channel is capable of carrying more information than a pair of copper wires designed for the plain-old-telephone service (POTS). Associated with each channel there is a quantity known as the capacity, C, which indicates how much information it can carry reliably [12].

Important milestones in the area of channel coding are described in Tables 1.1, 1.2 and 1.3.

Year	*Milestone*
1948	Shannon's Capacity Theorem [12].
1950	Hamming codes were discovered by Hamming [21].
1954	Reed [22] and Muller [23] present Reed-Muller (RM) codes.
1955	Elias introduces convolutional codes [24].
1957	Prange introduces cyclic codes [25].
1959	Hocquenghem [26] and ...
1960	Bose and Chaudhuri [27] proposed BCH codes.
	Reed and Solomon defined (RS) codes over certain finite Galois fields [28].
	Peterson designed a BCH decoder [29].
1961	Peterson's book on Error Correction Codes (ECC) [30].
1962	Gallager invents LDPC codes [31].
	2400 BPS modem commercially available (4-PSK)(see [32]).
1963	Fano algorithm introduced for decoding convolutional codes [33].
	Massey describes threshold decoding [34].
1966	Forney's introduction of concatenated codes [35]
	and generalized minimum distance decoding [36].
1967	Berlekamp designs an efficient algorithm for BCH/RS decoding [37].
	Rudolph initiates the study of finite geometries for coding [38].
	4800 BPS modem commercially available (8-PSK)(see [32]).
1968	Berlekamp, documents Algebraic Coding Theory [39].
	Gallager publishes, Information theory and reliable communications [40].
1969	Jelinek defines the stack algorithm for decoding convolutional codes [41].
	Massey introduces his BCH decoding algorithm [42].
	Reed-Muller code used on Mariner deep space probes.
1971	Viterbi algorithm for Maximum Likelihood (ML) decoding of convolutional codes [43].
	9600 BPS modem commercially available (16-QAM) see [32].

Table 1.1: Milestones in channel coding (1948-1971) [14, 44]

Year	*Milestone*
1972	Bahl *et al.* invents the Maximum A-Posteriori (MAP) algorithm [45].
	Chase introduces his soft-decision-based block decoding algorithm [46].
	Peterson and Weldon revise their book [47].
1973	Forney further interprets the Viterbi algorithm [48].
1974	Bahl *et al.* describe the symbol based MAP algorithm [49].
1975	Sugiyama *et al.* invokes the Euclidean algorithm for decoding [50].
1977	MacWilliams and Sloane write The Theory of Error Correcting Codes [51].
	Voyager deep space mission uses a concatenated RS/convolutional code (see [52]).
1978	Wolf introduces trellis-decoding of block codes [53].
1980	14,400 BPS modem commercially available (64-QAM) (see [32]).
	Sony and Phillips standardize the compact disc, including a shortened RS code.
1981	Goppa introduces Algebraic-Geometry (AG) codes [54, 55].
1982	Ungerböck invents trellis-coded modulation (TCM) [56].
1983	Textbook on Error control coding by Lin and Costello [57].
	Blahut publishes his channel coding book [58].
1984	14,400 BPS TCM modem commercially available(128-TCM) (see [32]).
1985	19,200 BPS TCM modem commercially available(160-TCM) (see [32]).
1988	Divsalar and Simon discover multiple trellis-coded modulation [59].
1989	Hagenauer and Hoeher present the Soft-Output Viterbi Algorithm (SOVA) [60].
1990	Koch and Baier describe a reduced complexity MAP algorithm [61].
1992	Zehavi introduces Bit-Interleaved Coded Modulation (BICM) [62].
1993	Berrou, Glavieux, and Thitimajshima discover turbo codes [13].
	Honary, Markarian and Farrell *et al*. presented low complexity trellis decoding of array [63] and Hamming codes [64].
1994	The Z_4 linearity of certain families of nonlinear codes is announced [65].
	Erfanian, Pasupathy and Gulak describe the Max-log-MAP algorithm [66].
1995	MacKay revives LDPC codes [67].
	Wicker publishes his textbook [68].
	Robertson, Villebrun and Hoeher desribe Log-MAP algorithm [69].
1996	Hagenauer, Offer and Papke propose turbo-BCH codes [70].
	33,600 BPS modem (V.34) modem is commercially available (see [71]).
	Sidorenko, Markarian and Honary presented a novel trellis design technique [72] for block and convolutional codes resulting in low complexity Viterbi decoding.
1997	Tarokh, Seshadri and Calderbank introduce space-time trellis coding (STTC) [73].
	Nickl, Hagenauer and Burkett report approaching the Shannon limit over Gaussian channels [74] within 0.27 dB.
	Schlegel writes his book on trellis coding [75].
	Ritcey and Li introduce Bit-Interleaved Coded Modulation with Iterative Decoding (BICM-ID) [76].

Table 1.2: Milestones in channel coding (1972-1997) [14, 44]

Year	*Milestone*
1998	Turbo trellis-coded modulation (TTCM) introduced by Robertson and Wörz [77].
	Alamouti introduces space-time block coding [78].
	Guruswami and Sudan present a list decoder for RS and AG codes [79].
1999	Ritcey and Li combine TCM with BICM-ID [80].
2000	Aji and McEliece [81] (and others [82]) synthesize
	several decoding algorithms using message passing ideas.
	Proakis publishes fourth edition of his textbook [83].
2002	Hanzo, Liew, and Yeap characterize turbo algorithms in [14].
	Siwamogsatham and Fitz introduce MTCM assisted STBC [84].
2003	Jafarkhani and Seshadri propose super-orthogonal STTC (SOSTTC) [85].
	Koetter and Vardy extend the GS algorithm for soft-decision
	decoding of RS codes [86].
2004	Lin and Costello publish second edition of their textbook [87].
2005	Moon publishes his textbook [44].
	Simon and Alouini write Digital Communications over Fading Channels [88].
	Song *et al.* introduce SOSTTC combined with QAM [89].

Table 1.3: Milestones in channel coding (1998-2005) [14, 44]

1.3 Organisation of Thesis

The outline of the thesis is presented below with reference to Figure 1.3:

- **Chapter 2:** This chapter discusses iterative detection aided coded modulation scheme designed for transmission over non-dispersive propagation environments. It is demonstrated that concatenated codes are capable of achieving a near-capacity performance, as opposed to non-iterative schemes. Hence iterative detection aided Self-Concatenated Trellis Coded Modulation (SECTCM) schemes are explored, which have a simple structure owing to using a single encoder and a single decoder, and yet deliver a turbo-like performance. We design SECTCMs with the aid of symbol-based EXtrinsic Information Transfer (EXIT) charts. The symbol based Maximum A-Posteriori (MAP) algorithm operating in the logarithmic domain is also highlighted.

- **Chapter 3:** The symbol-based EXIT chart discussed in Chapter 2 was found to be fairly accurate in predicting the SNR threshold required for achieving decoding convergence, despite the inaccurate simplifying assumption that the *extrinsic* information and the systematic information of each SECTCM symbol are independent of each other, which has a limited validity. Self-Concatenated Convolutional Coding (SECCC) using iterative detection is designed with the

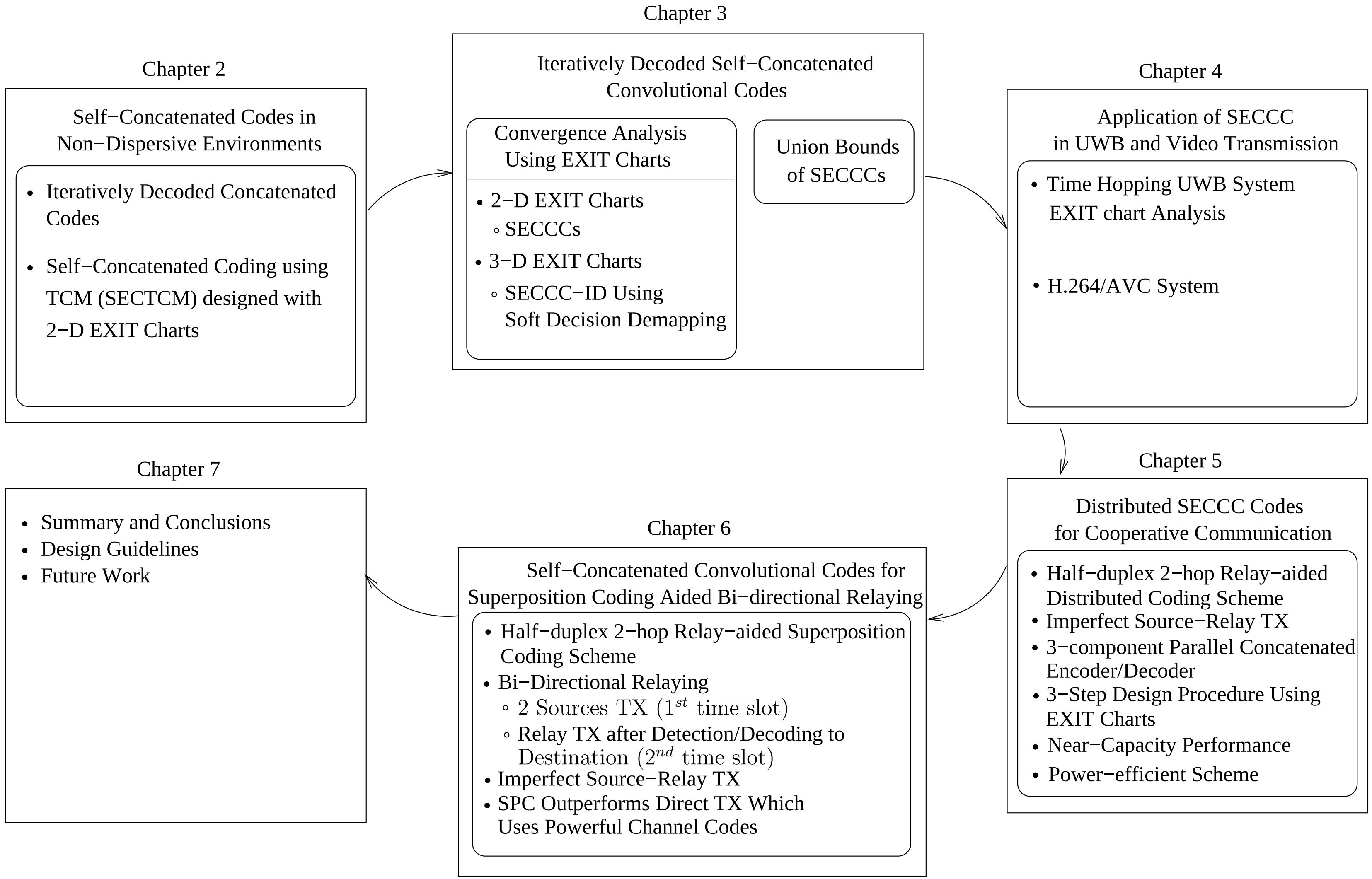

Figure 1.3: Thesis outline

aid of EXIT charts. Then we further developed the SECCC schemes to arrange for the exchange of soft-information with the demapper. The resultant scheme is termed Self-Concatenated Convolutional Coding using Iterative Decoding (SECCC-ID).

- **Chapter 4:** Based on the SECCC designed in Chapter 3 we exemplify their applications in UltraWideBand (UWB) and video transmission environments. The chapter presents a historical perspective on advances in UWB systems and their basic terminology is introduced. We then design a near-capacity Time Hopping (TH) Pulse Position Modulated (PPM) UWB Impulse Radio (IR) system employing SECCCs. In our other application example we then briefly portray the state-of-the-art H.264 Audio/Video Coding (AVC) standard. Finally, we design a robust H.264 coded wireless video transmission scheme using SECCCs.

- **Chapter 5:** In order to mitigate the effects of large-scale shadow fading on the performance of wireless communication systems, we design a distributed coding scheme for cooperative communications employing SECCCs that is capable of providing substantial diversity-, throughput- as well as coding-gains for the case of single-user scenario. The proposed Distributed Self-Concatenated Convolutional Coding scheme using Iterative Decoding (DSECCC-ID) is a half-duplex relaying system, where the source-relay (SR) and source-destination (SD) link employs a SECCC code, while the relay node employs a simple RSC encoder instead of a SECCC encoder. Therefore, the iterative decoder employed at the destination exchanges information between the SECCC decoder and an RSC decoder.

- **Chapter 6:** The chapter presents the basic concepts of Superposition Coding (SPC) and Successive Interference Cancellation (SIC). A two-user bidirectional single-relay-aided cooperative communication system employing SECCCs is studied in interference-limited scenarios. The two nodes communicate with each other via a relay node, which receives information from both nodes in the first transmission period. At the relay node we combined a powerful SPC scheme with a SECCC scheme. The SIC receiver and SECCC decoder iterate by exchanging extrinsic information between each other in order to exchange their mutual information and hence eliminate the residual interference.

- **Chapter 7:** The main findings of the thesis are summarised, design guidelines are presented and future research directions are discussed.

1.4 Novel Contributions:

The dissertation is based on the following publications [1–9]. The novel contributions of the thesis are summarised as follows:

- The design of near-capacity SECTCM schemes was carried out with the aid of symbol-based EXIT charts. Good constituent TCM codes were found for assisting the SECTCM scheme in attaining decoding convergence at the lowest possible E_b/N_0 value, when communicating over both AWGN and uncorrelated Rayleigh fading channels [1].
- We analyse bit-based SECCC codes and design flexible SECCC schemes that are capable of near-capacity operation over both AWGN and uncorrelated Rayleigh fading channels. Bit-based SECCCs eliminate the mismatch inherited by their symbol-based counterparts between the bit-by-bit Monte Carlo-simulation based decoding trajectory and its predicted 2-D EXIT curves, which is a consequence of the correlation of the bits within each coded symbol. The design of near-capacity SECCC schemes based on their decoding convergence analysis which carried out with the aid of bit-based 2D-EXIT charts [2].
- Some information is lost due to the employment of bit-based schemes. We demonstrate that in order to recover the entropy- or capacity-reduction owing to employing binary schemes, soft decision feedback is required between the SISO MAP decoder and the soft demapper. To analyse the exchange of information between the SISO MAP decoder and the soft demapper we employ 3-D EXIT charts. Some of the proposed schemes can perform reliably within about 1 dB from both the AWGN and Rayleigh fading channels' capacity [3].
- We derive the union bound of SECCCs employing BPSK modulation, that are derived for communications over both AWGN and uncorrelated Rayleigh fading channels, based on a novel interleaver concept [4].
- We design a near-capacity iteratively decoded TH-PPM-UWB-IR-SECCC system using EXIT charts. More explicitly, the powerful tool of EXIT charts is used to select the SECCCs for the sake of achieving an infinitesimally low BER for near-capacity operation. Quantitatively, the proposed TH-PPM-UWB-IR-SECCC design becomes capable of performing within about 1.41 dB of the Nakagami-m fading channel's capacity at a BER of 10^{-3} [5].

- A low complexity iteratively decoded binary SECCC is used for the transmission of the source coded stream. This technique is suitable for low-complexity video-telephony, which requires a low transmission power. Furthermore, the practically achievable interactive video performance trends are quantified, when using state-of-the-art video coding techniques, such as H.264/AVC. It is demonstrated that an E_b/N_0 gain of 6 dB may be attained using SECCCs in comparison to the identical-rate state-of-the-art benchmarker over correlated Rayleigh fading channels [6].

- We proposed a power-efficient distributed scheme employing SECCC for cooperative communications. A novel three-component parallel concatenated decoder is invoked. The proposed scheme is designed by a systematic and widely applicable procedure using EXIT charts. The corresponding complexity analysis was also carried out and it was demonstrated that the proposed scheme has a low complexity. The SR link is imperfect, yet this simplified scheme is capable of approaching the Discrete-input Continuous-output Memoryless Channels's (DCMC) capacity [7, 8].

- The half-duplex 2-hop relay-aided SPC scheme assumes that decoding errors may be encountered at the relay node. The relay node then broadcasted this information in the second transmission period after re-encoding it, again, using a SECCC encoder. At the destination, an amalgamated SIC-SECCC block then detected and decoded the signal either with or without the aid of *a priori* information. Our simulation results demonstrated that the proposed scheme is capable of reliably operating at a low BER for transmission over both AWGN and uncorrelated Rayleigh fading channels [9].

Having presented an overview of the thesis, let us now commence our detailed discourse on coded modulation schemes designed for AWGN and Rayleigh channels in the following chapter.

Chapter 2

Self Concatenated Codes in Non-dispersive Environments

The philosophy of concatenated coding schemes was proposed by Forney in [35] for the purpose of achieving high coding gains, where the probability of error decreased exponentially, while maintaining a reasonable decoding complexity by dividing the code into low-complexity constituent codes. This involves combining two or more coding schemes in a serial or parallel manner. Turbo codes constitute a class of FECs, which were developed in 1993 in a contribution by Berrou, Glavieux and Thitimajshima in [13]. The discovery of turbo codes was a breakthrough in coding theory, because they are high-performance codes capable of operating near the Shannonian limit [12]. Since their invention they have found diverse applications in bandwidth-limited communication systems, where the maximum achievable information rate has to be supported in the presence of transmission errors due to the AWGN and channel fading.

2.1 Turbo Coding Schemes

This section briefly outlines three major types of iteratively decoded concatenated coding schemes. The major scientific contributions on iterative detection and its convergence analysis are summarised in Tables 2.1 and 2.2 of Section 2.2. A procedure devised for finding the decoding convergence thresholds of Iteratively-Decoded Self-Concatenated Trellis Coded Modulation (SECTCM) using symbol-based 2-D EXIT charts is presented in Section 2.3. Finally, we present our conclusions in Section 2.5.

2.1.1 Parallel Concatenated Codes

These are the original turbo codes, as described by Berrou *et al.* in 1993 [13] which consist of two or more parallel constituent codes. The component codes are usually systematic. In general, each component code independently encodes the information, whereas an interleaver is used between the two to make the corresponding coded data statistically independent of each other, as shown in Figure 2.1. The overall rate of the parallel concatenated code (PCC) [90] is

$$R_{PCC} = \frac{1}{\frac{1}{R_A} + \frac{1}{R_B} - 1} \, . \tag{2.1}$$

For two identical component encoders, each having a rate R, we have

$$R_{PCC} = \frac{R}{2 - R} \, . \tag{2.2}$$

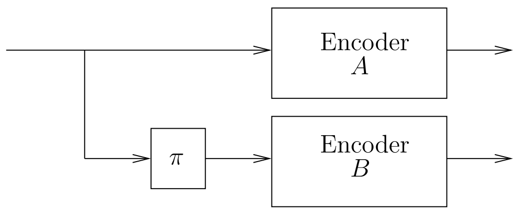

Figure 2.1: The schematic of a parallel concatenated code.

The encoders used were Recursive Systematic Convolutional (RSC) encoders which produce both systematic and parity bits. Hence two codewords are generated that contain the same information part. The parity bits of the two streams can be punctured to generate higher overall coding rates. Therefore the redundant parts of both codes may be transmitted, plus a single copy of the information part. At the decoder, two RSC decoders are used. The decoder operates iteratively. Various TTCM schemes were proposed in [91], [92] and [77], which have a similar architecture to turbo codes, but employ TCM constituent codes [93]. It was shown in [77] that TTCM is capable of outperforming classic Turbo Codes (TC).

2.1.2 Serial Concatenated Codes

The serial concatenation of an outer and an inner encoder is shown in Figure 2.2. These codes were discovered by Benedetto *et al.* [94]. Typically the inner code is a weaker code and the outer code is a stronger code, which are separated by an interleaver. The overall rate of the serial concatenated code (SCC) is

$$R_{SCC} = R_A R_B \, . \tag{2.3}$$

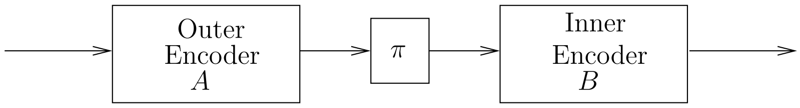

Figure 2.2: The schematic of a serial concatenated code.

If two identical component codes are used, then naturally, the overall rate will decrease. To obtain higher code rates we may employ puncturing. Serially concatenated convolutional codes have been shown to yield a performance comparable, and in some cases superior, to turbo codes.

2.1.3 Self-Concatenated Codes

Trellis Coded Modulation (TCM) was proposed by Ungerböck [56], where a rate $n/(n+1)$ trellis code is combined with an $M = 2^{n+1}$- point signal constellation in order to produce a coded modulation scheme, which imposes no bandwidth expansion relative to an uncoded 2^n-point modulation of the same type, it simply increases the number of bits per symbol. At the same time, it is capable of achieving significant coding gains over power and band-limited channels. Iteratively-Decoded Self-Concatenated Trellis Coded Modulation (SECTCM) schemes were proposed by Benedetto *et al.* [95] and Loeliger [96]. They constitute another attractive family of iterative detection aided schemes. SECTCMs exhibit a low complexity, since they invoke only a single encoder as depicted in Figure 2.3 and a single decoder. The overall rate of the self concatenated code is

$$R_{SECTCM} = R/2 \ . \tag{2.4}$$

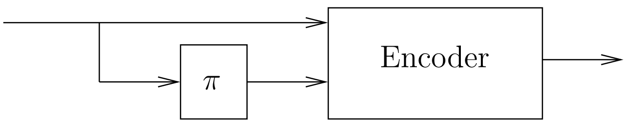

Figure 2.3: The schematic of a self concatenated code.

2.2 Iterative Decoding and Convergence Analysis of Concatenated Codes

At the time of the conception of concatenated codes [35] they were deemed to have an excessive complexity and hence they failed to stimulate immediate research interest. It was not until the discovery of turbo codes [13] that efficient iterative decoding of concatenated codes became a reality at a low complexity by employing simple constituent codes. Since then, the appealing iterative decoding of concatenated codes has inspired numerous researchers to extend the technique to other transmission schemes consisting of a concatenation of two or more constituent decoding stages [76, 80, 95, 97–108]. In [102] iterative decoding was carried out by exchanging information between an outer convolutional decoder and an inner TCM decoder. The research of [103, 104] presented a unified theory of Bit-Interleaved Coded Modulation (BICM) and in [105] the iterative detection principle for BICM between the multilevel soft demapper and the channel decoder was employed. The research efforts of the ensuing era demonstrated that the employment of iterative processing techniques is not limited to traditional concatenated coding schemes. In other words, the "turbo principle" is applicable to numerous other algorithms that can be found in digital communications, for example in turbo equalisation [109] and spectrally efficient modulation [76]. In addition, turbo multiuser detection and channel decoding was proposed in [107] for channel coded code-division multiple-access (CDMA) schemes. Finally, in [108] an iteratively detected scheme was proposed for the Rayleigh fading MIMO channel, where an orthogonal STBC scheme was considered as the inner code combined with an additional block code as the outer channel code. It was shown in [110] that a recursive inner code is needed in order to maximise the interleaver gain and to avoid having a BER floor, when employing iterative decoding. This principle has been adopted by several authors designing serially concatenated schemes, where unity-rate inner codes were employed for designing low complexity iterative detection aided schemes suitable for bandwidth- and power-limited systems having stringent BER requirements [111–115].

The concept of EXtrinsic Information Transfer (EXIT) charts was proposed by ten Brink in [116, 117] as a tool designed for analysing the convergence behaviour of iteratively decoded systems. EXIT charts constitute an efficient tool created for independently analysing each component of an iterative system. Amongst their other benefits detailed in Sections 2.3.2, 3.2.2, 3.3.2 and 5.3 they are capable of predicting the SNR value, where an infinitesimally low BER can be achieved without performing time-consuming bit-by-bit decoding employing a high number of decoding iterations. More specifically, they analyse the input/output mutual information characteristics of a Soft-Input-Soft-Output (SISO) constituent decoder by modelling the *a priori* LLRs and computing the corresponding mutual information between the hard-decision based bits and the extrinsic LLRs. However, the EXIT chart based BER performance-prediction accuracy erodes unless we assume the employment of a sufficiently long interleaver, where the Log-Likelihood Ratio (LLR) values may be rendered Gaussian distributed. The 'waterfall-like' region in the BER curve of a concatenated code can be successfully predicted with the aid of EXIT charts. The computation of EXIT charts was further simplified in [118] to a time averaging, when the Probability Density Function (PDF) values of the information communicated between the input and output of the constituent decoders are both symmetric and consistent. A tutorial introduction to EXIT charts can be found in [119]. The concept of EXIT chart analysis has been extended to three-stage concatenated systems in [120–122]. The major scientific contributions on iterative detection and its convergence analysis are summarised in Tables 2.1 and 2.2.

2.3 Decoding convergence analysis of SECTCM[1]

Symbol-based EXIT charts of non-binary serial and parallel concatenated schemes have been studied in [135], [136] and [137], respectively. Near-capacity codes have been designed with the aid of EXIT charts in [118] and [138]. However, EXIT charts have not been used for designing SECTCM schemes. An EXIT chart based analysis of the iterative decoder provides an insight into its decoding convergence behaviour and hence it is helpful for finding the best constituent codes for SECTCMs.

The applications of TCM for wireless communication channels have been explored in [139] and [140]. The Self-Concatenated Trellis Coded Modulation (SECTCM) philosophy was proposed by Benedetto *et al.* [95] and a similar scheme was proposed by Loeliger [96]. Our goal is to design high-performance constituent TCM codes for communicating over both uncorrelated Rayleigh fading and AWGN channels. At the receiver, iterative decoding is invoked for exchanging extrinsic information between the hypothetical decoder components as detailed in Section 2.3.2. The convergence behaviour of the decoder is analysed with the aid of symbol-based EXIT charts in Section 2.3.2.2. Similarly, the search conducted in Section 2.3.2.2 for finding the best TCM constituent codes is also based on EXIT chart analysis. Finally, we demonstrate that the selected codes are capable of operating within 1 dB from the SNR threshold of the corresponding channel capacity.

[1]This section is based on [1]

Year	*Milestone*
1962	Gallager invented LDPC codes [31].
1966	Forney [35] proposed a novel concatenated coding scheme.
1974	Bahl *et al*. [49] invented the MAP algorithm.
1993	Berrou *et al*. [13] invented the Turbo Codes (TC) and showed that the iterative decoding is an efficient way of improving the attainable performance.
1995	Robertson *et al*. [69] proposed the log-MAP algorithm that results in similar performance to the MAP algorithm but at a significantly lower complexity.
	Divsalar *et al*. [97] applied turbo principle to multiple PCCs.
	Douillard *et al*. [109] presented turbo equalisation, where iterative decoding was invoked for exchanging extrinsic information between a soft-output symbol detector and an outer channel decoder in order to overcome the multipath propagation effects in Gaussian and Rayleigh channels.
1996	Benedetto *et al*. [98] extended the turbo principle to serially concatenated block and convolutional codes.
1997	Loeliger proposed turbo-like codes using a single trellis for their decoding [96].
	Benedetto *et al*. [102] proposed an iterative detection scheme where iterations were carried out between the outer convolutional code and an inner TCM decoder.
	Caire *et al*. [103, 104] presented the BICM concept along with its design rules.
	Ritcey and Li [76] introduced Bit-Interleaved Coded Modulation using Iterative Decoding (BICM-ID).
1998	Robertson and Wörz introduced turbo trellis-coded modulation (TTCM) [77].
	Benedetto *et al*. [94, 95] studied multiple SCCs combined with interleavers.
	Benedetto *et al.* proposed self-concatenated trellis coded modulation (SECTCM) schemes.
	ten Brink *et al*. [105] introduced a soft demapper between the multilevel demodulator and the channel decoder in an iteratively detected coded system.
1999	Wang *et al*. [107] proposed iterative multiuser detection and channel decoding for coded CDMA systems.
	Acikel and Ryan [123] designed high-rate punctured TCs.
2000	Divsalar *et al*. [111, 112] employed unity-rate inner codes for designing low-complexity iterative schemes for bandwidth/power limited systems having stringent BER requirements.
	ten Brink [116] proposed the employment of EXIT charts for analysing the convergence behaviour of iteratively detected systems.
2001	Lee [114] studied the effect of precoding on SCC systems for transmission over ISI channels.
	ten Brink [117, 120] extended the employment of EXIT charts to three-stage PCCs.
	El Gamal *et al*. [124] used SNR measures for studying the convergence behaviour of iterative decoding.

Table 2.1: Major concatenated schemes and iterative detection (1966-2001).

Year	*Milestone*
2001	Ramamurthy and Ryan [125] proposed the serial concatenation of convolutional differential encoders (accumulate codes), whose performance is better than those of PCCs.
2002	Tüchler *et al*. [118] simplified the computation of EXIT charts.
	Tüchler *et al*. [126] compared several algorithms predicting the decoding convergence of iterative decoding schemes.
	Tüchler *et al*. [121] extended the EXIT chart analysis to three-stage SCCs.
2003	Sezgin *et al*. [108] proposed an iterative detection scheme, where a block code was used as an outer code and STBC as an inner code.
2004	Tüchler *et al*. [127] proposed a design procedure for creating systems exhibiting beneficial decoding convergence depending on the block length.
2005	Lifang *et al*. [115] showed that non-square QAM constellations can be decomposed into aparity-check block encoder having a recursive nature and a memoryless modulator. Iterative decoding was implemented in combination with an outer code for improving the system performance.
	Brännström *et al*. [122] considered EXIT chart analysis for multiple concatenated codes using 3-dimensional charts and proposed a way for finding the optimal activation order.
	Luo and Sweeney proposed the employment of cross-entropy as a novel method of predicting the convergence threshold of a TC, which achieved without imposing the usual conditions of either having a Gaussian distribution for the *a priori*/extrinsic information or perfect knowledge of the source information [128].
	Douillard and Berrou [129] showed that double-binary TCs are capable of achieving a better performance in comparison to classic TCs [13].
2006	Chatzigeorgiou *et al.* proposed a novel technique of finding the transfer function of a punctured turbo code designed for optimal performance [130].
2008	Carson *et al.* proposed a novel optimal bit-to-symbol mapping scheme for an 8PSK modulated BICM-ID system for transmission over quasi-static fading channels [131].
	Ng *et al*. [132] used EXIT charts and union bound analysis to compare the performance of near-capacity TTCM schemes.
	Maunder *et al*. [133] designed irregular variable length codes for the near-capacity operation of joint source and channel coding aided systems.
2009	Berrou *et al*. [134] proposed a low-complexity decoding algorithm for improving the performance of TCs in the 'turbo-cliff' region with the introduction of a rate-1 post-encoder applied in a classic TC scheme at the cost of imposing 10% increase in complexity.

Table 2.2: Major concatenated schemes and iterative detection (2001-2009).

2.3.1 SECTCM System Model

In this section we design an SECTCM scheme using TCM as constituent codes. We consider a half-rate SECTCM scheme using QPSK modulation and both the AWGN and uncorrelated Rayleigh fading channels are considered. As shown in Figure 2.4, the input bit sequence $\{b_1\}$ of the self-concatenated encoder is interleaved for yielding the bit sequence $\{b_2\}$. The resultant bit sequences are input to the TCM constituent encoder. At the output of the encoder the interleaved bit sequence is punctured. Hence, the output of the encoder is composed of the combined systematic bit sequence and parity bit sequence.

The TCM constituent encoder has a coding rate of $R_0 = 2/3$, where two input bits, namely b_1 and b_2 are fed to the TCM encoder for generating three output bits, namely b_0, b_1 and b_2, during each encoding instance. However, the interleaved bit b_2 is punctured for attaining a higher rate of $R = 1/2$ as compared to a 1/3-rate scenario, when bit b_2 was not punctured. The systematic and parity bits, b_0 and b_1, are mapped to a QPSK symbol as $x = \mu(b_0 b_1)$, where $\mu(.)$ is the Set Partitioning (SP) based mapping function [139]. The QPSK symbol x is then transmitted over the communication channel.

At the receiver side the received symbol is given by:

$$y = hx + n, \tag{2.5}$$

where h is the channel's non-dispersive fading coefficient and n is the AWGN having a variance of $\frac{N_0}{2}$ per dimension. This signal is then used by a soft demapper for calculating the conditional PDF of receiving y, when $x^{(m)}$ was transmitted:

$$P(y|x^{(m)}) = \frac{1}{\pi N_0} \exp\left(-\frac{\left|y - hx^{(m)}\right|^2}{N_0}\right), \tag{2.6}$$

where $x^{(m)} = \mu(b_0 b_1)$ is the hypothetically transmitted QPSK symbol for $m \in \{0, 1, 2, 3\}$. Then these PDFs are passed to a soft depuncturer for computing the conditional PDF of the $(n + 1) = 3$-bit coded symbol:

$$P(y|\tilde{x}^{(l)}) = P(y|x^{(m)})P(b_2), \tag{2.7}$$

where $\tilde{x}^{(l)}$ is the hypothetically transmitted 3-bit symbol related to b_0, b_1 and b_2 for $l \in \{0, 1.., 7\}$. Since b_2 was punctured, the probability of transmitting b_2 is given by

$$P(b_2) = 0.5, \tag{2.8}$$

The $2^3 = 8$-valued PDF $P(y|\tilde{x}^{(l)})$ characterising each 3-bit symbol is then passed to the SECTCM decoder shown in Figure 2.4.

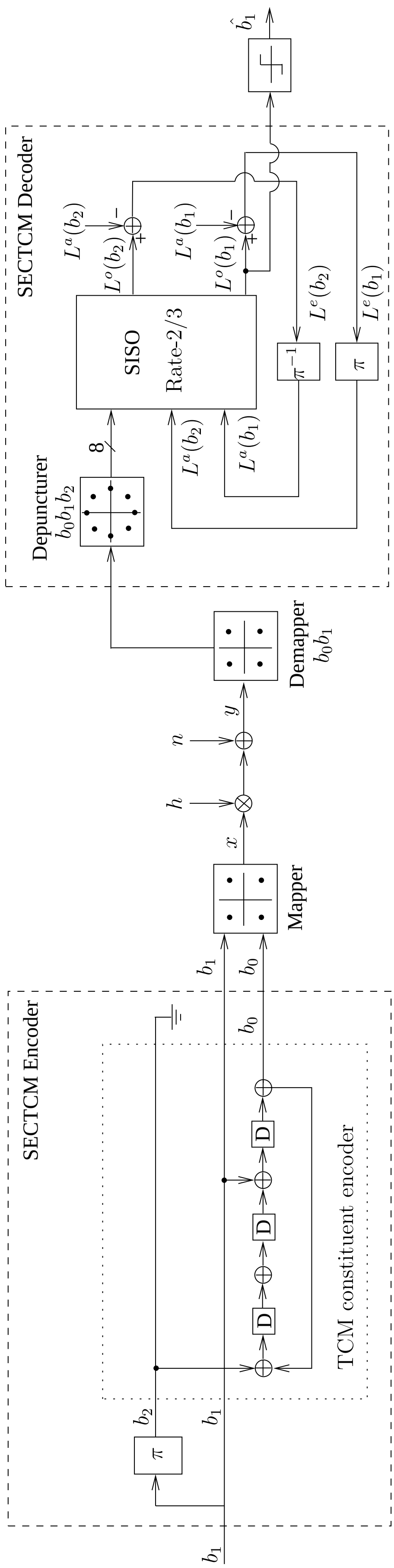

Figure 2.4: SECTCM system

The decoder is a self-concatenated decoder using a symbol-based MAP decoding algorithm proposed in [77] and discussed in Chapter 24 of [11] in detail. It first calculates the extrinsic LLR of the information bits, namely $L_e(b_1)$ and $L_e(b_2)$. Then they are appropriately interleaved to yield the *a priori* LLRs of the information bits, namely $L_a(b_1)$ and $L_a(b_2)$, as shown in Figure 2.4. The choice of the specific generator polynomial seen in Figure 2.4 will be detailed in Section 2.3.2.2. The self-concatenated decoding process of Figure 2.4 proceeds, until a fixed number of iterations is reached. It can be seen in Figure 2.5 that the performance of the code improves by increasing the self-iterations, hence exhibiting a turbo like behaviour for the case of AWGN channels. Similarly for uncorrelated Rayleigh fading channels the performance improvement is shown in Figure 2.6.

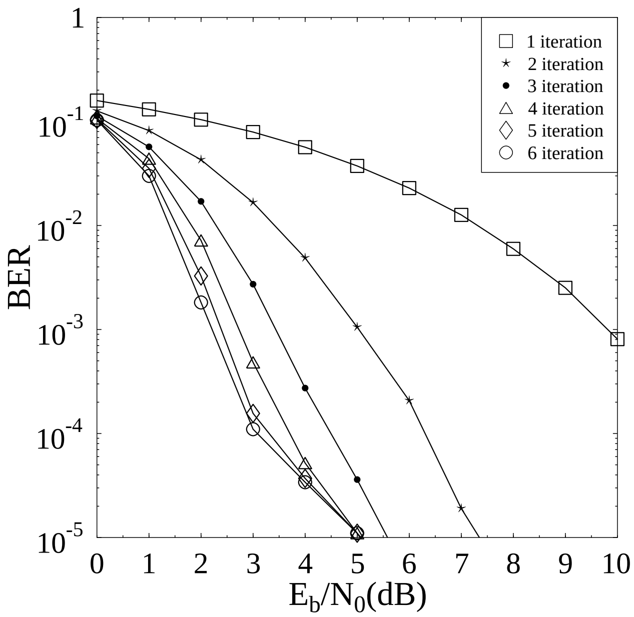

Figure 2.5: Simulations results for an 8-state, rate-1/2 SECTCM code, when communicating over AWGN channels.

2.3.2 SECTCM Code Design Using EXIT Charts

2.3.2.1 Decoding Model

The decoding architecture of the SECTCM scheme is seen in the schematic of Figure 2.7, which corresponds to the symbol-based SECTCM decoder of Figure 2.4. A decoding model was introduced in [141], which was widely applicable to decoding problems including PCCs, SCCs, LDPC and RA codes. The symbol based decoding model is similar to the ones presented in [137, 142]. Random variables (r.v.s.) are denoted by capital letters and their corresponding realizations using lower case letters. Sequences of random variables are indicated by underlining them. For example,

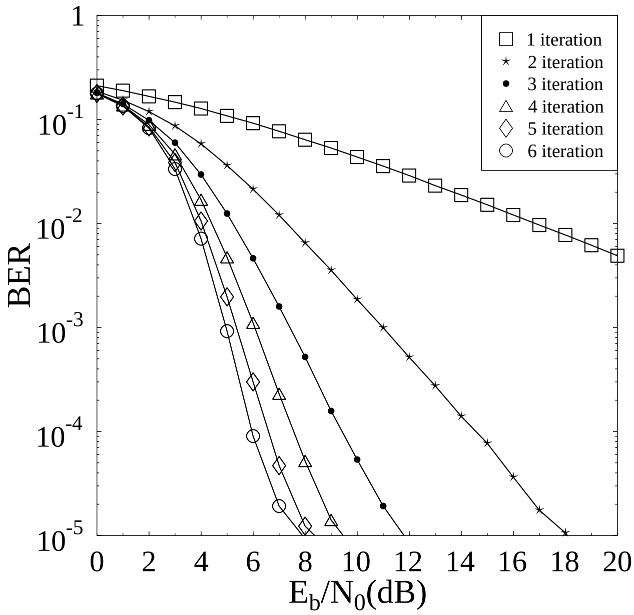

Figure 2.6: Simulations results for 8-state, rate-1/2 SECTCM code, when communicating over uncorrelated Rayleigh fading channels.

the information bit sequence is $\underline{U}$, whose realization is $\underline{u}$, where $\underline{U}$ is encoded by the SECTCM Encoder of Figure 2.4, yielding the coded symbol sequence $\underline{X}$, which is then transmitted over the communication channel. The received symbol sequence is given by $\underline{Y}$, which is then fed to the SISO SECTCM decoder. The *a priori* channel 1 models the *a priori* probabilities of the information bit sequence $\underline{U}$ by $\underline{A}(U)$ and the *a priori* channel 2 models its interleaved version $\underline{W}$ by $\underline{A}(W)$. The SECTCM SISO decoder then computes both the *a posteriori* bit probabilities $\underline{O}(U)$ and the *extrinsic* bit probabilities $\underline{E}(U)$ and $\underline{E}(W)$. An EXIT chart plots the *extrinsic* information I_E as a function of the *a priori* information I_A. In the context of SECTCM, I_A is the joint *a priori* information of U and W, and I_E is the joint *extrinsic* information of U and W.

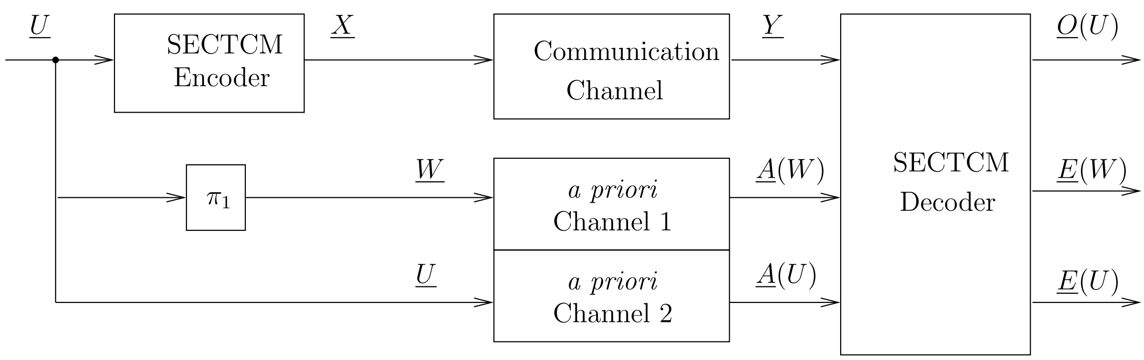

Figure 2.7: Decoding model for an SECTCM scheme.

2.3.2.2 Code Design Procedure

The EXIT chart based code design procedure can be explained using the example of a memory $\nu = 3$ rate-2/3 TCM encoder shown in Figure 2.4. The connections shown in the encoder of Figure 2.4 between the information bits and the modulo-2 adders are uniquely determined by the generator polynomials. The feed-forward generator polynomials are denoted as g_i for $i \in \{1, 2 \ldots, n\}$, while the feed-back generator polynomial is denoted as g_r. As shown in Figure 2.4, there are four possible connection points, when there are $\nu = 3$ shift register stages, each denoted by D. For example, the generator polynomial corresponding to the first information bit b_1 is given by $g_1 = [0010]_2$, which indicates that b_1 is connected only to the third modulo-2 adder from the left. In general, the four binary digits seen in the generator polynomials indicate the presence or absence of connections. The entire code generator is expressed in octal format as $G = [g_r \ g_1 \ g_2]_8 = [11 \ 2 \ 10]_8$.

When designing a non-iteratively decoded TCM scheme, the generator polynomials are typically designed as detailed in Chapter 2 of [14]. However, our goal here is to design the best possible iteratively decoded scheme, hence we are not aiming for maximising the minimal distance, we can fix the generator polynomial connections of the information bits and then only search for the best generator polynomial creating the parity bit, as was done in [132]. The feed-back generator polynomial is denoted as $g_r = [1\text{xx}1]_2$, where the first and the last digits of g_r are fixed to one and the rest of the two digits can be either x= 0 or x= 1, giving rise to only four possible devices for g_r for the $\nu = 3$ TCM code. These four feed-back generator polynomials are given by $[11 \ 2 \ 10]_8$, $[13 \ 2 \ 10]_8$, $[15 \ 2 \ 10]_8$ and $[17 \ 2 \ 10]_8$. *We plot the corresponding EXIT curves for all these polynomials and then identify the specific code having the best decoding convergence by choosing the one that has an open EXIT tunnel at the lowest signal-to-noise ratio (SNR).*

The EXIT charts of self-concatenated codes are typically similar to those of the parallel concatenated TTCM schemes [13, 136, 137], where an open EXIT tunnel exists if the EXIT curve does not intersect with the straight line connecting the point ($I_A = 0$, $I_E = 0$) to the point ($I_A = 2$, $I_E = 2$) in the EXIT chart. In [132] EXIT charts were successfully used to compare the performance of different TTCM schemes by employing the same method to one of the component decoders.

The EXIT curves for three of the $\nu = 5$ constituent TCM codes are shown in Figure 2.8, where it was found that the code associated with the generator polynomial $[77 \ 2 \ 10]_8$ has an open EXIT tunnel at the lowest E_b/N_0 value of 3.02 dB. Figure 2.9

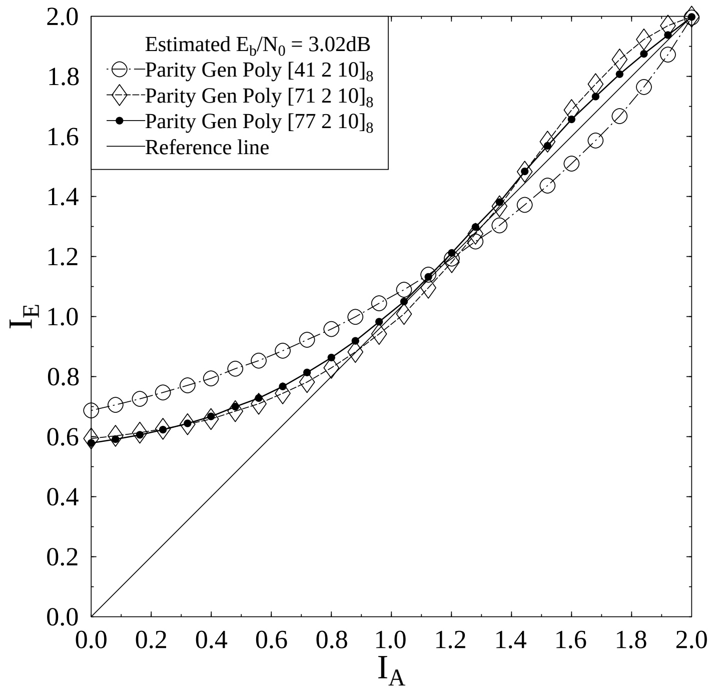

Figure 2.8: Comparison of EXIT curves for various $\nu = 5$ half-rate QPSK-assisted SECTCM codes at $E_b/N_0 = 3.02$ dB using a block length of 10^4 symbols.

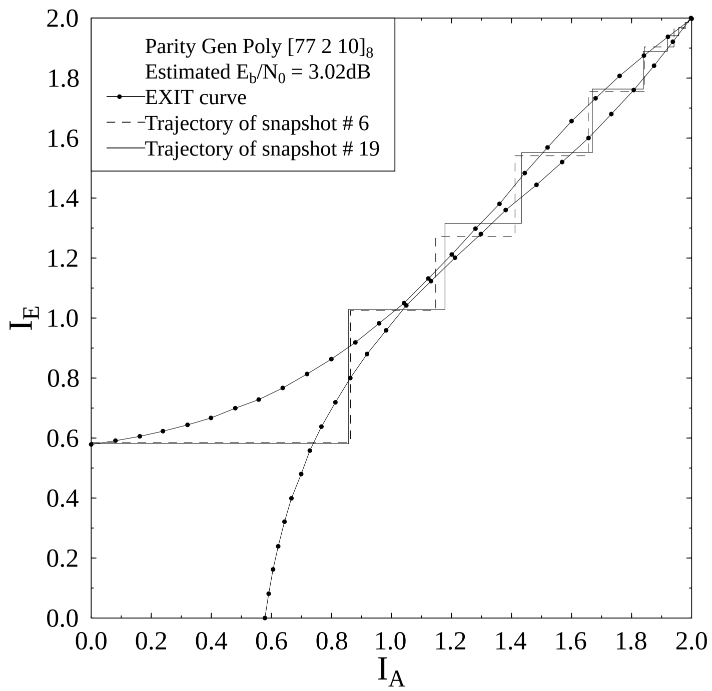

Figure 2.9: EXIT chart and two snapshot decoding trajectories for half-rate QPSK-assisted SECTCM using a block length of 10^4 symbols and $\nu = 5$ at $E_b/N_0 = 3.02$ dB.

depicts the EXIT curves of the constituent codes having a generator polynomial of $[77\ 2\ 10]_8$ together with two of its Monte-Carlo simulation based decoding trajectory snapshots. The two EXIT curves are for two hypothetical decoder components of SECTCM iterating between each other. Since these are identical components, therefore we have to compute the EXIT curve of only one of the components and the other is its mirror image. It is for the same reason that in Figure 2.8 only one EXIT curve (of a particular generator polynomial) has been compared against a 45 degree diagonal line. The EXIT curves of the hypothetical decoder components are plotted on the same EXIT chart together with its decoding trajectory for the sake of visualizing the transfer of extrinsic information between the decoders. Similar to the EXIT curves of the TTCM schemes, the decoding trajectories based on bit-by-bit simulations do not exactly match the predicted EXIT curves [132]. The main reason for the mismatch is that the EXIT charts were generated based on the assumption that the *extrinsic* information and the systematic information of each TCM encoded symbol are independent of each other, which has a limited validity since both the systematic and the parity bits are transmitted together as a single 2^{n+1}-ary symbol. For a symbol-based decoder, a mismatch between its decoding trajectory and its predicted EXIT curves is due to the correlation of the bits in each coded symbol [132, 136, 137]. However, we found that the EXIT charts of the SECTCM scheme can be used as upper bounds since the actual EXIT chart tunnel is always wider than the predicted EXIT chart tunnel. Furthermore, the best TCM code found based on the EXIT charts also exhibits the best BER performance based on bit-by-bit simulations, as we will see in Section 2.3.2.3.

2.3.2.3 Results and Discussions

More quantitatively, the above mentioned EXIT chart method was used to find the best constituent TCM codes for $\nu = \{3, 4, 5\}$, when communicating over both AWGN and uncorrelated Rayleigh fading channels. The corresponding generator polynomials and the channel capacity limits are shown in Table 2.3 together with the predicted and actual convergence thresholds expressed in E_b/N_0.

The predicted convergence threshold is based on the EXIT chart analysis as explained in Section 2.3.2, while the actual convergence threshold is based on the corresponding BER curve given by the specified E_b/N_0 value, where there is a sudden drop of BER after a certain number of decoding iterations. It becomes possible to attain an infinitesimally low BER beyond the convergence threshold, provided

ν	Code Polynomial (Octal)	AWGN Channel E_b/N_0 (dB)			Rayleigh Channel E_b/N_0 (dB)		
		Predicted	Actual	ω	Predicted	Actual	ω
3	$[17\ 2\ 10]_8$	1.19	1.0	0.19	3.32	3.00	1.83
4	$[37\ 2\ 10]_8$	1.06	0.7		3.09	2.70	
5	$[77\ 2\ 10]_8$	1.02	0.7		3.02	2.60	

Table 2.3: The code polynomials of the best TCM constituent codes and their decoding convergence thresholds, where ω denotes the corresponding channel capacity limit.

that the block length is sufficiently long and the number of decoding iteration is sufficiently high. The BER versus E_b/N_0 performance curves of the various QPSK-assisted SECTCM schemes recorded from symbol-by-symbol simulations are shown in Figures 2.10, 2.11 and 2.12. A block length of 10^4 symbols was considered and the number of decoding iterations (I) was fixed to 20 in the simulations.

For the best constituent TCM codes having a fixed code memory ν, the distance from the channel capacity to their convergence threshold has been shown in Figures 2.10, 2.11 and 2.12.

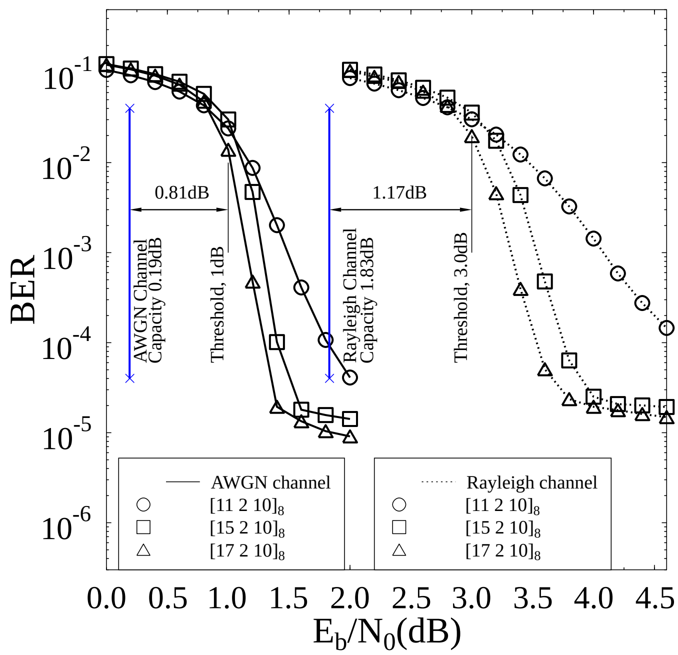

Figure 2.10: The BER versus E_b/N_0 performance of various $\nu = 3$ half-rate QPSK-assisted SECTCM schemes when employing a block length of 10^4 symbols and $I = 20$ decoding iterations.

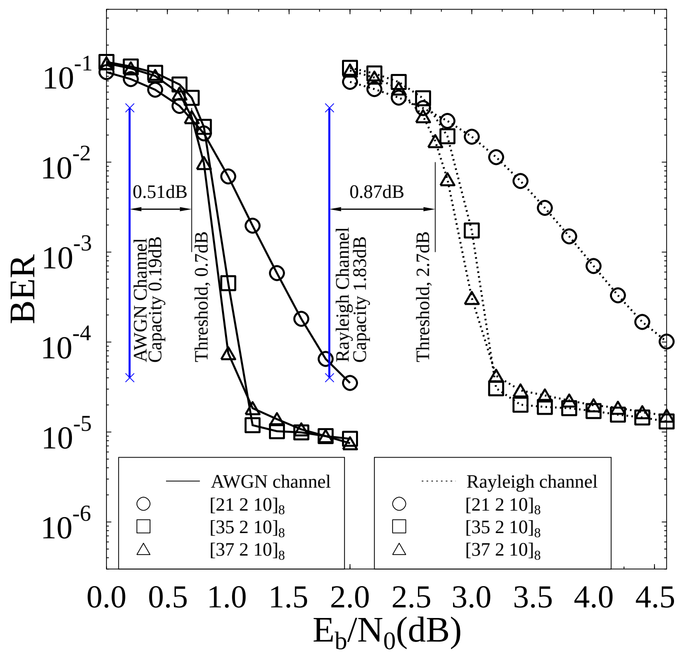

Figure 2.11: The BER versus E_b/N_0 performance of various $\nu = 4$ half-rate QPSK-assisted SECTCM schemes when employing a block length of 10^4 symbols and $I = 20$ decoding iterations.

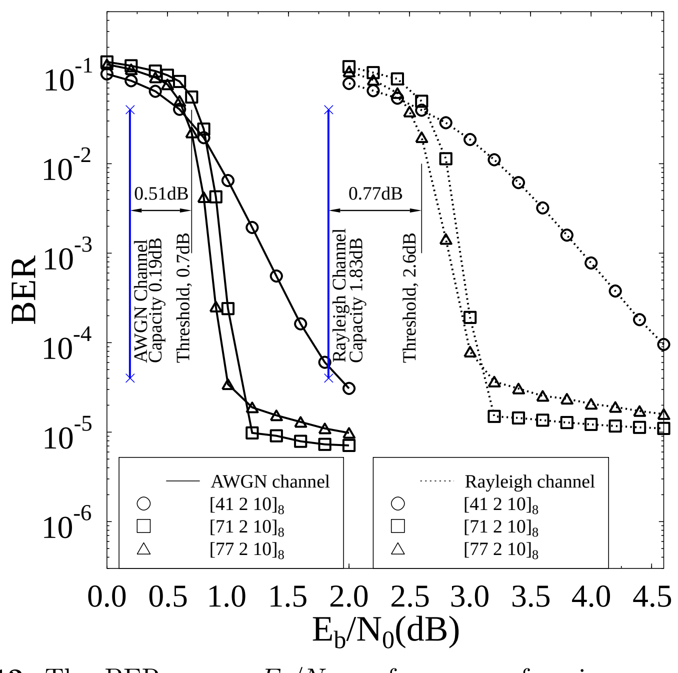

Figure 2.12: The BER versus E_b/N_0 performance of various $\nu = 5$ half-rate QPSK-assisted SECTCM schemes when employing a block length of 10^4 symbols and $I = 20$ decoding iterations.

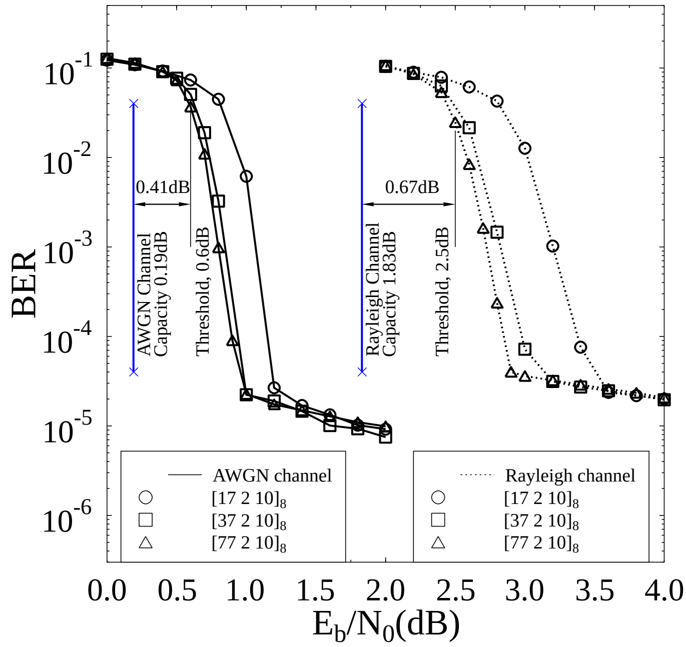

Figure 2.13: The BER versus E_b/N_0 performance of best codes among $\nu = 3$, 4 and 5, half-rate QPSK-assisted SECTCM schemes when employing a block length of 10^4 symbols and $I = 50$ decoding iterations.

It can be observed from Figures 2.10 and 2.11 that upon increasing the code memory ν from 3 to 4 there is a modest 0.3 dB gain in case of both AWGN and uncorrelated Rayleigh fading channels, which is achieved at the rather high 'cost' of doubling the complexity. However, when ν is increased from 4 to 5 as observed from Figures 2.11 and 2.12, no additional gain is achieved in case of the AWGN channel, and only a modest gain of 0.1 dB is achieved in case of the uncorrelated Rayleigh fading channel, despite further doubling the complexity.

As we can see from Table 2.3, the actual achievable convergence threshold is about 0.3 dB lower than the convergence threshold predicted by the EXIT chart. However, the best code found for a given code memory also exhibits the best BER performance among the top three codes considered for that particular code memory, as we can see from Figures 2.10 to 2.12. Hence, the symbol-based EXIT chart is useful for finding the best TCM constituent codes, when designing SECTCM schemes for having a decoding convergence at the lowest possible E_b/N_0 value. In conclusion, minimum distance is is no longer the most important optimization criterion when analysing the BER floor, nor is the distance profile, unless we aim for the so-called 'truncated' union bound analysis [132]. In general, a reduced BER floor may be attained by increasing the block length [132] without increasing the decoder's complexity.

The E_b/N_0 values required for attaining a capacity of 1 bit/s/Hz are 0.19 dB and 1.83 dB for the QPSK-based discrete-input AWGN and Rayleigh fading channels, respectively [11, 143]. As seen in Figures 2.10 to 2.12, the codes found from the EXIT chart based design are capable of approaching the channel capacity of both the AWGN and uncorrelated Rayleigh fading channels. We then further increased the number of decoding iterations from $I = 20$ to 50 and plotted the BER curves of best codes for $\nu = 3$, 4 and 5 in Figure 2.13.

When the number of iterations is increased from 20 to 50, a further 0.1 dB gain is achieved by employing a generator polynomial of $[77\ 2\ 10]_8$ for communicating over either the AWGN or uncorrelated Rayleigh fading channels, as seen in Figures 2.12 and 2.13. Finally, we can see from Figure 2.13, that the $\nu = 5$ SECTCM scheme is only 0.41 dB and 0.67 dB away from the AWGN and Rayleigh fading channel's capacity, respectively.

In terms of the complexity of the schemes we can compare them by calculating the total number of trellis states, multiplied by the number of iterations at the corresponding decoders. This determines the number of Add-Compare-Select (ACS) arithematic operations of a systolic array based silicon chip. For $I = 50$ decoding iterations of a memory-$\nu = 3$ SECTCM decoder, $I \times 2^{\nu} = 50 \times 8 = 400$ ACS operations are required. By contrast, a memory-$\nu = 5$ SECTCM decoder requires quadrupled number of ACS operations given by $I \times 2^{\nu} = 50 \times 32 = 1600$.

2.4 Performance Analysis of Coded Modulation Schemes

In order to investigate the performance of the SECTCM scheme, we compared the TCM, BICM, TTCM and BICM-ID schemes [11] and [93], in the presence of AWGN and Rayleigh fading channels. We considered equivalent-complexity QPSK assisted coded modulation schemes, which are characterized, in Figures 2.14, 2.15 and 2.16 for coded frame length of 1000, 4000 and 10,000 symbols. As shown in Figures 2.14(a) and 2.14(c), four iterations are used for the TTCM scheme exchanging extrinsic information between two component codes, therefore an 8-state component code exhibits a total compolexity associated with $2 \times 4 \times 8 = 64$ trellis states, therefore it has a complexity similar to that of a 64-state TCM and BICM scheme. In the case of SECTCM the two identical code components iterate four times exchanging extrinsic information with each other, hence we have fixed the number of iterations to eight. Hence the complexity of an 8-state SECTCM code characterized in Figures 2.14(a)

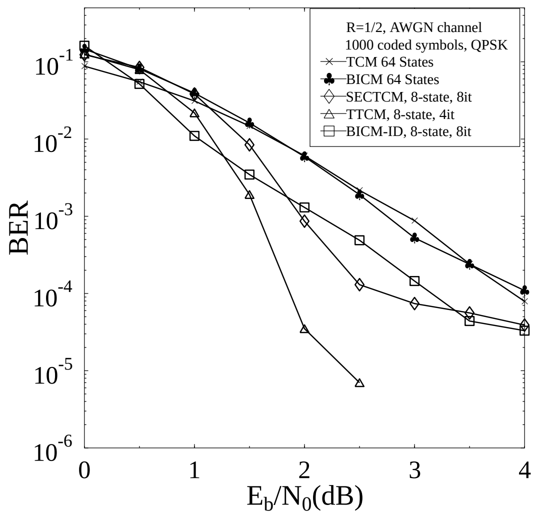

(a) 8 iterations

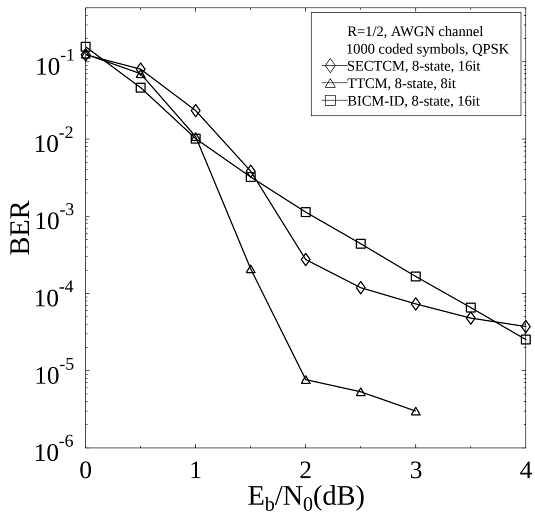

(b) 16 iterations

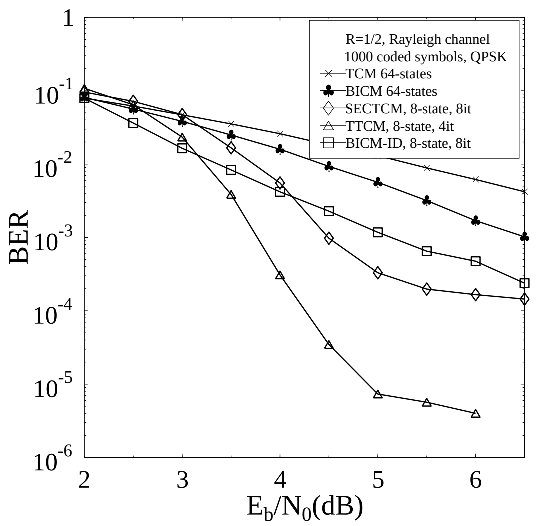

(c) 8 iterations

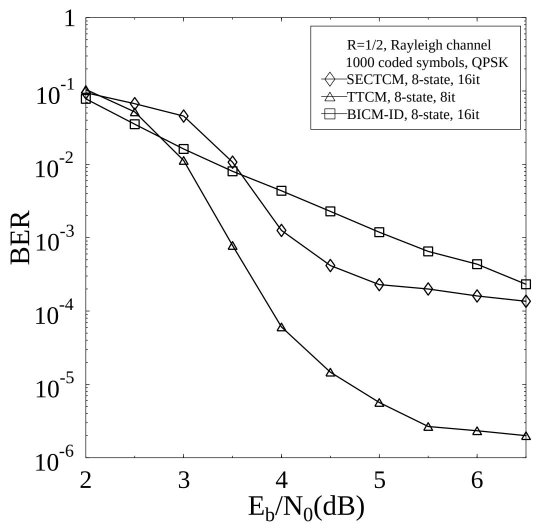

(d) 16 iterations

Figure 2.14: Performance of QPSK assisted equivalent-complexity TCM, BICM, SECTCM, TTCM and BICM-ID schemes under AWGN and Rayleigh fading channel conditions when the interleaver depth is 1000 symbols.

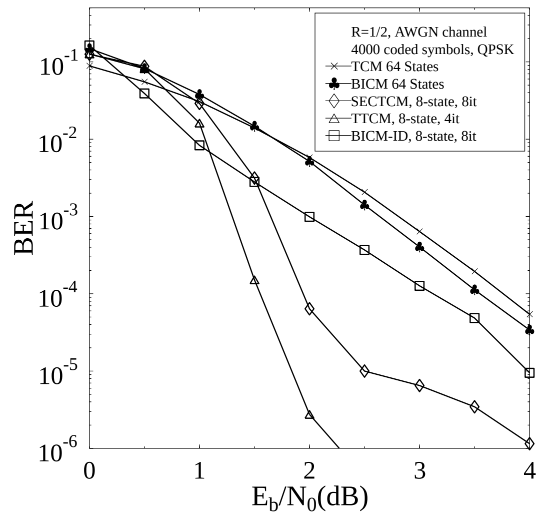

(a) 8 iterations

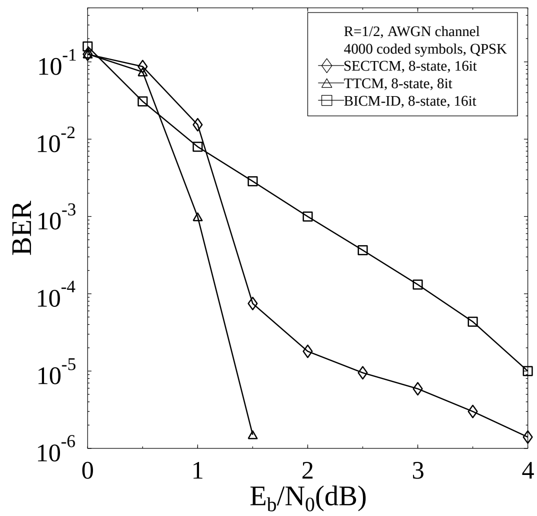

(b) 16 iterations

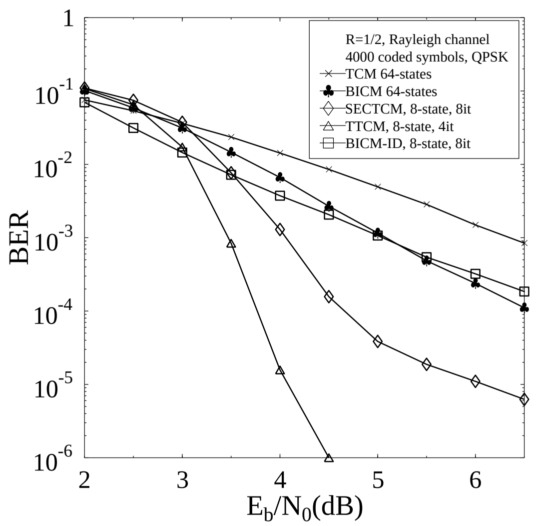

(c) 8 iterations

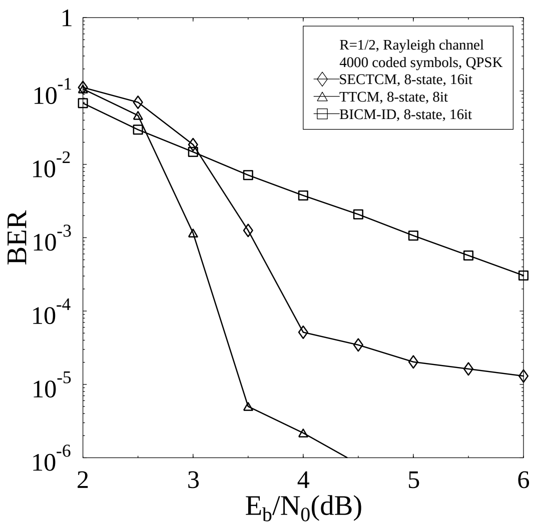

(d) 16 iterations

Figure 2.15: Performance of QPSK assisted equivalent-complexity TCM, BICM, SECTCM, TTCM and BICM-ID schemes under AWGN and Rayleigh fading channel conditions when the interleaver depth is 4000 symbols.

and 2.14(c) is also that of an $8 \times 8 = 64$ state trellis code. As seen in Figures 2.14 the performance of TTCM is superior to that of all the other schemes. However, the equivalent-complexity SECTCM arrangement performs better compared to TCM, BICM and BICM-ID, as shown in Figures 2.14, 2.15 and 2.16. When the number of iterations is increased from 8 to 16, the attainable coding gain remains modest for the 1000-symbol interleaver and its performance in comparison to TTCM remains inferior. However, when we increase the interleaver size to 4000-symbols the performance improves. When the number of coded symbols is 4000 and we have a memory of $\nu = 3$, Figure 2.15(a) shows our comparison of 64-state TCM and BICM with 8-state SECTCM, TTCM and BICM-ID having 8 decoding iterations. The TTCM scheme shows a superior performance over that of the other schemes. When analysed under AWGN channel conditions, it may be observed that TTCM performs 0.35 dB better than SECTCM at a BER of 10^{-4}, since the E_b/N_0 value recorded at a BER of 10^{-4} for the case of SECTCM is 1.95 dB, whereas it is 1.60 dB for TTCM. By contrast, SECTCM shows a gain of 1.20 dB in comparison to BICM-ID and a gain of 1.85 dB over TCM. We can observe in Figure 2.15(a) that BICM performs better than TCM. The performance difference between the SECTCM and TTCM schemes reduces to 0.25 dB at a BER of 10^{-4}, when we increase the number of decoding iterations from 8 to 16, as shown in Figure 2.15(b), since the E_b/N_0 value recorded at a BER of 10^{-4} for the case of SECTCM is 1.45 dB, whereas it is 1.20 dB for TTCM. There is a marked gain of 0.5 dB in case of SECTCM, when we increase the number of iterations from 8 to 16. Similar trends are observed, when we analyse the above-mentioned coding schemes at an interleaver length of 10,000 coded symbols.

When fixing the interleaver-length to 4000 symbols and the code memory to 3 under uncorrelated Rayleigh fading channel conditions the performance of an 8-state SECTCM, TTCM and BICM-ID scheme having 8 decoding iterations is compared again to that of 64-state TCM and BICM schemes in Figure 2.15(c). The performance trends are similar to those in case of the AWGN channel, as characterized in Figure 2.15(c) and discussed earlier. The SECTCM scheme performs better than the identical-complexity TCM, BICM and BICM-ID schemes. TTCM exhibits a 0.9 dB better performance in comparison to an equivalent-complexity SECTCM code at a BER of 10^{-4}, since the E_b/N_0 value recorded at a BER of 10^{-4} for the case of SECTCM is 4.70 dB, whereas it is 3.80 dB for TTCM. However upon increasing the number of decoding iterations to 16 the SECTCM narrows this gap to 0.6 dB, as shown in Figure 2.15(d), since the E_b/N_0 value recorded at a BER of 10^{-4} for the case of SECTCM is 3.90 dB, whereas it is 3.30 dB for TTCM. Similar trends are

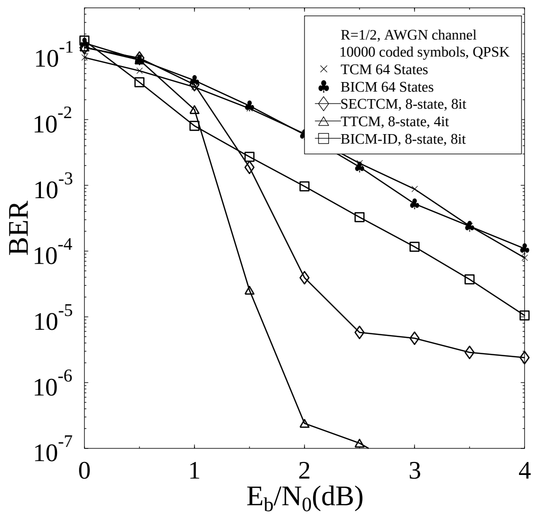

(a) 8 iterations

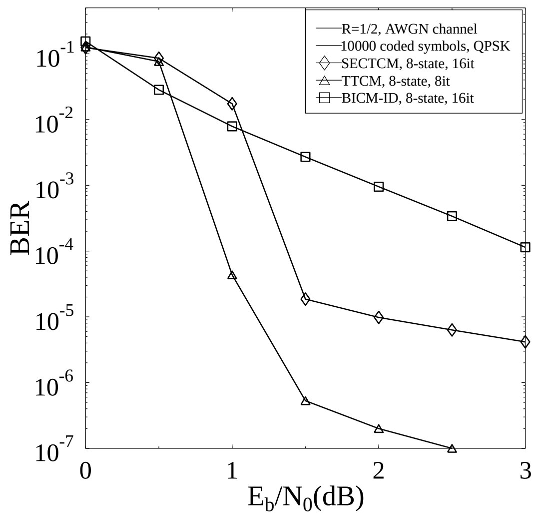

(b) 16 iterations

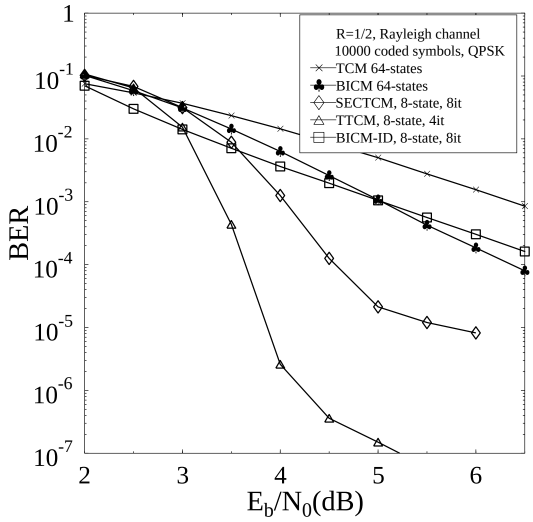

(c) 8 iterations

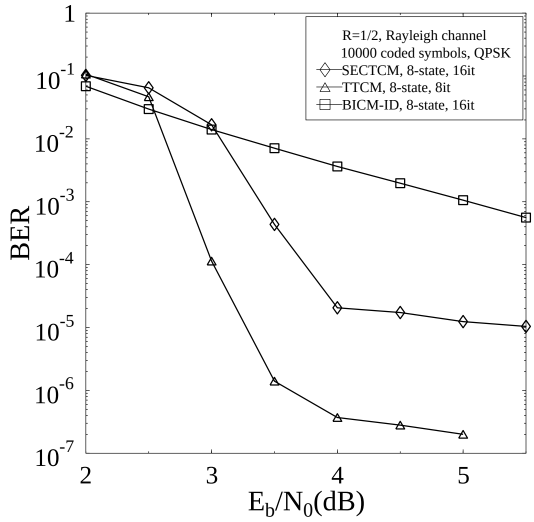

(d) 16 iterations

Figure 2.16: Performance of QPSK assisted equivalent-complexity TCM, BICM, SECTCM, TTCM and BICM-ID schemes under AWGN and Rayleigh fading channel conditions when the interleaver depth is 10,000 symbols.

observed, when we consider an interleaver length of 10,000 coded symbols.

2.5 Chapter Conclusions

We have designed near-capacity SECTCM schemes based on their decoding convergence analysis, as detailed in Figures 2.8 and 2.9 in Section 2.3. The symbol-based EXIT chart discussed in Section 2.3 was found to be fairly accurate in predicting the decoding convergence threshold, despite the inaccurate simplifying assumption that the *extrinsic* information and the systematic information of each SECTCM symbol was independent of each other, which has a limited validity. Good constituent TCM codes were found for assisting the SECTCM scheme in attaining decoding convergence at the lowest possible E_b/N_0 value, when communicating over both AWGN and uncorrelated Rayleigh fading channels. It was seen in Figure 2.13 that the SECTCM schemes designed are capable of operating within about 0.5 dB and 1.0 dB from the AWGN and Rayleigh fading channel's capacity, respectively.

2.6 Chapter Summary

In this chapter we provided an introduction to concatenated coding schemes. Our design procedure relying on finding the decoding convergence thresholds of SECTCMs using symbol-based 2-D EXIT charts was presented in Section 2.3. It was shown in Section 2.4 that although TTCM using half-rate constituent codes performs better than SETCM, as shown in Figures 2.14, 2.15 and 2.16, it fails to offer much flexibility in terms of the choice of coding rates.

As seen in Figures 2.14, 2.15 and 2.16, the performance of TTCM is superior in comparison to the other schemes. However, the equivalent-complexity SECTCM scheme performs better than TCM, BICM and BICM-ID, as shown in Table 2.4. When the number of iterations is increased from 8 to 16, the additional coding gain remains modest for the case of a 1000-symbol interleaver, hence its performance remains modest in comparison to TTCM. However, when we increase the interleaver length to 4000 symbols the performance improves. When the interleaver-length is 4000-symbols and the code memory is $\nu = 3$, Table 2.4 shows our comparison of 64-state TCM and BICM with 8-state SECTCM, TTCM and BICM-ID having either 8 or 16 decoding iterations. TTCM exhibits a superior performance over that of the other schemes. When considering AWGN channel conditions, it may be observed

Channel				AWGN			Uncorrelated Rayleigh		
Modulation				QPSK					
Decoder				Approximate Log-MAP					
Symbols per frame				1000	4000	10,000	1000	4000	10,000
Code	ν	Gen. Poly.	Iterations	E_b/N_0 (dB) at BER of 10^{-4}					
TCM	6	$[117\ 26]_8$	0	3.85	3.80	3.85	11.30	8.00	8.30
BICM	6	$[133\ 171]_8$	0	4.00	3.50	4.00	7.50	6.55	6.35
SECTCM	3	$[17\ 2\ 10]_8$	8	2.75	1.95	1.80	7.50	4.70	4.60
SECTCM	3	$[17\ 2\ 10]_8$	16	2.65	1.45	1.30	7.40	3.90	3.75
TTCM	3	$[13\ 6]_8$	4	1.85	1.60	1.35	4.25	3.80	3.65
TTCM	3	$[13\ 6]_8$	8	1.60	1.20	0.90	3.90	3.30	3.05
BICM-ID	3	$[15\ 17]_8$	8	3.20	3.15	3.05	7.20	7.00	6.95
BICM-ID	3	$[15\ 17]_8$	16	3.30	3.15	3.00	7.25	7.00	6.80

Table 2.4: Performance of QPSK assisted equivalent complexity TCM, BICM, SECTCM, TTCM and BICM-ID schemes under AWGN and Rayleigh fading channels when the interleaver depth are 1000, 4000 and 10,000.

that TTCM performs about 0.25 dB better for transmission over AWGN channels and 0.6 dB better for Rayleigh fading channel conditions than SECTCM at a BER of 10^{-4} in the case of a 4000-symbols interleaver, when employing 16 decoding iterations. Similar trends are observed, when we consider an interleaver length of 10,000 symbols.

In the following chapter we will design flexible bit-based self-concatenated codes, which will be shown to be capable of operating close to the capacity of both the AWGN and of the uncorrelated Rayleigh fading channel.

Chapter 3

Iteratively Decoded Self-Concatenated Convolutional Codes

3.1 Introduction

In chapter 2 convergence behaviour of the SECTCMs was analysed with the aid of symbol-based EXIT charts, when communicating over both uncorrelated Rayleigh fading and AWGN channels. It was seen in Figure 2.4 that the SECTCM is a low-complexity scheme employing a single encoder. In this chapter we will design various Self-Concatenated Convolutional Codes (SECCC) and Self-Concatenated Convolutional Codes Iteratively Decoding with a soft demapper (SECCC-ID). We invoke 2D- and 3D-bit-based EXIT charts, respectively. It will be shown that flexible bit-based SECCC schemes can be designed using the proposed method, which is not possible for the symbol-based case of SECTCM and TTCM schemes. Furthermore, it will be demonstrated that SECCCs and SECCC-IDs are capable of exhibiting lower error floors as compared to an equivalent-complexity SECTCM scheme. EXIT charts are helpful in analysing the convergence behaviour of SECCCs. We discuss in detail the specific design procedure using 2D-EXIT charts in Section 3.2.2 and 3D-EXIT charts in Section 3.3.2. It will be argued that bit-based SECCC lend themselves to more accurate EXIT-chart-based design than their symbol-based SECTCM counterparts, because the bits of a SECTCM symbol are not uncorrelated with each other, although this is a prerequiste for the accurate match between the EXIT curves and the Monte-Carlo simulation based decoding trajectories. Finally, in Section 3.4 we derive the union bounds for an SECCC scheme, which is an upper bound on the bit error probability, our derivation is based on following the concept of uniform interleavers used in [110] and [144] for PCCC and SCCC in order to analyse their error floor. The union bound constitutes a useful code design technique [75, 132, 145–149], which was also employed for the design of antenna selection schemes [150]. More explicitly, in Section 3.4 the union bounds of SECCCs are derived for communication over both AWGN and uncorrelated Rayleigh fading channels, which involves the computation of the distance spectrum [145] of the code. In [145] it was shown that the error floor that occurs at moderate SNRs is a consequence of the relatively low free distance of the code. Which is further aggravated by having several low-distance spectral components. It should be noted that for a large codeword length, it is computationally expensive or even potentially unrealstic to compute the entire distance spectrum. Hence the union bound is approximated by considering the contribution of the several smallest non-zero distance spectrum terms [146]. This approximation of the union bound is termed as the Truncated Union Bound (TUB). The TUBs of SECCCs are very useful for studying the corresponding BER floors. All concatenated coding schemes including SECCCs tend to exhibit a BER floor in the medium to high SNR region [145]. However, the BER floor of SECCCs has not been analyzed in the literature. While EXIT chart analysis [151] is only accurate when a sufficiently long interleaver is used, the BER floor analysis using the so-called TUB [132] is valid for arbitrary interleaver lengths. Hence, the BER floor analysis is important for code design.

The novelty and rationale of this chapter can be summarised as follows:

1. ***Binary SECCC Code Design:*** *We analyse bit-based SECCC codes and design flexible SECCC schemes that are capable of near-capacity operation over both AWGN and uncorrelated Rayleigh fading channels. Bit-based SECCCs eliminate the mismatch, inherited by its symbol-based counterpart between its decoding trajectory and its predicted 2-D EXIT curves due to the correlation of the bits in each coded symbol.*

2. ***Binary SECCC-ID Using Soft Decision Demapping:*** *Some information is lost due to the employment of bit-based schemes. We demonstrate that in order to recover the entropy- or capacity-reduction owing to employing binary schemes, soft decision feedback is required between the SISO MAP decoder and the soft demapper. To analyse the exchange of information between the SISO MAP decoder and soft demapper we use 3-D EXIT charts. Some of the proposed schemes perform less than 1 dB from both the AWGN and Rayleigh fading*

channels' capacity.

3. ***Union Bound of SECCC:*** *We derive the union bound of SECCCs employing BPSK modulation, that are derived for communications over both AWGN and uncorrelated Rayleigh fading channels, based on the novel uniform self-interleaver concept.*

3.2 Binary SECCC

SECCC is a low-complexity scheme involving only a single encoder and a single decoder. An EXIT chart based analysis of the iterative decoder provides an insight into its decoding convergence behaviour and hence it is helpful for finding the best coding schemes for creating SECCCs. An SECTCM scheme was designed using TCM as constituent codes with the aid of EXIT charts in chapter 2 and appeared in [1]. The proposed design was symbol-based, therefore it had the inherent problem of exhibiting a mismatch between the EXIT curve and the bit-by-bit decoding trajectory. The main reason for the mismatch was that the EXIT charts were generated based on the assumption that the *extrinsic* information and the systematic information part of each TCM encoded symbol are independent of each other, which had a limited validity, since both the systematic and the parity bits were transmitted together as a single 2^{n+1}-ary symbol. More explicitly, the coded bits in each coded symbol are correlated [136, 137], hence they cannot convey the maximum possible information, which is equivalent to an entropy- or capacity-loss. Nonetheless, we found that the EXIT charts of the symbol-based SECCC scheme can be beneficially used, since the actual EXIT chart tunnel is always wider than the predicted EXIT chart tunnel. Hence, the analysis was still valid, since it assisted us in finding the convergence SNR. In the following Section we present our proposed binary SECCC scheme which eliminates the mismatch inherited by the symbol-based TCM design.

3.2.1 Binary SECCC System Model[1]

The scheme employs binary RSC codes as constituent codes to eliminate the mismatch inherited by the symbol-based TCM design of Figure 2.4 by proposing a bit-based SECCC design in order to create flexible SECCC schemes capable of efficiently operating for transmission over both AWGN and uncorrelated Rayleigh fading channels. EXIT charts have been used to characterize the convergence behaviour of these

[1]This section is based on [2]

schemes. It will be shown that some of the proposed SECCC schemes perform within about 1 dB from the AWGN and Rayleigh fading channels' capacity. The scheme used Gray-coded QPSK modulation in all the examples. The SECCC system model is depicted in Figure 3.1.

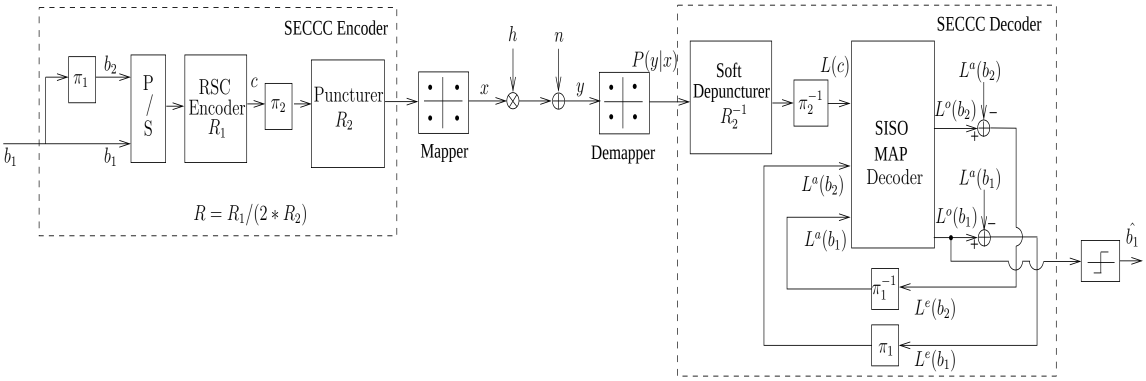

Figure 3.1: Binary SECCC scheme [2], which is different from the SECTCM schematic of Figure 2.4, since the RSC constituent encoder is followed by an interleaver, a puncturer and a modulator. By contrast, in the case of the SECTCM scheme of Figure 2.4 the TCM constituent encoder generates its output after puncturing the systematic bits. This makes the SECCC scheme more flexible.

We consider a rate $R = 1/2$ SECCC scheme as an example, in order to highlight the various system concepts considered in this section. Both the AWGN and the uncorrelated Rayleigh fading channels are considered. The notation $L(.)$ in Figure 3.1 represents the LLR of the bit probabilities. The notations b and c in the round brackets (.) in Figure 3.1 denote the information bits and the coded symbols, respectively. The specific nature of the probabilities and LLRs is represented by the subscripts a, o and e, which denote in Figure 3.1, *a priori*, *a posteriori* and *extrinsic* information, respectively. As shown in Figure 3.1, the input bit sequence $\{b_1\}$ of the self-concatenated encoder is interleaved for yielding the bit sequence $\{b_2\}$. The resultant bit sequences are parallel-to-serial converted and then fed to the RSC encoder using the generator polynomials $(g_r = 13, g_1 = 15, g_2 = 17)_8$ expressed in octal format and having a rate of $R_1 = 1/3$ and memory $\nu = 3$, where g_r specifies the feedback polynomial. Hence for every bit input to the SECCC encoder there are six output bits of the RSC encoder. At the output of the encoder there is an interleaver and then a rate $R_2 = 1/3$ puncturer, which punctures (does not transmit) two bits out of three encoded bits[2]. Hence, the overall code rate, R can be derived based

[2] $R_2 = lx/ly$ is the puncturing rate, where $(ly - lx)$ bit(s) are punctured for every ly-bit segment. The interleaver π_2 is before the puncturer in Figure 3.1, therefore the bits being punctured could be either the parity or the systematic bit.

on [152] as:

$$R = \frac{R_1}{2 \times R_2} = \frac{1}{2}\left(\frac{1}{3\left(\frac{1}{3}\right)}\right) = \frac{1}{2}. \tag{3.1}$$

Therefore, at the output of the puncturer the number of encoded bits reduces from six to two bits, namely (c_1c_0). Puncturing is used in order to increase the achievable bandwidth efficiency η. It can be observed that different codes can be designed by changing R_1 and R_2. These bits are then mapped to a QPSK symbol as $x = \mu(c_1c_0)$, where $\mu(.)$ is the Gray-coded mapping function. Hence the bandwidth efficiency is given by $\eta = R \times \log_2(4) = 1$ bit/s/Hz assuming a zero Nyquist roll-off-factor. The QPSK symbol x is then transmitted over the communication channel. At the receiver side the received symbol is given by:

$$y = hx + n, \tag{3.2}$$

where h is the channel's non-dispersive fading coefficient and n is the AWGN having a variance of $N_0/2$ per dimension. This signal is then used by the demapper for calculating the conditional PDF of receiving y, when a complex-value $x^{(m)}$ was transmitted:

$$P(y|x = x^{(m)}) = \frac{1}{\pi N_0}\exp\left(-\frac{\left|y - hx^{(m)}\right|^2}{N_0}\right), \tag{3.3}$$

where $x^{(m)} = \mu(c_1c_0)$ is the hypothetically transmitted QPSK symbol for $m \in \{0, 1, 2, 3\}$. Then these PDFs are passed to a soft depuncturer, which converts the PDFs to bit-based LLRs and inserts zero LLRs at the punctured bit positions. These LLRs are then deinterleaved and fed to the SISO MAP decoder. The self-concatenated decoding procedure is similar to that described in Section 2.3.1 using a TCM constituent code.

The employment of the interleaver, π_1 seen in Figure 3.1 and used in all of the schemes considered in Table 3.1 renders the information bits, more-or-less uncorrelated. This is a necessary requirement for the employment of EXIT charts, because they require the LLRs of the information bits to be Gaussian distributed. The interleaver used after the RSC encoder of Figure 3.1, namely π_2, randomises the coded bits before the puncturer.

3.2.2 Decoding Convergence Analysis with 2-D EXIT Charts

The decoder architecture of the SECTCM scheme shown in Figure 2.7 also applies to the proposed SECCC scheme. The EXIT charts of self-concatenated codes are typically similar to those of the family of parallel concatenated codes [13, 136, 137], where an open EXIT tunnel exists, if the EXIT curve does not intersect with the line connecting the point ($I_A = 0$, $I_E = 0$) to the point ($I_A = 1$, $I_E = 1$) in the EXIT chart. In Figures 2.8 and 2.9 of Section 2.3 EXIT charts were successfully used to compare the performance of non-binary SECCC schemes. This chapter uses the same method by finding the threshold E_b/N_0 point by calculating the EXIT curve of the identical decoder components and then plotting them together in the EXIT chart, as shown in Figures 3.2 and 3.3 of the Appendix of this chapter. The E_b/N_0 value, where the two EXIT curves touch each other is termed as the threshold E_b/N_0 point denoted by Λ, which is the point where the 'turbo-cliff' [13] region starts and beyond which the EXIT tunnel becomes 'just' open, as shown in Figures 3.4 and 3.5. If uncorrelated extrinsic information is available, then all of the symbol-by-symbol decoding trajectories will reach the $(I_A, I_E) = (1, 1)$ point [117] for E_b/N_0 values higher than Λ. The various coding schemes considered in this chapter are characterised in Table 3.1. They are identified by the code rate (R_1), puncturing rate (R_2), the overall code rate (R), code memory ν and bandwidth efficiency η, expressed in bit/s/Hz. Furthermore, I denotes the number of inner self-concatenated iterations. In all the codes considered in Table 3.1 the thresholds are calculated for $I = 40$ iterations and for Gray Mapping (GM) schemes. Finally, the channel capacity limit ω is also expressed in dBs [11], as tabulated in Table 3.1. For $R_1 = 1/2$ and $\nu = 2$, the generator polynomial $G = (7, 5)_8$ is used, whereas for $\nu = 3$, $G = (13, 15)_8$ is employed. For $R_1 = 1/3$ and $\nu = 3$, $G = (13, 15, 17)_8$ is used, where the first number in the generator polynomial represents the feedback polynomial.

Again, the EXIT charts recorded for the binary SECCC schemes of Table 3.1 are shown in Appendix A. The GM-based RSC-coded SECCC systems having rates of $R_1 = 1/2$ and $R_2 = 3/4$ have been plotted in Figures 3.4 and 3.5. The two EXIT curves represent the two hypothetical decoder components of the SECCC scheme, while the stair-case-shaped trajectories correspond to the Monte-Carlo simulation based decoding trajectories, when iterating between them. Since these are identical components, we only have to compute the EXIT curve of one component and the other is its mirror image with respect to the diagonal line. The EXIT curves of the hypothetical decoder components are plotted within the same EXIT chart together with their corresponding decoding trajectory for the sake of visualizing the transfer of extrinsic information between the decoders. The EXIT curves of the proposed scheme accurately match the decoding trajectories computed from the bit-by-bit simulations which was not the case for the symbol-based EXIT charts of Figure 2.9 recorded for the TCM constituent codes.

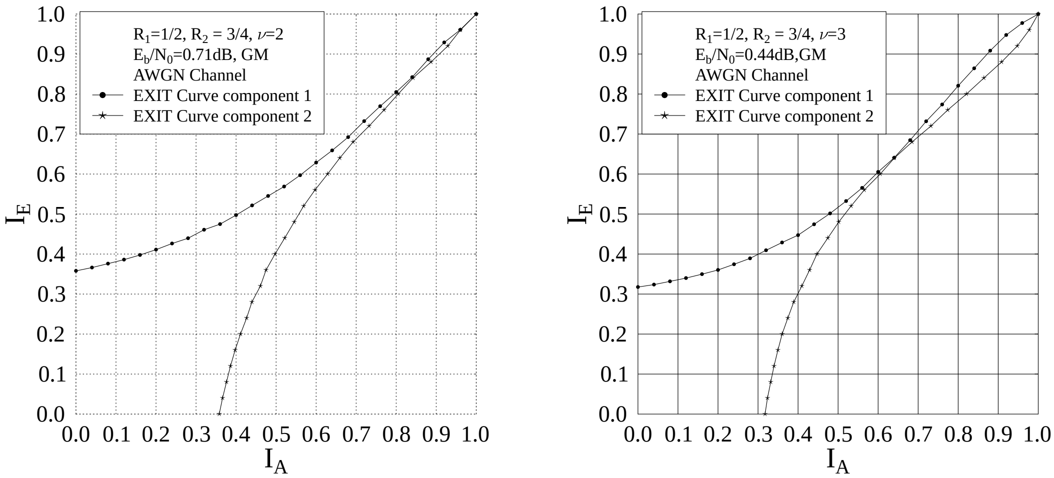

(a) $\nu = 2$ (b) $\nu = 3$

Figure 3.2: Threshold calculation of GM-based RSC-coded SECCC systems for $R_1 = 1/2$ and $R_2 = 3/4$ outlined in Table 3.1 for the case of AWGN channel.

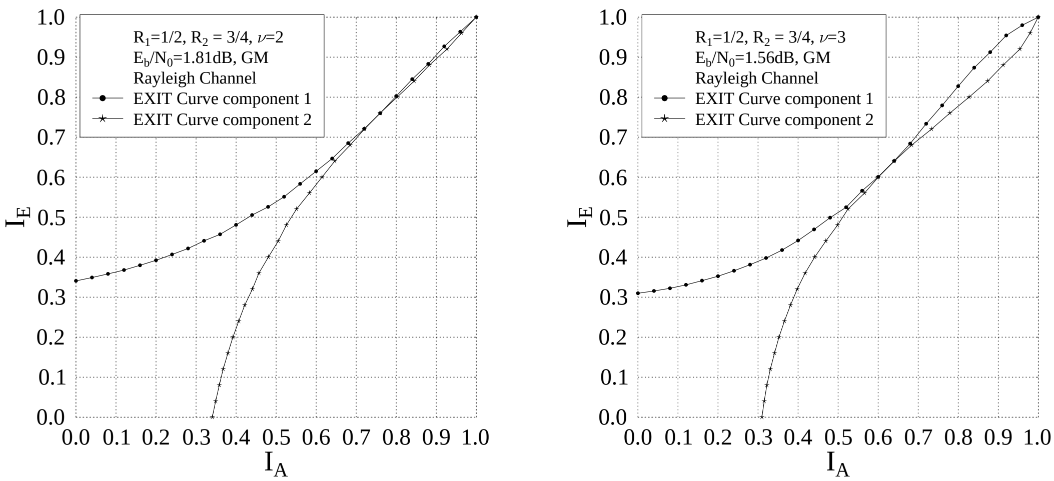

(a) $\nu = 2$ (b) $\nu = 3$

Figure 3.3: Threshold calculation of GM-based RSC-coded SECCC systems for $R_1 = 1/2$ and $R_2 = 3/4$ outlined in Table 3.1 for the case of Rayleigh fading channel.

The EXIT curves and two randomly choosen decoding trajectories were recorded for the specific binary SECCC scheme operating closest to the AWGN and Rayleigh channel's capacity in Fig. 3.4 and 3.5, respectively. These were recorded by using 10 transmission frames, each consisting of 24×10^3 information bits for calculating the EXIT curve and 10 frames each consisting of 120×10^3 information bits for calculating the decoding trajectories.

SECCC Gray Mapping	ν	η (bit/s/Hz)	AWGN Channel E_b/N_0 (dB)		Rayleigh Channel E_b/N_0 (dB)	
			Λ	ω	Λ	ω
R_1=1/2, R_2=3/4, R=1/3	2 3	0.67	0.71 0.44	-0.49	1.81 1.56	0.54
R_1=1/2, R_2=1/2, R=1/2	2 3	1	1.45 1.2	0.19	3.4 **3.2**	1.83
R_1=1/2, R_2=1/3, R=3/4	2 3	1.5	3.44 3.24	1.65	8.54 **8.09**	4.98
R_1=1/3, R_2=2/3, R=1/4	3	0.5	0.17	-0.86	0.96	-0.09
R_1=1/3, R_2=1/3, R=1/2	3	1	1.28	0.19	**3.3**	1.83
R_1=1/3, R_2=1/4, R=2/3	3	1.33	2.43	1.06	5.95	3.65

Table 3.1: Various SECCC schemes and their successful decoding thresholds.

The near-capacity SECCC schemes summarised in Table 3.1 are capable of operating within about 1 dB of the AWGN channel's capacity. For the scheme employing $\nu = 3$, $R_1 = 1/2$ and $R_2 = 3/4$, the E_b/N_0 distance between the capacity and the threshold E_b/N_0 point is 0.93 dB and 1.02 dB in case of AWGN and Rayleigh fading channels, respectively. For a bandwidth efficiency of 0.67 bit/s/Hz, the capacity of the $\nu = 3$, $R_1 = 1/2$ and $R_2 = 3/4$ scheme [11] is -0.49 dB and 0.54 dB for the QPSK-based discrete-input AWGN and Rayleigh fading channels, respectively. Another scheme, which performs close to capacity is that employing $\nu = 3$, $R_1 = 1/3$ and $R_2 = 2/3$, as shown in Table 3.1. The E_b/N_0 difference for this scheme for AWGN and Rayleigh fading channels' capacity of -0.86 dB and -0.09 dB, as measured from their respective threshold points is 1.03 dB and 1.05 dB.

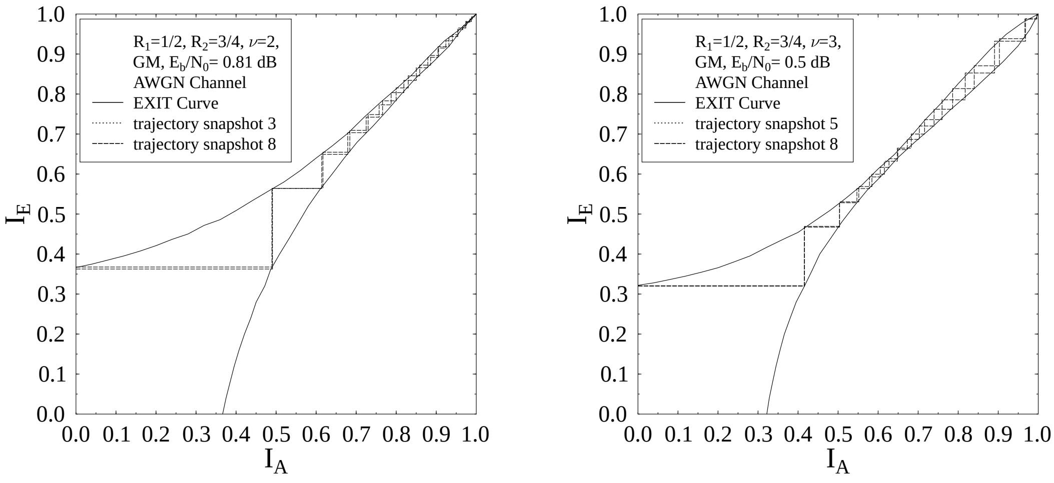

(a) $\nu = 2$ (b) $\nu = 3$

Figure 3.4: EXIT chart and two 'snap-shot' decoding trajectories for R_1=1/2 and R_2=3/4, QPSK-assisted SECCC, $\eta = 0.67$ bit/s/Hz, for transmission over an AWGN channel.

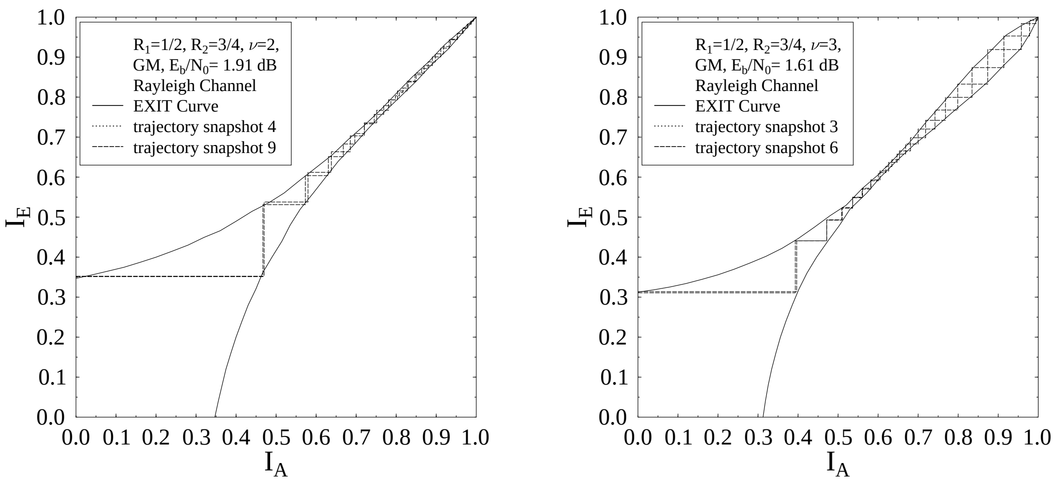

(a) $\nu = 2$ (b) $\nu = 3$

Figure 3.5: EXIT chart and two 'snap-shot' decoding trajectories for R_1=1/2 and R_2=3/4, QPSK-assisted SECCC, $\eta = 0.67$ bit/s/Hz, for transmission over a Rayleigh fading channel.

3.2.3 Results and Discussions

The EXIT charts discussed in Section 3.2.2 were used to find the SECCC schemes for $\nu = \{2, 3\}$, when communicating over AWGN and uncorrelated Rayleigh fading channels. The convergence threshold predicted by the EXIT chart analysis detailed in Section 3.2.2, closely matches the actual convergence threshold observed in the BER curve given by the specified E_b/N_0 value. This convergence threshold is defined as the E_b/N_0 values where there is a sudden drop of the BER after a certain number of decoding iterations, as confirmed in Figure 3.6 by the BER versus E_b/N_0 performance of $R_1 = 1/2$, $R_2 = 3/4$ and $\nu = 2$ scheme under Rayleigh fading channel conditions. Hence it becomes possible to attain an infinitesimally low BER beyond the convergence threshold, provided that the block length is sufficiently long and the number of decoding iterations is sufficiently high.

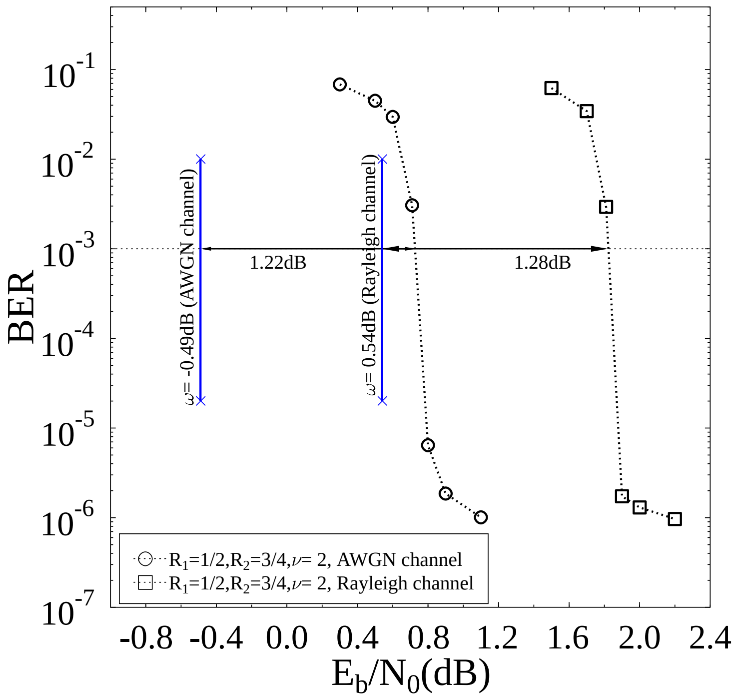

Figure 3.6: The BER versus E_b/N_0 performance of Gray mapped QPSK-assisted SECCC schemes, using $R_1 = 1/2$, R_2=3/4, and $I = 40$ decoding iterations for $\nu = 2$, when operating over AWGN and Rayleigh fading channels.

As we can see by studying Table 3.1 and Figure 3.6 the actual BER convergence threshold is exactly the same as the convergence threshold predicted by the EXIT charts for the case of $\nu = 2$, $R_1 = 1/2$ and $R_2 = 3/4$. The corresponding successful decoding threshold is at 0.71 dB and 1.81 dB in case of AWGN and Rayleigh fading channels, respectively. Hence, the binary EXIT chart is useful for finding the best SECCC schemes for having a decoding convergence at the lowest possible E_b/N_0 value. The BER performance of the SECCC scheme shown in Figure 3.6 and employing $\nu = 2$, $R_1 = 1/2$ and $R_2 = 3/4$ has a distance from capacity, which is 1.22 dB and 1.28 dB at a BER of 10^{-3} in case of AWGN and Rayleigh fading channels, respectively.

3.3 Binary SECCC-ID Using Soft Decision Demapping[3]

It was suggested in [153] that a symbol-based scheme always has a lower convergence threshold compared to an equivalent binary scheme. In order to recover the information loss due to employing binary rather than non-binary schemes, we will demonstrate that soft decision feedback is required between the SISO MAP decoder and the soft demapper [154].

An attractive approach to design Repeat-Accumulate (RA) codes using iterative detection and decoding using EXIT charts has been proposed in [151]. The RA code is a serial-concatenated coding scheme where a repetition code is employed as the outer code and a bit-by-bit accumulator is employed as the inner encoder. By contrast the SECCC scheme can be viewed as a parallel-concatenated coding scheme employing an odd-even separated turbo interleaver as discovered in [4]. Hence, the SECCC scheme is not the same as the RA code. Another major difference is that the RA codes in [151] are irregular and hence they tend to be more complex than our SECCC-ID scheme. Similar to Bit-Interleaved Coded Modulation using the Iterative Decoding (BICM-ID) concept [155], we also employ iterations between the SECCC and the Soft Demapper in our SECCC-ID scheme. However, instead of using N parallel bit interleavers as in BICM-ID, we only have one bit interleaver in our system. Note that the optimized mapping of [156] and the multidimensional mapping of [157] can also be employed for the SECCC-ID scheme. Furthermore, SECCC-ID codes have not been characterised in the literature in terms of their decoding convergence.

Two-stage iterative receivers can be analysed with 2-D EXIT charts, while their three-stage counterparts require 3-D EXIT charts, which were proposed in [121] and further studied in [122, 158, 159]. We will show that 3-D EXIT charts provide a unique insight into the design of near-capacity SECCC-ID codes. To elaborate a little further, in conventional 2-D EXIT charts a new EXIT curve is generated for each new channel SNR or channel model, while our 3-D EXIT chart representation of

[3]This section is based on [3]

the SECCC component is channel-independent and hence has to be computed only once, regardless of the channel SNR. Hence we characterise each SECCC component code using two 3-D EXIT charts, which can then be used for designing an iterative decoding aided system employing any demapper type. Extrinsic information is exchanged across three concatenated decoder stages and the achievable decoding convergence is studied using 3-D EXIT charts. Finally, it is demonstrated that the best SECCC schemes perform within about 1 dB of both the AWGN and Rayleigh fading channels' capacity.

3.3.1 Binary SECCC-ID System Model

The proposed binary SECCC-ID system model employing SP based QPSK modulation is shown in Figure 3.7. The notations $P(.)$ and $L(.)$ in Figure 3.7 denote the logarithmic-domain symbol probabilities and the LLR of the bit probabilities, respectively. The rest of the notations used in Figure 3.7 have been defined in Section 3.2.1. The binary SECCC scheme depicted in Figure 3.1 does not have the ability of exchanging soft information with the demapper.

The QPSK symbol x is then transmitted over the communication channel. At the receiver side the received symbol is given by Equation 3.2 as: $y = hx + n$. This signal is then used by the demapper for calculating the conditional PDF of receiving y, when x^m was transmitted as in Equation 3.3:

$$P(y|x = x^{(m)}) = \frac{1}{\pi N_0} \exp\left(-\frac{\left|y - hx^{(m)}\right|^2}{N_0}\right).$$

These PDFs are then passed through the Symbol to 'Bit Probability Converter' of Figure 3.7, which performs the following three steps:

1. Calculating the *a posteriori* probability of the transmitted signal
$$P^o(x|y) = \frac{P(y|x)P(x)}{P(y)}, \tag{3.4}$$
where $P(y)$ is a constant term and can be ignored. For a symbol based system the probability of the transmitted signal $P(x)$ can be assumed to be a constant value. However, in a bit based system iterative decoding exchanging extrinsic information between the demodulator and decoder can be invoked based on $P(x)$.

2. From Bayes' rule and assuming that bits c_1 and c_0 are independent, we have
$$P(x) = P(c_1c_0) = P(c_1|c_0)P(c_0) = P(c_1)P(c_0). \tag{3.5}$$

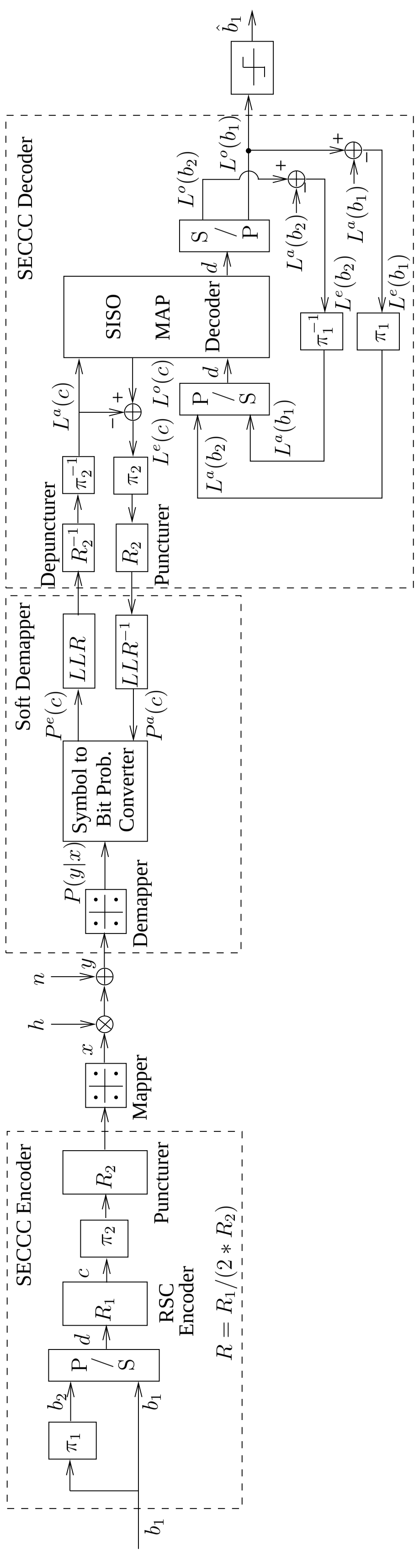

Figure 3.7: Binary SECCC-ID system, which is different from the SECCC scheme of Figure 3.1, since the Soft Demapper in this case exchanges extrinsic information with the SISO MAP decoder.

Therefore,

$$P^o(x|y) \approx P(y|x)P(c_1)P(c_0). \tag{3.6}$$

3. The symbol probabilities are then converted to bit probabilities. The *a posteriori* probability of the coded bit $c_i = b$ is given by

$$P^o(c_i = b|y) = \sum_{x \in \chi(i,b)} \left(P(y|x) \prod^{\text{all}_j} P(c_j) \right), \tag{3.7}$$

where $\chi(i,b) = \{\mu(c_1c_0), \forall c_1, c_0 \in \{0,1\}|c_i = b\}$, which contains two phasor combinations of the QPSK modulated signal x. The bit index is specified by $i \in \{0,1\}$ and the value of the bit by $b \in \{0,1\}$. For higher order modulations the bits required are $m = \log_2(M)$, where M is the number of constellation points. The extrinsic probability of c_i is then calculated as

$$P^e(c_i = b|y) = \sum_{x \in \chi(i,b)} \left(P(y|x) \prod_{j \neq i}^{\text{all } j} P(c_j) \right). \tag{3.8}$$

The extrinsic bit probabilities are then converted to the corresponding bit-based LLRs by the block denoted as *LLR* in Figure 3.7, which are then passed through a soft depuncturer inserting zero LLRs at the punctured bit positions. The LLRs are then deinterleaved and fed to the SISO MAP decoder [102]. The decoder of Figure 3.7 is a self-concatenated decoder. It first calculates the extrinsic LLRs of the information bits, namely $L^e(b_1)$ and $L^e(b_2)$. Then they are appropriately interleaved to yield the *a priori* LLRs of the information bits, namely $L^a(b_1)$ and $L^a(b_2)$, as shown in Figure 3.7. Self-concatenated decoding proceeds, until a fixed number of iterations is reached. The extrinsic LLRs of the codeword denoted by $L^e(c)$ at the output of the SISO decoder are fed back to the Soft Demapper of Figure 3.7, which are interleaved by π_2 and then punctured according to R_2. These are then converted to the *a priori* bit probabilities $P_b^a(c)$ by the block denoted as LLR^{-1} in Figure 3.7, to be fed to the APP demapper, which first converts them to symbol probabilities and then provides the improved extrinsic LLR $L^e(c)$ of the codeword at its output, thus completing the outer iteration between the SISO decoder and Soft Demapper. Apart from having inner self-concatenated iterations in the outer SECCC decoder, a fixed number of outer iterations exchange extrinsic information between the decoder and soft-demapper to yield the decoded bits $\hat{b}_1$.

3.3.2 Decoding Convergence Analysis with 3-D EXIT Charts

EXIT charts constitute powerful tools designed for analysing the convergence behaviour of concatenated codes without time-consuming bit-by-bit simulation of the actual system. They analyse the input/output mutual information characteristics of a SISO decoder by modelling the *a priori* LLRs either by an AWGN process or by its experimentally determined histogram and then computing the corresponding mutual information between the extrinsic LLRs as well as the corresponding bit-decisions. More explicitly, the employment of EXIT charts assumes having a sufficiently high interleaver length, so that the extrinsic LLRs can be rendered Gaussian distributed. The SNR value, where the turbo-cliff [13] in the BER curve of a concatenated code appears can be successfully predicted with the aid of EXIT charts.

The decoding model of the SECCC-ID scheme is portrayed in Figure 3.8. It corresponds to either one of the hypothetical component decoders. Random variables (r.v.s.) are denoted with capital letters and their corresponding realizations with lower case letters. Sequences of random variables are indicated by underlining them. The information bit sequence is $\underline{B}$, which is interleaved and then parallel to serial converted. The resultant bits are denoted by $\underline{D}$, that are then encoded to yield the coded bit sequence $\underline{C}$ of Figure 3.8, and transmitted over the communication channel often termed as the *a priori* channel 1 [160], which gives the *a priori* probabilities of the codeword $\underline{A}(C)$ as its output. The received symbol sequence is given by $\underline{Y}$, which is then fed to the SISO SECCC decoder. By contrast, the *a priori* channel 2 of Figure 3.8 models the *a priori* probabilities $\underline{A}(D)$ constituted by the combination of the information bits and their interleaved version referred to as the hypothetical dataword $\underline{D}$. The SECCC SISO decoder of Figure 3.8 then computes the *extrinsic* bit probabilities revelant for both the codeword $\underline{E}(C)$ and the dataword $\underline{E}(D)$.

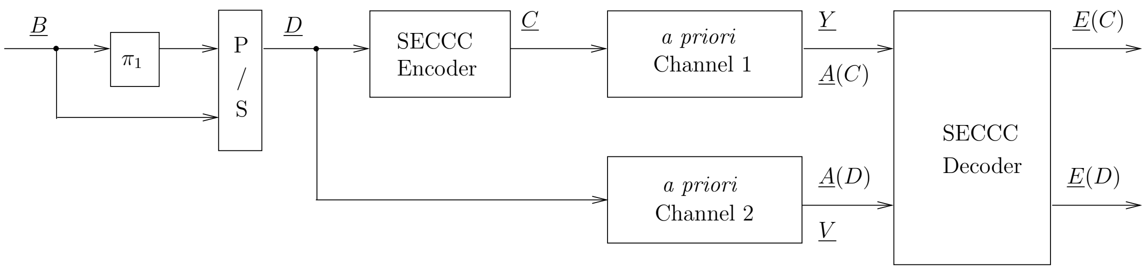

Figure 3.8: Decoding model for an SECCC-ID scheme [1]. Note that the architecture of the SECTCM decoder shown in Figure 2.7 represents both the hypothetical component decoders. By contrast, the decoding model presented here outlines only one of the hypothetical component decoders.

EXIT charts [117] visualize the input/output characteristics of the constituent SECCC decoder in terms of the average mutual information transfer. In the context of the SECCC decoder of Figure 3.8, the EXIT chart visualises the following mutual information exchange:

1. average mutual information of $\underline{D}$ and $\underline{A}(D)$:

$$I_A(D) = \frac{1}{N_D} \sum_{k=1}^{N_D} I[D_k; A(D_k)] \ ; \tag{3.9}$$

2. average mutual information of $\underline{C}$ and $\underline{A}(C)$:

$$I_A(C) = \frac{1}{N_C} \sum_{k=1}^{N_C} I[C_k; A(C_k)] \ ; \tag{3.10}$$

3. average mutual information of $\underline{D}$ and $\underline{E}(D)$:

$$I_E(D) = \frac{1}{N_D} \sum_{k=1}^{N_D} I[D_k; E(D_k)] \ ; \tag{3.11}$$

4. average mutual information of $\underline{C}$ and $\underline{E}(C)$:

$$I_E(C) = \frac{1}{N_C} \sum_{k=1}^{N_C} I[C_k; E(C_k)] \ , \tag{3.12}$$

where the number of symbols in the sequences $\underline{D}$ and $\underline{C}$ are given by N_D and N_C, respectively. As depicted in Figure 3.9, component 1 and 2 of SECCC decoders are associated with four mutual information transfers according to Eqs. (3.9)–(3.12). Hence two three-dimensional EXIT charts [121, 159] are required for visualising the mutual information transfer between the hypothetical SECCC component decoders (namely for portraying each of the two outputs as a function of two inputs) and the EXIT curve of the combined SECCC decoder and the soft demapper (a two input, single output block).

Provided that the binary MAP [13] decoder discussed in Chapter 5 of [14] is used, the average *extrinsic* mutual information of $\underline{D}$ and $\underline{A}(D)$ may be computed from Eqs. (10) and (11) of [137] as follows:

$$\begin{aligned} I_E(D) &= \frac{1}{N_D} \sum_{k=1}^{N_D} H(D_k) - H(D_k|E(D_k)) \\ &= \log_2(\mathcal{M}_D) - \frac{1}{N_D} \sum_{k=1}^{N_D} \mathrm{E}\left[\sum_{m=1}^{\mathcal{M}_D} E(D_k^{(m)}) \log_2(E(D_k^{(m)})) \right] \ , \end{aligned} \tag{3.13}$$

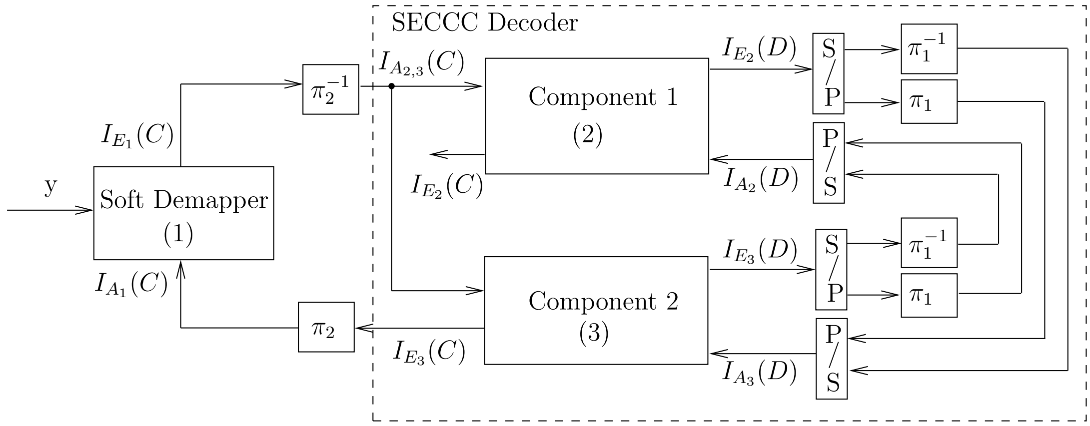

Figure 3.9: Mutual information exchange between the three components of an SECCC-ID scheme [161].

where $E(D_k^{(m)}) = P(D_k^{(m)}|\underline{Y}, \underline{V}_{[k]})$ is the extrinsic probability of the hypothesized transmitted symbol $D_k^{(m)}$, for $m \in \{1, \ldots, \mathcal{M}_D\}$, which is provided by the MAP decoder. Here $\mathcal{M}_D = 2^{L_D}$ and L_D is the number of information bits[4] in the SECCC input symbol of Fig. 3.8. Notice that the expectation in Eq. (3.13) may be removed, when N_D is sufficiently large, yielding:

$$I_E(D) = \log_2(\mathcal{M}_D) - \frac{1}{N_D} \sum_{k=1}^{N_D} \sum_{m=1}^{\mathcal{M}_D} E(D_k^{(m)}) \log_2[E(D_k^{(m)})] \ . \tag{3.14}$$

Similarly, we have [137]:

$$I_E(C) = \log_2(\mathcal{M}_C) - \frac{1}{N_C} \sum_{k=1}^{N_C} \sum_{m=1}^{\mathcal{M}_C} E(C_k^{(m)}) \log_2[E(C_k^{(m)})] \ , \tag{3.15}$$

where $E(C_k^{(m)}) = P(C_k^{(m)}|\underline{Y}_{[k]}, \underline{V})$ is the extrinsic probability of the hypothesized transmitted symbol $C_k^{(m)}$, for $m \in \{1, \ldots, \mathcal{M}_C\}$, generated by the MAP decoder and N_C is assumed to be sufficiently large. Here, $\mathcal{M}_C = 2^{L_C}$, where L_C is the number of coded bits in the SECCC symbol.

The average *a priori* mutual information of both $\underline{D}$ and $\underline{C}$ may be modelled using the following assumptions [137, 162]:

1. the LLRs of the bits are Gaussian distributed: the LLR of an information or parity bit s, which can be either from the sequence $\underline{D}$ or $\underline{C}$, is given by [117]:

$$z = h_A s + n_A \ , \tag{3.16}$$

   where the variance of the AWGN n_A is σ_A^2 per dimension and the equivalent 'fading factor' is given by $h_A = \sigma_A^2/2$ [117];

[4]For binary EXIT chart, $L_D = 1$

2. the bits in a symbol are assumed to be independent of each other and uniformly distributed: the average *a priori* mutual information of a symbol sequence $\underline{D}$ (or $\underline{C}$), where each symbol D_k (or C_k) consists of L_D (or L_C) bits, is L_D (or L_C) times the average *a priori* mutual information of a bit in the symbol.

The average *a priori* mutual information of a certain bit denoted as $s \in \{s^{(1)} = +1, s^{(2)} = -1\}$ and its LLR z may be expressed as:

$$I(S;Z) = 1 - \frac{1}{2}\sum_{m=1}^{2} \mathrm{E}\left[\log_2 \sum_{n=1}^{2} \exp(\Psi_{m,n}^{A}) \middle| \, s^{(m)}\right] , \tag{3.17}$$

where we have $\exp(\Psi_{m,n}^{A}) = p(z|s^{(n)})/p(z|s^{(m)})$ and the conditional Gaussian PDF is given by:

$$p(z|s) = \frac{1}{\sqrt{2\pi\sigma_A^2}} \exp\left(\frac{(z - h_A s)^2}{2\sigma_A^2}\right) , \tag{3.18}$$

while the exponent is given by:

$$\Psi_{m,n}^{A} = \frac{-\left|(\sigma_A^2/2)(s^{(m)} - s^{(n)}) + n_A\right|^2 + |n_A|^2}{2\sigma_A^2} . \tag{3.19}$$

Note that another interpretation of Eq. (3.17) was given in [Eq. (14)] [117]. We have a function $I_A = I(S;Z) = J(\sigma_A)$, with $J(\sigma_A)$ being monotonically increasing and therefore invertible. Hence, at a given I_A value we may find the corresponding σ_A value from $J^{-1}(I_A)$. Finally, one may compute the corresponding LLR value z from Eq. (3.16). The *a priori* mutual information of an L_D-bit symbol D_k is given by:

$$I(D_k; Z_{(k)}) = \sum_{i=1}^{L_D} I[s_{(k,i)}^{D}; z_{(k,i)}^{D}] , \tag{3.20}$$

where $z_{(k)}^{D} = \{z_{(k,1)}^{D}, \ldots, z_{(k,L_D)}^{D}\}$ is the LLR sequence, which is related to the L_D bits of D_k and $z_{(k,l)}^{D}$ is the LLR of $s_{(k,l)}^{D}$, which is the lth bit in the kth symbol D_k.

The various coding schemes considered in this section are characterised in Table 3.2. They are identified by the code rate (R_1), puncturing rate (R_2), the overall code rate (R), code memory ν and bandwidth efficiency η, expressed in bit/s/Hz similar to presented in Table 3.1. Furthermore, O denotes the total number of iterations of SECCC-ID scheme and I denotes the total number of iterations of SECCC scheme. In all the codes considered in Table 3.2 the thresholds are calculated for $O = 40$ and $I = 40$ for the SECCC and SECCC-ID schemes, respectively. In the case of SECCC the two identical code components iterate 20 times exchanging extrinsic information with each other, while in the case of SECCC-ID the two identical code components iterate 20 times with the demapper. The EXIT charts recorded

SECCC/ SECCC-ID Schemes	Mapping	ν	η (bit/s /Hz)	AWGN Channel E_b/N_0 (dB)		Rayleigh Channel E_b/N_0 (dB)	
				Λ	ω	Λ	ω
R_1=1/2,	GM	2	0.67	0.71	-0.49	1.81	0.54
R_2=3/4,	SP			**0.25**		**1.35**	
R=1/3	GM	3		0.44		1.56	
	SP			0.5		1.55	
R_1=1/2,	GM	2	1	1.45	0.19	3.4	1.83
R_2=1/2,	SP			**1.0**		3.4	
R=1/2	GM	3		1.2		**3.2**	
	SP			1.25		3.3	
R_1=1/2,	GM	2	1.5	3.44	1.65	8.54	4.98
R_2=1/3,	SP			**3.2**		8.4	
R=3/4	GM	3		3.24		**8.09**	
	SP			3.2		8.1	
R_1=1/3,	GM	3	0.5	0.17	-0.86	0.96	-0.09
R_2=2/3,	SP			**0.07**		**0.82**	
R=1/4							
R_1=1/3,	GM	3	1	1.28	0.19	**3.3**	1.83
R_2=1/3,	SP			**1.23**		3.4	
R=1/2							
R_1=1/3,	GM	3	1.33	2.43	1.06	5.95	3.65
R_2=1/4,	SP			**2.37**		**5.7**	
R=2/3							

Table 3.2: Various SECCC and SECCC-ID schemes and their thresholds.

for the binary SECCC-ID schemes of Table 3.2 are shown in Figures 3.10, 3.11, 3.12 and 3.13.

The mutual information exchange between the components of an SECCC-ID scheme is portrayed in Figure 3.9, which shows the SECCC-ID decoder of Figure 3.7 as two hypothetical component decoders. The hypothetical component 2 of the SECCC decoder of Figure 3.9 receives inputs from and provides outputs for both the soft demapper and the hypothetical component 1 SECCC decoder of Figure 3.9. Hence we have two EXIT surfaces in Figure 3.10, the first one corresponding to the component 2 decoder's average mutual information $I_{E_3}(C)$ provided for the soft demapper, while the second one corresponding to $I_{E_3}(D)$ supplied for the component

1 SECCC decoder, as shown in Figure 3.9. The same procedure can be used to calculate the two EXIT surfaces for the average mutual information of the component 1 decoder. One of the EXIT surfaces corresponds to the mutual information $I_{E_2}(C)$ provided for the soft demapper (not used) in Figure 3.9. Similarly, the component 1 SECCC decoder has the other EXIT surface characterising its average mutual information $I_{E_2}(D)$ forwarded to the hypothetical component 2 SECCC decoder of Figure 3.9. By contrast, the soft demapper has a single EXIT surface characterising its average mutual information $I_{E_1}(C)$ forwarded to component 1 and 2 of the SECCC decoder of Figure 3.9.

The scheme using $R_1 = 1/2$, $R_2 = 3/4$, $\nu = 2$ and employing the SP based Soft Demapper is shown in Figures 3.10 and 3.11.

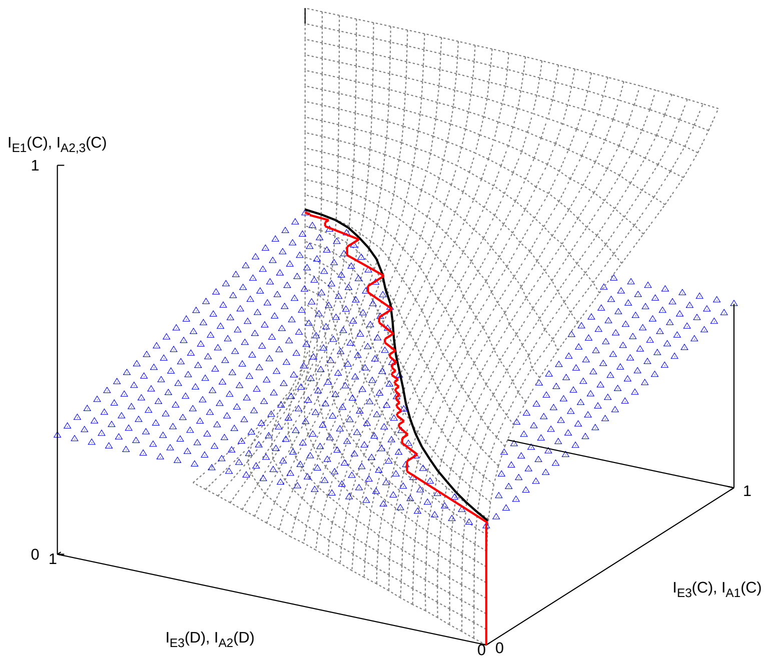

Figure 3.10: 3-D EXIT surfaces of SECCC decoder (dotted) and Soft Demapper (triangles) along with a 'snap-shot' decoding trajectory for R_1=1/2 and R_2=3/4, QPSK-assisted SECCC-ID, $\nu = 2$, $\eta = 0.67$ bit/s/Hz at $E_b/N_0 = 1.55$ dB using SP mapping, for transmission over an uncorrelated non-dispersive Rayleigh fading channel.

Specifically, the EXIT surface marked with triangles in Figure 3.10 was computed based on the Soft Demapper's output $I_{E_1}(C)$ at the given $I_{E_3}(D)$ value of the component 2 SECCC Decoder and $I_{A_1}(C)$ of the Soft Demapper's abscissa values. By contrast, the steeply rising EXIT surface drawn using dotted lines in Figure 3.10 was computed based on the component 2 decoder's outputs $I_{E_3}(C)$ and $I_{E_3}(D)$ at the given $I_{A_{2,3}}(C)$ value. Note that the Soft Demapper characteristic is independent of $I_{E_3}(D)$ gleaned from the output of the component 2 decoder, as seen in

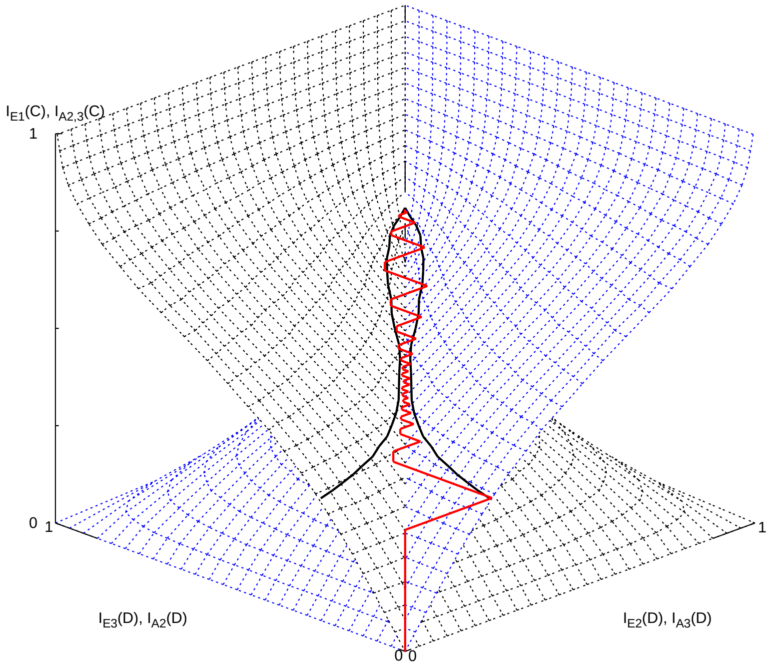

Figure 3.11: 3-D EXIT surfaces of the two identical hypothetical SECCC decoder components and a 'snap-shot' decoding trajectory for R_1=1/2 and R_2=3/4, QPSK-assisted SECCC-ID, $\nu = 2$, $\eta = 0.67$ bit/s/Hz at $E_b/N_0 = 1.55$ dB using SP mapping for transmission over an uncorrelated non-dispersive Rayleigh fading channel.

Figure 3.9. As we can see from Figure 3.10, the decoding trajectory is computed at $E_b/N_0 = 1.55$ dB[5]. The Monte-Carlo simulation-based symbol-by-symbol decoding trajectory (solid line) relies on the average mutual information of the component 2 SECCC decoder's output, namely on $I_{E_3}(C)$, and it evolves within the space under the EXIT surface marked with triangles but above the EXIT surface drawn using dotted lines, which means that it matches the 3-D EXIT curves.

Similarly, the EXIT surface of Figure 3.11 spanning from the horizontal line $[I_{A_2}(D) = \{0 \rightarrow 1\}, I_{E_2}(D) = 0, I_{A_{2,3}}(C) = 0]$ to the horizontal line $[I_{A_2}(D) = \{0 \rightarrow 1\}, I_{E_2}(D) = 1, I_{A_{2,3}}(C) = 1]$, represents the first hypothetical SECCC decoder component. Since in case of SECCCs these are identical components, we only have to compute the EXIT surface of a single component and the other is its mirror image [1]. The EXIT surfaces of the two hypothetical decoder components are plotted within the same EXIT chart together with their corresponding decoding trajectory for the sake of visualizing the exchange of extrinsic information between the decoders. The EXIT surfaces of the proposed scheme match exactly the decoding

[5]Note that there is a small but still beneficial vertical step in the decoding trajectory (Figs. 3.10 and 3.11) after each iteration of the SECCC decoder and the Soft Demapper. This justifies the use of 3-D EXIT charts as compared to 2-D EXIT charts, where this gain cannot be observed.

trajectories computed from the bit-by-bit simulations.

The 3-D EXIT surfaces of the SECCC decoder and the two distinct decoding trajectories - one for SP (iterating solid line) and the other for Gray mapping (iterating bold solid line) based Soft Demapper - were recorded for the binary SECCC schemes operating closest to the Rayleigh channel's capacity, which are given in Figure 3.12.

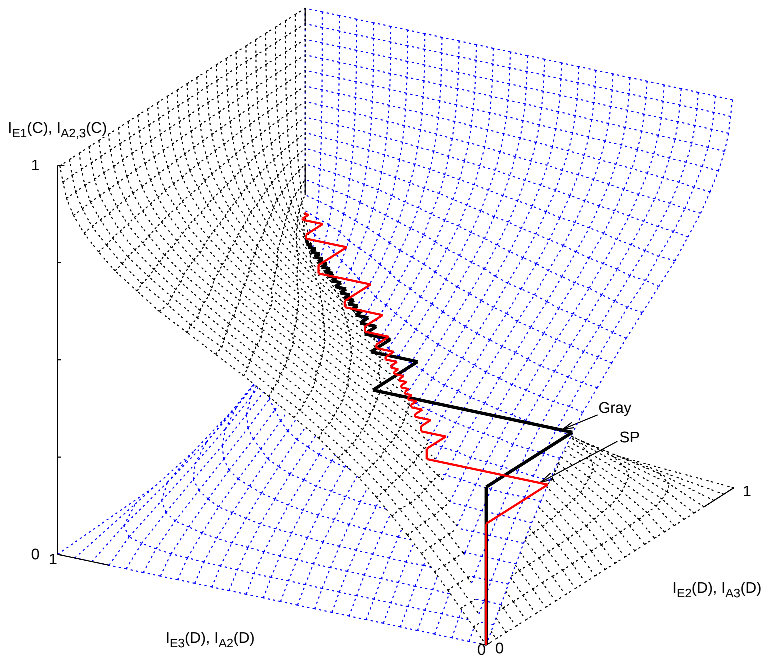

Figure 3.12: 3-D EXIT chart and two 'snap-shot' decoding trajectories for R_1=1/2 and R_2=3/4, QPSK-assisted SECCC-ID, $\nu = 2$, $\eta = 0.67$ bit/s/Hz at $E_b/N_0 = 1.55$ dB using SP mapping and at $E_b/N_0 = 1.9$ dB using Gray mapping, for transmission over an uncorrelated non-dispersive Rayleigh fading channel.

Each EXIT surface was calculated based on 10 transmission frames, each consisting of 24×10^3 information bits. Each Monte-Carlo-simulation based snapshot decoding trajectory was computed based on a block length of 120×10^3 information bits.

In Figure 3.12, the scheme using $R_1 = 1/2$, $R_2 = 3/4$, $\nu = 2$ and employing Gray mapping acquires an open EXIT tunnel at E_b/N_0=1.9 dB, when communicating over an uncorrelated Rayleigh fading channel. For this scheme the threshold Λ is at 1.81 dB as recorded in Table 3.2, which is 1.27 dB away from the Rayleigh channel's capacity.

The 2-D EXIT curves recorded for the case of Rayleigh fading channel are shown in Figure 3.13(a). These exemplify the method of finding thresholds for the Gray mapped SECCC-ID scheme using $\nu = 2$, $R_1 = 1/2$ and $R_2 = 3/4$. 2-D EXIT curves have been used for the case of Gray mapping because there is no mutual information exchange gain between the soft demapper and the decoder. Hence, the threshold can be calculated using 2-D EXIT charts for the case of Gray mapping[6]. We found that when employing the $\nu = 2$ RSC code, all SECCC schemes exhibited EXIT curves having similar trends to those in Figure 3.13(a), where the tunnel at the top-right corner becomes very narrow. Hence, a higher SNR was required for the decoding trajectory to pass through the tunnel. As a result, their performance tends to be farther away from the channel capacity. The threshold of E_b/N_0=1.81 dB is shown in Figure 3.13(a) and in Table 3.2, which is 1.27 dB away from the Rayleigh fading channel's capacity.

By contrast, to calculate the threshold of a given SP mapping based SECCC-ID scheme, we have to rely on 3-D EXIT charts to analyse the mutual information exchange gain achieved, while iterating between the soft demapper and the decoder. This is shown in Figure 3.10 and 3.11. The intersection of the surfaces in Figure 3.10 represents the points of convergence between the SNR-dependent soft demapper and the SNR-independent SECCC-ID decoder. At these intersection points we have shown a solid line. The corresponding $I_{E_2}(D)$ values associated with the curve of intersection of the surfaces in Figure 3.10 and its mirror image are projected onto the surfaces seen in Figure 3.11. Figure 3.11 also shows the Monte-Carlo-simulation based decoding trajectory matching these EXIT curves. These EXIT curves are projected onto $I_{E_1}(C) = 0$ for yielding Figure 3.13(b). The 2-D projection seen in Figure 3.13(b) for the Rayleigh fading channel has a threshold of 1.35 dB. Hence, an overall gain of 0.46 dB is attained compared to the Gray mapping performance seen in Figure 3.13(a).

3.3.3 Results and Discussions

The EXIT charts discussed in Section 3.3.2 were used to find near capacity SECCC-ID schemes for $\nu = \{2, 3\}$, when communicating over AWGN and uncorrelated non-dispersive Rayleigh fading channels.

The threshold predicted by the EXIT chart analysis detailed in Section 3.3.2 closely matches with the actual threshold observed in the BER curve given by the specified E_b/N_0 value, where there is a sudden drop of the BER after a certain number of decoding iterations, as shown in Figures 3.14 and 3.15. Hence it becomes possible

[6]Note that it is possible to simply use the 3-D EXIT chart of the SECCC-ID scheme when using the Gray mapper, without having to compute another 2-D EXIT curve for the SECCC scheme at a given SNR or channel model.

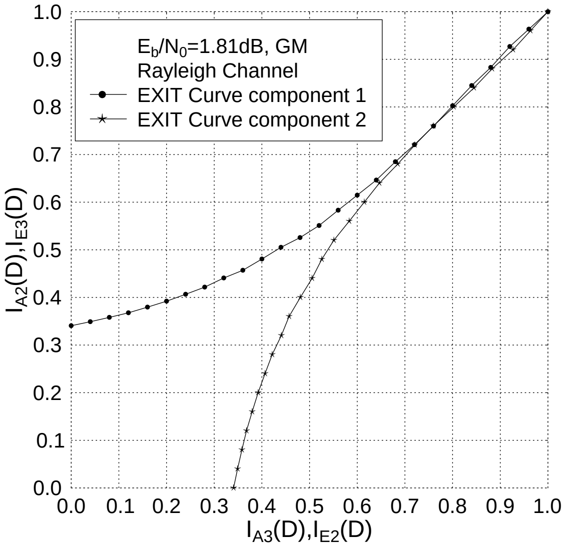

(a) Gray Mapping

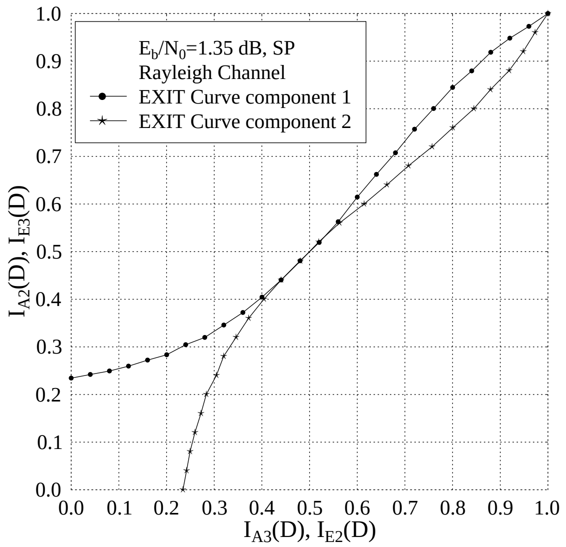

(b) 2D Projection of SP Mapping

Figure 3.13: EXIT curves of the R_1=1/2 and R_2=3/4, $\nu = 2$, SECCC-ID scheme to find the corresponding thresholds, operating over an uncorrelated non-dispersive Rayleigh fading channel.

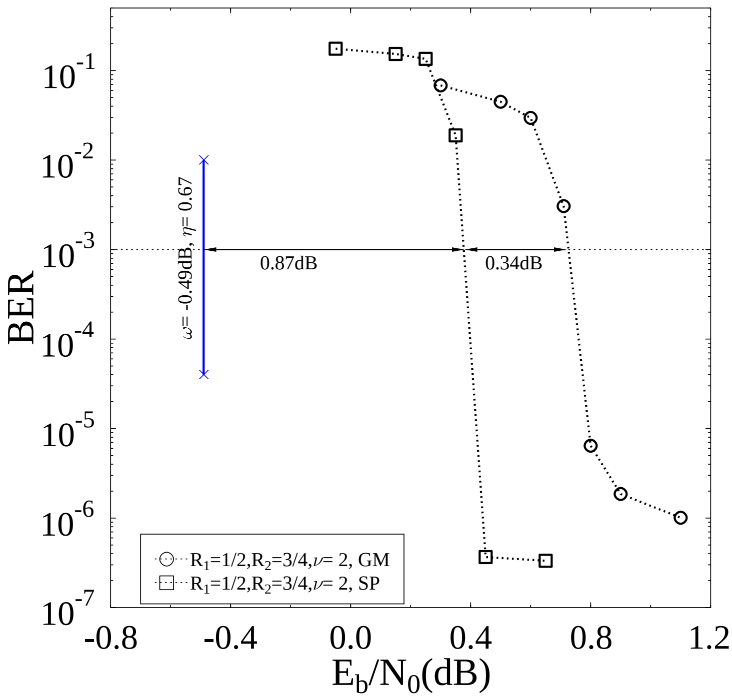

Figure 3.14: The BER versus E_b/N_0 performance of Gray and SP mapped QPSK-assisted SECCC-ID schemes, $R_1 = 1/2$, R_2=3/4, and $I = 40$ decoding iterations for $\nu = 2$, operating over an AWGN channel.

to attain an infinitesimally low BER beyond the threshold, provided that the block length is sufficiently long and the number of decoding iterations is sufficiently high.

Again, the BER versus E_b/N_0 performance curves of the best performing QPSK-assisted SECCC-ID schemes having $R_1 = 1/2$ and $R_2 = 3/4$, recorded from our bit-by-bit simulations are shown in Figures 3.14 and 3.15. We considered an information block length of 120×10^3 bits per frame, for 10^3 frames and the number of decoding iterations (I) are fixed to 40. Figures 3.14 and 3.15 show the E_b/N_0 difference between the channel capacity and the system operating at a BER of 10^{-3} marked by dotted lines, which was recorded for the SECCC-ID scheme having a code memory of $\nu = 2$. The SP mapping scheme operates 0.93 dB away from Rayleigh fading channel capacity, which is 0.35 dB better compared to the Gray mapping scheme at a BER of 10^{-3}, as shown in Figure 3.15. For the scheme employing $\nu = 2$, $R_1 = 1/2$ and $R_2 = 3/4$, the distance from capacity is 0.87 dB when communicating over AWGN channel, which is 0.34 dB better compared to the Gray mapping scheme at a BER of 10^{-3}, as shown in Figure 3.14. Another scheme, which performs close to capacity, employs $\nu = 3$, $R_1 = 1/3$ and $R_2 = 2/3$, as shown in Table 3.2. This scheme is

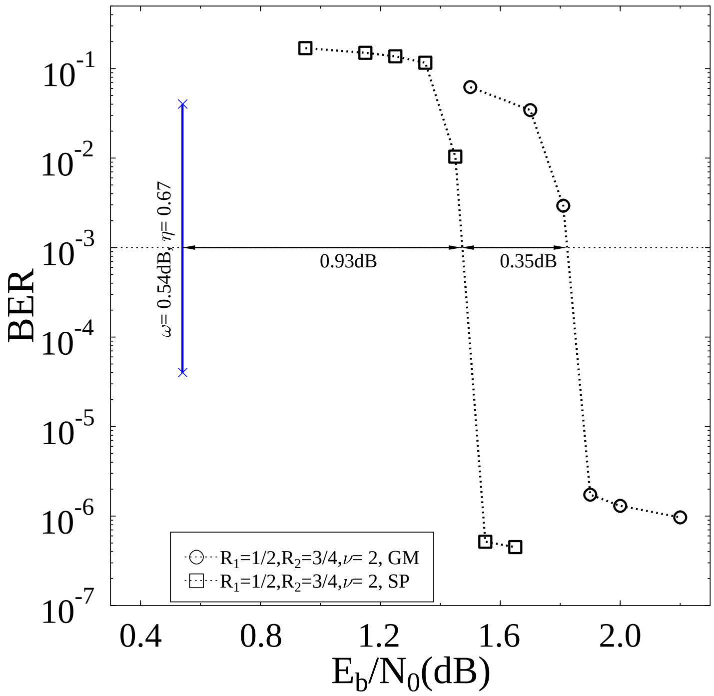

Figure 3.15: The BER versus E_b/N_0 performance of Gray and SP mapped QPSK-assisted SECCC-ID schemes, $R_1 = 1/2$, R_2=3/4, and $I = 40$ decoding iterations for $\nu = 2$, operating over an uncorrelated Rayleigh fading channel.

capable of operating within (0.07+0.86)=0.93 dB and (0.82+0.09)=0.91 dB from the capacity of the AWGN and Rayleigh fading channels, respectively, while employing the SP mapper.

As we can see by studying Table 3.2 and Figures 3.14 and 3.15, the BER thresholds are accurately predicted by the EXIT charts. Hence, the binary EXIT chart is useful for finding the best SECCC-ID schemes that are capable of decoding convergence at the lowest possible E_b/N_0 value. We apply the same method of calculating the BER thresholds for a range of SECCC-ID schemes, as detailed in Table 3.2.

The complexity of the schemes can be compared by calculating ACS operations as discussed in Section 2.3.2.3. For $I = 40$ decoding iterations a memory-$\nu = 2$ SECCC decoder requires $I \times 2^{\nu} = 40 \times 4 = 160$ ACS operations, which is the same as that of a memory-$\nu = 2$ SECCC-ID decoder using $O = 40$ decoding iterations (i.e. $O \times 2^{\nu} = 40 \times 4 = 160$).

3.4 Union Bounds of Self-Concatenated Convolutional Codes[7]

The union bound is a popular code design technique [75, 132, 145–149], which assists us in analysing the error floor of a turbo-like code. In this section we derive the union bounds of an SECCC scheme for communications over both AWGN and uncorrelated Rayleigh fading channels. As discussed in Section 3.1, the calculation of the union bound involves the computation of the distance spectrum [145] of the code and for a high codeword length, it may become computationally prohibitive to compute the entire distance spectrum. Hence the TUB is considered here, which takes into account the contribution of the lowest non-zero distance spectrum terms [146] rather than only the minimum distance. This technique is useful for studying the corresponding BER floors, regardless of the interleaver lengths.

We first study the similarities and differences between PCCCs and SECCCs in Section 3.4.1. Then, we highlight the union bound derivation for conventional CCs in Section 3.4.2, before we derive the union bound of SECCCs in Section 3.4.3 which is then compared to our simulation results in Section 3.4.4.

3.4.1 System Model for Union Bound Analysis

The schematic of the SECCC encoder employing a $R_1 = 1/2$ RSC encoder and a $R_2 = 1/2$ puncturer is shown in Figure 3.16. As seen from Figure 3.16, the bit sequence $\mathbf{b}_2 = [b_{2,1}\ b_{2,2}\ b_{2,3} \ldots]$ is simply the interleaved version of the original bit sequence $\mathbf{b}_1 = [b_{1,1}\ b_{1,2}\ b_{1,3} \ldots]$. After the parallel-to-serial (P/S) conversion, we can compute the information sequence of the hypothetical upper SECCC component code as $\mathbf{b}^{(1)} = [b_{1,1}\ b_{2,1}\ b_{1,2}\ b_{2,2} \ldots]$. Interestingly, we can view the information sequence of the hypothetical lower SECCC component code $\mathbf{b}^{(2)}$ as the interleaved version of $\mathbf{b}^{(1)}$ using an Odd-Even Separation (OES) based interleaver π_{oes}. More explicitly, the OES interleaver consists of two component interleavers, where the odd position of the bit sequence is permuted based on the mapping of $\pi_o = \pi$, while the even position of the bit sequence is permuted based on the inverse of the mapping π, namely on $\pi_e = \pi^{-1}$.

We apply a puncturer that removes the interleaved bit sequence $\mathbf{b}_2$ as well as all parity bits corresponding to the bit sequence $\mathbf{b}_1$ in order to yield the output sequence $\mathbf{c}^{(1)}$, as shown in Figure 3.16. The resultant puncturing rate is given by $R_2 = 1/2$ and the SECCC output sequence $\mathbf{c}^{(1)}$ consists of only the input bit sequence $\mathbf{b}_1$ as

[7]This section is based on [4]

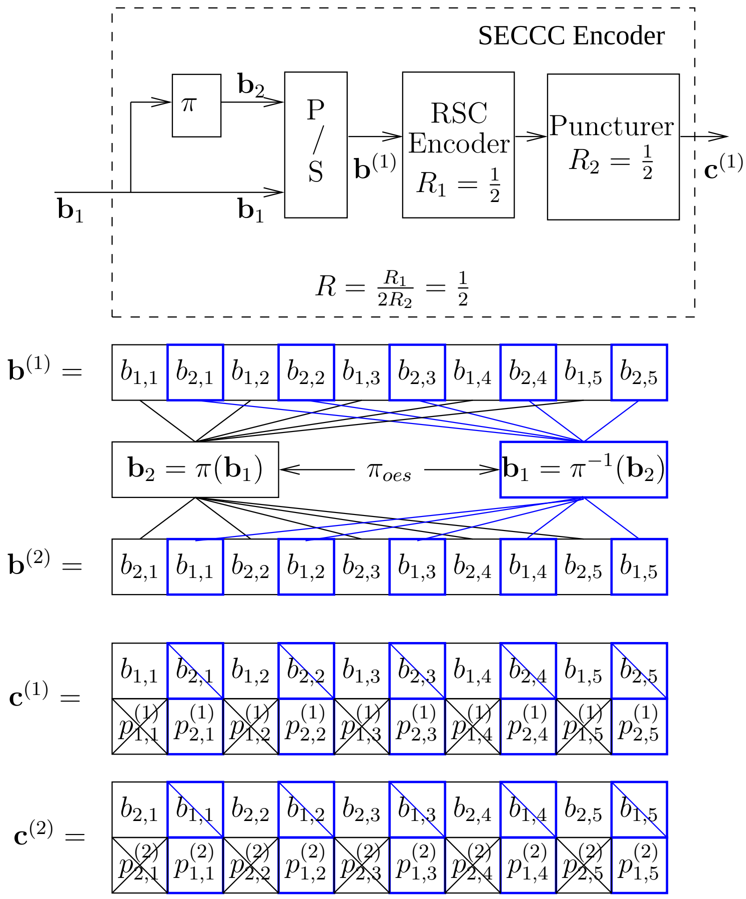

Figure 3.16: Schematic of the SECCC encoder. The notations $\mathbf{b}^{(1)}$ and $\mathbf{b}^{(2)}$ denote the information sequences of the hypothetical upper and lower component encoder, respectively, while the puncturer output sequences of the hypothetical upper and lower component encoder are denoted as $\mathbf{c}^{(1)}$ and $\mathbf{c}^{(2)}$, respectively.

well as the parity bit sequence corresponding to $\mathbf{b}_2$, as shown in Figure 3.16. The SECCC encoder consists of both the rate-R_1 RSC encoder and the rate-R_2 puncturer. Hence, the coding rate of the SECCC encoder, as shown in Figure 3.16, is given by $R = R_1/(2R_2) = 1/2$.

Although $\mathbf{b}_2$ is punctured from $\mathbf{c}^{(1)}$, we can obtain the LLR of the bits in $\mathbf{b}_2$ by interleaving the LLRs associated with the bits in $\mathbf{b}^{(1)}$ obtained from the MAP decoder, as shown in Figure 3.17. Hence, the output sequence $\mathbf{c}^{(1)}$ seen in Figure 3.16 is similar to that of the upper component encoder of a turbo code, where all parity bits corresponding to the odd-position information bits are punctured. Similarly, all parity bits corresponding to the odd-position information bits at the output sequence of the hypothetical lower component code $\mathbf{c}^{(2)}$, as seen in Figure 3.16, are punctured.

Based on these observations, we are able to compute the union bound of SECCCs, as detailed in Section 3.4.3.

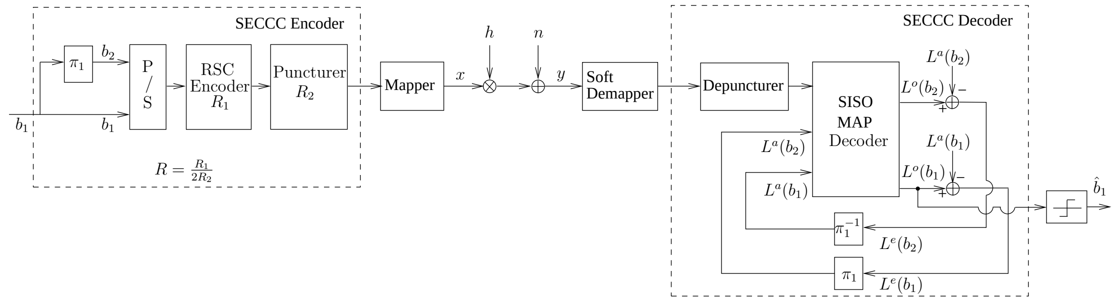

Figure 3.17: Schematic of the SECCC encoder and decoder. The notation $L(b)$ denotes the LLR of bit b and the the superscripts a, o and e denote the *a priori*, *a posteriori* and extrinsic nature of the LLRs, respectively. This schematic is different from Figure 3.1, since the interleaver π_2 seen in Figure 3.1 after the RSC encoder is not used here in order to make the analysis simpler, as also augmented in Figure 3.16.

3.4.2 Union Bounds of Convolutional Codes

The Pair-Wise Error Probability (PWEP) is defined as the probability that the modulated symbol sequence $\mathbf{x} = [x_1\ x_2\ \ldots]$ is wrongly decoded as another modulated symbol sequence $\hat{\mathbf{x}} = [\hat{x}_1\ \hat{x}_2\ \ldots]$. The PWEP, which depends on both the modulation scheme as well as on the code structure and the communication channel, can be expressed as [75]:

$$P(\mathbf{x} \to \hat{\mathbf{x}}) \;=\; \mathrm{Q}\left(\sqrt{\frac{\gamma}{2} d^2(\mathbf{x}, \hat{\mathbf{x}})}\right), \tag{3.21}$$

where γ is the SNR, while $d^2(\mathbf{x}, \hat{\mathbf{x}})$ is the squared *Euclidean distance* between the modulated symbol sequences $\mathbf{x}$ and $\hat{\mathbf{x}}$, when communicating over an AWGN channel, which is given by:

$$d^2(\mathbf{x}, \hat{\mathbf{x}}) \;=\; \sum_{t \in \beta} |x_t - \hat{x}_t|^2, \tag{3.22}$$

where β represents the set of indices t satisfying the condition of $x_t \neq \hat{x}_t$. The number of elements in the set β is given by $\Delta_H = \Delta_H(\mathbf{x}, \hat{\mathbf{x}})$, which quantifies the number of erroneous modulated symbols in the sequence $\hat{\mathbf{x}}$, when compared to the correct sequence $\mathbf{x}$. When communicating over uncorrelated Rayleigh fading channels, the PWEP can be shown to be [163]:

$$P(\mathbf{x} \to \hat{\mathbf{x}}) \;\leq\; \frac{1}{2} \prod_{t \in \beta} \left(1 + \frac{\gamma}{4} |x_t - \hat{x}_t|^2\right)^{-1}. \tag{3.23}$$

In this treatise, we will derive the union bound of SECCCs based on BPSK modulation. Note that when BPSK modulation is employed, we have $|x_t - \hat{x}_t|^2 = 4$, whenever $x_t \neq \hat{x}_t$ since $\{x_t, \hat{x}_t\} = \{\pm 1\}$. Based on this simplification, the PWEP for the AWGN channel can be expressed from Eq. (3.21) as:

$$P(\mathbf{x} \to \hat{\mathbf{x}}) \;=\; \mathrm{Q}\left(\sqrt{2\gamma\Delta_H}\right) \; . \tag{3.24}$$

Similarly, the PWEP for the uncorrelated Rayleigh fading channel can be simplified from Eq. (3.23) as:

$$P(\mathbf{x} \to \hat{\mathbf{x}}) \;\leq\; \frac{1}{2}(1+\gamma)^{-\Delta_H} \; , \tag{3.25}$$

where Δ_H is also referred to as the *effective Hamming distance*, which quantifies the diversity order of the code.

The union bound of the average BER of a coding scheme can be expressed as [75]:

$$P_b \;\leq\; \frac{1}{k}\sum_{\Delta_H} B_{\Delta_H} P(\mathbf{x} \to \hat{\mathbf{x}}) \; , \tag{3.26}$$

where k is the number of information bits per n-bit coded symbol and B_{Δ_H} is the distance spectrum of the code, given by:

$$B_{\Delta_H} \;=\; \sum_{w} \frac{w}{N} \cdot A_{w,\delta} \; ; \quad \text{for} \quad \Delta_H = w + \delta \; , \tag{3.27}$$

where w is the information weight denoting the number of erroneous information bits in an encoded sequence and δ is the parity weight quantifying the number of erroneous parity bits in an encoded sequence. More explicitly, $A_{w,\delta}$ is the two-dimensional Weight Enumerating Function (WEF), quantifying the average number of sequence error events having an information weight of w and a parity weight of δ. Hence, the Hamming distance is given by $\Delta_H = w + \delta$.

3.4.3 Union Bounds of SECCCs

The WEF of SECCCs can be expressed as:

$$A_{w,\delta} = A^{(1)}_{2w,\delta^{(1)}} \cdot A^{(2)}_{2w,\delta^{(2)}} \cdot P_{\pi}^{N,w} \; , \tag{3.28}$$

where $A^{(1)}_{2w,\delta^{(1)}}$ and $A^{(2)}_{2w,\delta^{(2)}}$ are the WEFs of the hypothetical upper and lower component codes, respectively, while the effective parity weight of an SECCC is given by:

$$\delta = \delta^{(1)} + \delta^{(2)}, \tag{3.29}$$

where $\delta^{(1)}$ and $\delta^{(2)}$ are the parity weights of the hypothetical upper and lower component codes, respectively. The above procedure is similar to that devised for the

TTCM scheme of [132] employing two TCM constituent codes, where the parity bits of the upper and lower TCM encoded symbols are punctured at the even and odd symbol indices, respectively. As we can see from Figure 3.16, the information sequence of the upper component encoder $\mathbf{b}^{(1)}$ consists of the original information sequence $\mathbf{b}_1$ and its interleaved version $\mathbf{b}_2$. Hence, if the original information sequence $\mathbf{b}_1$ has an information weight of w, then the information sequence of the upper component encoder $\mathbf{b}^{(1)}$ will have an information weight of $2w$. The same also applies to the lower component code. Hence, we have $A^{(1)}_{2w,\delta^{(1)}}$ and $A^{(2)}_{2w,\delta^{(2)}}$ in Eq. (3.28).

The term $P^{N,w}_{\pi}$ in Eq (3.28) denotes the probability of occurrence for all the associated error events having w information bit errors, when employing a self-concatenated bit-interleaver having a length of N bits. The evaluation of $P^{N,w}_{\pi}$ is based on the novel uniform self-interleaver concept, which may be interpreted as the extension of the uniform bit-interleaver concept proposed in [144]. More specifically, a uniform self-interleaver may be partitioned into two bit-interleavers, as defined in Definition 1.

Definition 1 *A uniform self-interleaver of length N bits is a probabilistic device, which maps a given input sequence of length N bits having an information weight of w bits into all possible permutations in the odd and even partitions of an equivalent odd-even-separation based interleaver of length $2N$ having an information weight of $2w$, with equal probability of $P^{N,w}_{\pi}$ given by:*

$$P^{N,w}_{\pi} = P^{N,w} \cdot P^{N,w} , \tag{3.30}$$

where $P^{N,w} = 1/\binom{N}{w}$, which characterizes the traditional N-bit uniform interleaver having an information weight of w bits. If there are w bit errors in the information sequence, then there will be w bit errors in the 'odd' sequence $\mathbf{b}_1$ as well as another w bit errors in the 'even' sequence $\mathbf{b}_2$, since $\mathbf{b}_2$ is simply the interleaved version of the $\mathbf{b}_1$ sequence.

The WEF $A_{w,\delta}$ for an SECCC having a block length of N encoded symbols and a total of M number of trellis states can be calculated as follows. We can define the State Input-Redundancy WEF (SIRWEF) for a block of N SECCC-encoded symbols as:

$$\mathbf{A}(N,S,W,Z) = \sum_{w}\sum_{\delta} A_{N,S,w,\delta} \cdot W^{w} Z^{\delta} , \tag{3.31}$$

where $A_{N,S,w,\delta}$ is the number of paths in the trellis entering state S at symbol index N, which have an information weight of w and a parity weight of δ. The notations W and Z represent dummy variables. For each n-bit coded symbol at index t, the term $A_{t,S,w,\delta}$ can be calculated recursively as follows:

$$A_{t,S,w,\delta} = \sum_{S',S:u_t} A_{t-1,S',w',\delta'} \ , \ (1 \le t \le N) \ , \tag{3.32}$$

where u_t represents the specific k-bit input symbol that triggers the transition from state S' at index $(t-1)$ to state S at index t, while the terms w and δ can be formulated as:

$$w = w' + i(S', S) \ \ ; \ \ \delta = \delta' + \Phi(S', S) \ , \tag{3.33}$$

where w' and δ' are the information weight and the parity weight, respectively, of the trellis paths entering state S' at index $(t-1)$. Furthermore, $i(S', S) \in \{0, 1, \ldots, k\}$ is the information weight of the k-bit information symbol u_t that triggers the transition from state S' to S and $\Phi(S', S) \in \{0, 1, \ldots, n-k\}$ is the parity weight between $\hat{c}_t$ and c_t, where $\hat{c}_t$ is the encoded n-bit symbol corresponding to the trellis branch in the transition from state S' to S and c_t is the actual encoded n-bit symbol at index t. Again, all the parity bits in $\{c_t\}$ (or $\{\hat{c}_t\}$) corresponding to the odd-position information bits are punctured. Note that the parity weight contribution corresponding to a punctured parity bit equals to zero.

Let the encoding process commence from state 0 at index 0 and terminate at any of the M possible states at index N. Then the WEF used in Eq. (3.27) is given by:

$$A_{w,\delta} = \sum_{S} A_{N,S,w,\delta} \ . \tag{3.34}$$

Note that for linear codes [87] the distance profile of the code is independent of which particular encoded symbol sequence is considered to be the correct one. Hence, for the sake of simplicity, we can assume that the all-zero encoded symbol sequence is transmitted.

Based on all the above equations, the union bound of an SECCC employing BPSK modulation can be shown to be:

$$P_b \le \sum_{\Delta_H} \sum_{w} \frac{A^{(1)}_{2w,\delta^{(1)}} \cdot A^{(2)}_{2w,\delta^{(2)}}}{\binom{N}{w} \cdot \binom{N}{w}} \cdot \frac{w \cdot \mathrm{Q}\left(\sqrt{2\gamma\Delta_H}\right)}{kN} \ , \tag{3.35}$$

when communicating over AWGN channels and

$$P_b \le \sum_{\Delta_H} \sum_{w} \frac{A^{(1)}_{2w,\delta^{(1)}} \cdot A^{(2)}_{2w,\delta^{(2)}}}{\binom{N}{w} \cdot \binom{N}{w}} \cdot \frac{w \cdot (1+\gamma)^{-\Delta_H}}{2kN} \ , \tag{3.36}$$

when communicating over uncorrelated Rayleigh fading channels, where $\Delta_H = w + \delta^{(1)} + \delta^{(2)}$.

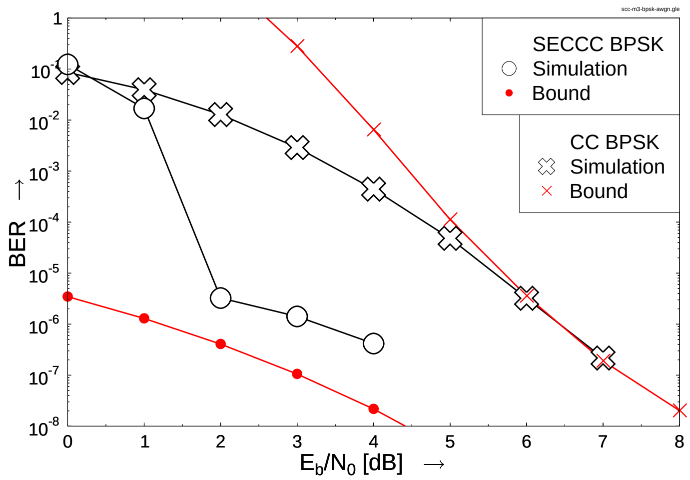

Figure 3.18: Simulations and TUBs of BPSK-assisted CC and SECCC, when communicating over AWGN channels. The union bounds are truncated at a maximum Hamming distance of $\Delta_{H\,\max} = 20$. The SECCC employs an interleaver of length 12 000 bits and 16 decoding iterations.

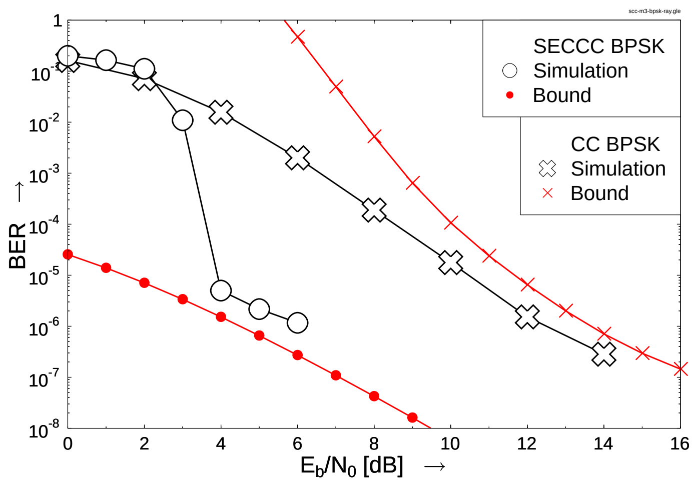

Figure 3.19: Simulations and TUBs of BPSK-assisted CC and SECCC, when communicating over uncorrelated Rayleigh fading channels. The union bounds are truncated at a maximum Hamming distance of $\Delta_{H\,\max} = 20$. The SECCC employs an interleaver of length 12 000 bits and 16 decoding iterations.

3.4.4 Results and Discussions

Let us now compare the BER performance of CCs and SECCCs to their union bounds truncated at a maximum Hamming distance of $\Delta_{H\,\max} = w_{\max} + \delta_{\max} = 20$, where the maximum information and parity weights considered are $w_{\max} = 10$ and $\delta_{\max} = 10$, respectively. Figures 3.18 and 3.19 shows the BERs of our simulations and bounds of the CCs and SECCCs employing BPSK modulation, when communicating over both AWGN and uncorrelated Rayleigh fading channels. Both the CC and SECCC employ an RSC code based on a generator polynomial of $G = [13\ 15]$ expressed in octal format.

As shown in Figures 3.18 and 3.19, the truncated union bound quantifies the BER floor of SECCCs quite accurately. Hence, we can design various SECCCs having various desired BER floors using the proposed TUB.

3.5 Comparison of SECTCM, SECCC and SECCC-IDs

Let us now compare the performance of the SECTCM, SECCC and SECCC-ID schemes in the presence of AWGN and Rayleigh fading channels. The equivalent-complexity QPSK assisted schemes are characterized in Figures 3.20, 3.21 and 3.22 for coded-frame length of 1000, 4000 and 10,000 symbols. Similar to the case of the SECTCM, where the two identical components iterate four times with each other hence we define the overall iterations as eight, the SECCC has two identical components which iterate four times with each other by exchanging extrinsic information, therefore the overall number of iterations is eight. For the SECCC-ID scheme, the two identical components iterate with each other and then with the soft demapper by exchanging extrinsic information. This is activated four times, hence the overall number of iterations is eight as well. The complexity of all the 8-state codes characterized in Figures 3.20, 3.21 and 3.22 is $8 \times 8 = 64$. Figures 3.20 and 3.21 present similar trends for the schemes considered. They show that although the SECTCM schemes achieve an early convergence, its error floor is high as compared to those of the SECCC and SECCC-ID schemes. By contrast, the SECCC and SECCC-ID schemes perform almost equivalently around the error floor region in the case of $R_1 = 1/2$ and $R_2 = 1/2$, albeit the SECCC achieves an early convergence compared to the SECCC-ID scheme. However, when we increase the interleaver depth to 10,000, as shown in Figure 3.22, the error floor is seen to be lower for the SECCC-ID scheme.

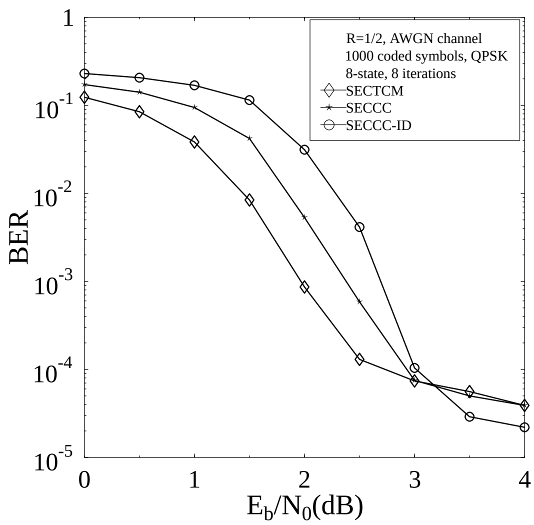

(a) 8 iterations

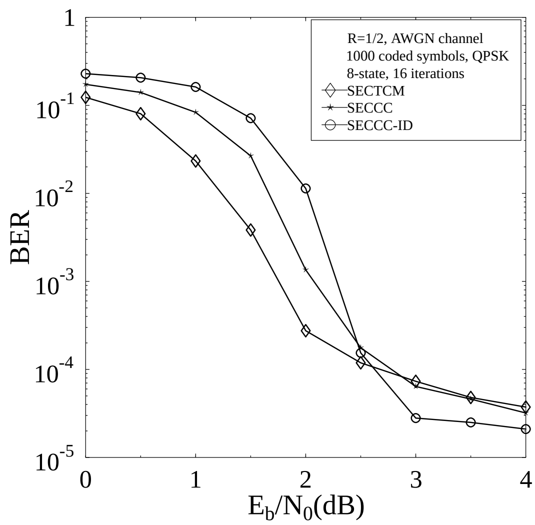

(b) 16 iterations

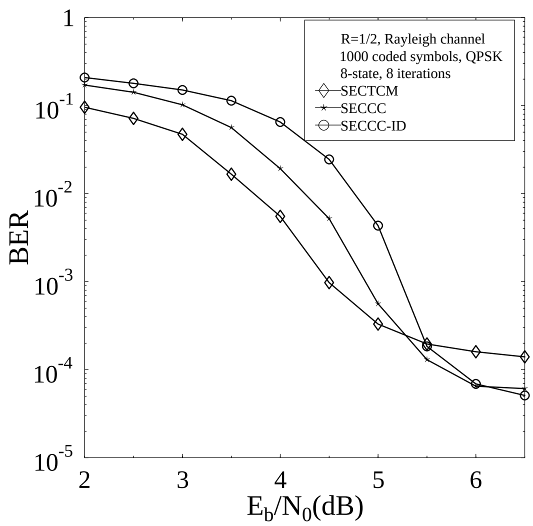

(c) 8 iterations

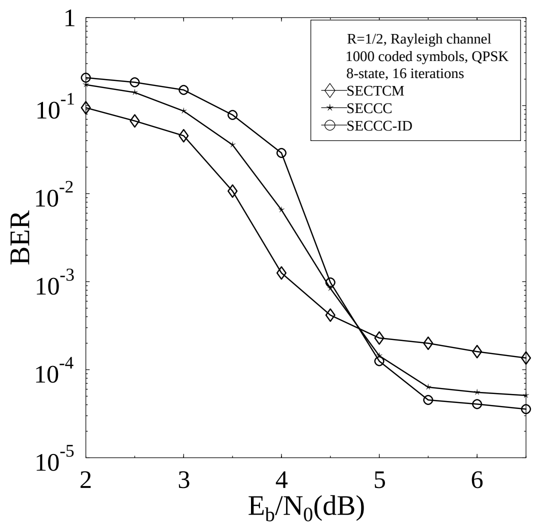

(d) 16 iterations

Figure 3.20: Performance of the QPSK-assisted equivalent-complexity SECTCM, SECCC and SECCC-ID schemes for AWGN and Rayleigh fading channels, when the interleaver depth is 1000.

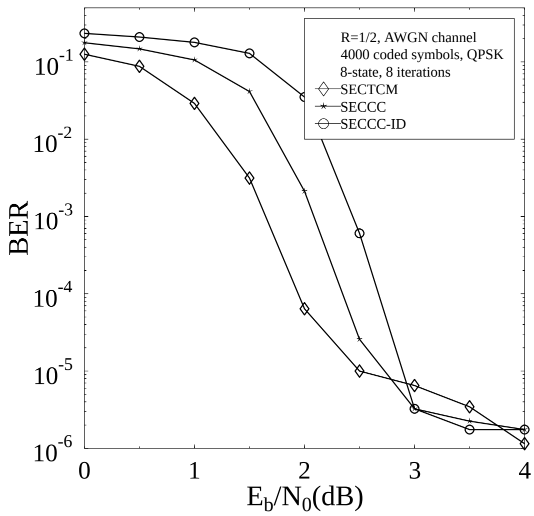

(a) 8 iterations

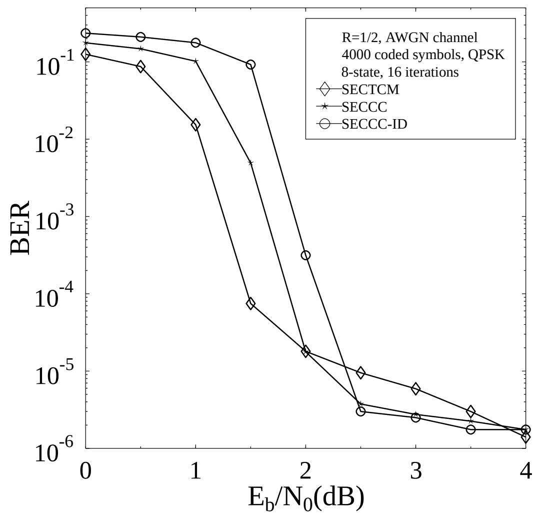

(b) 16 iterations

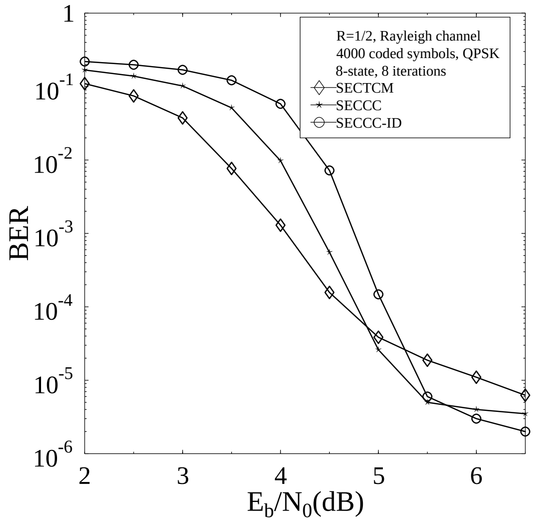

(c) 8 iterations

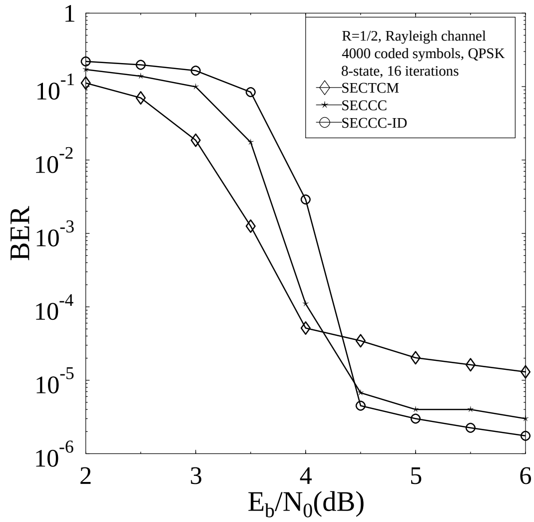

(d) 16 iterations

Figure 3.21: Performance of the QPSK-assisted equivalent-complexity SECTCM, SECCC and SECCC-ID schemes for AWGN and Rayleigh fading channels, when the interleaver depth is 4000.

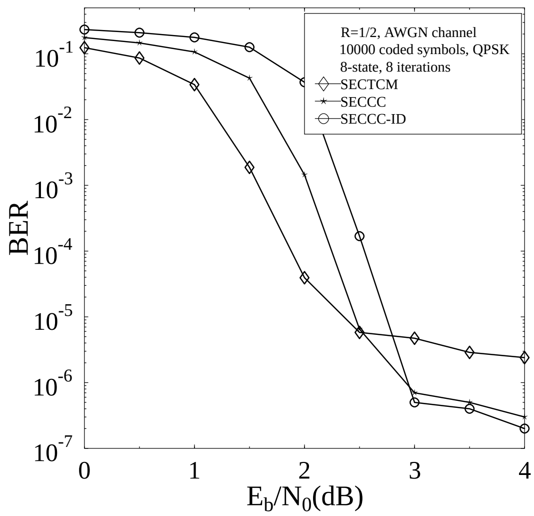

(a) 8 iterations

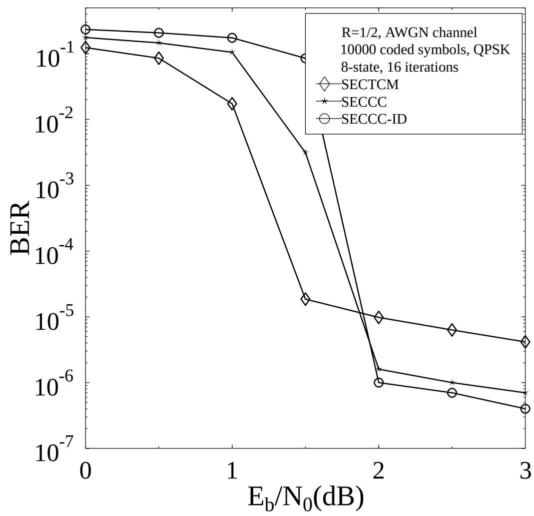

(b) 16 iterations

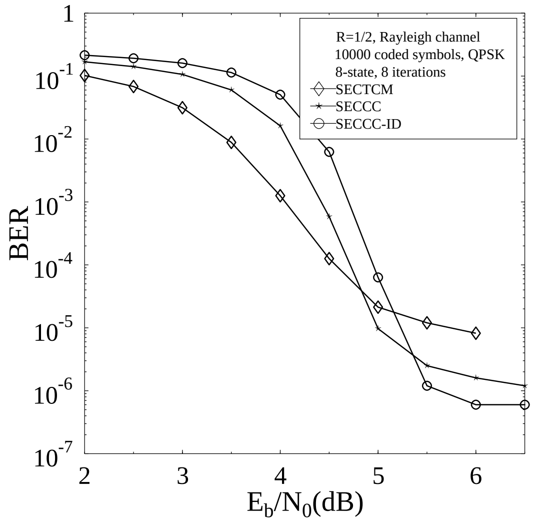

(c) 8 iterations

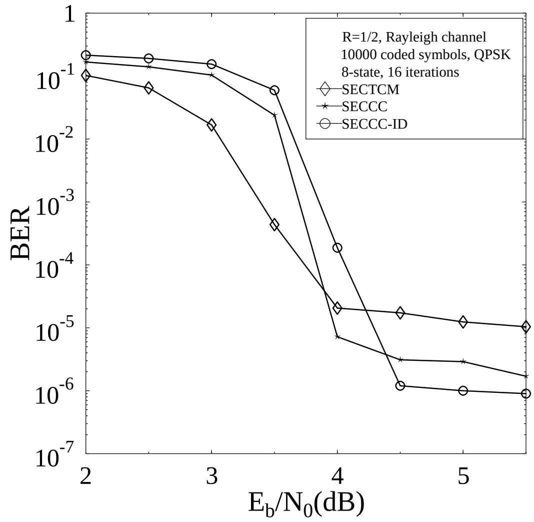

(d) 16 iterations

Figure 3.22: Performance of the QPSK-assisted equivalent-complexity SECTCM, SECCC and SECCC-ID schemes for AWGN and Rayleigh fading channels, when the interleaver depth is 10,000.

3.6 Chapter Conclusions

Section 3.3 focused on designing near-capacity binary self-concatenated codes using different constituent schemes using a procedure which was based on their EXIT-chart aided decoding convergence analysis. The SECCC schemes invoke binary RSC codes and different puncturing rates. The puncturer is used to increase the achievable bandwidth efficiency. The interleaver placed before the puncturer helps randomise the puncturing pattern. Good SECCC parameters were found for assisting the SECCC scheme in attaining decoding convergence at the lowest possible E_b/N_0 value, when communicating over both AWGN and uncorrelated Rayleigh fading channels. We have demonstrated that 3-D EXIT charts are useful for designing near-capacity SECCC-ID codes. Furthermore, 3-D EXIT charts may also be used to design a SECCC-ID scheme concatenated with an outer codec, such as a video codec for enabling soft information exchange between the SECCC-ID decoder and the video decoder. The SECCC-ID schemes designed are capable of operating less than 0.5 dB and 1.0 dB from the AWGN as well as Rayleigh fading channel's capacity.

A useful union bound has been derived for BPSK-based SECCCs in Section 3.4, when communicating over both AWGN and uncorrelated Rayleigh fading channels. We also demonstrated that the union bound can be truncated in order to conveniently analyze the BER floor of SECCCs. This union bound can be used together with EXIT charts in order to design near-capacity SECCCs operating at a given desired BER floor. It can also be extended to high-order modulation schemes for designing bandwidth efficient SECCCs.

3.7 Chapter Summary

The self-concatenated code design proposed in Chapter 2 was symbol-based, therefore it had the inherent problem of exhibiting a mismatch between the EXIT curve and the bit-by-bit decoding trajectory. The EXIT charts assume the data to be uncorrelated, but in our scheme the data was correlated, since both the systematic and the parity bits were transmitted together within a single 2^{n+1}-ary symbol. EXIT charts of the symbol-based SECCC scheme can be used as upper bounds because we found that the EXIT-charts corresponding to independent data exhibited a wider open tunnel and hence the Monte-Carlo simulation based decoding trajectory always successfully passed through it. The design proposed in Section 3.2.1 is a bit-based design, which eliminates the mismatch inherited by the symbol-based design. However, due to the employment of bit-based SECCC schemes there is a loss of information. It was then shown in Figures 3.10, 3.11 and 3.12 that 3-D EXIT charts are helpful in designing binary SECCC-IDs, which exchange extrinsic information with the soft-decision demapper, in order to recover the lost information and hence to approach channel capacity.

Channel				AWGN			Uncorrelated Rayleigh		
Modulation				QPSK					
Decoder				Approximate Log-MAP					
Symbols per frame				1000	4000	10,000	1000	4000	10,000
				E_b/N_0 (dB) at BER					
Code	ν	Gen. Poly.	Iterations	10^{-4}	10^{-5}	10^{-5}	10^{-4}	10^{-5}	10^{-5}
SECTCM	3	$[17\ 2\ 10]_8$	8	2.75	2.50	2.38	7.50	6.10	5.75
SECTCM	3	$[17\ 2\ 10]_8$	16	2.65	2.50	2.00	7.40	6.40	5.50
SECCC	3	$[13\ 15]_8$	8	2.90	2.75	2.45	5.70	5.30	5.00
SECCC	3	$[13\ 15]_8$	16	2.80	2.20	1.85	5.25	4.50	3.95
SECCC-ID	3	$[13\ 15]_8$	8	3.00	2.90	2.75	5.80	5.40	5.25
SECCC-ID	3	$[13\ 15]_8$	16	2.60	2.38	1.90	5.10	4.50	4.30

Table 3.3: Performance of QPSK assisted equivalent complexity SECTCM, SECCC and SECCC-ID schemes under AWGN and Rayleigh fading channels for interleaver depths of 1000, 4000 and 10,000.

In order to provide further insights, we extracted the results of Table 3.3 from Figures 3.20, 3.21 and 3.22. For an interleaver length of 1000 coded symbols we observe the E_b/N_0 values required for a BER of 10^{-4} from Figure 3.20. It can be seen that upon increasing the number of decoding iterations from 8 to 16, SECCC-ID performs better at a BER of 10^{-4}, since it requires $E_b/N_0 = 2.60$ dB and 5.10 dB for the case of AWGN and Rayleigh fading channels, respectively. However, for the case of an interleaver length of 4000 and 10,000 coded symbols it is observed in Figures 3.21 and 3.22 that at a BER of 10^{-5} the performance of SECCC and SECCC-ID are comparable, but better than that of SECTCM, provided that the number of decoding iterations is increased to 16. For example, in the case of an interleaver length of 10,000 coded symbols and Rayleigh fading channel we require $E_b/N_0 = 5.50$ dB for SECTCM, whereas SECCC and SECCC-ID necessitate 3.95 and 4.30 dB, respectively. In Figures 3.23 and 3.24 we will characterize the performance of SECCC and SECCC-ID schemes having different code rates and demonstrate that indeed, the SECCC-ID scheme has a lower error floor as compared to an equivalent SECCC scheme.

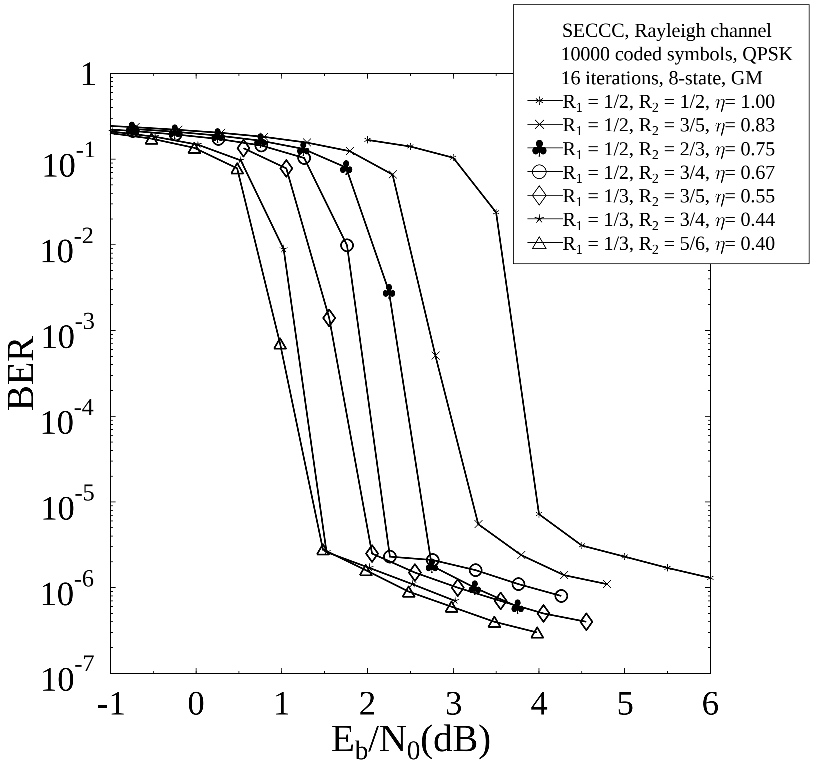

Figure 3.23: Performance of various QPSK-assisted SECCC schemes for transmission over Rayleigh fading channels when the interleaver depth is 10,000 symbols.

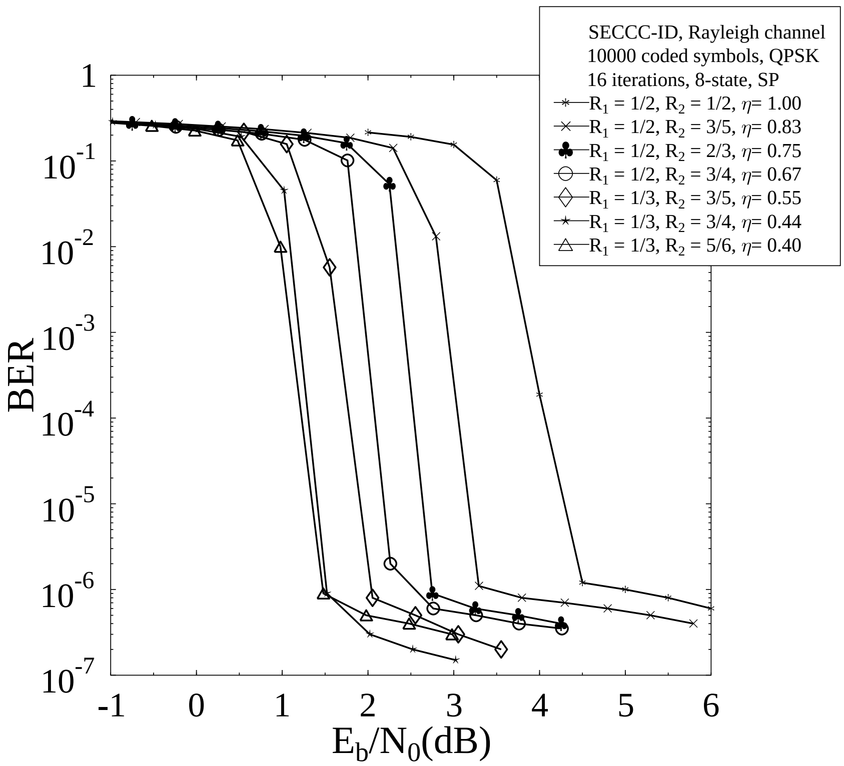

Figure 3.24: Performance of various QPSK-assisted SECCC-ID schemes for transmission over Rayleigh fading channels when the interleaver depth is 10,000 symbols.

Observe in Figures 3.23 and 3.24 that our proposed schemes are flexible, since we can obtain the desired overall coding rates by varying the values of R_1 and R_2. These are studied for the case of uncorrelated Rayleigh fading channels using an interleaver depth of 10,000 symbols. Figure 3.23 illustrates the BER performance of GM SECCC schemes, whereas Figure 3.24 is depicting the performance for the case of a SP mapped SECCC-ID scheme. It can be observed that in the case of the GM SECCC scheme convergence is attained at a lower E_b/N_0 value, however the SP mapped SECCC-ID scheme has a lower error floor.

Lastly, the union bounds of SECCCs were derived for communications over both AWGN and uncorrelated Rayleigh fading channels. The TUBs of SECCCs are very useful for studying the corresponding BER floors. Based on the TUBs, various SECCCs can be designed for a desired BER floor without the need of time-consuming Monte-Carlo simulations.

Chapter 4

Application of Self-Concatenated Convolutional Codes in UWB and Video Systems

4.1 Introduction

In Section 3.2.1 we invoked binary SECCCs employing iterative decoding for communicating over both uncorrelated Rayleigh fading and AWGN channels. Recursive systematic convolutional codes were selected as constituent codes and an interleaver was used for randomising the extrinsic information exchange of the constituent codes, while a puncturer assisted us in adjusting the bandwidth efficiency. At the receiver, self-iterative decoding was employed for exchanging extrinsic information between the hypothetical decoder components. The convergence behaviour of the decoder was analysed with the aid of bit-based EXIT charts. In this chapter we analyse applications of SECCCs in the important areas of UltraWideBand (UWB) and video transmission.

UWB transmission techniques constitute a family of wireless transmission schemes whose bandwidth (B) is more than 25 percent of the carrier frequency, or more than 1.5GHz [164, 165]. Alternatively, according to the Federal Communications Commission (FCC), UWB signals occupy a bandwidth of at least 500MHz in the 7.5GHz chunk of spectrum between 3.1GHz and 10.6GHz [166]. An UWB radio communicates using baseband pulses of very short duration, typically on the order of a nanosecond, thereby spreading the energy of the radio signal very 'thinly' (about a few μW per MHz) from near DC to a few GigaHertz. Because of the broad spectrum of this signal, which we typically associate with an appropriately shaped signalling impulse, this system is also often referred to as Impulse Radio (IR) [165]. It is a baseband system having a Power Spectral Density (PSD) that occupies frequencies stretching from near DC to a few Gigahertz [167]. The terminology of a carrierless system implies that it could be manufactured inexpensively. Furthermore, its baseband operation at low frequencies improves its capability of penetrating materials that tend to become more opaque at higher frequencies. Many properties of UWB systems are fundamentally different from those of RF communications. Again, instead of using a carrier frequency, as in traditional systems, UWB systems transmit high-bandwidth carrierless radio impulses using extremely accurate timing [168].

Naturally, impulse radio signals are also subject to propagation impairments, even in benign propagation environments, which determine the achieveable SNR and hence the attainable transmission rate. However, UWB systems benefit from a high diversity order, since owing to their high bandwidth, they have a high number of independently fading multipath components. Furthermore, they are capable of accommodating a high number of users even in multipath environments, as a benefit of their high bandwidth [164]. Hence UWB systems may revolutionize home media networking, facilitating the downloading of images from a digital camera to a computer, distributing HDTV signals from a single receiver to multiple TV sets around the home, connecting printers to computers, and potentially replacing any electronic signalling cables on the premises [181], except of course for mains cables.

UWB impulses are transmitted in sub-nanosecond intervals, which inherently leads to a high bandwidth and - as a benefit - to an accurate spatial resolution, which can be taken advantage of in positioning applications [176, 177, 180]. The associated high signalling impulse rates facilitate high connection speeds over short distances. Since UWB signals occupy a broad spectrum, low transmission powers must be used in order to avoid interference with existing Radio Frequency (RF) systems [182]. A common approach is to set the UWB power levels so low that the signals cannot be distinguished from external noise imposed by other systems operating at overlapping frequencies. However, the concepts have mainly been used in radar-based applications only, since the timing and synchronization requirements of UWB communications have been too challenging for creating cost-effective consumer products. Recent developments in semiconductor technology have brought the applications closer to realization and the regulatory steps taken in the US also indicate a trend towards accelerating research efforts [166]. Table 4.1 gives an overview of past advances in the field of UWB communications.

Year	*Milestone*
1954	Rosa *et al*. [169] patented a random pulse generation based communication system, which used a modulated carrier for minimising the risk of jamming by the enemy.
1968	Ross [170] proposed a time-domain model for creating wideband radiating elements. It was shown that by limiting the duration of the impulse response, excellent transient behaviour can be achieved for the radiating antenna.
1973	Ross [171] was awarded a patent for the transmission and reception method of very short duration base-band signalling pulses, which were unaffected by other communication systems or noise.
1978	Bennett and Ross *et al*. [172] introduced the baseband pulse generation concept and discussed its application in radar and communications theory.
1980	Harmuth [173] derived a class of useful non-sinusoidal signals developed for synthetic aperture radar.
1990	The Defense Advanced Research Projects Agency (DARPA) and the Office of Secretary of Defense (OSD) contracted the Battelle Corp. to convene a panel of experts and examine the UWB technology [174].
1993	Scholtz [175] highlighted the potential offered by a time-hopping Pulse Position Modulated (PPM) waveform having a duration on the order of a nanosecond, which resulted in a low-cost receiver.
2002	Federal Communications Commission (FCC) [166] changed the rules to allow operation of UWB transmission systems in a broad range of frequencies. The UWB Precision Asset Location (PAL) system [176] was built, which gave accurate results for locating cargo containers in multipath environments.
2005	Gezici *et al*. [177] conceived high time resolution based accurate UWB positioning systems for sensor networks.
2006	Molisch *et al*. [178] proposed a comprehensive statistical model for UWB propagation channels that was accepted by the IEEE 802.15.4a Task Group as the standard model for the evaluation of UWB system proposals.
2007	Bacci *et al*. [179] designed a game-theoretic model for studying power control designed for UWB wireless networks operating in frequency-selective multipath environments.
2009	Dardari *et al*. discussed the potential of UWB in systems requiring accurate localization capabilities by utilising low-complexity time-of-arrival (TOA) based ranging techniques [180].

Table 4.1: UWB advancements

In this chapter, we will provide channel coding solutions approaching the UWB system's capacity. Another attractive design alternative is that of employing sophisticated binary SECCCs using different puncturing rates, as presented in Section 3.2.1, which will be used to construct a low-complexity near-capacity Time-Hopping (TH) Pulse Position Modulated (PPM) UWB Impulse Radio (IR) system having a moderate interleaver size.

Interactive wireless video telephony constitutes an attractive service. However, the band-limited nature of communication networks imposes the constraint of maintaining a low bit-rate, associated with highly compressed video. Unfortunately, the employment of standard video coding techniques, such as variable length coding, make the coded stream sensitive to channel-induced errors. Therefore, some form of FEC must be employed to protect the compressed video stream. Various error protection schemes utilising both source and channel coding for video communication using turbo-style transceivers have been designed in [183]. Furthermore, the secure transmission of H.264 coded video using iterative Joint Source-Channel Decoding (JSCD) was investigated in [184].

New concepts and coding tools have been introduced in state-of-the-art video coding standards [185]. Various error resilient features, such as Flexible Macroblock Ordering (FMO), Data Partitioning (DP) and slice structuring of video pictures were also incorporated in video coding standards such as H.264/AVC [186]. However, in reality the source codes designed without taking into account the presence of channel decoding errors tend to have a poor performance. In a high-compression source codec even a low number of erroneous bits within an entropy coded sequence typically results in a high video distortion in the reconstructed sequence. This imposes stringent BER requirements on the channel coding scheme employed in order to attain an acceptable video quality at the receiver. Various error resilient schemes have been proposed in [183] in order to alleviate these problems, but the price paid is a potential reduction of the achievable compression efficiency and an increased computational complexity. Instead of the traditional serial concatenation of the classic Variable Length Codes (VLC) with a channel code, a parallel concatenated coding scheme was presented in [187], where the VLCs were combined with a turbo code. An optimised bit rate allocation scheme using a rate-1 inner channel encoder along with 3 to 6-bit source mapping was proposed in [188], and its performance was evaluated relative to conventional JSCD using a rate-$\frac{1}{2}$ Recursive Non-Systematic Convolutional (RNSC) inner code.

The novelty and rationale of this chapter can be summarised as follows:

1. *We design a near-capacity iteratively decoded TH-PPM-UWB-IR-SECCC system [5] using EXIT charts. More explicitly, the powerful tool of EXIT charts is used to appropriately select the coding rates of the SECCCs in order to shape the inverted EXIT curve of the TH-PPM-UWB-IR-SECCC system and hence to match it with that of the inner decoder for the sake of achieving an infinitesimally low BER at near-capacity SNR values. Quantitatively, the proposed TH-PPM-UWB-IR-SECCC design becomes capable of performing within about 1.41 dB of the Nakagami-m fading channel's capacity at a BER of* 10^{-3} *[5].*

2. *In [6] low complexity iteratively decoded binary SECCCs, were proposed, which used only a single encoder and a single decoder for the transmission of source coded stream. This technique is suitable for low-complexity video-telephony, which requires a low transmission power. Furthermore, the practically achievable interactive video performance trends are quantified, when using state-of-the-art video coding techniques, such as H.264/AVC. Explicitly, we will demonstrate that an* E_b/N_0 *gain of* 6 *dB may be attained using SECCCs in comaprison to the identical-rate state-of-the-art benchmarker.*

This chapter is organised as follows. In Section 4.2 the near-capacity TH-PPM-UWB-IR-SECCC concept is presented, along with an overview of the UWB system architecture. Section 4.2.5 presents our EXIT chart based performance analysis. The performance of the H.264/AVC using SECCCs is characterised in Section 4.3.3, while our overall performance results are presented in Section 4.3.4. Finally, we offer our conclusions in Section 4.4 and summary in Section 4.5.

4.2 Near-Capacity TH-UWB Design Using SECCCs

4.2.1 Transmitted Signal

The UWB-TH-IR signal is formulated as [165]

$$s^{(k)}(t) = \sum_{j=-\infty}^{\infty} \Psi(t - jT_f - \upsilon_j^{(k)} T_c - \zeta_j^{(k)} T_h), \tag{4.1}$$

where $\Psi(t)$ is the OPSWF signalling pulse shape, T_f is the frame duration, $\upsilon_j^{(k)}$ represents the PN code based TH pattern assigned to user k, T_c is the time shift based on the TH code, where the code repeats after a certain interval, $\zeta_j^{(k)}$ corresponds to the data symbols of user k, while Λ is small shift in the pulse position, either forward or

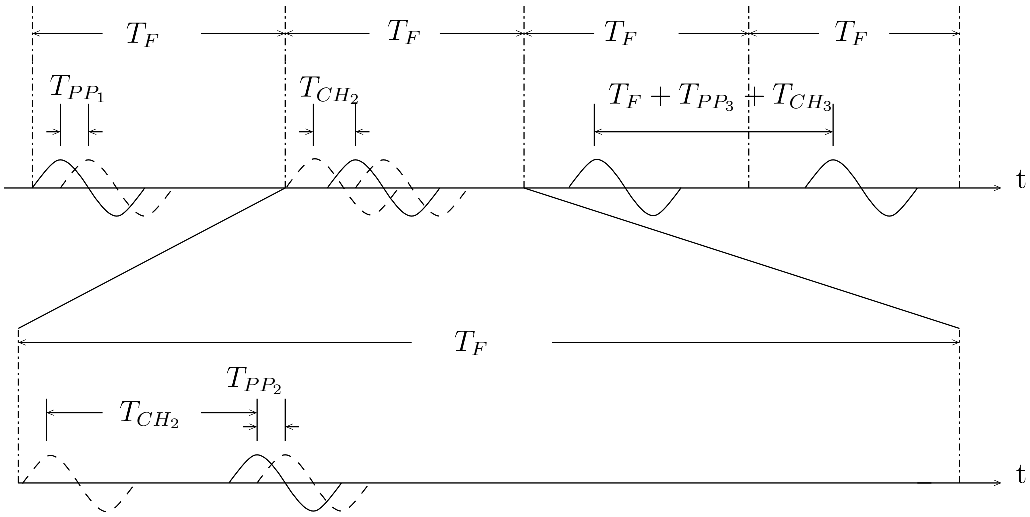

Figure 4.1: A binary TH-PPM system output.

backward to represent the modulating data symbol. The Pulse Repetition Frequency (PRF) is the reciprocal of T_F. The frame time T_F will be of the order of 1000 times the actual pulse width.

In Figure 4.1, we show the output of a simple TH aided binary PPM UWB transmitter, where T_F is the frame duration, T_{PP_n} is the PPM-related shift in the pulse position, either forward or backward with respect to the nominal signalling instant to represent the binary stream, T_{CH_n} is the time shift based on the unique time hopping code of a specific user, where the code repeats after a certain interval.The schematic characterises a single-user scenario, which can be readily extended to the multi-user scenario by using different time-hopping PN codes for the different users, as seen in Figure 4.2.

4.2.2 Nakagami-m Fading

TH-UWB is evaluated using UWB multipath channel model based on indoor channel measurements between 3.1 GHZ to 10.6 GHz over a range of less than 10 meters. The model accepted by the IEEE 802.15.3 standard and considered here may be expressed as [189]

$$h(t) = \sum_{u=1}^{U} h_u e^{j\phi_u} \delta(t - uT_\psi), \tag{4.2}$$

where U represents the number of resolvable multipaths, h_u and ϕ_u are the gain and phase of the *uth* resolvable multipath component, while uT_ψ represents the corresponding delay of the *uth* multipath component.

According to [190], measurements suggest that the UWB channels obeys the

Nakagami distribution, which has been validated by using the Kolmogorov-Smirnov testing with a significance level of 1 percent. Hence explicitly, the fading amplitude h_u is assumed to obey an independent Nakagami-m distribution having a PDF [191]

$$P_{h_u}(r) = \frac{2m_u^{m_u} r^{2m_u-1}}{\Gamma(m_u)\Omega_u^{m_u}} e^{\frac{-m_u r^2}{\Omega_u}}, \qquad r > 0 \tag{4.3}$$

where m_u is the Nakagami fading parameter defined as:

$$m_u = \frac{E^2\left[r^2\right]}{var(r^2)}, \tag{4.4}$$

where the parameter Ω_u is given by

$$\Omega_u = E\left[r^2\right]. \tag{4.5}$$

The vth moment of the random variable r is given by:

$$E\left[r^v\right] = \frac{\Gamma\left(m_u + \frac{v}{2}\right)}{\Gamma(m_u)} \left(\frac{\Omega}{m_u}\right)^{\frac{v}{2}}, \tag{4.6}$$

while $\Gamma(\cdot)$ is the gamma function defined as

$$\Gamma(m_u) = \int_0^\infty x^{m_u-1} e^{(-x)} dx. \tag{4.7}$$

We assume in our analysis that the phase rotation due to fading channel is uniformly distributed in $[0, 2\pi]$.

4.2.3 MMSE Detection

The received signal vector can be expressed for the TH-UWB system as [192]

$$\mathbf{y} = \mathbf{J}\mathbf{b} + \mathbf{n}, \tag{4.8}$$

where $\mathbf{J}$ is the overall system matrix, $\mathbf{b}$ is the information symbol vector, while $\mathbf{n}$ denotes the AWGN vector having $E[\boldsymbol{n}\boldsymbol{n}^H] = 2\sigma_n^2 \boldsymbol{I}$ with $\boldsymbol{I}$ being the identity matrix of appropriate dimension. The MMSE multiuser detector's weight vector $\mathbf{P}$ [192] can be expressed as:

$$\begin{aligned} \mathbf{P} &= \mathbf{R}_b \mathbf{J}^H (\mathbf{J}\mathbf{R}_b\mathbf{J}^H + \mathbf{R}_n)^{-1} \\ &= (\mathbf{J}^H \mathbf{R}_n^{-1} \mathbf{J} + \mathbf{R}_b^{-1})^{-1} \mathbf{J}^H \mathbf{R}_n^{-1}, \end{aligned} \tag{4.9}$$

where $\mathbf{R}_b$ is the covariance matrix of information symbols and $\mathbf{R}_n$ is the covariance matrix of the noise.

4.2.4 System Model

We will use the binary SECCC scheme detailed in Section 3.2.1 to design a near-capacity TH-PPM based UWB Impulse Radio (IR) system. We contrive the iteratively detected SECCC arrangements employing powerful design technique of EXIT charts. The Orthogonal Prolate Spheroidal Wave Function (OPSWF) based signalling pulse shapes are used for the sake of minimizing the Multi-User Interference (MUI) and ISI. RSC codes are employed as constituent codes combined with an interleaver for randomising the extrinsic information exchange between the constituent codes. Furthermore, a puncturer assists us in removing redundant bits, hence increasing the achievable bandwidth efficiency. Iterative decoding is invoked for exchanging extrinsic information between the hypothetical decoder components at the receiver end. The convergence behaviour of the decoder is analysed with the aid of bit-based EXIT charts. Finally, we propose a novel TH-PPM-UWB-IR-SECCC system configuration, which is capable of operating within about 1.41 dB of the information-theoretic limits at a BER of 10^{-3}.

Figure 4.2 shows the baseband model of the iteratively detected TH-PPM-UWB-IR-SECCC system. We have used OPSWF signalling pulses and PPM for transmission over uncorrelated Nakagami-m fading channels, with $m = 1$ for which Rayleigh fading is recovered. As explained in Section 3 we employ Gray-coded QPSK modulated SECCC scheme and combine it with various system components of Figure 4.2. More explicitly, as shown in Figure 4.2, the input bit sequence $\{b_1\}$ of the self-concatenated encoder is interleaved for yielding the bit sequence $\{b_2\}$. The resultant bit sequences are parallel-to-serial converted and then fed to the RSC encoder of coding rate $R_1 = 1/2$ using the generator polynomial $G = (7, 5)_8$ for $\nu = 2$ and $G = (13, 15)_8$ for $\nu = 3$ as detailed in Section 3.2.1. The bits b seen in Figure 4.2 are then sent to the bit-to-symbol conversion buffer. The resultant symbols are then pulse position modulated, while obeying the OPSWF pulse shapes in order to minimize the effects of ISI and MUI. Finally, the TH-PPM-UWB-IR-SECCC encoded transmitted signal is formed by invoking a PN generator for creating the required TH patterns obeying the corresponding PPM signalling delays, as shown in Figure 4.2. The resultant transmitted signal was characterized in Section 4.2.1.

After transmission over a non-dispersive Nakagami-m fading channel contaminated by AWGN having a variance of $N_0/2$ per dimension, the received signal y is fed into a pulse-position MMSE detector, as shown in Figure 4.2. The closed-form matrix description of the receiver was detailed in Section 4.2.1. After the TH-UWB-PPM-IR

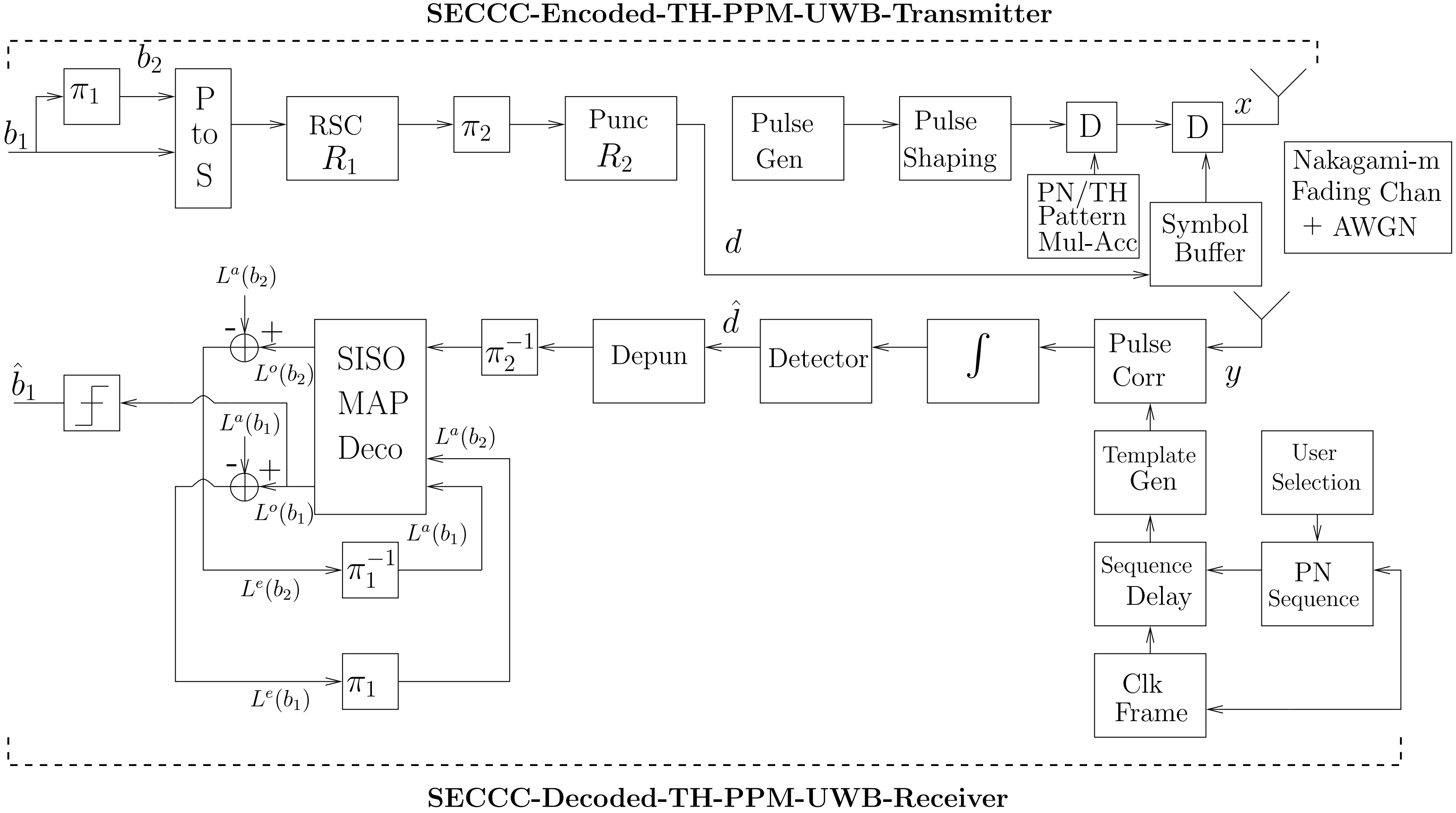

Figure 4.2: TH-PPM-UWB-IR-SECCC system. The schematic incorporates the SECCC scheme of Figure 3.1. Following encoding, interleaving and puncturing the data is then stored in the symbol buffer and transmitted in the baseband without carrier modulation. Similarly, after detection the received signal is passed through a depuncturer, de-interleaver and SISO MAP decoder.

detector of Figure 4.2 the signal $\hat{d}$ is then used by a soft demapper for calculating the conditional PDF of receiving y, when $x^{\{(k),(m)\}}$ was transmitted, where k is the number of users and the set $m \in \{0, 1, 2, 3\}$ represents the legitimate quarternary modulated symbols. Then, the resultant soft-values are passed to a soft depuncturer, which converts them to bit-based LLRs and zero LLRs are inserted at the punctured bit positions. These LLRs are then deinterleaved and fed to the self-concatenated SISO MAP decoder of Figure 4.2 whose iterative procedure has been explained in Section 2.3.1. Self-concatenated decoding proceeds, until the affordable number of iterations is reached. Let us now analyze the performance of the iteratively detected TH-PPM-UWB-IR-SECCC system of Figure 4.2 with the aid of EXIT charts.

4.2.5 EXIT Chart Based Performance Analysis

As detailed in Section 3.2.2, the EXIT charts of self-concatenated codes are typically similar to those of the parallel concatenated TTCM schemes [136, 137], where an open EXIT tunnel exists if the EXIT curve does not intersect the straight line connecting the point ($I_A = 0$, $I_E = 0$) to the point ($I_A = 1$, $I_E = 1$) in the EXIT chart. The coding schemes considered in this section are characterised in Table 4.2. They are identified by the code rate (R_1), puncturing rate (R_2), overall code rate (R), code memory ν and bandwidth efficiency η expressed in bit/s/Hz. The E_b/N_0 decoding convergence threshold, beyond which the EXIT tunnel becomes "just" open is denoted by Λ, although this does not necessarily imply that the (I_A, I_E)=(1,1) point of 'perfect convergence' can be reached, because some of the decoding trajectories are curtailed owing to the limited interleaver length used. Again, this is why the slightly different term, tunnel was introduced, which specifies the E_b/N_0 value, where there is a more widely open EXIT tunnel leading to the (1,1) point and where decoding convergence to an infinitesimally low BER value can always be achieved, provided that the interleaver length is large and the number of decoding iterations is sufficiently high [117]. Furthermore, the channel capacity limit ω is also expressed in dBs [11], as tabulated in Table 4.2. For R_1=1/2 and $\nu = 2$, the octally represented generator polynomial of $G = (7, 5)$ is used, whereas for $\nu = 3$, $G = (13, 15)$ is employed.

The EXIT charts recorded for the TH-PPM-UWB-IR-SECCC system of Table 4.2 are shown in Figure 4.3. The two EXIT curves represent the two hypothetical decoder components of the SECCC scheme, while the stair-case-shaped trajectory "snapshots" correspond to iterating between them as discussed in Section 3.2.2. These are identical components, hence, we only have to compute the EXIT curve of one

TH-PPM-UWB-IR-SECCC System	ν	η (bit/s/Hz)	Nakagami-m Channel E_b/N_0 (dB)	
			Λ	ω
Code 1 (R_1=1/2, R_2=3/4, R=1/3)	2	0.67	2.5	0.54
	3	0.67	1.8	0.54
Code 2 (R_1=1/2, R_2=1/2, R=1/2)	2	1	4.5	1.83
	3	1	3.5	1.83

Table 4.2: The TH-PPM-UWB-IR-SECCC system's decoding convergence thresholds (Λ), ν: memory of SECCC, η: bandwidth efficiency, ω: channel capacity limit.

component and the other is its mirror image with respect to the diagonal line. The EXIT curves of the hypothetical decoder components are plotted within the same EXIT chart together with their corresponding decoding trajectory for the sake of visualizing the transfer of extrinsic information between the decoders. The EXIT curves of the proposed scheme exactly match the decoding trajectories computed from the bit-by-bit simulations.

The EXIT curves and the two distinct decoding trajectories were recorded for the TH-PPM-UWB-IR-SECCC system operating closest to the Nakagami-m channel's capacity, which are given in Figure 4.3 for a specific bit-by-bit Monte-Carlo simulation. Similar decoding trajectory snapshots were found for all our simulations.

In Figure 4.3, the scheme using Code 1, $R_1 = 1/2$, $R_2 = 3/4$, $\nu = 3$ succeeds in creating an open EXIT tunnel at E_b/N_0=1.9 dB, when communicating over an uncorrelated Nakagami-m fading channel. For this scheme the threshold Λ is reached at 1.8 dB according to Table 4.2, which is 1.26 dB away from capacity.

The EXIT charts of Figure 4.3 were used to find the TH-PPM-UWB-IR-SECCC system parameters for $\nu = \{2, 3\}$, when communicating over uncorrelated Nakagami-m fading channels. The convergence threshold predicted by the EXIT chart analysis, as seen in Figure 4.3, closely matches the actual convergence threshold observed in the BER curve given by the specific E_b/N_0 value, where there is a sudden drop of the BER after a certain number of decoding iterations, as shown in Figure 4.4. Hence it becomes possible to attain an infinitesimally low BER beyond the convergence threshold Λ, provided that both the block length and the number of decoding iterations are sufficiently high.

The BER versus E_b/N_0 performance curves of the various TH-PPM-UWB-IR-

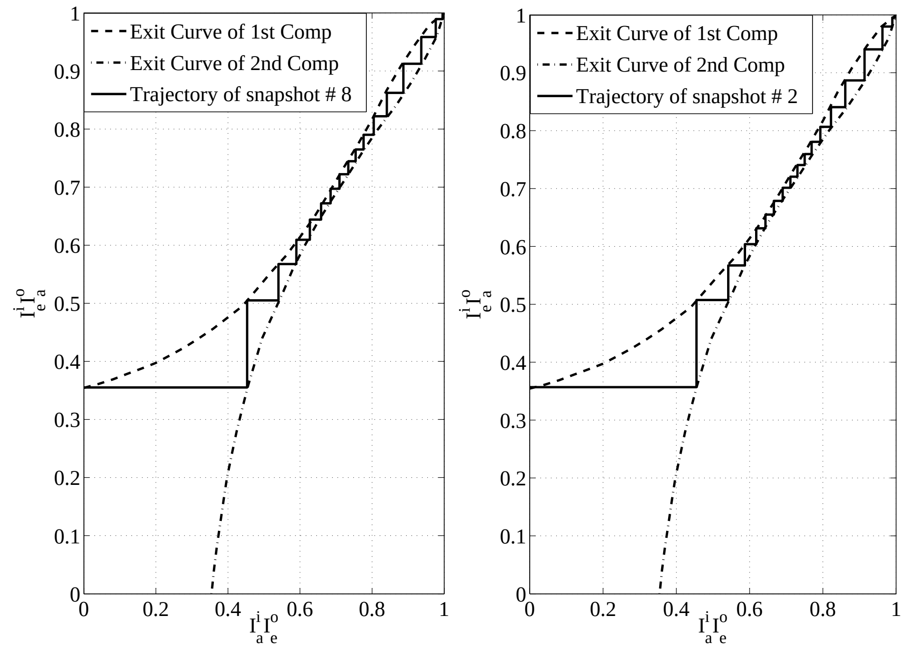

Figure 4.3: EXIT chart and decoding trajectories for Code 1 (R_1=1/2 and R_2=3/4), TH-PPM-UWB-IR-SECCC, $\nu = 3$, $\eta = 0.67$ bit/s/Hz at $E_b/N_0 = 1.9$ dB, for transmission over a Nakagami-m fading channel.

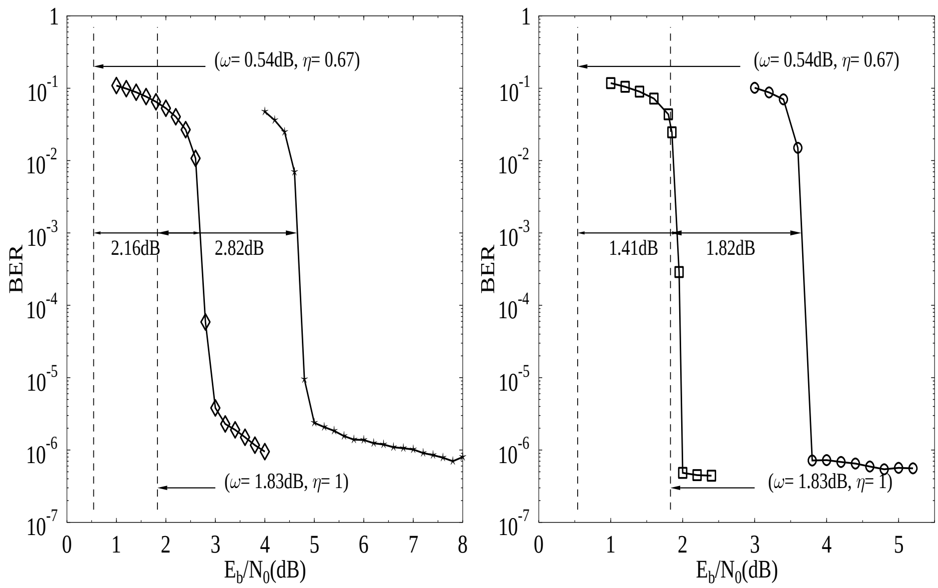

Figure 4.4: The BER versus E_b/N_0 performance of various TH-PPM-UWB-IR-SECCC systems, with Code 1 employing $I = 80$ decoding iterations for $\nu = 2$ (diamond shaped) and $I = 50$ for $\nu = 3$ (square). Similarly, Code 2 employs $I = 80$ for $\nu = 2$ (star) and $I = 50$ for $\nu = 3$ (circle). All the schemes are operating over uncorrelated Nakagami-m fading channel.

SECCC systems recorded from our bit-by-bit simulations are shown in Figure 4.4. As mentioned, we considered an information block length of 120×10^3 bits per frame, transmitted 10^3 frames and the number of decoding iterations (I) was varied from 50 to 80. Figure 4.4 shows the E_b/N_0 difference between the capacity and the convergence threshold Λ for the proposed TH-PPM-UWB-IR-SECCC system at a given code memory ν. It can be observed from Figure 4.4 that the system using Code 1 and $\nu = 2$ is capable of operating within 2.16 dB whereas, for the system using Code 2 and $\nu = 2$ is capable of operating within 2.82 dB, of the Nakagami-m fading channel's capacity, respectively at a BER of 10^{-3}.

As we can see by studying Table 4.2 and Figure 4.4, the actual BER convergence threshold is exactly the same as the convergence threshold predicted by the EXIT charts. Hence, the binary EXIT chart is useful for finding the best TH-PPM-UWB-IR-SECCC system parameter required for attaining a decoding convergence at the lowest possible E_b/N_0 value. The near-capacity SECCC schemes characterized in Figure 4.4 and found from the EXIT chart based design approach are summarised in Table 4.2. For the scheme employing Code 1 and $\nu = 3$ and characterized in Table 4.2, the distance from capacity is 1.41 dB at a BER of 10^{-3} in case of Nakagami-m fading channels. For a bandwidth efficiency of 0.67 bit/s/Hz, the capacity of this scheme [11] is 0.54 dB for Nakagami-m fading channels.

4.3 H.264/AVC Codec Using SECCCs

Wireless systems typically suffer from limited bandwidth and transmit power. Therefore, a video coding standard has to be carefully designed by striking a balance between compression efficiency, signal processing complexity and error resilience etc. [183]. In Section 4.3.2 we will briefly discuss the history of the H.264 Audio/Video Coding (AVC) standard. Its error resilient features are highlighted in Section 4.3.1, while in Section 4.3.3 we present our low-complexity video transceiver using SECCCs.

H.264/AVC coding standard [193] was completed as a joint project between the ITU-T Video Coding Experts Group (VCEG) and the ISO/IEC Moving Picture Experts Group (MPEG). H.264/AVC is a highly efficient video codec, which is resilient to transmission errors and it is capable of, supporting both real-time interactive applications such as video conferencing and video telephony as well as non-real-time applications, such as video streaming and digital television broadcast applications [185].

The recent research advances in the area of H.264/AVC are summarised in Table 4.3. The design of H.264/AVC was defined in form of two layers known as the Video Coding Layer (VCL) and Network Adaptation Layer (NAL) [186]. The core compression scheme of H.264/AVC is based on the above-mentioned VCL, which consists of different sub-levels known as blocks, macroblocks (MB) and slices. It was designed to be as network-independent as possible and consists of various so-called compression 'tools' which improve the attainable coding efficiency and error-resilience of the coded video stream.

4.3.1 Error Resilience of H.264/AVC

Real-time two-way interactive applications such as video conferencing and video telephony have stringent delay requirements. Transmission errors due to for example, IP-packet loss events owing to statistical multiplexing, congestion at the routes and link-layer imperfections are difficult to avoid. Therefore, error resilient features have to be incorporated in the video coding standards [185]. Some of the error resilient features of H.264/AVC are briefly described below;

4.3.1.1 Flexible Macroblock Ordering

Flexible Macroblock Ordering (FMO) allows for the allocation of MBs to slices using various MB allocation maps, each allowing for different error resilient features [185]. Therefore, when using FMOs, MBs can be discrete cosine transformed and transmitted in an order out of the natural raster scan sequence.

4.3.1.2 Arbitrary Slice Ordering

Arbitrary Slice Ordering (ASO) allows the arbitrary decoding order of MBs within a slice. This achieves a reduced decoding delay in case of out of order delivery of NAL units caused by, for example, using different routes in the Internet [185].

4.3.1.3 Data Partitioning

Data Partitioning (DP) allows for the creation of up to three partitions per slice having different error sensitivity for transmission of coded information. In contrast to previous standards, where the coded information was partitioned into header and motion information, in H.264 the last partition is separated into intra-frame coded and inter-frame coded information. This provided unequal error protection for the different partitions based on their relative importance [194].

4.3.1.4 Intra MBs Update

The Intra MB update allow us to curtail error propagation in coded sequences due to packet loss or bit error events in the bit-stream, since the inclusion of image blocks in intra mode allows the prompt recovery from error propagation. H.264 also allows the intra-frame coding of MBs, which cannot be efficiently motion predicted. Furthermore, H.264 also allows us to perform the selection of intra-frame coded MBs either in a random fashion or using channel-adaptive rate distortion optimisation [186]. The employment of intra MB updates results in significant performance improvements, when the error rate is high. Generally speaking, channel adaptive intra-frame update results in more beneficial performance improvements than pure random intra-frame updates.

4.3.1.5 Redundant Coded Slices

Redundant coded slices may be transmitted to assist the decoder in eliminating the effects of errors in the corresponding primary coded picture. An example of this redundant coding technique is the Video Redundancy Coding (VRC) technique [195].

It is important to note that all these error resilient techniques generally result in an increased data rate for the coded video without improving the error-free video quality. Therefore, their application should always be carefully considered in the light of the compression efficiency. For further details on the features of the H.264 codec and for related system design principles please refer to [183].

4.3.2 History of H.264/AVC

A brief history of H.264/AVC codec is summarised in Table 4.3.

4.3.3 System Overview

The schematic of the proposed system is shown in Figure 4.5. We considered a rate-1/2 binary SECCC scheme of Section 3.2.1 as an example to evaluate its performance benefits relative to those of conventional RSC codes. Additionally, we considered the transmission of Gray-coded QPSK modulated symbols over correlated Rayleigh

Year	*Milestone*
2001	Video Coding Experts Group (VCEG) and Moving Picture Experts Group (MPEG) formed a Joint Video Team (JVT) to finalise the draft of the H.264/AVC video coding standard.
2003	ITU-T: H.264/AVC standard was recommended by JVT for all video applications, ranging from mobile services and video conferencing to IPTV, HDTV and HD video storage [193].
	Wiegand *et al*. [196] reviewed the technical features of the H.264/AVC standard, its history and its potential applications.
	Wenger [197] showed that the concepts of parameter sets, multiple slices, FMO and DP on the video coding layer of H.264/AVC significantly improves IP-based systems' performance.
	Stockhammer [186] proposed a range of error-resilient techniques for error prone wireless conversational services using H.264/AVC.
2004	Stockhammer and Bystrom [198] demonstrated that by appropriately partitioning the video bit-stream into different sensitivity classes and protecting them by different-rate codes the overall video performance may be substantially improved.
	Ostermann *et al*. [185] presented new tools, and characterized the features as well as the complexity of H.264/AVC. It was shown that coding tools of H.264/AVC allow for a bit-rate reduction of about 50% compared to MPEG-4 and MPEG-2, which come at the price of an increased complexity. However, the performance improvement of the associated VLSI circuitry meant that in 2004 H.264/AVC was deemed more implementable than MPEG-2 in 1994.
2006	Marpe *et al*. [199] proposed the so-called Fidelity Range Extensions (FRExt) for the H.264 standard.
	Chang *et al*. [200] conceived a novel low-complexity Unequal Error Protection (UEP) for the H.264/AVC-compressed bit-stream using adaptive hierarchical 16-QAM.
2007	Hanzo *et al*. [183] published a broad ranging research monograph on diverse aspects of video compression and communications.
2008	Liu *et al*. [187] designed a parallel concatenated coding scheme, where the variable-length coded (VLC) video was protected by a turbo code.
	Adrat *et al*. [188] proposed an optimised bit-rate allocation scheme using a rate-1 inner channel encoder along with 3 to 6-bit source mapping.
2009	Nasruminallah and Hanzo proposed Iterative Joint Source and Channel Decoding (JSCD) for the error-resilient transmission of the H.264 coded video stream [184].

Table 4.3: H.264/AVC advances.

fading channels. As shown in Figure 4.5, the video source signal is encoded using the H.264 video codec. The error resilient feature of slice structuring of video pictures in the H.264 codec was employed, which results in the partitioning of each video frame into multiple slices, each independently coded from the others. Additionally, we also incorporated DP, which results in three different sensitivity video coded streams per video slice, containing different coding elements and parameters. In our system setup, we organised each type of stream with multiple occurrence in each frame for the different slices, into a single stream of each type. Subsequently, the three streams are concatenated, to generate a single stream b_1 as shown in Figure 4.5, before being encoded using the SECCC encoder considered. The input of the self-concatenated encoder is interleaved using the bit-interleaver π_1 of Figure 4.5 to generate the bit-sequence b_2. The resultant bit-sequences b_1 and b_2 are parallel-to-serial converted, before they are fed to the RSC encoder. More specifically, we used a rate $R_1 = 1/2$ RSC encoder having generator polynomials of $g_r = 7$, $g_1 = 5$ and a memory of $\nu = 2$. The SECCC encoded bits are interleaved using the interleaver π_2 of Figure 4.5, in order to randomise the coded bits, and are subsequently punctured using the rate $R_2 = 1/2$ puncturer of Figure 4.5. The employment of puncturing results in an increased bandwidth efficiency η. Each of the puncturer blocks of Figure 4.5 punctures a single bit out of the two SECCC encoded bits. Hence the overall code rate R can be calculated from Eq. 3.1 as:

$$R = \frac{R_1}{2 \times R_2} = \frac{1}{2}\left(\frac{1}{2(\frac{1}{2})}\right) = \frac{1}{2}.$$

The resultant bits are then mapped to the QPSK symbol sequence x before transmission over the communication channel. At the receiver side the AWGN contaminated signal $y = hx+n$ is received, where h is the channel's non-dispersive fading coefficient and n is the AWGN having a variance of $N_0/2$ per dimension. The resultant signal is then fed into the soft-demapper in order to generate the conditional PDF given in Equation 3.3

$$P(y|x = x^{(m)}) = \frac{1}{\pi N_0}\exp\left(-\frac{\left|y - hx^{(m)}\right|^2}{N_0}\right),$$

of receiving x, provided that $x^{(m)}$ was transmitted, where $m \in \{0, 1, 2, 3\}$.

Then, the resultant soft-values are passed to a soft depuncturer, which converts them to bit-based LLRs and zero LLRs are inserted at the punctured bit positions. These LLRs are then deinterleaved and fed to the self-concatenated SISO MAP decoder of Figure 4.2 whose iterative procedure has been explained in Section 2.3.1. Self-concatenated decoding proceeds, until the affordable number of iterations is

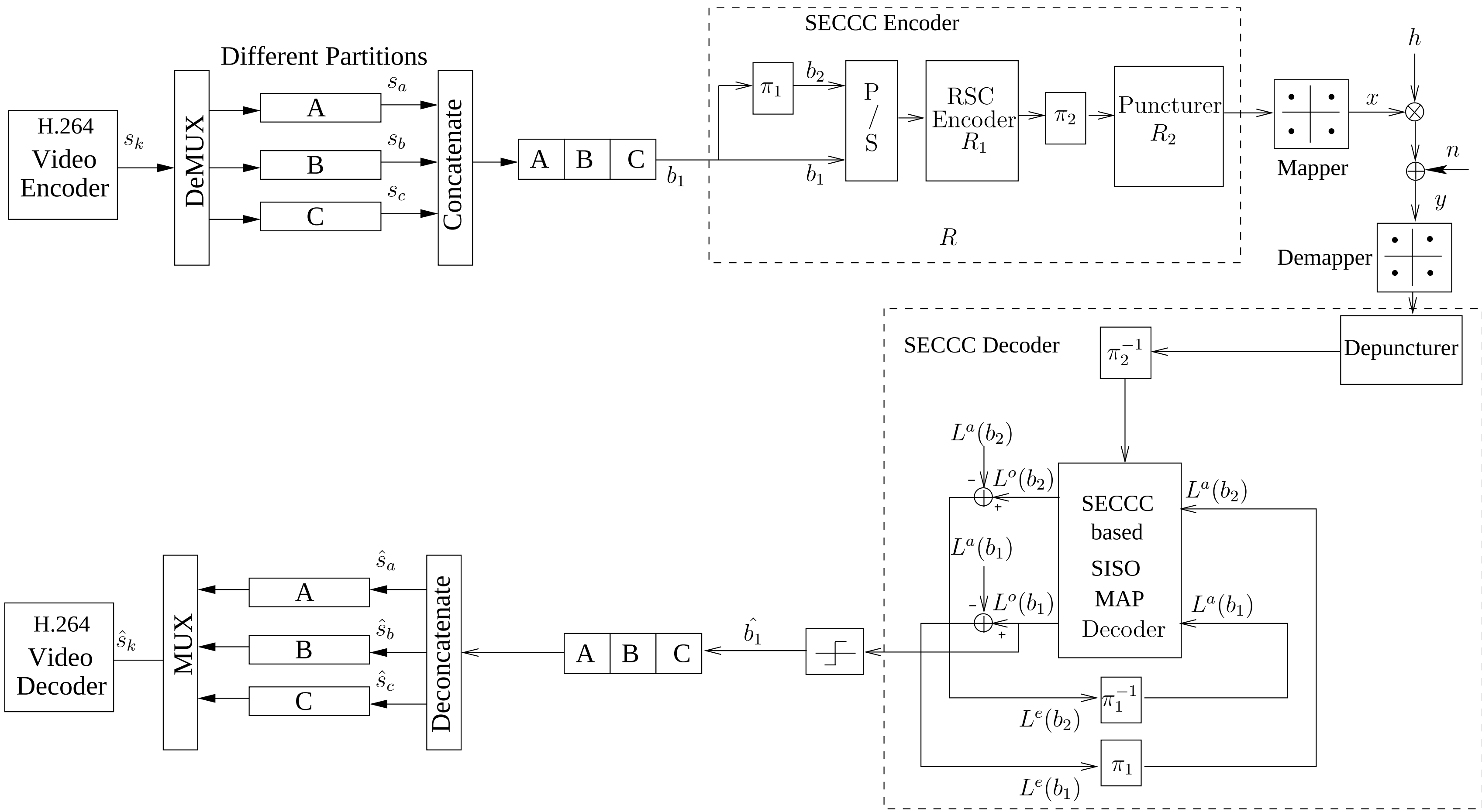

Figure 4.5: The proposed SECCC aided iterative system decoding model. The schematic incorporates the SECCC scheme of Figure 3.1. The H.264 video encoder passes the source coded bits to an SECCC encoder followed by an interleaver, a puncturer and a modulator. The receiver the received signal is passed through the demapper, depuncturer, de-interleaver and the SECCC decoder, followed by the H.264 video decoder. We can see that Figure 4.2 can be incorporated in the proposed schematic, hence new system architecture relying on the H.264/AVC, SECCC and UWB schemes emerges.

reached.

Table 4.4: Code rates for different Error Protection schemes

Error Protection Scheme	Code Rate		
	Outer Code	Inner code	Overall
SECCC Scheme	SECCC $R = \frac{1}{4}$	Puncturer $R_2 = \frac{1}{2}$	1/2
Benchmarker Scheme	RSC $R = \frac{1}{4}$	Puncturer $R_2 = \frac{1}{2}$	1/2

4.3.4 System Performance Results

In this section we present our performance results characterising the proposed system. We provided the video source signal generated by the H.264/AVC as input to our proposed system model of Figure 4.5. The performance of this system was evaluated for the *Akiyo* video test sequence represented in (176×144)-pixel Quarter Common Intermediate Format (QCIF) resolution. The test sequence was encoded using the H.264 codec at 15 frames-per-second (fps), with a target bitrate of 64 kbps. Various error resilient features of the H.264 video codec, such as the slice-based structure of the video frame and data partitioning DP were also exploited. Each frame was partitioned into 11 MBs per slice and there were 9 slices per QCIF frame. Additionally, intra-frame coded MB update of three randomly distributed MBs per QCIF frame was also incorporated, which associated us in avoiding avalanche like error propagation to the successive frames. Each intra or 'I' frame was followed by 44 predicted or 'P' frames, which curtailed error propagation beyond the 45-frame boundary. Therefore, the video sequence was refreshed with the aid of an 'I' frame after every 3-second interval. Additionally, the motion search was restricted to only the immediately preceding frame, in order to reduce the computational complexity of the video encoding/decoding process. For reasons of reduced computational complexity, we also avoided the insertion of bi-directionally predicted 'B' pictures, which would result in unacceptable loss of lip-synchronisation owing to its processing delay. Similarly, in order to keep the encoder's complexity realistic for the real-time videophone implementation, the error resilient FMO [186] was turned off, because it typically results in modest video performance improvements in low-motion video sequences, despite its substantial increase in computational complexity. Additional source codec parameters include the employment of quarter-pixel-accuracy motion estimation, intra-frame MB update and the use of Universal Variable Length Coding (UVLC) type entropy coding. The remaining system parameters of our experimental setup are listed in Table 4.5.

Table 4.5: Systems parameters

System Parameters	Value	System Parameters	Value
Source Coding	H.264/AVC	No of MB's/Slice	11
Source Bit-Rate	64Kbps	Intra-frame MB	3
Frame Rate	15fps	update/frame	
No of Slices/frame	9		
Inner module	Puncturer	Over-all Code Rate	1/2
Modulation Scheme	QPSK	Channel	Correlated
Number of	1		Rayleigh
Transmitter Antennas			Fading
Number of	1	Normalised	
Receiver Antennas		Doppler	0.01
Interleaver Length	≈ (128000/15)	Frequency	

The performance of the system was evaluated while considering $I_t = 10$ iterations within the joint SECCC system module. Additionally, for the sake of increasing the confidence in our results, we repeated each 45-frame video transmission experiment 200 times with a specific number of system iterations and averaged the results generated.

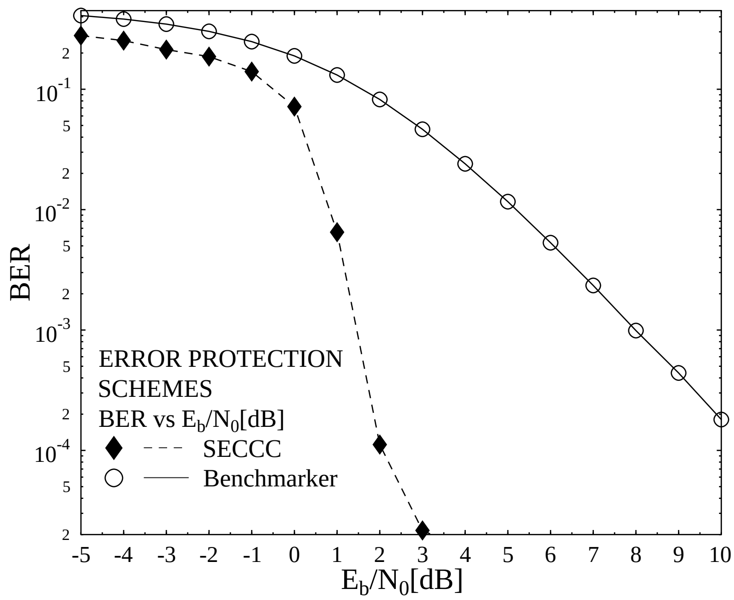

Figure 4.6: BER versus E_b/N_0 performance of the various error protection schemes summarised in Table 4.4. The system's schematic is seen in Figure 4.5.

The BER performance of the proposed error protection schemes is shown in Figure 4.6. It can be observed from Figure 4.6 that as expected, the SECCC scheme results in the best BER performance, when compared to the identical-rate RSC-coded benchmarker scheme.

Furthermore, the $PSNR$ versus E_b/N_0 curve of the proposed error protection

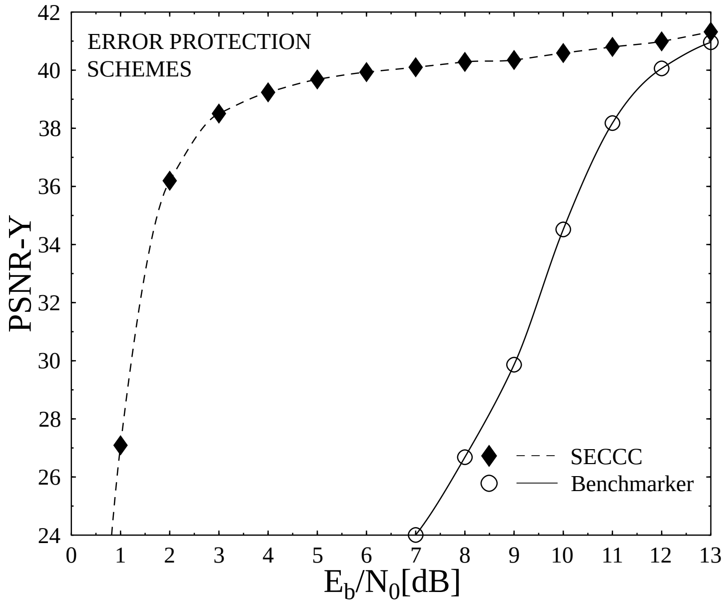

Figure 4.7: PSNR-Y versus E_b/N_0 performance of various error protection schemes summarised in Table 4.4. The system's schematic is seen in Figure 4.5.

schemes is portrayed in Figure 4.7. It may be observed in Figure 4.7 that the SECCC scheme employing $R_1 = 1/2$, $R_2 = 1/2$ and $I_t = 10$ iterations results in the best PSNR performance across the entire E_b/N_0 region considered. Quantitatively, when using the SECCC scheme of Table 4.4, an E_b/N_0 gain of upto 6 dB may be achieved relative to the RSC-coded benchmarker scheme at the PSNR degradation point of 2 dB, as shown in Figure 4.7 and summarised in Table 4.6.

Finally, the subjective video quality of the error protection schemes employed is characterised in Figure 4.8. In order to have a pertinent subjective video quality comparison, the video frames presented in Figure 4.8 were obtained by averaging

Figure 4.8: Subjective video quality of the 45^{th} "*Akiyo*" video sequence frame using SECCC Scheme (top) and Benchmarker scheme (bottom) summarised in Table 4.4 at E_b/N_0 values of (from left) 5 dB, 6 dB, 7 dB and 8 dB.

H.264/AVC System Parameters	Channel Code Paramaters	I_t	E_b/N_0 (dB) at 2 dB PSNR degradation
Table 4.5	**SECCC:** R_1=1/2, R_2=1/2, R=1/2, ν=2, QPSK, 3600 bits/frame 40 frame video repeated 200 times	10	6
Table 4.5	**RSC:** R_1=1/2, R_2=1/2, R=1/2, ν=2, QPSK, 3600 bits/frame 40 frame video repeated 200 times	0	12

Table 4.6: Performance of SECCC coded H.264/AVC scheme. The corresponding system schematic is seen in Figure 4.5 and the system parameters were summarised in Tables 4.4 and 4.5.

the results after the repeated transmission of both the luminance and chrominance components of the *Akiyo* video sequence 30 times. Observe from Figure 4.8 that an unimpaired video quality is attained by the SECCC scheme at an E_b/N_0 value of 5 dB. However, video impairment persist for the RSC-coded benchmarker scheme even at the relatively high E_b/N_0 values of 6 dB, 7 dB, and 8 dB, as shown in Figure 4.8.

4.4 Chapter Conclusions

The conclusive findings of the chapter are:

- We have designed near-capacity SECCC-ID schemes based on their decoding convergence analysis provided in Section 4.2. The SECCC-ID schemes designed are capable of operating within about 1 dB from the AWGN as well as Rayleigh fading channel's capacity, as detailed in Section 3.2.1. Based on this design, a near-capacity TH-PPM-UWB-IR system was proposed in Section 4.2, which invoked iteratively detected SECCCs and employed the powerful design technique of EXIT charts. The convergence behaviour of the decoder was analysed with the aid of bit-based EXIT charts. Finally, in Section 4.2.5 we proposed a novel TH-PPM-UWB-IR-SECCC system configuration, which is capable of operating within about 1.41 dB of the information-theoretic limits at a BER of 10^{-3}.

- Finally, we proposed a robust H.264 coded wireless video transmission scheme using an iteratively decoded SECCC. The performance of the system was evaluated using the H.264/AVC source codec for interactive video telephony. We demonstrate the efficiency of this approach by showing that the video quality was significantly improved, when using the binary SECCC scheme. More explicitly, the proposed system exhibits an E_b/N_0 gain of 6 dB at the PSNR degradation point of 2 dB in comparison to the identical-rate benchmarker carrying out RSC coding and puncturing, while communicating over correlated Rayleigh fading channels.

4.5 Chapter Summary

Based on the design of the SECCCs of Section 3.2.1, in Section 4.2 we constructed an iteratively decoded near-capacity TH-PPM-UWB-IR-SECCC system using EXIT charts. More explicitly, the powerful tool of EXIT charts was used to appropriately select the coding rates of the SECCCs in order to shape the inverted EXIT curve of the TH-PPM-UWB-IR-SECCC system and hence to match it to that of the inner decoder for the sake of achieving an infinitesimally low BER at near-capacity SNR values. The associated iterative decoding convergence behaviour was characterized by EXIT charts. In Figure 4.4 of Section 4.2.5 we demonstrated that Code 1 of memory $\nu = 3$ proposed in the TH-PPM-UWB-IR-SECCC design of Figure 4.2 became capable of performing within about 1.41 dB of the Nakagami-m fading channel's capacity at a BER of 10^{-3}, as seen in Figure 4.4. By contrast, Code 2 having the same memory length is about 1.82 dB away from the Nakagami-m fading channel's capacity as seen in Figure 4.4.

Additionally, in this system design study we used the low complexity iteratively decoded binary self-concatenated codes of Figure 3.1, involving only a single encoder and a single decoder for the transmission of the source coded stream. This technique is suitable for low-complexity video-telephony, which requires a low transmission power. Furthermore, the practically achievable interactive video performance trends were quantified, when using state-of-the-art video coding techniques, such as H.264/AVC.

In Table 4.6 we have summarised the achievable performance improvement attained by the H.264/AVC codec using SECCC in comparison to the identical-rate state-of-the-art benchmarker scheme. Explicitly, we observed in Figure 4.7 that an E_b/N_0 gain of 6 dB was attained using SECCC in comparison to the identical-rate state-of-the-art benchmarker.

Chapter 5

Distributed Self-Concatenated Coding for Cooperative Communications

5.1 Introduction

In this chapter, we propose a Distributed Binary Self-Concatenated Coding scheme using Iterative Decoding (DSECCC-ID) for cooperative communications, which is designed with the aid of binary EXIT charts using the SECCCs of Chapter 3.

The research of MIMO wireless systems has recently attracted considerable attention [15, 19, 20, 84, 201]. The wireless communication systems of future generations are required to provide reliable transmissions at high data rates in order to offer a variety of multimedia services to commercial and private customers. In order to improve their performance by attaining a high diversity gain requires that the channel impulse response of the different transmit and the receive antenna remain uncorrelated or statistically independent. This is possible if the antenna spacing is sufficiently large so that the assumption of statistical independence of the different paths from the different antennas is justified. In case of colocated MIMO elements multiple antennas at the transmitter and receiver are connected physically to the same mobile station (MS)/device. However, the assumption of sufficient antenna spacing may be impractical for shirt-pocket-sized wireless devices, which are typically limited in size and hardware complexity to a single transmit antenna. Space time coding schemes [202], which employ multiple transmitters and receivers, are among the most efficient techniques designed for achieving a high diversity gain, again, provided that the associated MIMO channels [143, 203] experience independent fading.

5.1.1 Cooperative Communications

The philosophy of cooperative communications was recently introduced for the sake of attaining spatial diversity, where it is typically possible to guarantee the required spatial separation of the transmit antennas. This is due to the fact that the different antennas belong to different MSs, which are assumed to be far enough to attain statistically independent fading from the different antennas. Therefore, since the signals transmitted from different users undergo independent fading, spatial diversity can be achieved with the aid of the cooperating partners' antennas. Utilising cooperative techniques eliminates the correlation of the signals when creating a Virtual Antenna Array (VAA) from the single antennas of the mobiles which would be imposed by the limited affordable element-spacing of co-located MIMO elements.

Traditional direct transmission has its shortfalls, because when the MS roams at the hinge of the coverage region of the cell to another cell while a conversation is in progress, initiating a handoff might not be possible due to the unavailability of unused channels or the lack of sufficient signal level at the adjacent cell in order to initiate a handoff. The call may be dropped in that scenario. Cooperative communication comes to our help in this case. It can extend the coverage area of a cell by creating an alternative transmission path from the MS to the base station (BS) via the introduction of a relay, as shown in Figure 5.1. Another advantage of this is the creation of independent paths between the MS and the BS namely the direct path between the two and the one via the relay.

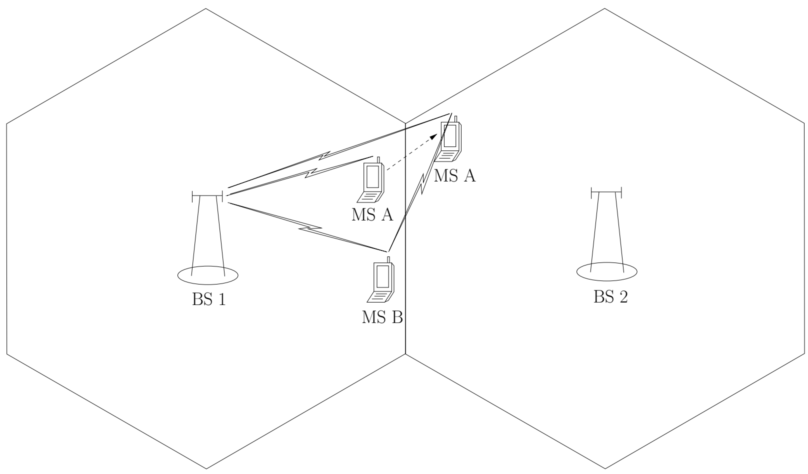

Figure 5.1: An example of a cooperative communication scenario, © Liu *et al.* [16], 2009.

There are various protocols that may be implemented at the relay channel. These can generally be organised into two families of schemes [16]:

- Fixed relaying;
- Adaptive relaying.

In fixed relaying schemes the channel resources are shared between the source and the relay in a time-invariant manner. They can be further divided into four categories [16, 204]:

- Amplify-And-Forward (AAF) [205];
- Decode-And-Forward (DAF) [205];
- Compress-And-Forward (CAF) [206, 207];
- Coded Cooperation [208].

The AAF scheme relies on a relay, which amplifies the received signal and then transmits it to the destination. Although the noise also gets amplified alongwith the signal, we still gain spatial diversity by transmitting the signal over two spatially independent channels. The DAF scheme has a relay which decodes the received signal transmitted by the source, re-encodes it and then forwards it to the destination, which combines all the copies in a proper way. In CAF relaying the relay transmits a quantised and compressed version of the received signal in the form of source encoded symbols. At the destination, the source encoded i.e. compressed version of the relay's transmitted signal is decoded by mapping the received bits into a set of values that estimate the source's transmitted message and then combined with the message directly received from the source. Finally, in coded cooperation incremental redundancy is introduced by the relay, which is then combined at the destination with the codeword sent by the source, resulting in a codeword benefitting from an increased amount of redundancy. While in some codes the information and redundancy are encoded in such a way that they are inseparable and only complete decoding can separate them, some redundancy can be removed from the codeword in the case of punctured concatenated codes.

Major cooperative communications techniques have been outlined in Tables 5.1 and 5.2. The basic idea behind cooperative communications can be traced back to the philosophy of the relay channel, which was introduced in 1971 by van der

Year	*Milestone*
1971	van de Meulen [209] introduced a simple relay channel modeled by three terminals: a source, a destination and a relay. He studied the problem of transmission of information as effectively as possible from the source to the destination assuming that the relay cooperate in the transmission process [210].
1979	Cover and El Gamal [206] provided a thorough capacity analysis of the full-duplex relay channel.
1998	Sendonaris *et al*. [211] generalised the relay model to multiple nodes that transmit their own data as well as serve as relays for each other.
2002	Hunter *et al*. [208] introduced coded cooperation to achieve diversity in which the idea of cooperation was combined with the classic error-control-coding.
	Dohler *et al*. [212] introduced the concept of virtual antenna arrays that emulates Alamouti's STBC for single-antenna-aided cooperating users.
2003	Sendonaris *et al*. [213, 214] presented a simple user-cooperation diversity based algorithm, where a cooperative CDMA system is implemented.
	Laneman *et al*. [215] developed different cooperative diversity protocols for exploiting spatial diversity in a cooperation scenario.
	Valenti and Zhao [216, 217] proposed a turbo coding scheme in a relay network.
2004	Laneman *et al*. [205] developed cooperative diversity protocols and compared the performance of DAF, AAF, selection relaying and incremental relaying in terms of their outage behaviour.
	Nabar *et al*. [218] analysed the spatial diversity performance of various signalling protocols.
	Janani *et al*. [17] presented two extensions to the coded cooperation framework [208]: increased the diversity of coded cooperation via ideas borrowed from space-time codes and applied turbo codes in the proposed relay framework.
	Stefanov *et al*. [219] analysed the performance of channel codes that are capable of achieving the full diversity provided by user cooperation in the presence of noisy interuser channels.
2005	Azarian *et al*. [220] proposed cooperative signalling protocols that are capable of striking an attractive diversity-multiplexing tradeoff.
	Sneessens *et al*. [221] proposed a soft decode-and-forward signalling strategy that can outperform the conventional DAF and AAF.
	Hu *et al*. [222] advocated Slepian-Wolf cooperation that exploits distributed source coding in wireless cooperative communication.
	Yu [223] compared the AAF and DAF signalling schemes in practical scenarios.
	Kramer *et al*. [207] addressed the information-theoretic aspects and considered DAF and CAF schemes for the wireless relay channels with many relays.

Table 5.1: Major cooperative communications techniques (1971-2005).

Year	*Milestone*
2006	Hunter *et al*. [224, 225] further developed the idea of coded cooperation [208] by computing BER and FER bounds as well as the outage probability of coded cooperation.
	Li *et al*. [226] employed soft information relaying in a BPSK modulated relay aided system employing turbo coding.
	Hu *et al*. [227] proposed Wyner-Ziv cooperation as a generalisation of the Slepian-Wolf cooperation [222] combined with a compress-and-forward signalling strategy.
	Hϕst-Madsen [228] derived upper and lower bounds for the capacity of four-node ad hoc networks having two transmitters and two receivers using cooperative diversity.
2007	Bui *et al*. [229] proposed soft information relaying where the relay's LLR values are quantised, encoded and superimposed, before being forwarded to the destination.
	Khormuji *et al*. [230] improved the performance of the conventional DAF strategy by employing constellation rearrangement in the source and the relay.
	Bao *et al*. [231] combined the benefits of AAF as well as DAF and proposed a new signalling strategy referred to as decode-amplify-forward.
	Xiao *et al*. [232] introduced the concept of network coding in cooperative communications.
2008	Yue *et al*. [233] compared the multiplexed coding and superposition coding in the coded cooperation system.
	Zhang *et al*. [234] proposed a distributed space-frequency coded cooperation scheme for communication over frequency-selective channels.
	Wang *et al*. [235] introduced the complex field network coding approach that can mitigate the throughput loss in conventional cooperative signalling schemes and attain full diversity gain.
2009	Hanzo *et al*. [15] presented low-complexity cooperative MIMO codes and distributed turbo codes designed for two users cooperating for the sake of improving their attainable BER performance.
	Liu *et al*. [16] authored a book on cooperative communications and networking.

Table 5.2: Major cooperative communications techniques (2006-2009).

Meulen [209]. Although full-duplex relaying and the associated capacity theorem derived for the discrete memoryless relay channel model have been proposed by Cover and El Gamal [206], practical cooperative diversity schemes were only proposed much later in [205, 213, 236, 237]. In [211] Sendonaris *et al.* generalised the conventional relay model, where there is one source, one relay and one destination, to multiple nodes that transmit their own data as well as serve as relays for each other. The scheme of [211] was referred to as "user cooperation diversity". Sendonaris *et al.* presented in [213, 214] a simple user-cooperation methodology based on a DAF signalling scheme using CDMA. Terminologies other than cooperative diversity Dohler *et al.* [212] introduced the concept of VAAs that emulates Alamouti's STBC for single-antenna-aided cooperating users. Space-time coded cooperative diversity protocols for exploiting spatial diversity in a cooperative scenario were proposed in [215]. In practice, each mobile collaborates with a single or a few partners for the sake of reliably transmitting both its own information and that of its partners jointly, which emulates a virtual MIMO scheme.

Cooperative communications have been shown to offer significant performance gains in terms of various performance metrics, including improved diversity gains [205, 215, 238] as well as multiplexing gains [220]. Hunter *et al.* [208] proposed the novel philosophy of coded cooperation schemes, which combine the idea of cooperation with the classic channel coding methods. Its extension to the framework of coded cooperation was presented in [17], where the diversity gain of coded cooperation was increased with the aid of ideas borrowed from the area of space-time codes. Additionally, a turbo coded scheme was proposed in [17] in the framework of cooperative communications. Furthermore, the analysis of the performance benefits of channel codes in a coded cooperation aided scenario was performed in [219]. Laneman *et al.* proposed fixed (DAF and AAF), selection and incremental relaying protocols and compared them in [205].

Recently, there have been substantial research interests in the idea of soft relaying, where the relay passes soft information to the destination. In [221], it was argued that the DAF signalling loses soft information and hence, it was proposed to use soft DAF signalling, where all operations are performed using the LLR based representation of soft information. It was shown in [221] that the soft DAF philosophy outperforms the DAF and the AAF signalling strategies. In [229] soft DAF was also used, where the soft information was quantised, encoded and superimposed before transmission to the destination. In [226] soft information based relaying was employed in a turbo coding scheme, where the relay derives parity checking BPSK symbol estimates for the received source information and forwards the symbols to the destination. In [221, 226, 229] soft information relaying has been used, where it was shown that soft DAF attains a better performance than hard DAF. Furthermore, in [222, 227] distributed source coding techniques have been adopted for employment in wireless cooperative communications in order to improve the attainable performance.

5.1.2 Distributed Coding Techniques

Distributed coding [239] constitutes another attractive cooperative diversity technique, where joint signal design and coding are invoked at the source and relay nodes. Distributed turbo codes [17, 217] have also been proposed for cooperative communications, although typically under the simplifying assumption of having a perfect communication link between the source and the relay nodes. These are half-duplex relay-aided systems, where the source transmits to both the relay and destination during the first transmission period and after decoding the information from the source the relay re-encodes it and sends it to the destination in the second transmission period. Hence half-duplex systems do not suffer from multi-access interference, which results in a simplified receiver structure at the cost of halving the spectral efficiency. As a more realistic design alternative, a turbo coded cooperation aided system having an imperfect source-relay (SR) communication link has been proposed in [240, 241]. In [240] the source node continues its transmission of the rest of the codeword in the second transmission period with the aim of achieving an improved bandwidth efficiency. Still referring to [240], the signals arriving from the source and relay are superimposed at the destination, where a *Maximum A Posteriori Probability* (MAP) detector and a turbo decoder exchange extrinsic information which were shown to be capable of operating near the capacity of ergodic flat fading channels. The scheme proposed in [241] considers a more complex irregular Low-density parity-check (LDPC) coded near-capacity system designed using EXIT charts and a design-procedure similar to that of [240]. It is demonstrated in [15, 242] that in the presence of Rayleigh fading, DAF cooperation-assisted systems are expected to outperform their non-cooperative counterparts. However an error floor is observed in [15] which can be mitigated by using soft-relaying [221, 226].

Against this background, the novelty and rationale [7, 8] of this chapter can be summarised as follows:

1. *In our proposed half-duplex relaying system the source-destination (SD) link employs a SECCC code, while the relay node employs simple RSC encoder in-*

stead of SECCC encoder. Therefore, the iterative decoding at the destination exchanges information between the SECCC MAP decoder and an RSC MAP decoder.

2. *The source employs a SECCC encoder, which reuses the same component instead of having two separate constituent codes. First SECCC iterative decoding is employed at the relay, which then re-encodes the decoded symbols by a low-complexity RSC encoder.*

3. *The relay frame is shorter than the source frame because of the puncturing of the systematic bits. Hence, the overall throughput is higher.*

4. *The motivation for using the proposed 3-stage decoder architecture is to effectively reduce the error-floor documented in Figs. 15.6-15.10 of [15] for the conventional two-stage architecture of Fig. 15.3 in [15].*

5. *The proposed scheme is designed by a systematic and widely applicable procedure using EXIT charts.*

6. *The SR link is imperfect, yet this simplified scheme is capable of approaching capacity.*

7. *We derive the theoretical lower and upper bounds on the Continuous-input Continuous-output Memoryless Channels's (CCMC) capacity as well as of the Discrete-input Continuous-output Memoryless Channels's (DCMC) [143, 160, 206, 243] capacity (constrained information rate) for independent and uniformly distributed (i.u.d.) sources.*

5.2 DSECCC-ID System Overview

The schematic of a two-hop half-duplex relay-aided system is shown in Figure 5.2, where the source node (s) transmits a frame of coded symbols $\mathbf{x}_s$ to both the relay node (r) and the destination node (d) during the first transmission period T_1, while the relay node first decodes the information, then re-encodes it and finally transmits a frame of coded symbols $\mathbf{x}_r$ to the destination node during the second transmission period T_2. In the time-division multiple access (TDMA) protocol used, the source transmits to both with the relay and destination during T_1, while in T_2, only the relay transmits to the destination. Hence, this protocol was termed as exhibiting degree-2 of broadcasting and no receive collision in [218]. The communication links

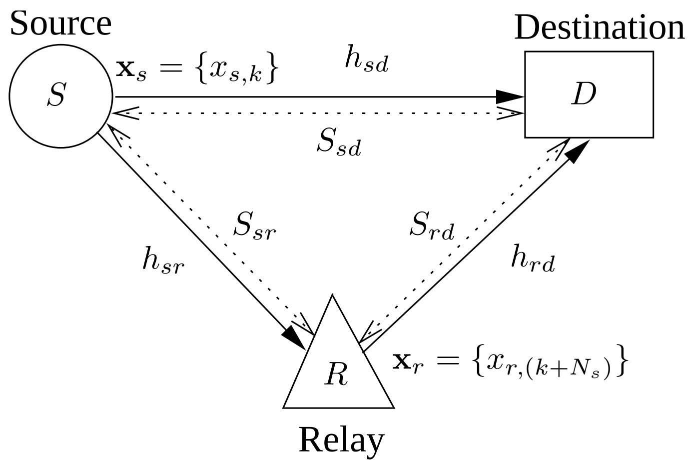

Figure 5.2: Schematic of a two-hop relay-aided system, where S_{ab} is the geographical distance between node a and node b.

seen in Figure 5.2 are subject to both free-space path loss as well as to short-term uncorrelated Rayleigh fading.

Let S_{ab} denote the geometrical distance between nodes a and b. The path loss between these nodes can be modelled by [216, 237]:

$$P(ab) = K/S_{ab}^{\alpha} \ , \tag{5.1}$$

where K is a constant that depends on the environment and α is the path loss exponent. For a free-space path loss model we have $\alpha = 2$. The relationship between the energy E_{sr} received at the relay node and that of the destination node E_{sd} can be expressed as:

$$E_{sr} = \frac{P(sr)}{P(sd)} E_{sd} = G_{sr} E_{sd} \ , \tag{5.2}$$

where G_{sr} is the power-gain (or geometrical gain) [237] experienced by the SR link with respect to the SD link as a benefit of its reduced distance and path loss, which can be computed as:

$$G_{sr} = \left(\frac{S_{sd}}{S_{sr}} \right)^2 \ . \tag{5.3}$$

Similarly, the power-gain for the relay-destination (RD) link with respect to the SD link can be formulated as:

$$G_{rd} = \left(\frac{S_{sd}}{S_{rd}} \right)^2 \ . \tag{5.4}$$

Naturally, the power-gain of the SD link with respect to itself is unity, i.e. $G_{sd} = 1$.

The kth received signal at the relay node during the first transmission period T_1, where N_s number of symbols are transmitted from the source node, can be written as:

$$y_{r,k}^{(T_1)} = \sqrt{G_{sr}}\; h_{sr,k}^{(T_1)}\; x_{s,k} + n_{r,k}^{(T_1)}\;, \tag{5.5}$$

where $k \in \{1, \ldots, N_s\}$ and $h_{sr,k}^{(T_1)}$ is the complex-valued Rayleigh fading channel coefficient between the source and the relay at instant k, while $n_{r,k}^{(T_1)}$ is the zero-mean complex AWGN having a variance of $N_0/2$ per dimension. By contrast, the kth symbol received at the destination during the period T_1, can be expressed as:

$$y_{d,k}^{(T_1)} = \sqrt{G_{sd}}\; h_{sd,k}^{(T_1)}\; x_{s,k} + n_{d,k}^{(T_1)}\;, \tag{5.6}$$

where $h_{sd,k}^{(T_1)}$ is the complex-valued Rayleigh fading channel coefficient between the source and the destination at instant k, while $n_{d,k}^{(T_1)}$ is the AWGN having a variance of $N_0/2$ per dimension. Similarly, the lth symbol received at the destination during the second period T_2, where N_r number of symbols are transmitted from the relay node, is given by:

$$y_{d,l}^{(T_2)} = \sqrt{G_{rd}}\; h_{rd,l}^{(T_2)}\; x_{r,l} + n_{d,l}^{(T_2)}\;, \tag{5.7}$$

where $l \in \{1 + N_s, \ldots, N_r + N_s\}$ and $h_{rd,l}^{(T_2)}$ is the complex-valued Rayleigh fading channel coefficient between the relay and the destination at instant l, while $n_{d,l}^{(T_2)}$ is the AWGN having a variance of $N_0/2$ per dimension.

5.2.1 DSECCC-ID Encoder

In our DSECCC-ID scheme, we consider a Quadrature Phase-Shift Keying (QPSK)-assisted SECCC encoder of Section 3.2.1 at the source as well as a QPSK-assisted RSC encoder at the relay. To elaborate a little further, we use an RSC encoder instead of a SECCC encoder at the relay, because we found in our informal investigations not included here that it is sufficient for the relay to transmit only the parity bits during the second transmission period to ensure that the systematic bits are transmitted only once to the destination. This is a plausible design choice, because it is in general more beneficial to transmit extra parity information to the destination, than several replicas of the original information bits. As seen in Figure 5.3 the relay detects the signals received from the source node using a SECCC scheme during the first transmission period. The notation π_r in Figure 5.3 denotes the random bit interleaver used at the relay to interleave the decoded bits before the RSC encoding. The encoders employed at both the source and relay transceiver nodes can be viewed as a three-component parallel-concatenated SECCC encoder[1], which is depicted in Figure 5.3.

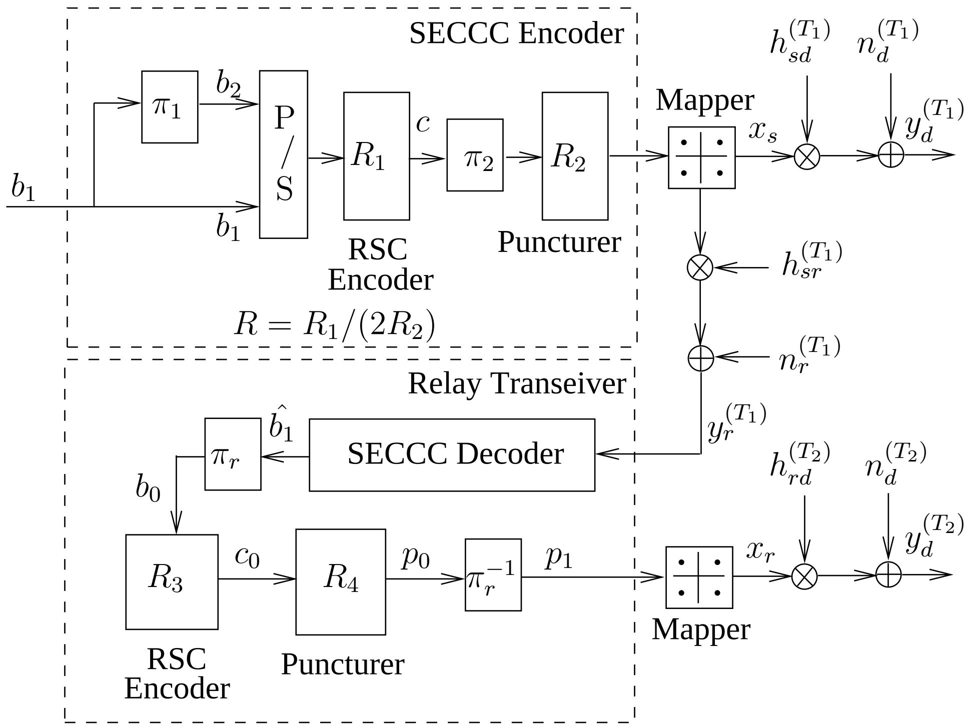

Figure 5.3: The schematic of the three-component arrangement using the self-concatenated encoder of Figure 3.1. This figure applies to the DSECCC-ID scheme, when the relay decodes the received symbols using the SECCC decoder of Figure 3.1 and then forwards the decoded symbols to the destination in the second phase.

The notation x_r used in Figure 5.3 denotes the 2-bit QPSK symbol at the relay node. The puncturer denoted as R_4 in Figure 5.3 is used to improve the overall throughput of the scheme. We found that a good performance can be achieved by transmitting only the parity bits generated at the output of the RSC encoder at the relay node.

At the source node we consider a rate $R = 1/3$ SECCC scheme of Section 3.2.1 operating close to uncorrelated Rayleigh fading channel's capacity and employing QPSK modulation. As shown in Figure 5.3 and discussed in Section 3.2.1, the input bit sequence $\{b_1\}$ of the self-concatenated encoder is interleaved for yielding the bit sequence $\{b_2\}$. The resultant bit sequences are parallel-to-serial converted and then fed to the RSC encoder having a rate of $R_1 = 1/2$. This stream is then passed through an interleaver and then a rate $R_2 = 3/4$ puncturer, as seen in Figure 5.3. Hence, the overall code rate evaluated from Equation 3.1 becomes $R = 1/3$. These bits are then mapped to a QPSK symbol as $x = \mu(c_1c_0)$, where $\mu(.)$ is the bit-to-symbol

[1]An SECCC encoder can be viewed as a two-component parallel-concatenated encoder [4]

mapping function. Hence the bandwidth efficiency is given by $\eta = R \times \log_2(4) =$ 0.67 bits/symbol (bps), assuming a zero Nyquist roll-off-factor. The QPSK symbol x_s is then transmitted over the channel. The overall throughput of this two-hop cooperative scheme can be formulated as:

$$\eta \;=\; \frac{N_i}{N_s + N_r}\ [\text{bps}]\ , \tag{5.8}$$

where N_i is the number of information bits transmitted within a duration of (N_s+N_r) symbol periods. Again, N_s is the number of modulated symbols per frame transmitted from the source node and N_r is the number of modulated symbols per frame arriving from the relay node. For our case we have $N_i = 120{,}000$ bits. Therefore, we transmit $N_s = 180{,}000$ symbols. Note that the number of symbols per transmission burst at the relay node is given by $N_r = 60,000$ due to the employment of QPSK modulation and a rate $R_4 = 1/2$ puncturer that removes all systematic bits from the output of the RSC encoder of rate $R_3 = 1/2$. Hence, the overall effective throughput of the DSECCC-ID scheme is given by $\eta = (N_i)/(N_s + N_r) = 0.5$ bps. The Signal to Noise Ratio (SNR) per bit is given by $E_b/N_0 = \text{SNR}/\eta$. Hence, the DSECCC-ID scheme suffers from a penalty of 1.25 dB in terms of E_b/N_0, when compared to the conventional SECCC scheme having a somewhat higher throughput of 0.67 bps.

5.2.2 DSECCC-ID Decoder

The novel decoder structure of the DSECCC-ID scheme is illustrated in Figure 5.4. The notations $P(.)$ and $L(.)$ in Figure 5.4 denote the logarithmic-domain symbol probabilities and the Logarithmic-Likelihood Ratio (LLR) of the bit probabilities, respectively. The notations b and c in the round brackets (.) denote information bits and coded bits, respectively. The specific nature of the probabilities and LLRs is represented by the subscripts a, o and e, which denote in Figure 5.4, *a priori*, *a posteriori* and *extrinsic* information, respectively.

For the SECCC decoder of Figure 3.1 in Chapter 3, denoted by (1) in Figure 5.4, the received signal arrives at the soft demapper. This signal is then used by the demapper for calculating the conditional probability density function (PDF) of receiving $\mathbf{y}_d^{(T_1)}$, when $\mathbf{x}_s$ was transmitted, yielding:

$$p(\mathbf{y}_d^{(T_1)}|\mathbf{x} = \mathbf{x}_s^m) = \frac{1}{\pi N_0} \exp\left(-\frac{\left|\mathbf{y}_d^{(T_1)} - \mathbf{h}_{sd}^{(T_1)}\mathbf{x}_s^m\right|^2}{N_0}\right), \tag{5.9}$$

where $\mathbf{x}_s^m = \mu(c_1c_0)$ is the hypothetically transmitted QPSK symbol for $m \in \{0,1,2,3\}$, $\mathbf{h}_{sd}$ is the channel's non-dispersive fading coefficient and $\mathbf{n}_d$ is the AWGN having a

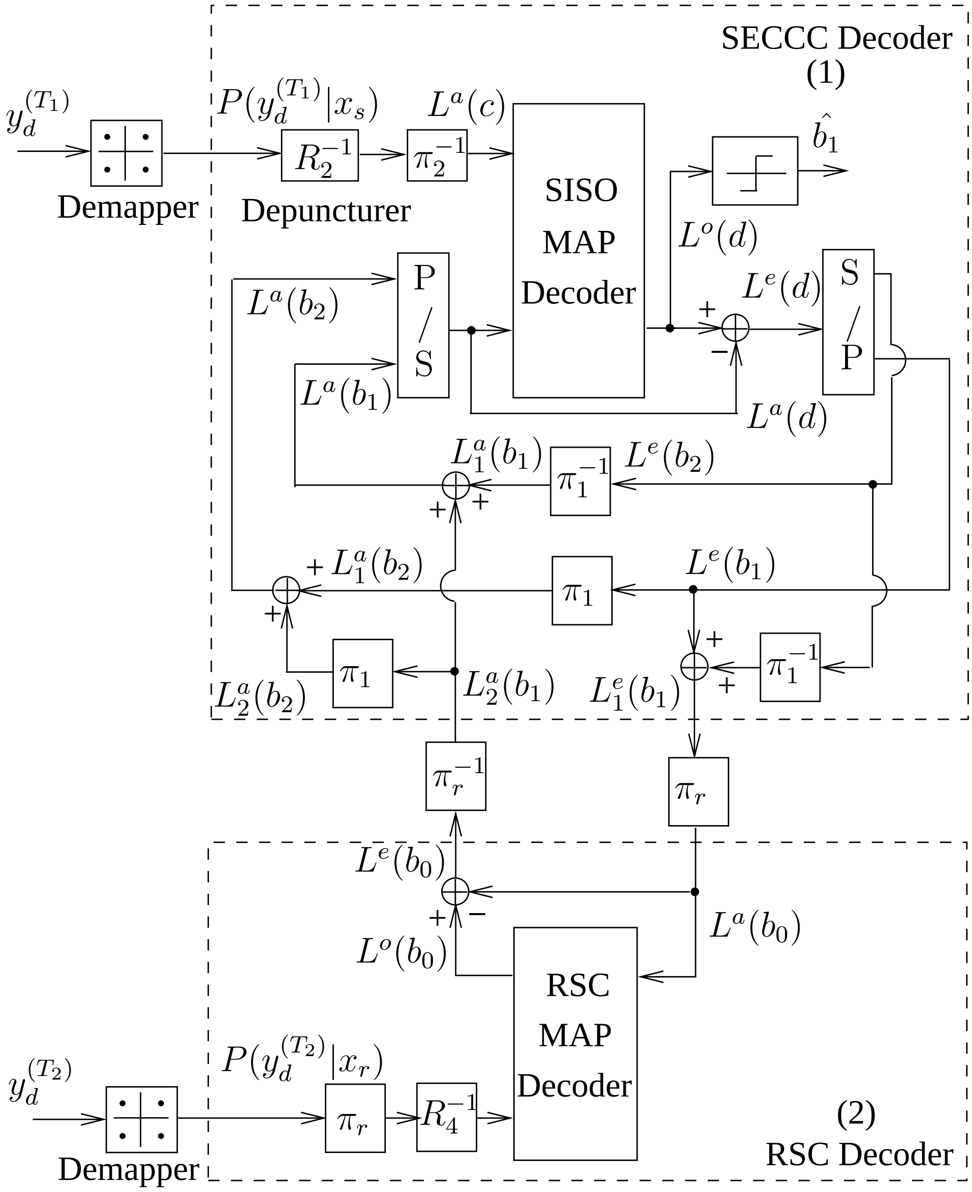

Figure 5.4: The schematic of the DSECCC-ID decoder. Note that the SECCC decoder is a modified version of the decoder of Figure 3.1 in order to make it capable of exchanging extrinsic information with the RSC decoder. The input of the SECCC decoder is generated by the QPSK demapper for the SD link, while the input of the RSC decoder is output by the QPSK demapper of the RD link.

variance of $N_0/2$ per dimension. The received signal that arrives at the soft demapper of the SECCC decoder (1) is given in Equation 5.9, while the received signal that arrives at the soft demapper of the RSC decoder, denoted by (2) in Figure 5.4 is used for calculating the conditional probability density function (PDF) of receiving $\mathbf{y}_d^{(T_2)}$, when $\mathbf{x}_r$ was transmitted, yielding:

$$p(\mathbf{y}_d^{(T_2)}|\mathbf{x} = \mathbf{x}_r^m) = \frac{1}{\pi N_0} \exp\left(-\frac{\left|\mathbf{y}_d^{(T_2)} - \mathbf{h}_{rd}^{(T_2)} \mathbf{x}_r^m\right|^2}{N_0} \right). \tag{5.10}$$

The bit probabilities are then passed through a soft depuncturer, which converts them to the corresponding bit-based LLRs and subsequently inserts zero LLRs at the punctured bit positions. The LLRs are then deinterleaved and fed to the Soft-Input Soft-Output (SISO) MAP decoder [102]. The decoder of Figure 5.4 is a self-concatenated decoder, which can be viewed as a three-component parallel-concatenated decoder, which first calculates the extrinsic LLRs of the information bits, namely $L^e(b_1)$ and $L^e(b_2)$. Then they are appropriately interleaved to yield the *a priori* LLRs of the information bits, namely $L^a(b_1)$ and $L^a(b_2)$, as shown in Figure 5.4. Self-concatenated decoding proceeds, until a fixed number of iterations is reached.

There are two inputs to the RSC MAP decoder block, which is denoted by (2) in Figure 5.4. The first is the extrinsic information of bit b_1 provided by the SECCC decoder, which is denoted by (1). As seen in Figure 5.4 this is obtained from the addition of $L^e(b_1)$ and the deinterleaved version of $L^e(b_2)$. The resultant $L_1^e(b_1)$ stream is interleaved by π_r to generate $L^a(b_0)$. The second input of the RSC MAP decoder (2) is the interleaved and depunctured version of the soft information provided by the QPSK demapper denoted as $P(y_d^{T_2}|x_r)$ in Figure 5.4. The RSC decoder of the relay seen in Figure 5.4 then provides the improved extrinsic LLR of the data bit b_0 namely $L^e(b_0)$ as its output, which is deinterleaved by π_r^{-1} to yield $L_2^a(b_1)$. The LLR $L_2^a(b_1)$ can be further interleaved using π_1 to generate $L_2^a(b_2)$. These *a priori* LLRs output by the RSC can be added to the SECCC decoder's *a priori* LLRs of b_1 and b_2, thus completing the iteration between the RSC and SECCC decoders.

It has been shown in [4] that an SECCC scheme may be viewed as two parallel-concatenated codes separated by an odd-even turbo interleaver. Hence the SECCC Decoder (1) of Figure 5.4 employed at the destination may be viewed as a two-component PCCC decoder, which exchanges extrinsic information with another parallel-concatenated RSC Decoder (2) as shown in Figure 5.4. Therefore, our proposed scheme can be viewed as a three-component parallel-concatenated scheme.

5.3 Design and Analysis

Similarly to the SECCC schemes of Section 3.2.1, we design and analyse the proposed scheme using EXIT charts in Section 5.3.1. Furthermore, the relay-aided system capacity is detailed in Section 5.3.2.

5.3.1 EXIT Chart Analysis

As argued in Section 3.2.2, binary EXIT charts are useful for finding the best SECCC schemes for having a decoding convergence at the lowest possible SNR value. The EXIT curves of the SECCC decoder components and a corresponding decoding trajectory were recorded for the binary SECCC schemes operating closest to the Rayleigh fading channel's capacity [2]. Since in case of SECCCs there are identical components, we only have to compute the EXIT curve of a single component and the other is its mirror image [2]. The EXIT curves of the two hypothetical decoder components are plotted within the same EXIT chart together with their corresponding decoding trajectory for the sake of visualizing the exchange of extrinsic information between the decoders. These were recorded by using 10 transmission frames, each consisting of 24×10^3 information bits for calculating the EXIT curve, while we consider a frame size of 120×10^3 information bits for calculating the decoding trajectories[2].

Our three-step design procedure using EXIT charts developed for the proposed distributed coded system is as follows:

Step 1:

Our code design procedure commences by calculating the decoding convergence of the SECCC scheme at the output of the communication link between the SR link, using EXIT charts. We found in Section 3.2.3 that the near-capacity QPSK-assisted SECCC scheme employs $R_1 = 1/2$, $R_2 = 3/4$ having $\eta = 0.67$ bps. As seen in Figure 5.5, we compare the SECCC scheme using $\nu = 2$ and $\nu = 3$ at a receive SNR of about -0.15 dB. For the $\nu = 3$-SECCC code a receive SNR of about -0.15 dB is needed in order to attain a decoding convergence to the (1,1) point of the EXIT chart, since at a receive SNR of -0.2 dB the EXIT-tunnel remains closed. By contrast, the EXIT tunnel for the $\nu = 2$-SECCC code, employing the generator polynomial

[2]We need large interleaver sizes for the trajectories to match the EXIT curves, whereas for the EXIT curves less bits can give us good prediction [117].

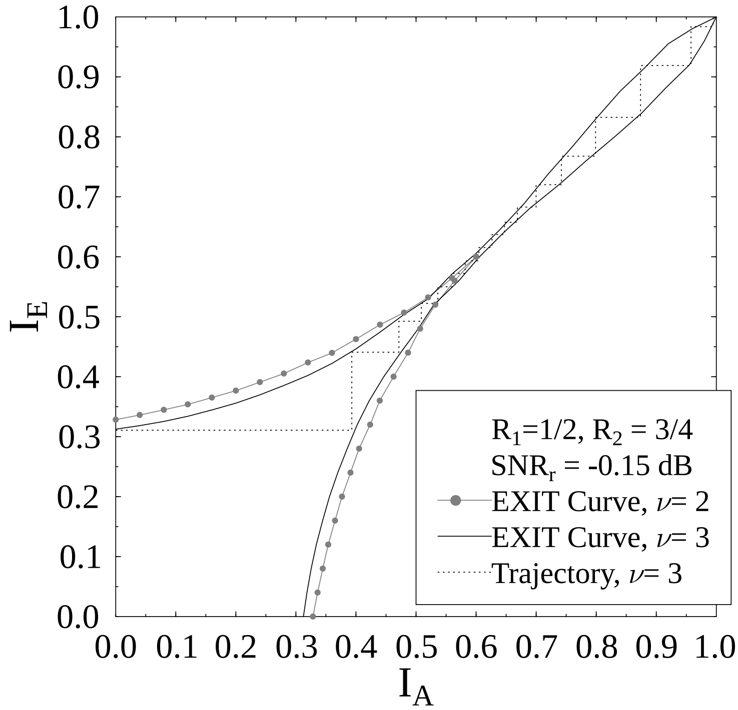

Figure 5.5: EXIT curves for $\nu = 2$ and $\nu = 3$, R_1=1/2 and R_2=3/4, QPSK-assisted SECCC using Gray mapping, η = 0.67 bps at SNR$_r$ = -0.15 dB for transmission over an uncorrelated Rayleigh channel. A decoding trajectory for $\nu = 3$ is also depicted. The 2-D EXIT chart is similar to that calculated for the SECCC scheme in Figure 3.5(b) at an equivalent E_b/N_0 value of 1.61 dB.

$(g_r = 7, g_1 = 5)_8$, remains closed at -0.15 dB. This can also be confirmed from Table 3.2, where the Gray mapped $\nu = 3$ SECCC scheme performs 0.25 dB better than the $\nu = 2$ scheme. Since the threshold ω of a $\nu = 2$ code is 1.81 dB in terms of E_b/N_0, whereas the $\nu = 3$ code requires an E_b/N_0 value of 1.56 dB. Consequently, we opted for $\nu = 3$, employing the octally represented generator polynomial of $(g_r = 13, g_1 = 15)_8$, as it requires a marginally reduced transmission power, noting that this may be deemed an unfavourable tradeoff, since it implies doubling the number of trellis states, i.e. the complexity. Figure 5.5 also corresponds to the performance of the SECCC scheme of the SR link. The receive SNR can be computed as:

$$\mathrm{SNR}_r = \mathrm{SNR}_e + 10\log_{10}(G_{sr}) \text{ [dB]} . \tag{5.11}$$

When there is no path-loss, the receive SNR equals the equivalent SNR[3], denoted by SNR$_e$ and G_{sr} was defined in Equation 5.3. Hence, a receive SNR of -0.15 dB can be achieved by various combinations of SNR$_e$ and G_{sr}. For the $\nu = 3$ SECCC

[3] To simply our analysis the term "equivalent SNR" is introduced, which is the ratio of the signal power at the transmitter (source/relay node) with respect to the noise level at the receiver (relay/destination node).

code the decoding convergence threshold[4] is at -0.2 dB, when employing $I = 40$ self-concatenated iterations, which is 1.05 dB away from the Rayleigh fading SR link capacity calculated as -1.20 dB at 0.67 bps from [11]. The corresponding capacity curve will be discussed later in the context of Figure 5.8 in detail. This scheme acquires an open EXIT tunnel[5] at SNR_r=-0.15 dB, when communicating over an uncorrelated Rayleigh fading channel.

In our analysis the relay node of the DSECCC-ID is assumed to be placed half-way between the source and relay nodes, i.e. we have $G_{sr} = G_{rd} = 4$, hence the minimum required equivalent SNR at the source node is $\mathrm{SNR}_e = -0.15 - 6.02 = -6.17$ dB.

Step 2:

In this section the decoding convergence of the three-component DSECCC-ID decoder used at the destination node is analysed. The EXIT curves of the SECCC decoder at the SD link employing $I_{sd} = 2$ self-concatenated iterations as well as that of the RSC decoder recorded at the RD link are plotted in Figure 5.6. Since this EXIT-chart reflects the destination decoder's convergence after the completion of the SECCC iterations only one of the pair of symmetric curves is shown and our goal at this stage is to examine the extrinsic information exchange between the SECCC decoder and RSC decoder having different memory lengths. The RD link employs rates of $R_3 = 1/2$, $R_4 = 1/2$. As explicity shown in Figure 5.6, we varied the memory of the RSC encoder in order to find the one, which has a low complexity, while simultaneoulsy matching the EXIT curve of the SECCC decoder of the SD link. It can be seen from Figure 5.6 that the EXIT curves associated with $\nu = 2$ and $\nu = 3$ do not intersect the EXIT curve of the SD link when we have $\mathrm{SNR}_e = -3.5$ dB at both the SD and at the RD link, while the $\nu = 4$-curve does intersect it at the same SNR. Since $\nu = 2$ is a lower-complexity code, therefore we opted for it for our proposed scheme.

The EXIT curves and corresponding decoding trajectory is shown in Figure 5.7. The number of iterations exchanging extrinsic information between the SECCC of

[4]The decoding threshold is the SNR value beyond which the EXIT tunnel becomes 'just' open, although this does not necessarily imply that the (I_A, I_E)=(1,1) point of 'perfect convergence' can be reached because some of the decoding trajectories are curtailed owing to the limited interleaver length used.

[5]An open EXIT tunnel specifies the receive SNR value where there is a more widely open EXIT tunnel leading to the (1,1) point and where decoding convergence to an infinitesimally low BER value can always be achieved, provided that the interleaver length is beyond a certain value and the number of iterations is sufficiently high [117].

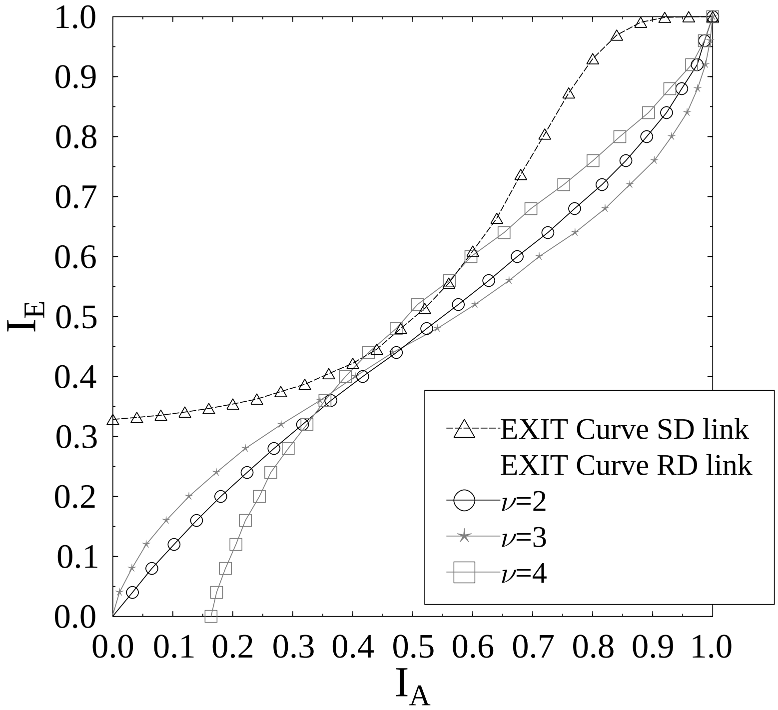

Figure 5.6: The EXIT curves for the DSECCC-ID scheme for a $\text{SNR}_e = -3.5$ dB both at the source as well as at the relay nodes. We portray the RD link's EXIT curves for three different values of ν.

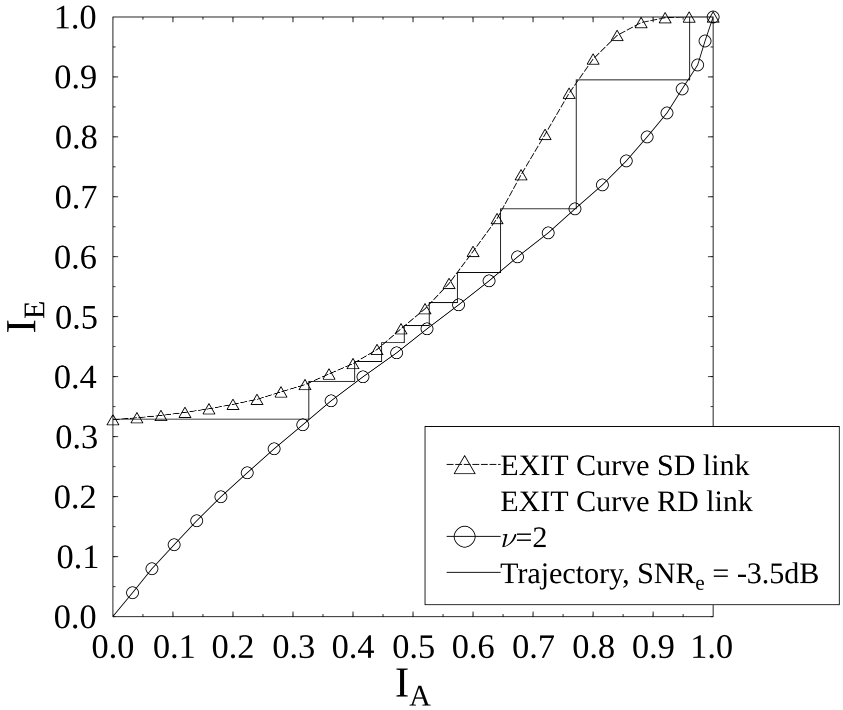

Figure 5.7: The EXIT curves and a decoding trajectory of the DSECCC-ID scheme for $\text{SNR}_e = -3.5$ dB both at the source as well as at the relay nodes. The number of iterations exchanging extrinsic information between the SECCC and RSC decoders at the destination node is limited to $I_{sd,rd} = 10$.

SD link and RSC decoders at the RD link is limited to $I_{sd,rd} = 10$.

Step 3:

The convergence threshold for the DSECCC-ID system can be calculated from the EXIT curves intersecting each other at SNR_e of -3.65 dB. Hence the trajectory will not reach the (1,1) point of perfect convergence to a vanishingly low BER. But once the system is operating at $\text{SNR}_e = -3.5$ dB at the SD link and again at $\text{SNR}_e = -3.5$ dB at the RD link, an open tunnel emerges. Since $\text{SNR}_e = -3.5$ dB is higher than the threshold of $\text{SNR}_e = -6.17$ dB, which guarantees an SECCC decoding convergence at the relay, the SR link may be deemed near-perfect. Another reason why we configure the system to operate at a higher SNR is because we want to have less self-concatenated iterations at the SR link's receiver, namely $I_{sr} = 8$ in this case. The proposed DSECCC-ID system's parameters are given in Table 5.3.

Coding Scheme at source	**SECCC: $\mathbf{R_1}$=1/2, $\mathbf{R_2}$=3/4, R=1/3, ν=3**
Coding Scheme at relay	**RSC: $\mathbf{R_1}$=1/2, $\mathbf{R_2}$=1/2, R=1/2, ν=2**
Modulation	QPSK
Bits per frame (N_i)	120,000
Symbols per frame from source (N_s)	180,000
Symbols per frame from relay (N_r)	60,000
Throughput of DSECCC-ID	0.5 bps
Number of frames	1000
Channel	Uncorrelated Rayleigh fading channel
Decoder	Approximate Log-MAP
I_{sr}	8
I_{sd}	2
$I_{sd,rd}$	10
pathloss	$G_{sr} = G_{rd} = 4$

Table 5.3: DSECCC-ID system parameters.

The EXIT chart analysis is verified by computing the corresponding Monte-Carlo simulation based decoding trajectory for the DSECCC-ID scheme. The distinct decoding trajectory based on a frame length of 120 000 bits is shown in Figure 5.7 for an equivalent SNR of -3.5 dB both at the source and at the relay. It matches the EXIT curves generated for the SD link, which employs the SECCC scheme and the RD link employing the RSC scheme, hence verifying the predicted results.

5.3.2 Relay Capacity

The two-hop half-duplex constrained relay-aided network capacity can be calculated by considering the capacity of the channel between the source, relay and the destination.

We first derive the upper and lower bounds on our half-duplex constrained relay-aided system's Continuous-Output Memoryless Channel (CCMC) capacity as well as those of the Discrete-Input Continuous-Output Memoryless Channel (DCMC) capacity (constrained information rate) based on the corresponding results derived for idealized full-duplex relay channels in [206]. More specifically, the upper bound of the full-duplex relay channel is given by [206]:

$$\begin{aligned} C_{Coop}^{U} \leq \max_{p(x_1,x_2,x)} \min\{&\lambda E[I(X_1;Y_1,Y)] + (1-\lambda)E[I(X_2;Y_2|X)], \\ &\lambda E[I(X_1;Y_1)] + (1-\lambda)E[I(X_2,X;Y_2)]\} \end{aligned} \tag{5.12}$$

and that of the lower bound on the CCMC and DCMC capacity of the full-duplex relay system is given in [206] as:

$$\begin{aligned} C_{Coop}^{L} \geq \max_{p(x_1,x_2,x)} \min\{&\lambda E[I(X_1;Y)] + (1-\lambda)E[I(X_2;Y_2|X)], \\ &\lambda E[I(X_1;Y_1)] + (1-\lambda)E[I(X_2,X;Y_2)]\}, \end{aligned} \tag{5.13}$$

where $I(A;B)$ represents the mutual information for the channel having the i.u.d. input A and the corresponding output B for the case of CCMC capacity. By contrast, for the case of DCMC the input A is constituted by PSK/Quadrature Amplitude Modulated (QAM) symbols. The signals X_1 and X_2 are transmitted from the source S in Figure 5.2 during T_1 and T_2, respectively, while Y_1 and Y_2 represent the corresponding signals received at the destination D of Figure 5.2 during the consecutive time slots. Furthermore, X and Y are the transmitted and received signals at the relay R of Figure 5.2, respectively. Still referring to Equations 5.12 and 5.13, $E(.)$ denotes the expectation with respect to the fading coefficients, $p(x_1, x_2, x)$ represents the joint probability of the signals transmitted from the source and the relay, while λ is the ratio of T_1 to the total frame duration, which is given by $\frac{N_s}{N_s+N_r} = \frac{3}{4}$. Similarly, we have $(1-\lambda) = \frac{N_r}{N_s+N_r} = \frac{1}{4}$. The term $E[I(X_1;Y_1,Y)]$ in Equation 5.12 represents the expected value of the mutual information between the signal transferred from the source node S and the signals received at both the relay and destination nodes during T_1, while the term $E[I(X_1;Y)]$ in Equation 5.13 considers the link spanning from the source node S to the relay node R in T_1. Furthermore, the term $E[I(X_2;Y_2|X)]$ in Equations 5.12 and 5.13 represents the expected value of the mutual information between the signal transferred from the source node and the signal received at the destination node in T_2, conditioned on the transmission of X from the relay node to the destination node. Similarly, the term $E[I(X_1;Y_1)]$ considers the transmission from the source node to the destination node in T_1. Finally, the term $E[I(X_2, X; Y_2)]$ represents the expected value of the mutual information between the signals transferred from both the source and relay nodes and the signal received at the destination node during T_2.

The upper and lower bound on the CCMC and DCMC capacity of a half-duplex relay-aided system can then be derived by setting $X_2 = 0$, because the source does not transmit in T_2. Hence we also have $E[I(X_2; Y_2|X)] = 0$ and $E[I(X_2, X; Y_2)] = E[I(X; Y_2)]$ in Equations 5.12 and 5.13. Consequently, the upper bound can be expressed as:

$$C^U_{Coop} \leq \max_{p(x_1,x)} \min\left\{\frac{3}{4}E[I(X_1; Y_1, Y)], \frac{3}{4}E[I(X_1; Y_1)] + \frac{1}{4}E[I(X; Y_2)]\right\}, \quad (5.14)$$

and the lower bound as:

$$C^L_{Coop} \geq \max_{p(x_1,x)} \min\left\{\frac{3}{4}E[I(X_1; Y)], \frac{3}{4}E[I(X_1; Y_1)] + \frac{1}{4}E[I(X; Y_2)]\right\}, \quad (5.15)$$

where the corresponding constrained information rates of $E[I(X_1; Y_1, Y)]$, $E[I(X_1; Y_1)]$, $E[I(X; Y_2)]$ and $E[I(X_1; Y)]$ can be computed by using the Monte-Carlo averaging method [143]. Using Equations 5.14 and 5.15 we can calculate the DCMC and CCMC capacity of the two-hop relay-aided network, which is graphically shown in Figure 5.8.

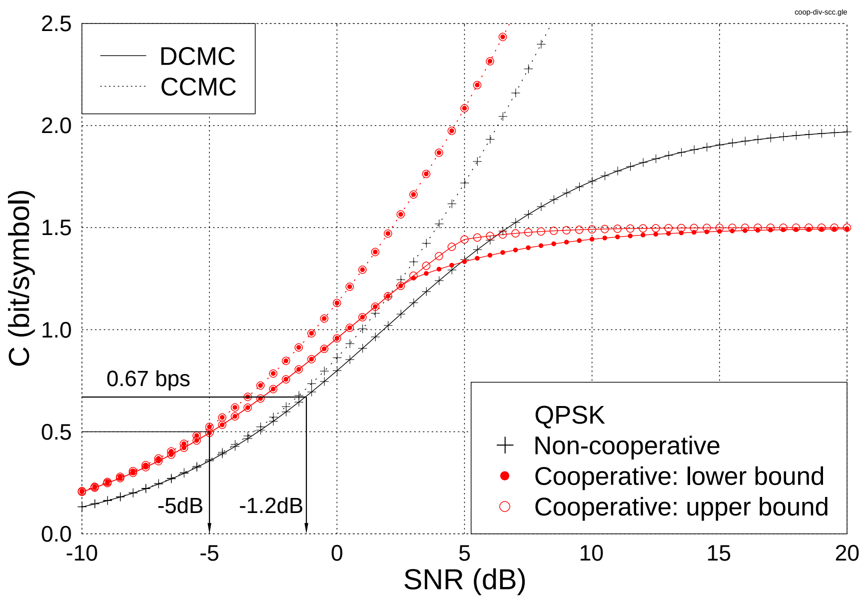

Figure 5.8: The DCMC and CCMC capacity curves of cooperative network and non-cooperative QPSK assisted schemes. It can be seen that the DCMC of a cooperative network is -5 dB at 0.5 bps. DCMC of a non-cooperative QPSK assisted scheme is -1.20 dB at 0.67 bps.

5.4 Results and Discussions

Finally, we compare the achievable performance of the DSECCC-ID scheme employing a realistic relay node, which potentially induces error propagation, to that of the non-cooperative SECCC scheme. The BER versus equivalent SNR performance of the DSECCC-ID and SECCC schemes is shown in Figure 5.9.

The SECCC scheme has a decoding threshold at -0.2 dB and the tunnel at -0.15 dB. It performs 1.05 dB away from the Rayleigh fading channels's capacity calculated as -1.20 dB from [11] and Figure 5.8 at a BER of 10^{-5}. The DSECCC-ID system has been analysed at -3.5 dB at the source and the relay employing the RSC encoder. Thus the DSECCC-ID outperforms the SECCC scheme by about 3.3 dB in SNR terms at a BER of 10^{-5}, which corresponds to $3.3 - 1.25 = 2.05$ dB in terms of E_b/N_0.

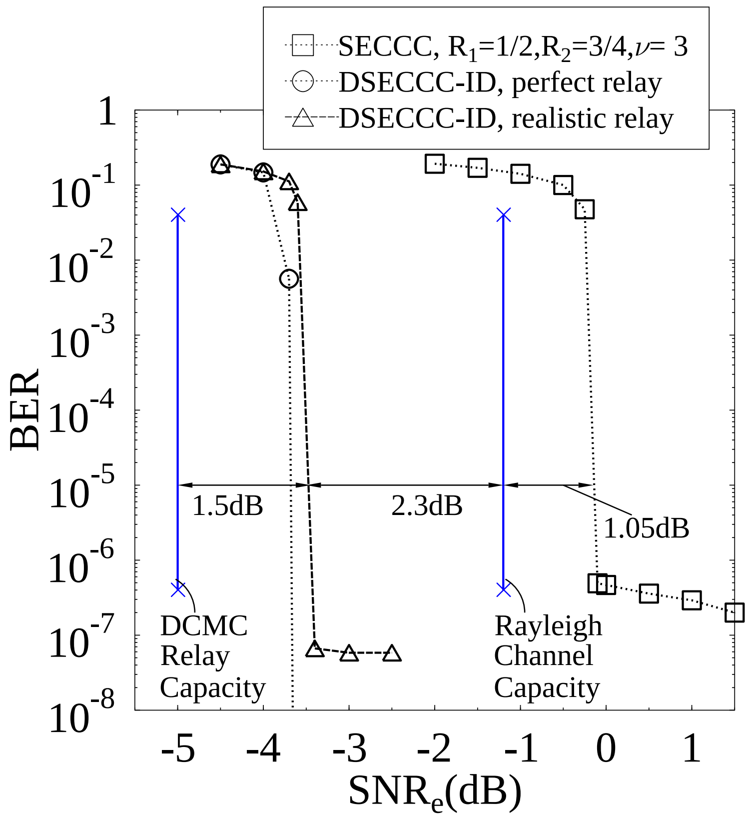

Figure 5.9: BER versus equivalent SNR performance of the DSECCC-ID and SECCC schemes for a frame length of 120,000 bits. The DCMC relay-aided network capacity is -0.5 dB at 0.5 bps as calculated from Figure 5.8.

As shown in Figure 5.9, the proposed DSECCC-ID system is capable of performing within about 1.5 dB from the two-hop relay-aided network's DCMC capacity of -5 dB at 0.5 bps, as inferred from Figure 5.8 at a BER of 10^{-5}. In comparison, for the scheme proposed in [240], the signals arriving from the source and relay are superimposed at the destination, where a MAP detector and a turbo decoder of memory $\nu = 4$ exchange extrinsic information, which were shown to be capable of achieving a BER of 10^{-5}, at about 1.43 dB away from the capacity of the ergodic flat-fading channel at an overall effective throughput of 0.44 bps. We compare the two schemes' complexity by calculating the total number of trellis states, multiplied by the number of iterations at the corresponding decoders to determines the number of ACS arithematic operations as discussed in Section 2.3.2.3. The total complexity of our proposed decoder is estimated as follows.

The number of decoding iterations at the SR link's memory-$\nu = 3$ decoder are $I_{sr} = 8$, therefore $I_{sr} \times 2^{\nu} = 8 \times 8 = 64$ ACS operations are required at the relay. The SD link employs $I_{sd} = 2$ iterations of a memory-3 decoder whereas the RD link employs a $\nu = 2$ code. The number of iterations exchanging extrinsic information between the SECCC and RSC decoders at the destination node is limited to $I_{sd,rd} = 10$. Hence, the number of ACS operations at the destination is given by $I_{sd} \times 2^3 \times 2^2 \times I_{sd,rd} = 640$. The overall ACS operations are therefore, $64 + 640 = 704$.

For the case of [240] the turbo decoder at the RD link employs 15 iterations between the two parallel concatenated turbo codes, while 15 iterations exchange extrinsic information between the MAP decoder and the turbo decoder of memory $\nu = 4$ at the destination. Hence the overall number of ACS operations required in [240] are $(15+15) \times 2 \times 2^4 = 960$, while the complexity incurred by the MAP detector has not been included in the calculation. Hence our proposed system is capable of exhibiting a similar performance while incurring a reduced overall complexity compared to the scheme in [240].

5.5 Chapter Conclusions

A power efficient DSECCC-ID scheme has been proposed for cooperative communications. A near-capacity code, such as the SECCC scheme is required at the relay in order to minimise the decoding error probability. Once the received SNR at the relay exceeds the error-free decoding threshold, the SECCC decoder employed at the relay becomes capable of reliably decoding the source signals. The relay node employs a simple RSC encoder and only its parity bits are transmitted to the destination. The EXIT chart of the three-component DSECCC-ID decoder reveals that the proposed system is capable of near-capacity operation at the destination, despite considering a potentially error-prone reception at the relay. The EXIT chart analysis also helps us reduce the total power required by an DSECCC-ID cooperative system by about 3.3 dB in SNR terms as compared to an non-cooperative SECCC system at a BER of 10^{-5}.

5.6 Chapter Summary

In this chapter, we propose a power-efficient DSECCC-ID for cooperative communications. The DSECCC-ID scheme is designed with the aid of binary EXIT charts. The source node transmits SECCC symbols to both the relay and the destination nodes during the first transmission period. The relay performs SECCC decoding, where it may or may not encounter decoding errors. It then re-encodes the information bits using a RSC code during the second transmission period. The resultant symbols transmitted from the source and relay nodes can be viewed as the coded symbols of a three-component parallel-concatenated encoder. At the destination node, three-component DSECCC-ID decoding is performed. The EXIT chart gives us an insight into operation of the distributed coding scheme, which enables us to significantly reduce the transmit power by about 3.3 dB in SNR terms as compared to a non-cooperative SECCC scheme at a BER of 10^{-5}. Finally, the proposed system is capable of performing within about 1.5 dB from the two-hop relay-aided network's capacity at a BER of 10^{-5}, even if there may be decoding errors at the relay as summarised in Table 5.4.

<table>
<tr><th>System</th><th>Paramaters</th><th>I_{sr}</th><th>I_{sd}</th><th>$I_{sd,rd}$</th><th>SNR$_e$ (dB) at BER 10^{-5}</th><th>DCMC Rayleigh Capacity (dB)</th></tr>
<tr><td>DSECCC-ID (perfect)</td><td rowspan="2">SECCC:
R$_1$=1/2, R$_2$=3/4, R=1/3,
ν=3, QPSK,
RSC:
R$_1$=1/2, R$_2$=1/2, R=1/2,
ν=2, QPSK,
0.5 bps
120,000 bits/frame</td><td>8</td><td>2</td><td>10</td><td>-3.7</td><td>-5</td></tr>
<tr><td>DSECCC-ID (realistic)</td><td>8</td><td>2</td><td>10</td><td>-3.5</td><td>-5</td></tr>
</table>

Table 5.4: Comparison of SECCC and DSECCC-ID schemes. These E_b/N_0 values were extracted from Figure 5.8. The corresponding system schematic is seen in Figures 5.3 and 5.4 and the system parameters were summarised in Table 5.3.

Chapter 6

Self-Concatenated Convolutional Codes for Superposition Coding Aided Bi-directional Relaying

6.1 Introduction

In Chapters 2, 3, 4 and 5 we discussed noise-limited environments. In order to introduce a further grade of realism, in this chapter we will discuss interference-limited scenarios. Superposition coding (SPC) constitutes a power-efficient, 'green' transmission technique, where each additional superimposed layer conveys a linearly increasing amount of information, as a function of power. Naturally, inter-layer interference is imposed, especially in scenarios, where the superimposed layers are imperfectly separated by non-orthogonal layer-specific spreading-sequences or interleavers transmitted over dispersive, co-channel-interference-contaminated environments. Hence they require the employment of some form of interference cancellation [10, 244]. As an attractive design alternative, Successive Interference Cancellation (SIC) has been explored in the literature [245–247] in intricate detail, but its employment in cooperative communications environments has been limited [220, 243, 248–250]. For the sake of improving the achievable diversity gain of practical relay-aided half-duplex networks, a new protocol called Dynamic Decode and Forward (DDF) was developed [220]. Recent studies calculated the fundamental limits of transmissions on the Gaussian relay channel in the context of multiple relay nodes [248], relay nodes operating in either full- or half-duplex mode [243] and over two-way relay channels [249]. In Chapter 5 a power-efficient distributed coding technique was presented, which employed low-complexity SECCCs for a relay-aided half-duplex single-user cooperative communications scenario. In this chapter our discussions evolve further and we present a design approach for the case of a two-user single-relay-aided cooperative communications arrangement by combining the benefits of SPC, SIC and SECCCs. A serially concatenated channel-coded bi-directional relaying arrangement is proposed, which was considered in the context of a relay-aided network-coded scenario in [251, 252] and in a two-user network-coded scenario in [253, 254].

In [255] SPC was introduced as a scheme broadcasting information from multiple sources, while outperforming other schemes based on orthogonal channel assignments, such as time or frequency division. To elaborate a little further, SPC constitutes a coding scheme, where the information of multiple sources is superimposed and appropriately rotated to form a composite signal, which results in a high throughput [256, 257]. Again, in contrast to the family of classic modulation schemes [11] obeying the logarithmic Shannon-Hartley law, SPC allows a linear increase of the throughput as a function of the transmit power. It was revealed in [245, 258] that the capacity of a Gaussian Multiple Access (GMA) channel may be approached by SIC combined with single-user decoding, provided that the users benefit from appropriate power allocation or rate allocation. SIC techniques provide a low-complexity design, which in theory approaches the ultimate Bayesian performance [245]. For the sake of eliminating the residual interference during interference cancellation and hence avoid the potential error propagation, an iterative SIC receiver has been advocated in [259].

Against this background, the novelty and rationale [9] of this chapter can be summarised as follows:

1. *We propose an SPC aided bi-directional relaying scheme, which receives information from the two communicating mobiles in the first transmission period and after detecting as well as decoding the information retransmits it to the corresponding destinations during the second transmission period.*

2. *In contrast to prior studies, the source-to-relay link is not assumed to be error free, which was the case in the Network Coding (NC) schemes of [253, 254].*

3. *In contrast to [256], the system proposed does not rely on temporal diversity and it requires a lower number of transmission periods than the solution advocated in [256].*

4. *Our performance results demonstrate that the relay-aided SPC arrangement requires a lower transmit power than the direct transmission of information between the two mobile users, while maintaining the same throughput (η) and delay (τ), because both the relay-aided and direct scheme require two transmission periods for their communications.*

The rest of the chapter is organized as follows. We aim for providing a brief unified treatment of SPC aided communications, commencing from the underlying theory of SPC in Section 6.2 and discussing the interference cancellation schemes considered in Section 6.3. We focus our attention on a sophisticated application employing SECCCs in Section 6.4, where we describe the architecture of the proposed bi-directional SPC-SECCC scheme. Section 6.5 is dedicated to our performance evaluations. Finally, we conclude our discourse in Section 6.6.

6.2 Superposition Coding

SPC can be interpreted as a specific modulation technique, where the complex-valued phasor constellation may be viewed as being Gaussian distributed, rather than obeying a predefined ordered structure, as in the classic QAM schemes [11]. SPC is also known as *superposition modulation* [256]. Similarly, the family of SPC schemes may also be viewed as being a multiplexing technique, where a high throughput is achieved by simultaneously transmitting in the form of multiple superimposed layers [257]. An SPC signal can be expressed as [260]:

$$x = \sum_{k=1}^{K} \rho_k e^{j\theta_k} x_k, \tag{6.1}$$

where $\rho_k, k \in [1, K]$ is a layer-specific amplitude scaling factor and $\theta_k, k \in [1, K]$ is a layer-specific phase rotation parameter of a particular layer or symbol $x_k \in \mathcal{A}_k$, which makes the super-symbol $x \in \mathcal{A}$ equiprobable and allows us to increase the cardinality of the set $|\mathcal{A}|$ hence increasing the number of bits conveyed by a SPC symbol. By appropriately choosing ρ and θ, almost arbitrary signalling constellations may be created. For the case of K=3 BPSK modulated layers, a total of $|\mathcal{A}| = 8$ distinct equiprobable signal constellation points can be created, thus a sum-rate of 3 symbols per super-symbol may be achieved as a maximum [257]. By increasing the number of SPC layers we can approach a Gaussian distribution, which is desirable from an information theoretic point of view, because it is capable of approaching the continuous-input continuous-output memoryless channel capacity derived by Shannon [12]. However, it renders the receiver more complex, since there is no clearly defined decision boundary as in the context of conventional modulation schemes [261]. As a result, classic stochastic estimation theory plays a crucial role in detecting such a composite SPC signal, for example by using Bayesian Inference [262].

The concept of SPC has already been adopted implicitly in many modern communications system designs, as summarised in Table 6.1. The most important one may be the family of Linear Dispersion Codes (LDC) [266], where each antenna transmits a weighted sum of the channel coded input symbols as in SPC and the weighting factor of each antenna's stream is typically found subject to a predefined design criterion [15]. Dirty Paper Coding (DPC) of [264] is also reminiscent of the SPC principle, where in addition to simply superimposing multiple layers in SPC, we also subtract the recognisable sources of interference prior to transmission which is reminiscent of writing on 'dirty paper' by avoiding the dirty segments, hence improving the readability. Importantly, the SPC concept is closely related to non-orthogonal multiuser communications in the cellular DownLink (DL) [269]. The intra-cell interference can be mitigated for example by employing orthogonal Direct Sequence Code Division Multiple Access (DS-CDMA) spreading sequences in the synchronous DL of the adjacent cells, while a non-orthogonal interference-limited scenario is encountered, when the inter-cell interference of multiple cells is taken into account from a system-level point of view. In fact, the non-orthogonal approach can be realized in a broader, generalised domain, which has typical instantiations such as for instance Trellis Coded Multiple Access (TCMA) [272, 273] where the separation of layers may be ensured by using orthogonal generator polynomials for a trellis code. By contrast, in Interleave Division Multiple Access (IDMA) [268, 274] we employ unique, user-specific or layer-specific interleavers. When these interleavers are applied to interleave the chips of a DS-CDMA spreading sequence, we arrive at the concept of chip-interleaved DS-CDMA [275]. An SPC scheme has also been invoked in a Cooperative Multiple Access(CMA) scenario [220], where multiple sources forming a cluster to jointly communicate with the destination, which is also known as Multiple Source Cooperation (MSC) [267, 271, 276]. The similarities between the SPC technique and the NC technique have been highlighted in [265, 270, 277], where the latter has been considered to be of high significance in future wireless networks, because it was shown to attain the maximum information flow in a multicast network. Furthermore, the SPC technique has also been employed in the context of HARQ mechanisms, leading to a novel Multiplexed HARQ (M-HARQ) scheme [260], where the main philosophy was that the M-HARQ jointly encodes the current new packet

Year	*Milestone*
1974	Bergmans and Cover proposed the novel concept of superposition coding [255].
1977	Imai and Hirakawa invented MultiLevel Coding (MLC) [263] which may also be viewed as a type of SPC. Explicitly, each bit of a multi-bit modulated constellation may be protected by a different code-rate. Both single-layer and multi-layer decoding techniques may be invoked.
1983	Costa presented Dirty Paper Coding (DPC) in [264], where the recognisable sources of interference are eliminated prior to transmission.
2000	Network Coding (NC) was proposed by Yeung *et al.* in [265], which refers to coding at the intermediate nodes in a bid to attain the maximum achievable throughput flow in a multicast network.
2002	Hassibi and Hochwald [266] discovered Linear Dispersion Codes (LDC), where each antenna transmits the linear combination of a number of substreams over space and time. The codes are designed to optimize the mutual information between the transmitted and received signals, hence they achieve substantial coding advantages.
2004	Ma and Ping advocated sigma mapping [257] which is a multiplexing technique, where a high throughput is achieved by simultaneously transmitting multiple superimposed layers.
	Multiple Source Cooperation (MSC) was proposed by Shalvi [267], where multiple sources form a cluster to jointly communicate with the destination.
	Interleave-Division Multiple Access (IDMA) was employed by Hoeher *et al.* in 4G and WLANs [268] using user-specific or layer-specific interleavers.
2005	Larsson and Vojcic analysed superposition modulation, where the information of multiple sources is superimposed and appropriately rotated to form a composite signal [256]. It was shown that the proposed scheme is capable of outperforming a classic DAF relaying scheme of the same complexity.
	Azarian *et al.* [220] invoked the SPC scheme for the sake of improving the achievable diversity gain of relay-aided half-duplex Cooperative Multiple Access (CMA) channels.
2006	Wang *et al.* compared orthogonal and non-orthogonal approaches designed for potential future wireless cellular systems in [269]. It was shown that the single-user rate can be increased by allocating multiple code streams to a user. This is the so-called Superposition Coded Modulation (SCM) scheme that provides a flexible means for rate adaptation.
	Chen *et al.* [270] investigated the diversity gain achieved using NC in wireless networks invoking a Distributed Antenna System (DAS) or supporting user cooperation.
2009	In [271] Zhang and Hanzo presented distributed Space-Time Coding for MSC, which employs a novel structured embedded (SE) random interleaver generation method allowing it to have autonomously generated random interleavers.
	Zhang and Hanzo [260] devised a SPC Aided Multiplexed Hybrid ARQ Scheme, capable of substantially improving the link layer's effective throughput for all transmitted packets and is particularly suitable for delay-sensitive services.

Table 6.1: SPC aided communications.

to be transmitted and any packets that are about to be retransmitted. Although the imposed retransmitted packet inflicts some additional interference, its delay is dramatically reduced.

6.3 Interference Cancellation

We employ an iterative interference cancellor (IC) to mitigate multiuser interference [244]. The goal of multiuser detection [278] is to correctly demodulate the information bits of interfering users. A maximum likelihood (ML) detector determines the performance bound for joint detection [244]. However, the ML detector's complexity increases exponentially with the number of users, while a range of suboptimal MUDs have been developed for striking attractive tradeoffs in terms of complexity, performance and channel estimation requirements. These can be divided into linear and non-linear detectors [244]. Linear detectors are constituted for example by the matched filter [278], as well as the decorrelating [279] and MMSE [280] detectors, which have a substantially reduced complexity compared to the ML detector. Non-linear detectors such as multistage, decision-feedback and IC detectors typically have a better performance than linear detectors. The family of IC schemes can be divided into three categories: Parallel Interference Cancellation (PIC), Successive (Serial) Interference Cancellation (SIC) and hybrid Parallel Arbitrated Successive Interference Cancellation (PASIC) schemes. SIC first ranks the users or streams based on their received signal power and then detects only the specific user having the strongest signal in each iteration. The detected and remodulated signal is then subtracted from the composite signal [281] until even the weakest signal was detected. By contrast, PIC simultaneously subtracts all of the users' signals from all of the others. Hence for equal-strength signals PIC typically performs better than SIC, while in case the signals have different strengths, the reverse is true [282]. A brief history of these schemes is summarised in Tables 6.2 and 6.3.

Year	*Milestone*
1990	Varanasi and Aazhang proposed a suboptimum Multi-User Detection (MUD) algorithm for a CDMA scheme, where interference-rejection was carried out in multiple parallel stages [283]. The detector has a computational complexity which is linear in the number of users.
1993	Yoon *et al*. [284] unveiled an uncoded Co-Channel Interference (CCI) cancellor designed for Direct Sequence Spread-Spectrum Multiple Access (DS-SSMA).

Table 6.2: Various multiuser detectors (1990-1993).

Year	*Milestone*
1994	Patel and Holtzman invented Successive (Serial) Interference Cancellation (SIC) [285], which is a low-complexity MUD scheme designed for DS-CDMA.
	Li and Steele [286] proposed a hybrid IC scheme and showed that it may perform better than an equivalent PIC scheme.
1995	Hallen *et al.* investigated MUD in CDMA systems [282] and demonstrated that in the presence of accurate power control PIC typically performs better than SIC, while in case the signals have distinctly different strengths owing to large power-control errors SIC is superior.
1996	Sanada and Nakagawa [287] analysed PIC in the context of multicarrier modulation, since multicarrier modulation is capable of providing a frequency diversity gain and coding gain.
1998	Verdu conceived a book on MUD [278].
	Divsalar *et al.* [288] proposed an advanced PIC scheme designed for CDMA, which involves a partial (soft) interference cancellation philosophy where the interference estimate is generated and its effects are cancelled using tentative decisions in multiple cancellation stages.
	Hui and Letaief [289] designed soft-SIC for multipath Rayleigh fading channels.
1999	Lampe and Huber [290] conceived an improved SIC scheme employing adaptive Minimum Mean-Square Error(MMSE) detection instead of matched filters.
	Wang and Poor [107] unveiled a novel nonlinear interference suppression technique conceived for coded CDMA, which employs both soft interference cancellation and linear MMSE filtering to approach the single user performance.
2001	Kobayashi *et al.* [291] presented low-complexity soft-SIC exchanging information with channel decoders, which also incorporated a channel parameter estimation step, in order to achieve a near-single-user performance at high channel loads.
	Poor wrote a popular primer on iterative MUD [292].
	Barriac and Madhow [293] put forth a scheme, where several parallel SICs are amalgamated in order to attain gains over standard SIC.
2002	Brännström *et al.* [272] considered an iterative multi-user detector designed for Trellis Coded Multiple Access (TCMA).
2006	Shi and Schlegel investigated Iterative MUD combined with channel coding for CDMA in [294].
2007	Gupta and Singer proposed a Joint Successive Interference Canceller (JSIC) that jointly detects users in an ordered set, as an evolved version of the conventional SIC [295].
2008	Song, de Lamare and Burr [296] proposed robust SIC schemes for STBC under doubly selective fading channels, providing much better performance than the SIC and the MMSE.
2010	Kong *et al.* [250] proposed a low-complexity SIC-based iteratively decoded space-time transmission architecture operating near the capacity.

Table 6.3: Various multiuser detectors (1994-2010).

6.4 SPC-SECCC for Cooperative Communications

6.4.1 Cooperation Model

The communication links seen in Figure 6.1 are subject to both free-space path loss as well as to short-term uncorrelated Rayleigh fading.

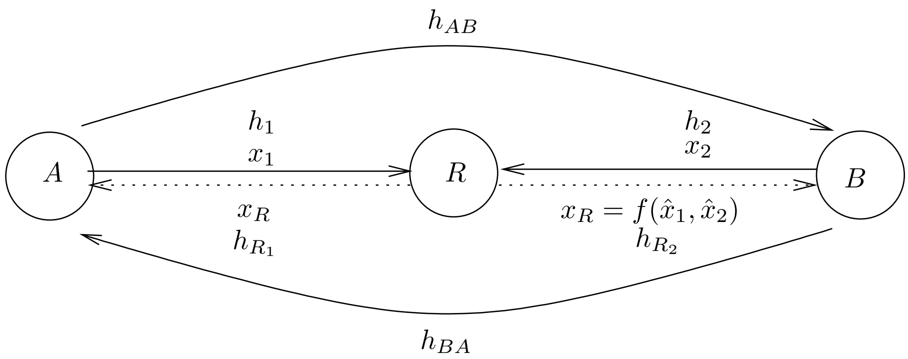

Figure 6.1: Schematic of the bi-directional relay aided system.

Let S_{ab} denote the distance between nodes a and b. The path-loss between these nodes can be modelled by [237] as in Equation 5.1:

$$P(ab) = K/S_{ab}^{\alpha} \ , \tag{6.2}$$

where K is a constant that depends on the environment and α is the path-loss exponent. For a free-space path-loss model we have $\alpha = 2$. The relationship between the energy E_{ar} received at the relay node and that of the destination node E_{ab} can be expressed as:

$$E_{ar} = \frac{P(ar)}{P(ab)} E_{ab} = G_{ar} E_{ab} \ , \tag{6.3}$$

where G_{ar} is the power-gain (or geometrical gain) [237] experienced by the source-relay link with respect to the source-destination link as a benefit of its reduced distance and path-loss, which can be computed as:

$$G_{ar} = \left(\frac{S_{ab}}{S_{ar}} \right)^2 \ . \tag{6.4}$$

Similarly, the power-gain of the relay-destination link with respect to the source-destination link can be formulated as:

$$G_{rb} = \left(\frac{S_{ab}}{S_{rb}} \right)^2 \ . \tag{6.5}$$

If $x_{a,j}$ is the jth symbol transmitted from node a, the average received Signal to Noise power Ratio (SNR) at node b is given as in Equation 5.11:

$$\mathrm{SNR}_r = \frac{\mathrm{E}\{G_{ab}\}\mathrm{E}\{|h_{ab,j}|^2\}\mathrm{E}\{|x_{a,j}|^2\}}{N_0} = \frac{G_{ab}}{N_0} \ ,$$

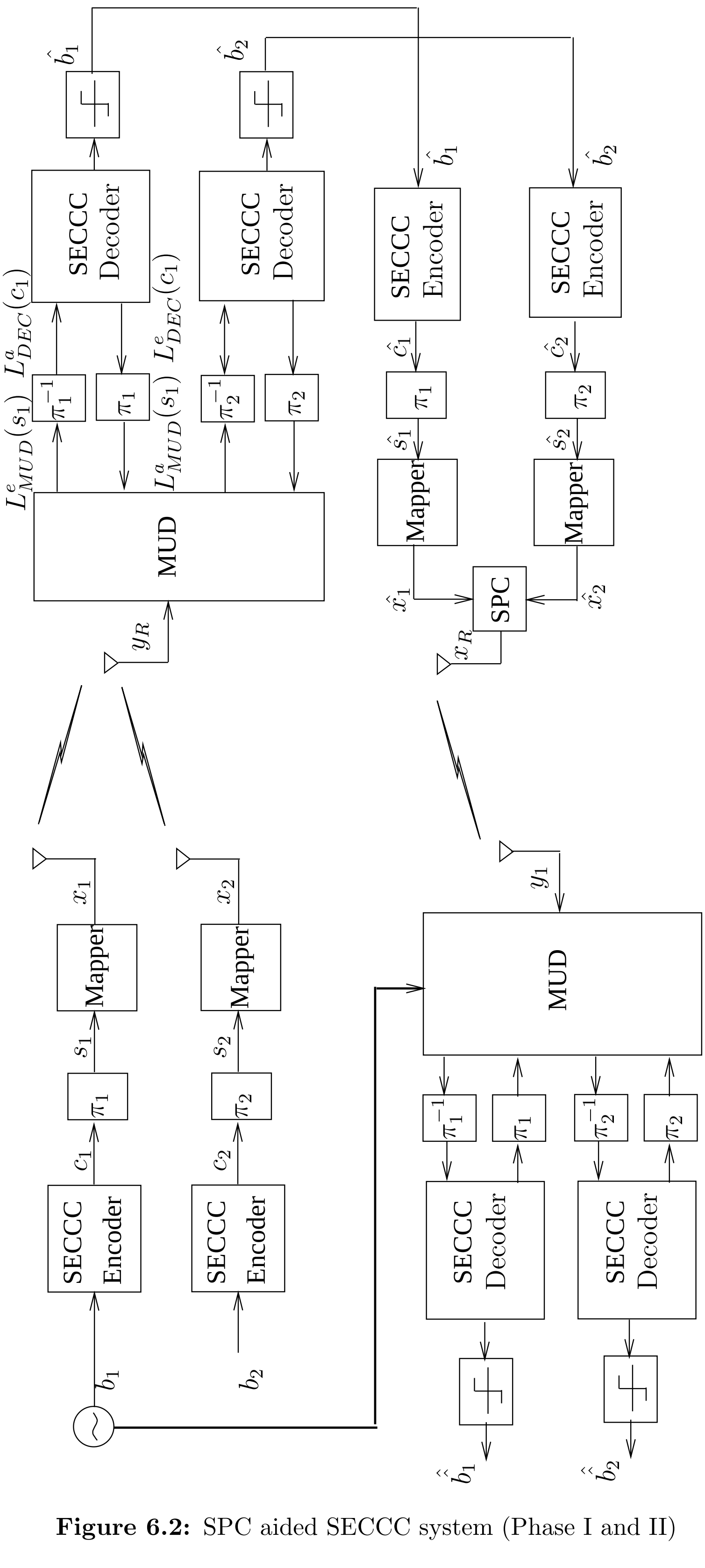

Figure 6.2: SPC aided SECCC system (Phase I and II)

where $\mathrm{E}\{|h_{ab,j}|^2\} = 1$ and $\mathrm{E}\{|x_{a,j}|^2\} = 1$. For ease of analysis, we define the ratio of the power transmitted from node a to the noise power encountered at the receiver of node b as:

$$\mathrm{SNR}_e = \frac{\mathrm{E}\{|x_{a,j}|^2\}}{N_0} = \frac{1}{N_0} \ , \tag{6.6}$$

which implies relating the noise and signal powers to each other at different points in space - therefore we refer to it as the equivalent SNRs denoted by SNR_e. Hence, we have:

$$\begin{aligned} \mathrm{SNR}_r &= \mathrm{SNR}_e \ G_{ab} \ , \\ \gamma_r &= \gamma_e + 10\log_{10}(G_{ab}) \ [\mathrm{dB}] \ , \end{aligned} \tag{6.7}$$

where $\gamma_r = 10\log_{10}(\mathrm{SNR}_r)$ and $\gamma_e = 10\log_{10}(\mathrm{SNR}_e)$. Therefore, we can achieve the desired SNR_r either by changing the transmit power or by selecting a relay at a different geographical location. In order to quantify SNR_r in terms of E_b/N_0, we have to consider the rate R of the SECCC encoder and the modulation, hence we have $E_b/N_0 = \gamma - 10\log_{10}(R \times \log_2(M))$.

The bi-directional relaying arrangement relies on three nodes, A, B and R, as shown in Figure 6.1. Node A and B intend to communicate with each other with the aid of node R. This can be achieved using any of the cooperation strategies outlined in Table 6.4.

Cooperation schemes	T_1	T_2	T_3	T_4
Conventional Relaying	A→R	R→B	B→R	R→A
Network Coding	A→R	B→R	R→A R→B	
SuperPosition Coding	A→R B→R	R→A R→B		

Table 6.4: Comparison of various cooperation philosophies.

- Conventional relaying - Node A transmits x_1 to R in the first transmission period (T_1), while R relays the message to Node B in the second transmission period (T_2). Node B transmits x_2 to R in the third slot (T_3), while R relays the message to Node B in the fourth transmission period (T_4).
- NC - Node A transmits x_1 to R in T_1. Node B transmits x_2 to R in T_2, while R relays the message to the intended destination in T_3[1].

[1]It is possible to achieve the same in two transmission periods by using Physical-Layer Network Coding (PNC) [297] at the 'cost' of the additional complexity of a specially designed mapping scheme.

- SPC - Only two transmission phases are required. Node A and B transmits x_1 and x_2 to R in T_1 (Phase-I) and R relays the message to the intended destination in T_2 (Phase-II).

6.4.2 Phase I - Source to Relay Transmission

The basic block diagram of the SPC-SECCC scheme is given in Figure 6.2, which relies on Phases I and II, representing two different transmission periods. The Phase-I transmission may be considered as a two-user UpLink (UL) multiple access scenario, where each user employs a powerful rate-R SECCC scheme and QPSK modulation, for their transmission to R, which plays the role of a BS. The two UL streams are separated by a user-specific bit-interleaver, resulting the well-known Bit-interleaved Coded Modulation [14, 298]. The discrete-time system model may be written as:

$$y_R = h_1 x_1 + h_2 x_2 + n_R, \tag{6.8}$$

where y_R, x_1 and x_2 denote the received signal at the relay and the two transmitted signals emerge from sources A and B, respectively. Furthermore, h_1 and h_2 denote the corresponding fading coefficient between source A and the relay R as well as between source B and the relay R, while n_R denotes the complex-valued AWGN.

6.4.2.1 SECCC Encoding at Source

At the source node we consider a rate $R = 1/3$ SECCC scheme of $R_1 = 1/2$, $R_2 = 3/4$ and memory $\nu = 3$ combined with QPSK modulation as shown in Figure 6.2 and explained in detail in Section 3.2.1. Both AWGN and uncorrelated Rayleigh fading channel conditions are considered. After SECCC encoding these bits are then mapped to a QPSK symbol as $x = \mu(c_1 c_0)$, where $\mu(.)$ is the bit-to-symbol mapping function. Hence the resultant bandwidth efficiency is given by $\eta = R \times \log_2(4) = 0.67$ bit/s/Hz, assuming a Nyquist roll-off-factor of 0. The QPSK symbol x_s is then transmitted over the channel. The corresponding SECCC decoder of Figure 6.2 has been further explained in Figure 3.1 of Chapter 3.

6.4.2.2 Multiuser Detection

A host of Multiuser Detection (MUD) schemes may be invoked, including the powerful but potentially complex Maximum Likelihood (ML) detection scheme, sphere decoding [244], etc. Here we opt for employing a low-complexity soft interference cancellation scheme [299].

Since a sufficiently long bit interleaver employed is capable of mitigating the correlation between consecutive symbols, we consider a particular symbol and aim for the detection of the jth source's symbol x_j, where Equation 6.8 may be rewritten as

$$y_R = h_j x_j + \sum_{i \neq j} h_i x_i + n, \tag{6.9}$$

where $\varrho = \sum_{i \neq j} h_i x_i$ is the residual interference and $\xi = \varrho + n$ represents the residual interference plus noise. By approximating ϱ as a joint Gaussian random vector, we can model the extrinsic symbol probability as:

$$P^e(x_j = x) \quad \propto \quad \exp\left[-|y_R - \hat{\varrho} - h_j x|^2 / 2V_\xi\right], \tag{6.10}$$

where $x \in \mathcal{A}$ is the particular realization drawn from the modulation alphabet $\mathcal{A}$. The estimated value of ϱ and the variance of ξ, namely V_ξ, may be expressed as:

$$\hat{\varrho} \;=\; \sum_{i=1}^{2} h_i \hat{x}_i - h_j \hat{x}_j, \tag{6.11}$$

$$V_\xi \;=\; \sum_{i=1}^{2} v_i |h_i|^2 + \sigma^2 - v_j |h_j|^2. \tag{6.12}$$

For $j = 1$ we have, $\hat{\varrho} = h_2 \hat{x}_2$ and $V_\xi = v_2 |h_2|^2 + \sigma^2$. The soft symbol $\hat{x}_i$ and the 'instantaneous' variance v_i are given by:

$$\hat{x}_i \;=\; \sum_{x \in \mathcal{A}} x P^a(x_i = x), \tag{6.13}$$

$$v_i \;=\; \sum_{x \in \mathcal{A}} |x|^2 P^a(x_i = x) - |\hat{x}_i|^2. \tag{6.14}$$

For the decoder of a binary code, the extrinsic non-binary symbol probability $P^e(x_j)$ may be converted to the bit-based extrinsic LLR $L^e_{MUD}(s_j = x^q_j), q \in [1, Q]$, where we have $x^q_j =$ the q^{th} bit of j^{th} source symbol, $Q = \log_2 |\mathcal{A}|$ and $|\mathcal{A}|$ is the cardinality, i.e. the number of phases in the modulation alphabet $\mathcal{A}$. The extrinsic LLR of the resultant bit is thus given by:

$$L^e_{MUD}(s_j = x^q_j) = \log_2 \frac{\sum_{x \in \mathcal{A}^+_q} P^e(x_j = x) P^a(x_j = x)}{\sum_{x \in \mathcal{A}^-_q} P^e(x_j = x) P^a(x_j = x)}, \tag{6.15}$$

where $\mathcal{A}^+_q$ and $\mathcal{A}^-_q$ denotes the two subsets of A hosting symbols with their qth bit being +1 and -1, respectively. It can be seen from Equation 6.15 that in the derivation of the extrinsic information $L^e_{MUD}(s_j = x^q_j)$, only the *a priori* symbol probability $P^a(x_j = x)$ is needed, which is given by:

$$P^a(x_j = x) = \prod_{q \in [1,Q]} \frac{1}{2} \left\{1 + x^q \tanh\left[L^a_{MUD}(s_j = x^q_j)/2\right]\right\},$$

where $x^q \in \{\pm 1\}$ is the qth bit's polarity in symbol x. This corresponds to a bit-LLR to symbol-probability conversion, where the bit LLR $L^a_{MUD}(s_j = x^q_j)$ is gleaned after interleaving using π_1 the extrinsic LLRs of the codeword denoted by $L^e_{DEC}(c)$ from the output of the SECCC decoder block. $L^a_{MUD}(s_j = x^q_j)$ is then fed back to the MUD of Figure 6.2 which generates $L^e_{MUD}(s_j = x^q_j)$. It is then deinterleaved using π_1^{-1} of Figure 6.2 to generate $L^a_{DEC}(c)$, thus completing the outer iteration between the SECCC decoder and the MUD. The SISO MAP SECCC decoder [102] first calculates the extrinsic LLR of the information bits, namely $L_e(b_1)$ and $L_e(b_2)$. Then they are appropriately interleaved to yield the *a priori* LLRs of the information bits, namely $L_a(b_1)$ and $L_a(b_2)$, as shown in Figure 6.2. Self-concatenated decoding proceeds, until a fixed number of iterations is reached. Apart from having inner self-concatenated iterations in the SECCC decoder, a fixed number of outer iterations exchange extrinsic information between the decoder and the MUD [14] in order to yield the decoded bits $\hat{b}_1$. A similar procedure is followed, when generating $\hat{b}_2$.

6.4.3 Phase II - Relay to Source Transmission

At the relay re-encoding of $\hat{b}_1$ and $\hat{b}_2$ is carried out using a rate-R SECCC encoder and the resultant QPSK modulated signals are $\hat{x}_1$ and $\hat{x}_2$. These are re-transmitted as x_R.

We hence focus our attention on source A, which received the signal $y_A = h_1 x_R + n_A$, where the transmitted signal x_R generated by the SPC scheme may be written as:

$$x_R = \rho\hat{x}_1 + (1-\rho)\hat{x}_2, \tag{6.16}$$

with ρ being the amplitude scaling factor used at the relay for SPC and we simply assume $\rho = 1/2$. Node A receives $y_1 = h_1 * f(\hat{b}_1) + h_1 * f(\hat{b}_2) + n_1$, where the function $f(.)$ represents the SECCC encoding. Since A has its own *a priori* information of b_1, it will first construct $f(b_1)$ using the same encoding function at the relay's transmiter and subtracts the information from the received signal y_1 and then decodes B's information as seen in Figure 6.2. However, in general $\hat{b}_1 \neq b_1$, hence $f(\hat{b}_2) \neq f(b_2)$. Given perfect self-information of x_1 at source A, we could simply initilise the detection process by the *a priori* information provided for source A according to its self-information. Note that this *a priori* information generated by pefect self-information may not be equal to the actual *a priori* information of our real transmitted packet, which is $\hat{x}_1$, unless pefect reception is assumed at the relay, when we have $\hat{x}_1 = x_1$, which may be referred to as the *idealized* scenario. By contrast, in a *realistic* scenario we have $\hat{x}_1 \neq x_1$. The receiver at source B follows the same design methodology.

6.5 Performance Evaluation

6.5.1 Assumptions and Parameters

We have investigated the performance of our system for transmission over both AWGN and uncorrelated Rayleigh fading channels. The SECCC scheme of Figure 6.2 used $R_1 = 1/2$, $R_2 = 3/4$, $\nu = 3$ and Gray mapping, hence its overall rate [152] R=1/3 from Equation 3.1. The bit-to-symbol mappers are QPSK mappers. Hence the resultant bandwidth efficiency is $\eta = R \times \log_2(4) = 0.67$ bps. The same encoder is used in our SPC-SECCC scheme, as depicted in Figure 6.2. Since there are two users, the normalized per-user transmission rate of the two users exchanging information in two transmission periods will be 2/3 bps. Similarly, the direct link based transmission between the two users each having a transmission rate of 2/3 bps also exchanges information in two different transmission periods, as shown in Figure 6.1. The SPC-SECCC scheme imposes the additional complexity of the twin-stream detector, but does not cause any throughput reduction compared to an SECCC scheme. We considered an information block length of 1000 bits per frame and the number of SECCC decoding iterations was fixed to $I_{sec} = 10$.

6.5.2 Simulation Results

We consider a relay node located at the mid-point between the source/destination nodes A and B. According to Equations 6.4 and 6.5, we have $G_{ar} = G_{br} = G_{ra} = G_{rb} = 4$, while $G_{ab} = 1$. Hence from Equation 6.7 we have, $[E_b/N_0]_r = [E_b/N_0]_e + 10\log_{10}(G_{ar})$. The achievable Phase-I performance is characterized in Figure 6.3 for transmission over both AWGN and uncorrelated Rayleigh fading channels. The various scenarios considered were denoted by the legends: '2u 1i', '2u 5i', and '1u', where (i) represents the number of outer iterations between the SPC and SECCC decoders, as follows:

- 2u 1i - 2 users and 1 iteration;
- 2u 5i - 2 users and 5 iterations;

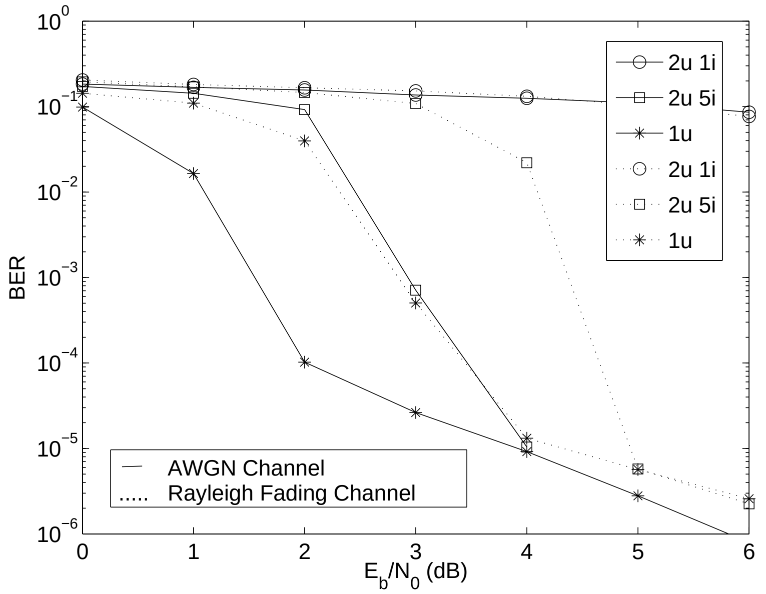

Figure 6.3: BER versus $E_b/N_0 = [E_b/N_0]_r$ of Phase-I of SPC-SECCC scheme for transmission over both AWGN and uncorrelated Rayleigh fading channels.

- 1u - 1 user.

Observe in Figure 6.3 that a marked improvement is exhibited by the BER curve both for AWGN and Rayleigh fading channels, when outer iterations are invoked. For the AWGN channel, represented by the solid line, at a BER of 10^{-4} the two-user scenario requires a 1.5 dB higher E_b/N_0 than the single-user case. Similar trends may be observed for Rayleigh fading channels, as indicated by the dashed lines in Figure 6.3.

The corresponding Phase-II performance is shown in Figure 6.4 for an AWGN scenario and in Figure 6.5 for a Rayleigh fading channel, respectively. The performance of the various scenarios is characterized by the four curves: '2u w 5i real', '2u wo 5i real', '2u w 1i', '1u dt', which represent the following scenarios:

- 2u w 5i real - with *a priori* information using $I_o = 5$ outer iterations for realistic error propagation at the relay;

- 2u wo 5i real - without *a priori* information using $I_o = 5$ outer iterations for realistic error propagation at the relay;

- 2u w 1i - with *a priori* information using $I_o = 1$ outer iteration and neglecting error propagation at the relay;

- 1u dt - when we consider having only a direct link between node A and B employing SECCC schemes. Due to the higher geographical distance between

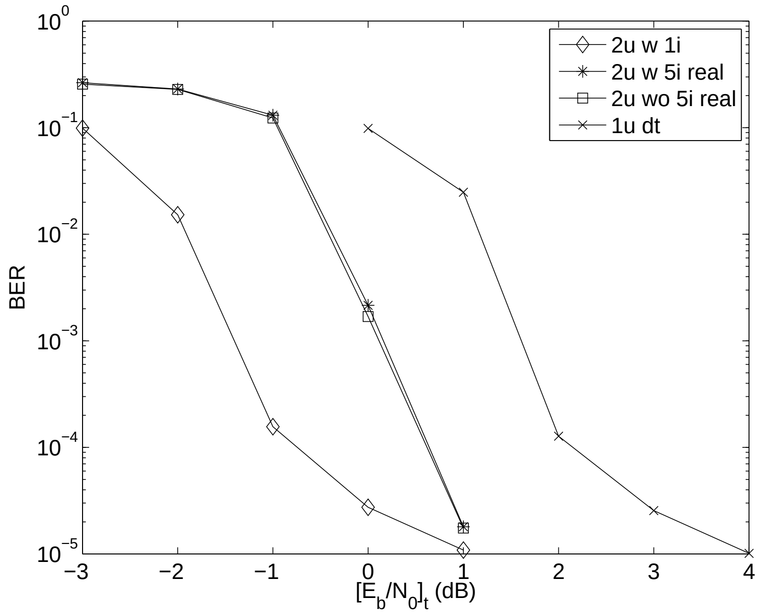

Figure 6.4: BER versus $[E_b/N_0]_e$ of Phase-II of the SPC-SECCC scheme for transmission over an AWGN channel.

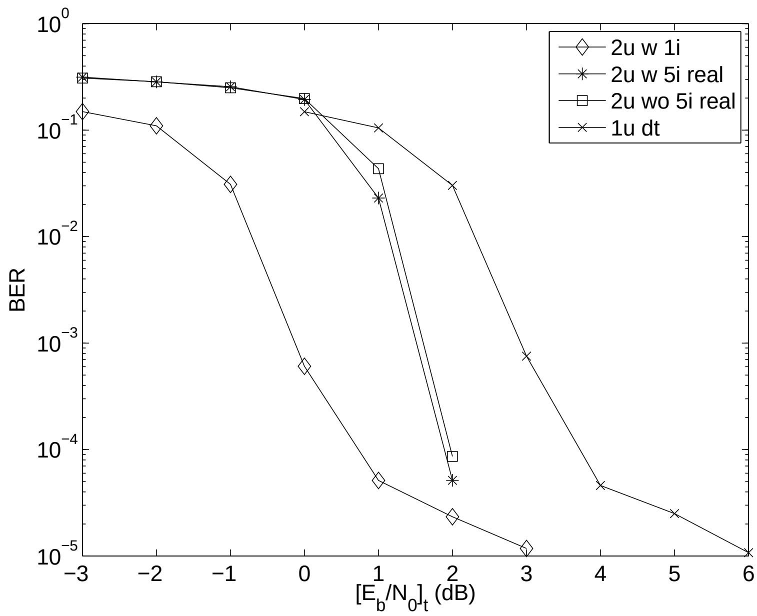

Figure 6.5: BER versus $[E_b/N_0]_e$ of Phase-II of the SPC-SECCC scheme for transmission over an uncorrelated Rayleigh fading channel.

the two nodes the attainable performance was degraded. The SPC-SECCC scheme performs better than the '1u dt' scheme, although they have the same throughput.

It was concluded that in the absence of errors at the relay, node A benefits from SPC. In Figure 6.4 the performance of the '2u w 1i' scenario was 3 dB better compared to '1u dt'. When assuming the presence of potential errors at the relay, node A still benefits from SPC and its performance is about 1.45 dB better than the single-user performance at a BER of 10^{-4} for the AWGN scenario and about 1.75 dB better for transmission over Rayleigh channels.

Coding Scheme at source	**SECCC: R_1=1/2, R_2=3/4, R=1/3, ν=3**
Coding Scheme at relay	**SECCC: R_1=1/2, R_2=3/4, R=1/3, ν=3**
Modulation	QPSK
Bits per frame	1000
Normalized per user transmission rate	2/3 bps
Channel	AWGN and Uncorrelated Rayleigh fading channels
Decoder	Approximate Log-MAP
Users	2
I_o with *a priori* (perfect relaying)	1
I_o with *a priori* (realistic relaying)	5
I_o without *a priori* (realistic relaying)	5
I_{sec}^{I}	10
I_{sec}^{II}	10
pathloss	$G_{ar} = G_{br} = G_{ra} = G_{rb} = 4$

Table 6.5: SPC-SECCC system parameters.

The proposed SPC-SECCC system's parameters are summarized in Table 6.5, where I_{sec}^{I} and I_{sec}^{II} are the number of SECCC iterations at the relay and destination node in Phase I and II, respectively. Furthermore, I_o^I and I_o^{II} represent the number of outer iterations between the SIC and SECCC block of Figure 6.2 at the relay in Phase-I and at the destination in Phase-II of the SPC-SECCC scheme of Figure 6.2.

6.6 Chapter Conclusions

In this chapter we have proposed the bi-directional relaying-aided transmission scheme of Figure 6.2 employing SPC and SECCC, which enabled us to reduce the number of transmission periods compared to both conventional relaying and NC, from four to two while keeping the normalized per-user throughput the same as that of two single users transmitting and receiving each other's information in two different transmission periods.

We may conclude from Figures 6.4 and 6.5 that the SPC technique is capable of striking an attractive tradeoff between the achievable *bandwidth efficiency* and power efficiency, as a benefit of its non-orthogonal code-multiplexing nature. We may also conclude that the SPC technique constitutes an attractive practical solution, since the error propagation effects of SIC may be mitigated with the aid of our iterative receiver, as evidenced by our cooperative communications design example of Section 6.4. Realistic transmission scenarios were considered, where the relay may encounter decision errors. The performance results gleaned from Figures 6.4 and 6.5 suggest that the SPC-SECCC system achieves a low BER even for realistic error-infested relaying. Our future work will concentrate on supporting an increased number of users under different channel conditions.

6.7 Chapter Summary

In this chapter, we considered coding schemes designed for two nodes communicating with each other via a relay node, which receives information from both nodes in the first transmission period of Figure 6.2. At the relay node seen in Figure 6.2 we combined a powerful SPC scheme with our SECCCs scheme, which exchanged mutual information between each other. It was assumed that decoding errors may be encountered at the relay node. The relay node then broadcasted this information in the second transmission period after re-encoding it, again, using a SECCC encoder. At the destination, an amalgamated SPC-SECCC block then detected and decoded the signal either with or without the aid of *a priori* information. Our simulation results demonstrated that the proposed scheme is capable of reliably operating at a low BER for transmission over both AWGN and uncorrelated Rayleigh fading channels. In Figure 6.4 and 6.5 we compared the proposed scheme's performance to a direct transmission link between the two sources having the same throughput. Additionally, as evidenced by Figures 6.4 and 6.5 the SPC-SECCC system achieved a low BER even for realistic error-infested relaying.

Table 6.6 presents a summary of the performance achieved by our realistic SPC-SECCC scheme in comparison to two users directly communicating with each other. In the absence of errors at the relay, node A benefits from SPC since the performance of an SPC-SECCC exploiting the availability of *a priori* information and using I_o^I=I_o^{II}=1 outer iteration between the SIC and the SECCC arrangements, was 3 dB better at a BER of 10^{-4} compared to the direct transmission scheme employing SECCC codes relying on I_{sec}^I=I_{sec}^{II}=40 decoding iterations. This was true for both

System	Parameters	No of users	I^{I}_{sec}	I^{II}_{sec}	I^{I}_{o} / I^{II}_{o}	E_b/N_{0_e} (dB) at BER 10^{-4} AWGN Channel		E_b/N_{0_e} (dB) at BER 10^{-4} Rayleigh Channel	
						w apri	wo apri	w apri	wo apri
Direct Transmission	R_1=1/2, R_2=3/4, R=1/3, ν=3, QPSK, normalized per user transmission rate: 2/3 bps, 1000 bits/frame	2	40	40	-	-	2.15	-	3.65
SPC-SECCC (perfect)		2	10	10	1	-0.75	-	0.65	-
SPC-SECCC (realistic)		2	10	10	5	0.7	0.7	1.9	2.0

Table 6.6: Comparison of SECCC and SPC-SECCC schemes (Phase I and Phase-II). These E_b/N_0 values were extracted from Figures 6.4 and 6.5. The corresponding system schematic is seen in Figure 6.2 and the system parameters were summarised in Table 6.5.

AWGN and Rayleigh fading channels when assuming the presence of potential errors at the relay, node A still benefits from SPC and its performance is about 1.45 dB better than the single-user performance at a BER of 10^{-4} for the AWGN scenario and about 1.75 dB better for transmission over Rayleigh channels, when exploiting the *a priori* information available and using I_o^I=I_o^{II}=5 outer iterations between the SIC and SECCC blocks. If no *a priori* information was available, the SPC-SECCC scheme's performance is about 1.45 dB better than the single-user performance at a BER of 10^{-4} for the AWGN and about 1.65 dB better for the case of Rayleigh fading channels, as shown in Figures 6.4 and 6.5 and summarized in Table 6.6.

Chapter 7

Conclusions and Future Research

In this final chapter, we will first provide our overall summary and conclusions in Section 7.1. Additionally, some useful design guidelines will be presented in Section 7.2. Then a range of topics concerning potential future research directions will be presented in Section 7.3.

7.1 Summary and Conclusions

In this treatise, we presented a suite of novel transceiver designs employing iteratively detected self-concatenated coding schemes in order to achieve a near-capacity performance, when operating in AWGN and Rayleigh fading channels. More specifically, we reported the following major findings:

- Chapter 1 presented a brief history of channel coding schemes and a general outline of the thesis.
- In Chapter 2, self-concatenated codes utilising TCM were analysed with the help of EXIT charts. We then discussed that concatenated codes are capable of attaining a near-capacity performance, which is only feasible for excessive-length non-iterative channel coding schemes. An SECTCM of Figure 2.4 relies on a single encoder and a single decoder and yet, it is capable of delivering a turbo-like performance. We designed new SECTCM schemes based on their decoding convergence analysis with the aid of symbol-based EXIT charts. The symbol based MAP algorithm operating in the logarithmic domain was used to decode the received signal. Meritorious, high performance constituent TCM codes were found for assisting the SECC scheme in attaining decoding convergence to a vanishingly low BER at the lowest possible E_b/N_0 value, when communicating

over both AWGN and uncorrelated Rayleigh fading channels.

- Chapter 3 discussed a suite of binary SECCCs, and a classic Turbo coding scheme which uses the idea of iterative decoding in order to achieve near-capacity performance. This chapter looked into the design of such schemes using EXIT charts in order to analyse the attainable convergence behaviour. In order to eliminate the mismatch between the EXIT-chart and the Monte-Carlo-simulation decoding trajectory experienced in the context of the TCM based scheme discussed in Chapter 2, we proposed a bit-based self-concatenated scheme employing an RSC based constituent code as shown in Figure 3.1. The mapper utilised Gray mapping, which mitigated the above mentioned EXIT-chart mismatch. However, as seen in Section 3.2.1 some information was lost because the coded bits in each coded symbol are correlated [136, 137], hence they cannot convey the maximum possible information, which is equivalent to an entropy- or capacity-loss. To recover this lost information, in Section 3.3 soft decision demapping was used. It was observed in Figures 3.14 and 3.15 that the proposed SECCC-ID scheme of Figure 3.7 while employing the SP demapper outperformed some of the GM based SECCC schemes. Subsequently the design of near-capacity codes was explored in Section 3.3.2 by varying the iterative detection configuration of the constituent decoders/demapper using the parameter configurations of Table 3.2. To analyse the exchange of extrinsic information between the SISO MAP decoder and the soft demapper of Figure 3.7 we employed 3-D EXIT charts in Figures 3.10 and 3.11. The accuracy of the 3-D EXIT chart based design was confirmed by the corresponding bit-by-bit Monte-Carlo BER simulations of Figures 3.14 and 3.15. Finally, in Section 3.4 we derived the union bound of SECCCs employing BPSK modulation, for communications over both AWGN and uncorrelated Rayleigh fading channels, based on the novel uniform self-interleaver concept.

- Based on the SECCCs designed in Chapter 3, in Chapter 4 we explored their applications in both UltraWideBand (UWB) and wireless video systems. In Section 4.1 we commenced by presenting a historical perspective on the recent advances in UWB systems. In Section 4.2 we then designed a near-capacity Time Hopping (TH) Pulse Position Modulated (PPM) UWB Impulse Radio (IR) scheme employing SECCCs using EXIT charts. More explicitly, the powerful tool of EXIT charts was used to select specific SECCCs for the sake of achieving an infinitesimally low BER. Quantitatively, Figure 4.4 demonstrated that the proposed TH-PPM-UWB-IR-SECCC design of Figure 4.2 was capable of performing within about 1.41 dB of the Nakagami-m fading channel's capacity at a BER of 10^{-3}. In Section 4.3.2 we then briefly portrayed the background on the state-of-the-art H.264 Audio/Video Coding (AVC) standard and then proposed a robust H.264 coded wireless video transmission scheme using SECCCs. In Section 4.3.3 a low-complexity iteratively decoded binary SECCC scheme was used for the transmission of the source coded stream. This technique is suitable for low-complexity video-telephony, which requires a low transmission power. The practically achievable interactive video performance trends were quantified in Tables 4.4 and 4.5, when using state-of-the-art video coding techniques, such as H.264/AVC. It was demonstrated in Figure 4.7 that an E_b/N_0 gain of 6 dB may be attained using SECCCs in comparison to the identical-rate state-of-the-art benchmarker. A more detailed system performance characterization was provided in Section 4.3.4.

- In Chapter 5 we proposed a power-efficient distributed scheme employing SECCCs for cooperative communications in order to mitigate the effects of large-scale shadow fading on the performance of wireless communication systems. Distributed Self-Concatenated Convolutional Coding using Iterative Decoding (DSECCC-ID) is a half-duplex relaying system, where the source-relay (SR) and source-destination (SD) link employs a SECCC code, while the relay node employs a low-complexity RSC encoder instead of an SECCC encoder, as portrayed in Figure 5.3. Therefore, the iterative decoder at the destination exchanges information between the SECCC and the RSC decoder components of Figure 5.4. The scheme is capable of providing substantial diversity-, throughput- as well as coding-gains for the case of a single-user scenario. Again, the novel three-component parallel concatenated decoder of Figure 5.4 is invoked. The proposed scheme was designed by conceiving the widely applicable design procedure of Section 5.3.1 using EXIT charts. The complexity analysis was carried out in Section 5.4 and it was demonstrated that the proposed scheme has a low complexity. Despite the fact that the SR link was prone to decision errors, this simplified scheme was capable of approaching the Discrete-input Continuous-output Memoryless Channel's (DCMC) capacity, as presented in Table 5.4.

- Chapter 6 applied the concept of Superposition Coding (SPC) and Successive Interference Cancellation (SIC) in order to improve the transmission efficiency of a cooperative communication scheme. In Section 6.4 a two-user bidirectional single-relay-aided cooperative communication system employing SECCCs was studied in order to investigate the effects of interference-limited scenarios. The two nodes communicate with each other via a relay node, which received information from both nodes in the first transmission period. As seen in Figure 6.2, at the relay node we combined a powerful SPC scheme with a SECCC scheme. The SIC receiver and SECCC decoder of Figure 6.2 iterate between each other to exchange mutual information and hence eliminate the deliterious effects of the residual interference. The half-duplex 2-hop relay-aided SPC scheme assumed that decoding errors may be encountered at the relay node. The relay node then broadcasts this information in the second transmission period after re-encoding it, again, using SECCC encoders and SPC. At the destination, an amalgamated SIC-SECCC block then detected and decoded the signal either with or without the aid of *a priori* information as seen in Figure 6.2. Our simulation results seen in Figures 6.4 and 6.5 and summarised in Table 6.6, demonstrated that the proposed scheme is capable of reliably operating at a low BER for transmission over both AWGN and uncorrelated Rayleigh fading channels.

7.2 Design Guidelines

- The first step in the design of FEC coding schemes in general and in SECCC and SECCC-ID coding schemes in particular is that of determining the code's specifications, such as the affordable decoding complexity expressed for example in terms of the number of ACS arithematic operations. This predetermines the resultant chip area versus decoding speed trade-offs, hence ultimately the maximum supported transmission rate.

- Another fundamental specification is the affordable delay, which determines the maximum tolerable interleaver length.

- Then the choice of the most appropriate SECCC component has to be resolved. In Chapter 2 we considered symbol-based TCM constituent codes, which require symbol-based EXIT charts. However, SECTCM codes exhibit a mismatch between the EXIT chart and the Monte-Carlo-Simulation based symbol-by-symbol decoding trajectory, because the bits of a symbol are not independent of each other. Additionally, we have less flexibility in terms of the choice of coding rates. However, they perform closer to capacity than their bit-based counterparts.

- As discussed in Chapter 3, bit-based SECCC schemes designed with the aid of 2-D EXIT charts are accurate in predicting the convergence thresholds and they have flexible coding- and puncturing-rates. Furthermore, more flexible three-stage SECCC-ID schemes may be designed with the aid of 3-D EXIT charts. We demonstrated in Section 3.4 that in order to have a complete and accurate code design procedure the Truncated Union Bound (TUB) is necessary, which can be used to predict the error-floors, while EXIT charts may be invoked to predict the turbo-cliff-SNR in the design of near-capacity SECCCs.

- In the light of the inherent trade-off between the lowest possible turbo-cliff SNR and the lowest possible residual error floor we can use the EXIT-chart based code-design procedures of Sections 2.3.2 and 3.3.2 and the generator polynomials exemplified in Tables 2.3 and 3.2 to meet the data-integrity requirements, such as the BER, SER or PER specifications.

- SECCCs provide the designer with a high degree of design-freedom, since they offer a vast range of options. These design options are exemplified by the type of component codes, their generator polynomials, code rate, puncturer schemes, interleaver designs and memory, bit-to-symbol mapping schemes such as Gray mapping, Anti-Gray mapping, Set-Partitioning, the choice of modulation schemes, such as coherent and non-coherent modems, irregular code designs, etc.

- When near-capacity operation is the over-riding design criterion, rather than that of minimizing the overall delay or complexity, the EXIT-chart-matching based designs of Chpater 3 suggest that 3-stage concatenated designs may have to be invoked. This is, because they are capable of reducing the area of the open EXIT-tunnel and hence they facilitate decoding convergence to an infinitesimally low BER at near-capacity SNRs.

- Hence it is important to emphasize that maximizing the minimum distance of the code or directly searching for the code having the best distance profile or weight-distribution is no longer the most paramount design criterion. The EXIT-charts provide us with a more insightful tool for designing codes for near-capacity operation.

- When designing SECCCs for supporting wireless cell-edge users for example, the distributed code design principles of Chapter 5 may be relied upon. More specifically, the distributed codes may move the constituent codes to separate relay nodes which have independently fading channels and hence provide a diversity gain. However, a powerful code is needed for all links of a relay-aided system, which suggests that the employment of a concatenated component code is of paramount importance at all nodes. Hence the coding scheme of the SR link has to be designed using EXIT charts, as detailed in Section 5.3.1. The propagation of decoding errors also has to be prevented along the RD link, which is achieved with the aid of another EXIT-chart matching procedure detailed in Section 5.3.1. Thus using DSECCC-ID schemes by employing a 3-stage decoder architecture, effectively reduces the potential error-floor often encountered in conventional 2-stage architectures. DSECCC-ID schemes impose a low complexity, where the ACS operations are distributed between the relay and destination nodes. Similarly to co-located constituent codes, it was demonstrated that EXIT charts are needed to design DSECCC-ID schemes using a widely applicable 3-step procedure:

- Decoding convergence threshold of the SECCC scheme of the SR link is calculated.
- EXIT curve of the SD link is matched against that of a suitable RD link EXIT curve.
- Convergence threshold of the DSECCC-ID scheme is then calculated. More explicity, by plotting the decoding trajectory of the DSECCC-ID scheme we can determine the number of iterations required between the SECCC and RSC decoders at the destination node in order to achieve perfect convergence to an infinitesimally low BER.

7.3 Future Work

The research presented in this thesis can be extended in several ways. In this section we present some ideas for potential future work and briefly elaborate on each idea.

7.3.1 Further Analysis of SECCC-ID Schemes

Our future research will focus on designing SECCC-ID schemes operating closer to capacity. Their coding gain versus code rate characteristics will be quantified to pursue this aim. Our proposed SECTCM design detailed in Chapter 2 and the SECCC-ID design outlined in Chapter 3 highlight the availability of different component codes. Additionally, the SECCC-ID schemes offer flexibility in terms of the choice of code- and puncturing-rates, memory, modulation scheme and facilitate iterative decoding by exchanging extrinsic information with either Sphere Packing or Anti-Gray Mapping [15]. Irregular variable length codes can help design a near capacity code, therefore they can be applied in a joint source and channel coded SECCC-ID scheme [133]. Furthermore, near-capacity irregular code design procedures may be conceived for SECCC schemes [133]. Another area to explore is that of finding the union bound for various coding rates of the SECCCs combined with higher-order modulation schemes, using the uniform puncturing concept of Section 3.4.

7.3.2 Differential SECCC-ID Schemes

As a further extension to the SECCC-ID schemes of Chapter 3, we can design differential SECCC-ID schemes that do not require any channel knowledge. Naturally, it is expected that differential schemes will have a 3 dB performance degradation, when compared to the corresponding coherent scheme assuming perfect channel knowledge at the receiver [15]. However, when realistic, imperfect channel estimation is employed, differential detection eliminates the complexity of channel estimation and we may even attain a better BER performance than that of the coherent scheme, when the channel estimation is inaccurate, as detailed in [15].

7.3.3 Near-capacity Non-coherently Detected DSECCC-ID Cooperative Schemes

Our future research will focus on enhancing the DSECCC-ID scheme of Chapter 5 designed for cooperative communications in order to operate near the capacity, while imposing a low complexity using differential encoding and non-coherent detection, and dispensing with channel estimation. We will study the attainable performance for different relay location scenarios and power allocations. Furthermore, we will investigate the performance of such DSECCC-ID schemes in differentially encoded, non-coherently detected cooperative systems [15].

The next challenging issue will be that of reducing the total power, including the transmit power and the DSP-related power consumption in a relay-aided network. The question arises in a multi-hop network without line of sight propagation, as to how we can better utilize distributed coding in this cooperative network.

The capacity of half-duplex relaying is a factor two lower than that of the equivalent non-cooperative scheme. This capacity reduction may be mitigated using the successive relaying aided regime of [300]. Furthermore, the previously mentioned irregular code design principles may be extended to the novel concept of viewing k cooperating relays as the k irregular code-components having different code-rates.

7.3.4 Multi-Functional Cooperative Communication Systems

The multi-functional MIMO scheme of [15] that combines the benefits of the Vertical Bell Labs Layered Space-Time (V-BLAST) scheme, of space-time codes as well as of beamforming can be beneficially extended to cooperative communication environments. More explicitly, this would benefit from the multiplexing gain of the V-BLAST, from the diversity gain of the space-time codes and from the SNR gain of beamforming [15]. A particular manifestation of the above-mentioned multi-functional MIMO scheme was referred to as a Layered Steered Space-Time Code (LSSTC) [15]. In order to further enhance the attainable system performance and to maximise the coding advantage of the proposed transmission scheme, the system characterized in [15] was combined with multidimensional SP-aided modulation. Hence, a potential research idea is to investigate the design of cooperative communication schemes that are characterised by diversity gain, multiplexing gain as well as beamforming gain. In other words, we are proposing to design multi-functional cooperative communication schemes. An uplink scheme can be implemented, where each MS may be equipped with a single antenna or a single antenna array. The users' actions may be coordinated in a way that the nearest users can transmit in a Space-Time Code (STC) manner, where the channels from the different MSs to the uplink receiver may be judiciously assumed to be statistically independent. Additionally, different groups of users employing STCs may transmit their data at the same time and using the same carrier frequency, like V-BLAST, in order to increase the attainable throughput of the system.

7.3.5 Soft-Relaying and Power-Optimisation in Cooperative Communication

In Chapter 5 we proposed a DSECCC-ID scheme that combines the concepts of cooperative communications and turbo coding. In the proposed scheme, we considered equal-power allocation for the two phases of cooperation as well as for the two users. However, in a practical scenario, the two cooperating users must be closer to each other than to the BS. Hence, their transmit power can be allocated more efficiently so that less power can be allocated for the cooperation phase and more power can be allocated to the second phase, while keeping the total transmit power in the two phases of cooperation constant. Additionally, the transmit power can be optimally shared between the two users so that the user benefitting from better channel conditions is assigned more transmit power.

On the other hand, soft relaying has been proposed as a powerful method of combining the main advantages of both AAF and DAF signalling strategies. In [221, 226, 229] soft DAF has been shown to outperform the DAF and AAF signalling, where it was argued that the DAF signalling loses soft information and hence all operations were performed in the LLR domain. Similarly, another beneficial extension to consider is to create a hybrid of the DAF or AAF as the optimal relaying scheme according to the specific position of relays. If the available relay is closer to the source DAF, gives a better performance, while if the relay is closer to the destination, then AAF is preferable [301]. Therefore, based on the performance improvements reported in the literature [301] while using soft information relaying, the DSECCC-ID scheme designed for a single user and the SPC-SECCC conceived for two users will transmit soft estimates of the other users' data instead of performing hard decoding, since the hard-decoding solution would lose the advantage of soft information.

7.3.6 Asynchronous Relaying in DSECCC-IDs

Asynchronous cooperative networks, where neither channel estimation nor symbol-level synchronisation is required at the cooperating nodes constitutes another promising direction to consider in our future research. The idea is to combine a differential SECCC-ID scheme with Loosely Synchronised (LS) codes [10]. This way we will be able to combat the effects of asynchronous uplink transmissions without any Channel State Information (CSI). Using a differential STC scheme, this design philosophy may be further extended to multiple relays.

7.3.7 Hierarchial Modulation in DSECCC-ID for Unequal Error Protection

Hierarchial modulation is used in Digital Video Broadcasting via Satellite services to Handhelds (DVB-SH) involving a high priority and a low priority bit stream, which are separately encoded. SECCCs can be used to mix these two streams so that the encoding of the less protected stream depends on the well protected. Hence at the decoder side we can involve soft decoding in order to improve the achievable performance of the low-priority stream.

Appendix **A**

Appendix to Chapter 3

In this appendix, the successful decoding threshold calculation of the Gray-mapped SECCC schemes introduced in Chapter 3 is presented in detail. All schemes use QPSK modulation. These have been summarised in Table 3.1.

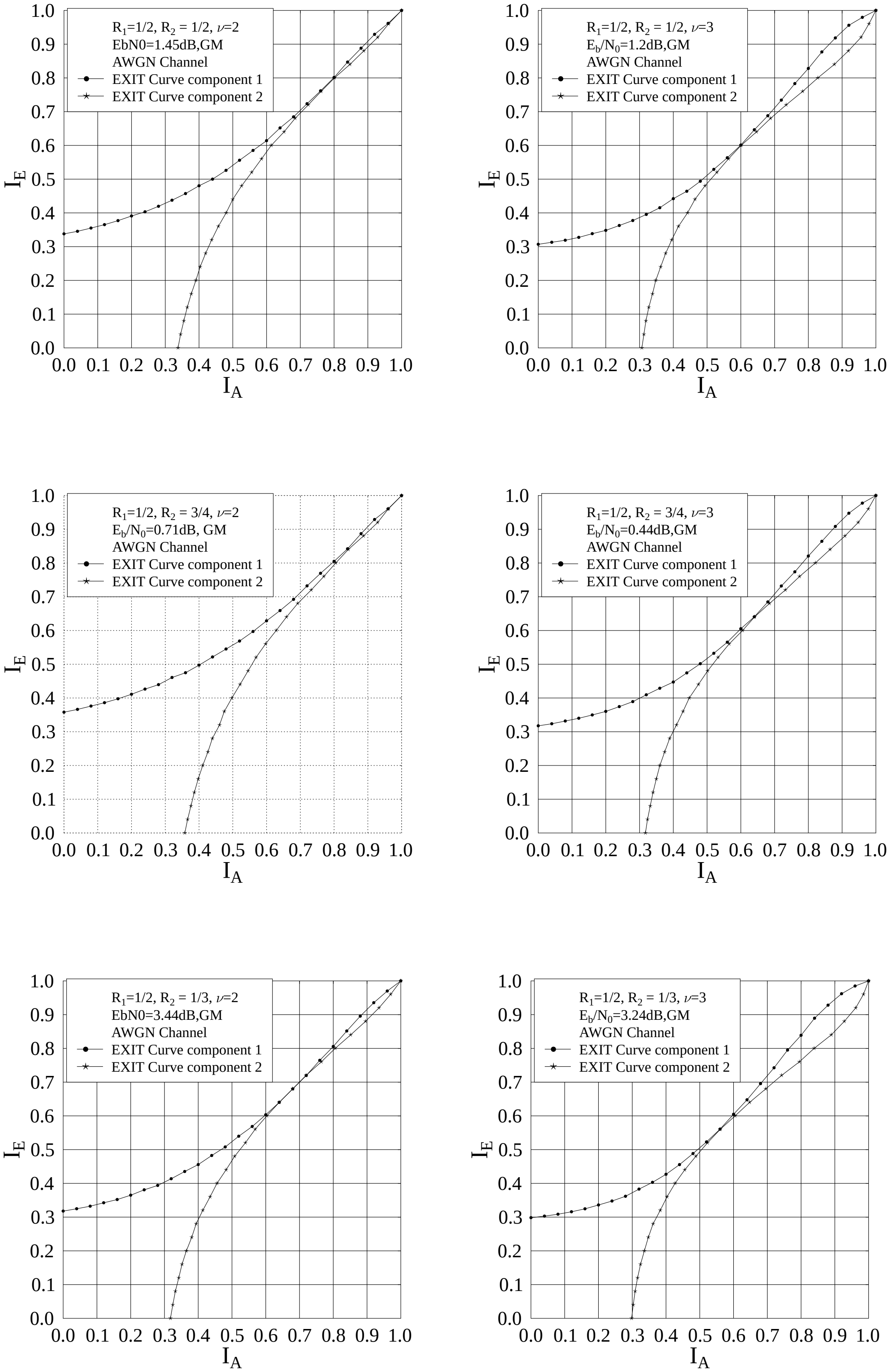

Figure A.1: Threshold calculation of GM-based RSC-coded SECCC systems for $R_1 = 1/2$ outlined in Table 3.1 for the case of AWGN channel.

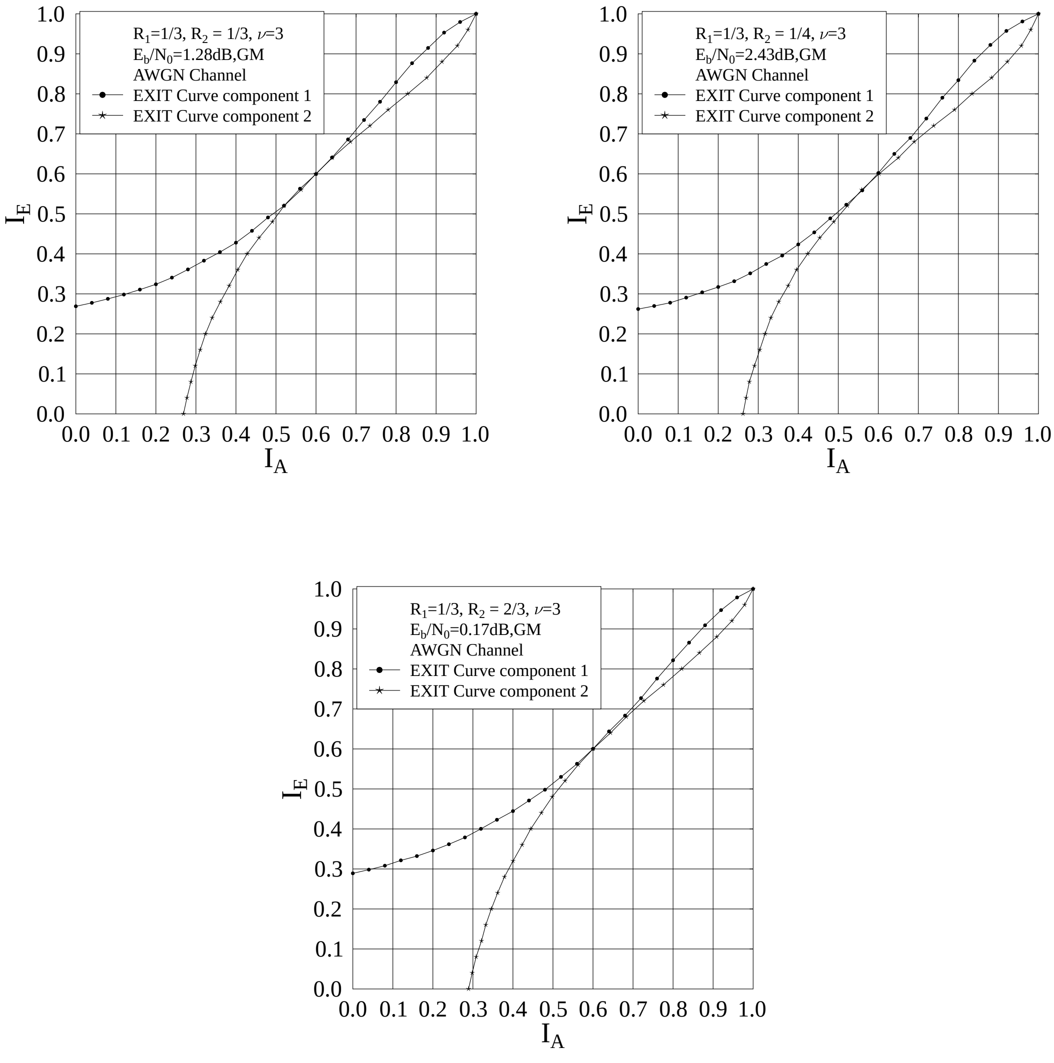

Figure A.2: Threshold calculation of GM-based RSC-coded SECCC systems for $R_1 = 1/3$ outlined in Table 3.1 for the case of AWGN channel.

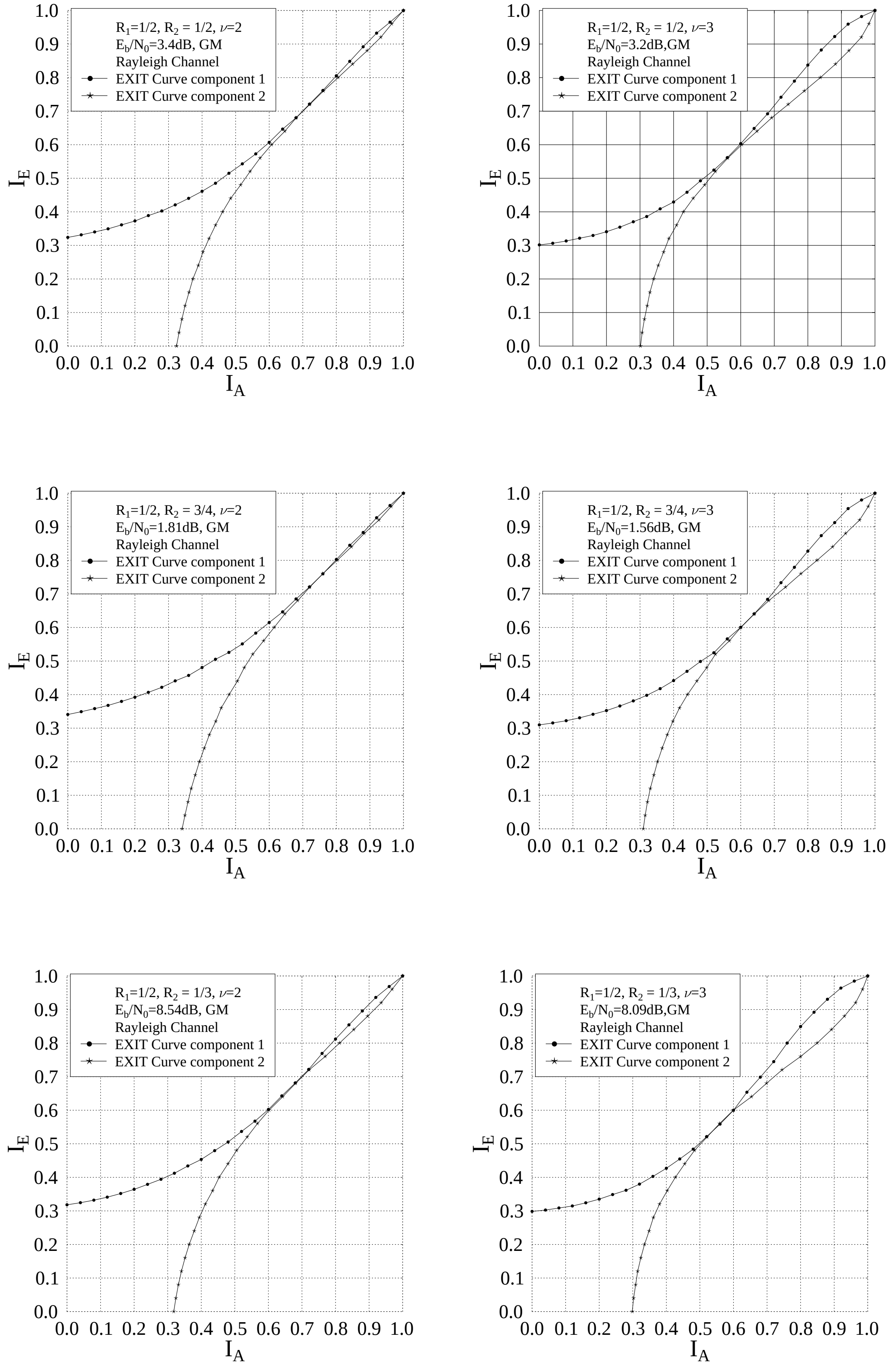

Figure A.3: Threshold calculation of GM-based RSC-coded SECCC systems for $R_1 = 1/2$ outlined in Table 3.1 for the case of Rayleigh fading channel.

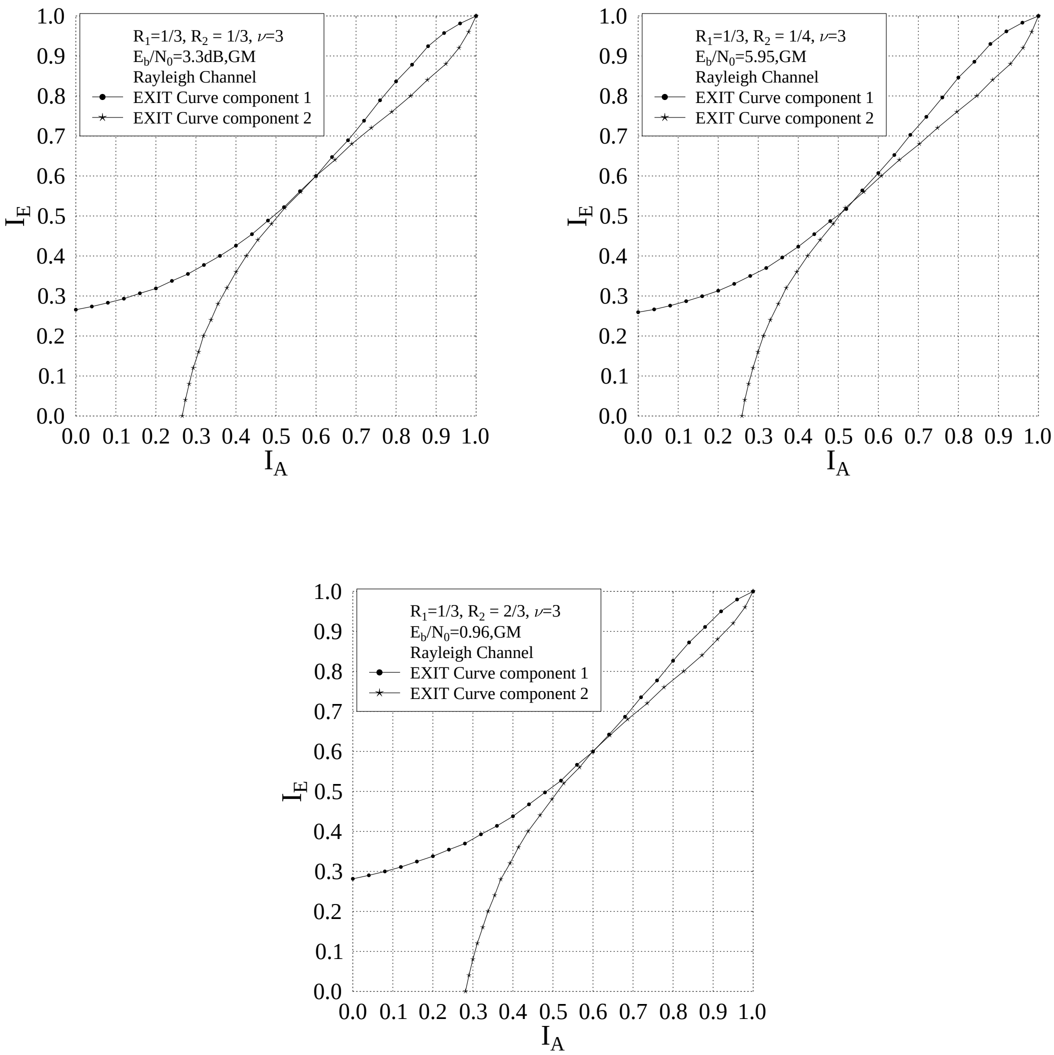

Figure A.4: Threshold calculation of GM-based RSC-coded SECCC systems for $R_1 = 1/2$ outlined in Table 3.1 for the case of Rayleigh fading channel.

Glossary

AAF	Amplify-And-Forward
AG	Algebraic-Geometry codes
ASO	Arbitrary Slice Ordering
AVC	Audio/Video Coding
AWGN	Additive White Gaussian Noise
BER	Bit Error Ratio, the number of the bits received incorrectly
BICM	Bit-Interleaved Coded Modulation
BICM-ID	Bit-Interleaved Coded Modulation with Iterative Decoding
bps	Bits per modulated symbol
BS	A common abbreviation for Base Station
CAF	Compress-And-Forward
CCI	Co-Channel Interference
CCMC	Continuous-input Continuous-output Memoryless Channel
CDMA	Code Division Multiple Access
CMA	Cooperative Multiple Access
CSI	Channel State Information
DAF	Decode-And-Forward
DARPA	Defense Advanced Research Projects Agency

DAS	Distributed Antenna System
DCMC	Discrete-input Continuous-output Memoryless Channel
DDF	Dynamic Decode and Forward
DL	DownLink
DP	Data Partitioning
DPC	Dirty Paper Coding
DS-CDMA	Direct Sequence Code Division Multiple Access
DS-SSMA	Direct Sequence Spread-Spectrum Multiple Access
DSECCC-ID	Distributed Self-Concatenated Coding using Iterative Decoding
DVB-SH	Digital Video Broadcasting - Satellite services to Handhelds
ECC	Error Correction Codes
EM	Electromagnetic Waves
EXIT	Extrinsic Information Transfer
FCC	Federal Communications Commission
FMO	Flexible Macroblock Ordering
fps	Frames-Per-Second
FRExt	Fidelity Range Extensions
GM	Gray Mapping
GMA	Gaussian Multiple Access
i.u.d.	Independent and Uniformly Distributed
IC	Interference Cancellation
IDMA	Interleave Division Multiple Access
IR	Impulse Radio
JSCD	Joint Source-Channel Decoding
JSIC	Joint Successive Interference Canceller

JVT Joint Video Team

LDC Linear Dispersion Codes

LLR Log-Likelihood Ratio

LOS Line Of Sight

LS Loosely Synchronised codes

LSSTC Layered Steered Space-Time Code

M-HARQ Multiplexed HARQ

MAP Maximum A Posteriori

MB Macroblock

MIMO Multi-Input Multi-Output

ML Maximum Likelihood

MLC MultiLevel Coding

MMSE Minimum Mean Square Error

MPEG Moving Picture Experts Group

MS A common abbreviation for Mobile Station

MSC Multiple Source Cooperation

MUD Multi-User Detection

MUI Multi-User Interference

NAL Network Adaptation Layer

NC Network Coding

OES Odd-Even Separation

OPSWF Orthogonal Prolate Spheroidal Wave Function

OSD Office of Secretary of Defense

PAL Precision Asset Location

PASIC Parallel Arbitrated Successive Interference Cancellation

PCC	Parallel Concatenated Code
PDF	Probability Density Function
PIC	Parallel Interference Cancellation
POTS	plain-old-telephone service
PPM	Pulse Position Modulated
PRF	Pulse Repetition Frequency
PSD	Power Spectral Density
PWEP	Pair-Wise Error Probability
QCIF	Quarter Common Intermediate Format
RA	Repeat-Accumulate
RD	Relay-Destination
RF	Radio Frequency
RNSC	Recursive Non-Systematic Convolutional
RS	Reed and Solomon codes
RSC	Recursive Systematic Convolutional
SCC	Serial Concatenated Code
SCM	Superposition Coded Modulation
SD	Source-Destination
SECCC	Self-Concatenated Convolutional Coding
SECCC-ID	Self-Concatenated Convolutional Coding with Iterative Decoding
SECTCM	Self-Concatenated Trellis Coded Modulation
SIC	Successive Interference Cancellation
SIRWEF	State Input-Redundancy WEF
SISO	Soft-Input-Soft-Output

SNR	Signal to Noise Ratio, noise energy compared to the signal energy
SOVA	Soft-Output Viterbi Algorithm
SP	Set Partitioning
SPC	SuperPosition Coding
SR	Source-Relay
STC	Space-Time Coding
TC	Turbo Codes
TCM	Trellis Coded Modulation
TCMA	Trellis Coded Multiple Access
TH	Time-Hopping
TOA	Time-of-Arrival
TTCM	Turbo Trellis Coded Modulation
TUB	Truncated Union Bound
UEP	Unequal Error Protection
UL	UpLink
UVLC	Universal Variable Length Coding
UWB	UltraWideBand
V-BLAST	Vertical Bell Labs Layered Space-Time
VAA	Virtual Antenna Array
VCEG	Video Coding Experts Group
VCL	Video Coding Layer
VLC	Variable Length Codes
VRC	Video Redundancy Coding
WEF	Weight Enumerating Function

Bibliography

[1] M.F.U. Butt, S.X. Ng and L. Hanzo, "EXIT chart aided design of near-capacity self-concatenated trellis coded modulation using iterative decoding," in *67th IEEE Vehicular Technology Conference, VTC-'08 Spring*, (Marina Bay, Singapore), pp. 734–738, May 2008.

[2] M.F.U. Butt, R.A. Riaz, S.X. Ng and L. Hanzo, "Near-capacity iteratively decoded binary self-concatenated code design using EXIT charts," in *IEEE Global Communications Conference, GLOBECOM '08*, (New Orleans, USA), Nov/Dec 2008.

[3] M.F.U. Butt, R.A. Riaz, S.X. Ng and L. Hanzo, "Near-Capacity Iterative Decoding of Binary Self-Concatenated Codes Using Soft Decision Demapping and 3-D EXIT Charts," *to appear in IEEE Transactions on Wireless Communications*, 2010.

[4] S.X. Ng, M.F.U. Butt and L. Hanzo, "On the union bounds of self-concatenated convolutional codes," *IEEE Signal Processing Letters*, vol. 16, pp. 754–757, September 2009.

[5] R. A. Riaz, M.F.U. Butt, S. Chen, and L. Hanzo, "Near-capacity UWB impulse radio using EXIT chart aided self-concatenated codes," in *70th IEEE Vehicular Technology Conference, VTC-'09 Fall*, (Alaska, USA), September 2009.

[6] Nasruminallah, M.F.U. Butt, S.X. Ng and L. Hanzo, "H.264 wireless video telephony using iteratively-detected binary self-concatenated coding," in *IEEE Vehicular Technology Conference, VTC-'10 Spring*, (Taipei, Taiwan), May 2010.

[7] M.F.U. Butt, R.A. Riaz, S.X. Ng and L. Hanzo, "Distributed self-concatenated codes for low-complexity power-efficient cooperative communication," in *70th IEEE Vehicular Technology Conference, VTC-'09 Fall*, (Anchorage, AK, USA), September 2009.

[8] M.F.U. Butt, R.A. Riaz, S.X. Ng and L. Hanzo, "Distributed Self-Concatenated Coding for Cooperative Communication," *to appear in IEEE Transactions on Vehicular Technology*, 2010.

[9] M.F.U. Butt, R. Zhang, S.X. Ng and L. Hanzo, "Superposition coding aided bi-directional relay transmission employing iteratively decoded self-concatenated convolutional codes," in *IEEE Vehicular Technology Conference, VTC-'10 Spring*, (Taipei, Taiwan), May 2010.

[10] L. Hanzo, L.-L. Yang, E.-L. Kuan and K. Yen, *Single and multi-carrier DS-CDMA: Multi-user detection, space-time spreading, synchronisation, networking and standards.* Chichester, England: John Wiley and Sons Ltd and IEEE Press, 2003.

[11] L. Hanzo, S.X. Ng, T. Keller and W. Webb, *Quadrature amplitude modulation: From basics to adaptive trellis-coded, turbo equalised and space-time coded OFDM, CDMA and MC-CDMA systems, 2nd Edition.* Chichester, England: John Wiley and Sons Ltd and IEEE Press, 2004.

[12] C. E. Shannon, "A mathematical theory of communication," *Bell Systems Technical Journal*, vol. 27, pp. 379/623–423/656, July/October 1948.

[13] C. Berrou, A. Glavieux and P. Thitimajshima, "Near Shannon limit error-correcting coding and decoding: Turbo-codes. 1," in *IEEE International Conference on Communications*, vol. 2, (Geneva), pp. 1064–1070, May 1993.

[14] L. Hanzo, T.H. Liew and B.L. Yeap, *Turbo coding, turbo equalisation and space time coding for transmission over fading channels.* Chichester, UK: Wiley: IEEE Press, 2002.

[15] L. Hanzo, O. Alamri, M. El-Hajjar and N. Wu, *Near-capacity multi-functional MIMO systems.* IEEE Press - John Wiley, April 2009.

[16] K.J.R. Liu, A.K. Sadek, W. Su and A. Kwasinski, *Cooperative communications and networking.* Cambridge University Press, 2009.

[17] M. Janani, A. Hedayat, T. Hunter and A. Nosratinia, "Coded cooperation in wireless communications: space-time transmission and iterative decoding," *IEEE Transactions on Signal Processing*, vol. 52, pp. 362–371, February 2004.

[18] T. S. Rappaport, *Wireless communications: Principles and practice.* Prentice Hall, 2002.

[19] A. Paulraj, R. Nabar and D. Gore, *Introduction to space-time wireless communications.* Cambridge University Press, 2003.

[20] H. Jafarkhani, *Space-time coding: Theory and practice.* Cambridge University Press, 2005.

[21] R.W. Hamming, "Error detecting and error correcting codes," *Bell Syst. Tech. Journal*, vol. 29, pp. 41–56, 1950.

[22] I. Reed, "A class of multiple-error-correcting codes and the decoding scheme," *IEEE Transactions on Information Theory*, vol. 4, pp. 38–49, September 1954.

[23] D. E. Muller, "Application of boolean switching algebra to switching cicuit design," *IEEE Transactions on Computers*, vol. 3, pp. 6–12, September 1954.

[24] P. Elias, "Coding for noisy channels," *IRE Conv. Rept.*, pp. 37–47, 1955.

[25] E. Prange, "Cyclic error-correcting codes in two symbols," *AFCRC-TN-57, 103, Air Force Cambridge Research Center, Cambridge, Mass.*, 1972.

[26] A. Hocquenghem, "Codes correcteurs d'erreurs," *Chiffres*, vol. 2, pp. 147–156, 1959.

[27] R.C. Bose and D.K. Ray-Chaudhuri, "On a class of error correcting binary group codes," *Information and Control*, vol. 3, pp. 68–79, March 1960.

[28] I.S. Reed and G. Solomon, "Polynomial codes over certain finite fields," *J. Soc. Ind. Appl. Math.*, vol. 8, pp. 300–304, June 1960.

[29] W.W. Peterson, "Encoding and error correction procedures for the Bose-Chaudhuri codes," *IRE Trans. Inform. Theory*, vol. IT-6, pp. 459–470, September 1960.

[30] W.W. Peterson, *Error-correcting codes.* Cambridge, MA and New York MIT Press and Wiley, 1961.

[31] R. Gallager, "Low-density parity-check codes," *IRE Transactions on Information Theory*, vol. 8, pp. 21–28, January 1962.

[32] G.D. Jr. Forney, R.G. Gallager, G.R. Lang, F.M. Longstaff and S.U. Qureshi, "Efficient modulation for band-limited channels," *IEEE Journal on Selected Areas in Communications*, vol. 2, pp. 632–647, September 1984.

[33] R. Fano, "A heuristic discussion of probabilistic decoding," *IEEE Transactions on Information Theory*, vol. 9, pp. 64–74, April 1963.

[34] J.L. Massey, *Threshold decoding.* MIT Press: Cambridge, Mass., 1963.

[35] G. Forney, *Concatenated codes.* Cambridge: MIT Press, 1966.

[36] G. Forney, "Generalized minimum distance decoding," *IEEE Transactions of Information Theory*, vol. 12, pp. 125–131, April 1966.

[37] E. Berlekamp, "Nonbinaty BCH decoding," *Intl. Symp. on. Info. Th.*, 1967.

[38] L. D. Rudolph, "A class of majority logic decodable codes," *IEEE Trans. Inform. Theory*, vol. 13, pp. 305–307, May 1967.

[39] E. Berlekamp, *Algebraic coding theory.* McGraw-Hill, New York, 1968.

[40] R. Gallager, *Information theory and reliable communication.* New York: Wiley, 1968.

[41] F. Jelinek, "Fast sequential decoding algorithm using a stack," *IBM J. Res. Develop.*, pp. 675–685, Nov 1969.

[42] J.L. Massey, "Shift-register synthesis and BCH decoding," *IEEE Trans. Information. Theory*, vol. IT-15, pp. 122–127, 1969.

[43] A. Viterbi, "Convolutional codes and their performance in communication systems," *IEEE Transactions on Communications [legacy, pre - 1988]*, vol. 19, pp. 751–772, October 1971.

[44] T.K. Moon, *Error correction coding: Mathematical methods and algorithms.* John Wiley Sons, Inc., 1st edition ed., 2005.

[45] L. Bahl, C. Cullum, W. Frazer and F. Jelinek, "An efficient algorithm for computing free distance," *IEEE Transactions on Information Theory*, vol. 18, pp. 437–439, May 1972.

[46] D. Chase, "A class of algorithms for decoding block codes with channel measurement information," *IEEE Transactions on Information Theory*, vol. IT-18, pp. 170–182, January 1972.

[47] W.W. Peterson and E.J. Jr. Weldon, *Error-correcting codes.* MIT Press: Cambridge, Mass., 2nd edition ed., 1972.

[48] G.D. Jr. Forney, "The Viterbi algorithm," *Proceedings of the IEEE*, vol. 61, pp. 268–278, March 1973.

[49] L. Bahl, J. Cocke, F. Jelinek and J. Raviv, "Optimal decoding of linear codes for minimizing symbol error rate," *IEEE Transactions on Information Theory*, vol. 20, pp. 284–287, March 1974.

[50] Y. Sugiyama, M. Kasahara, S. Hirasawa and T. Namekawa, "A method for solving key equation for Goppa codes," *Inf. and Control*, vol. 27, pp. 87–99, 1975.

[51] F.J. MacWilliams and J.A. Sloane, *The theory of error-correcting codes.* North-Holland, Amsterdam, 1977.

[52] R. McEliece and L. Swanson, *Reed-Solomon codes and their applications.* IEEE Press, New York, 1994.

[53] J. Wolf, "Efficient maximum likelihood decoding of linear block codes using a trellis," *IEEE Transactions on Information Theory*, vol. 24, pp. 76–80, January 1978.

[54] V. Goppa, "Codes on algebraic curves," *Soviet Math. Dokl.*, vol. 24, pp. 170–172, 1981.

[55] V.D. Goppa, *Geometry and codes.* Dordrecht [Netherlands] ; Boston : Kluwer Academic Publishers, 1988.

[56] G. Ungerböck, "Channel coding with multilevel/phase signals," *IEEE Transactions on Information Theory*, vol. 28, no. 1, pp. 55–67, 1982.

[57] S. Lin and D.J. Jr. Costello, *Error control coding: Fundamentals and applications.* Englewood Cliffs, N.J.: Prentice-Hall, 1983.

[58] R.E. Blahut, *Theory and practice of error control codes.* Reading, MA, USA: Addison-Wesley, 1983.

[59] D. Divsalar and M.K. Simon, "Multiple trellis coded modulation (MTCM)," *IEEE Transactions on Communications*, vol. 36, pp. 410–419, April 1988.

[60] J. Hagenauer and P. Hoeher, "A Viterbi algorithm with soft-decision outputs and its applications," in *IEEE Global Telecommunications Conference, GLOBECOM '89.*, (Dallas, TX), pp. 1680–1686, November 1989.

[61] W. Koch and A. Baier, "Optimum and sub-optimum detection of coded data disturbed by time-varying intersymbol interference," in *IEEE Global Telecommunications Conference, GLOBECOM '90.*, (San Diego, CA, USA), pp. 1679–1684, December 1990.

[62] E. Zehavi, "8-PSK trellis codes for a Rayleigh fading channel," *IEEE Transactions on Communications*, vol. 40, pp. 873–883, May 1992.

[63] B. Honary, G. S. Markarian and P. G. Farrell, "Generalised array codes and their trellis structure," *Electronics Letters*, vol. 29, pp. 541–542, March 1993.

[64] B. Honary and G. Markarian, "Low-complexity trellis decoding of Hamming codes," *Electronics Letters*, vol. 29, pp. 1114 –1116, June 1993.

[65] A.R. Hammons, P.V. Kumar, A.R. Calderbank, N.J.A. Sloane and P. Sole, "The Z_4-linearity of Kerdock, Preparata, Goethals and related codes," *IEEE Transactions on Information Theory*, vol. 40, p. 301, 1994.

[66] J.A. Erfanian, S. Pasupathy and G. Gulak, "Reduced complexity symbol dectectors with parallel structures for ISI channels," *IEEE Transactions on Communications*, vol. 42, pp. 1661–1671, 1994.

[67] MacKay and Neal, "Good codes based on very sparse matrices," in *IMA: IMA Conference on Cryptography and Coding, LNCS lately (earlier: Cryptography and Coding II, Edited by Chris Mitchell, Clarendon Press, 1992)*, 1995.

[68] S.B. Wicker, *Error control systems for digital communication and storage*. Englewood Cliffs, NJ, USA: Prentice-Hall, 1994.

[69] P. Robertson, E. Villebrun and P. Hoeher, "A comparison of optimal and sub-optimal MAP decoding algorithms operating in the Log domain," in *Proceedings of International Conference on Communications*, (Seattle, USA), pp. 1009–1013, June 1995.

[70] J. Hagenauer, E. Offer and L. Papke, "Iterative decoding of binary block and convolutional codes," *IEEE Transactions on Information Theory*, vol. 42, pp. 429–445, March 1996.

[71] G.D. Jr. Forney, L. Brown, M.V. Eyuboglu and J.L. III. Moran, "The V.34 high speed modem standard," *IEEE Communications Magazine*, vol. 34, pp. 28–33, December 1996.

[72] V. Sidorenko, G. Markarian and B. Honary, "Minimal trellis design for linear codes based on the Shannon product," *IEEE Transactions on Information Theory*, vol. 42, pp. 2048–2053, November 1996.

[73] V. Tarokh, N. Seshadri and A. Calderbank, "Space-time codes for high data rate wireless communications: Performance criterion and code construction," in *Proc IEEE International Conference on Communications '97*, (Montreal, Canada), pp. 299–303, 1997.

[74] H. Nickl, J. Hagenauer and F. Burkett, "Approaching Shannon's capacity limit by 0.27 dB using simple Hamming codes," *IEEE Communications Letters*, vol. 1, pp. 130–132, September 1997.

[75] C. Schlegel, *Trellis coding*. New York: John Wiley & Sons, September 1997.

[76] X. Li and J.A. Ritcey, "Bit-interleaved coded modulation with iterative decoding," *IEEE Communications Letters*, vol. 1, pp. 169–171, November 1997.

[77] P. Robertson and T. Wörz, "Bandwidth-efficient turbo trellis-coded modulation using punctured component codes," *IEEE Journal on Selected Areas in Communications*, vol. 16, pp. 206–218, February 1998.

[78] S.M. Alamouti, "A simple transmit diversity technique for wireless communications," *IEEE Journal on Selected Areas in Communications*, vol. 16, no. 8, pp. 1451–1458, 1998.

[79] V. Guruswami and M. Sudan, "Improved decoding of Reed-Solomon and algebraic-geometric codes," in *IEEE Symposium on Foundations of Computer Science*, pp. 28–39, 1998.

[80] X. Li and J.A. Ritcey, "Trellis-coded modulation with bit interleaving and iterative decoding," *IEEE Journal on Selected Areas in Communications*, vol. 17, pp. 715–724, April 1999.

[81] S.M. Aji and R.J. McEliece, "The generalized distributive law," *IEEE Transactions on Information Theory*, vol. 46, pp. 325–343, March 2000.

[82] F.R. Kschischang, B.J. Frey and H.-A. Loeliger, "Factor graphs and the sum-product algorithm," *IEEE Transactions on Information Theory*, vol. 47, pp. 498–519, February 2001.

[83] J.G. Proakis, *Digital communications.* McGraw Hill Higher Education, 4th edition ed., December 1, 2000.

[84] S. Siwamogsatham and M. Fitz, "Robust space-time coding for correlated Rayleigh fading channels," *IEEE Transactions on Signal Processing*, vol. 50, pp. 2408–2416, October 2002.

[85] H. Jafarkhani and N. Seshadri, "Super-orthogonal space-time trellis codes," *IEEE Transactions on Information Theory*, vol. 49, pp. 937–950, April 2003.

[86] R. Koetter and A. Vardy, "Algebraic soft-decision decoding of Reed-Solomon codes," *IEEE Transactions on Information Theory*, vol. 49, pp. 2809–2825, November 2003.

[87] S. Lin and D.J. Jr. Costello, *Error control coding: Second edition.* Upper Saddle River, New Jersey: Prentice-Hall, 2004.

[88] M.K. Simon and M.S. Alouini, *Digital communications over fading channels.* John Wiley Sons, Inc., 2nd edition ed., 2005.

[89] A. Song, G. Wang and X.G. Xia, "Some super-orthogonal space-time trellis codes based on non-PSK MTCM," *IEEE Transactions on Wireless Communications*, vol. 4, pp. 1214–1221, May 2005.

[90] M. Bossert, *Channel coding for telecommunications.* Wiley, 1999.

[91] S.L. Goff, A. Glavieux and C. Berrou, "Turbo-codes and high spectral efficiency modulation," in *IEEE International Conference on Communications*, (New Orleans, LA), pp. 645–649, 1994.

[92] S. Benedetto, D. Divsalar, G. Montorsi and F. Pollara, "Bandwidth efficient parallel concatenated coding schemes," *Electronics Letters*, vol. 31, pp. 2067–2069, November 1995.

[93] S.X. Ng, T.H. Liew, L-L. Yang and L. Hanzo, "Comparative study of TCM, TTCM, BICM and BICM-ID schemes," in *IEEE Vehicular Technology Conference*, (Rhodes, Greece), pp. 2450–2454, May 2001.

[94] S. Benedetto, D. Divsalar, G. Montorsi and F. Pollara, "Serial concatenation of interleaved codes: performance analysis, design and iterative decoding," *IEEE Transactions on Information Theory*, vol. 44, pp. 909–926, May 1998.

[95] S. Benedetto, D. Divsalar, G. Montorsi and F. Pollara, "Self-concatenated trellis coded modulation with self-iterative decoding," in *IEEE Global Telecommunications Conference*, vol. 1, (Sydney, NSW, Australia), pp. 585–591, 1998.

[96] H.-A. Loeliger, "New turbo-like codes," in *IEEE International Symposium on Information Theory*, (Ulm), p. 109, Jun/Jul 1997.

[97] D. Divsalar and F. Pollara, "Multiple turbo codes for deep-space communications," Telecommunications and Data Acquisition Progress Report 42-121, Jet Propulsion Laboratory, Pasadena, CA, May 1995.

[98] S. Benedetto and G. Montorsi, "Iterative decoding of serially concatenated convolutional codes," *Electronics Letters*, vol. 32, pp. 1186–1188, June 1996.

[99] D. Raphaeli and Y. Zarai, "Combined turbo equalization and turbo decoding," in *Proceedings of IEEE Global Telecommunications Conference (GLOBECOM)*, vol. 2, (Phoenix, AZ), pp. 639–643, November 1997.

[100] D. Raphaeli and Y. Zarai, "Combined turbo equalization and turbo decoding," *IEEE Communications Letters*, vol. 2, pp. 107–109, April 1998.

[101] M. Toegel, W. Pusch and H. Weinrichter, "Combined serially concatenated codes and turbo-equalization," in *2nd International Symposium on Turbo Codes*, (Brest, France), pp. 375–378, September 2000.

[102] S. Benedetto, D. Divsalar, G. Montorsi and F. Pollara, "A soft-input soft-output APP module for iterative decoding of concatenated codes," *IEEE Communications Letters*, vol. 1, pp. 22–24, January 1997.

[103] G. Caire, G. Taricco and E. Biglieri, "Bit-interleaved coded modulation," in *Proceedings of IEEE International Symposium on Information Theory (ISIT)*, (Ulm, Germany), p. 96, June/July 1997.

[104] G. Caire, G. Taricco and E. Biglieri, "Bit-interleaved coded modulation," *IEEE Transactions on Information Theory*, vol. 44, pp. 927–946, May 1998.

[105] S. ten Brink, J. Speidel and R.-H. Yan, "Iterative demapping and decoding for multilevel modulation," in *IEEE Global Telecommunications Conference (GLOBCOM)*, vol. 1, (Sydney,NSW), pp. 579–584, 1998.

[106] X. Li and J.A. Ritcey, "Bit-interleaved coded modulation with iterative decoding using soft feedback," *IEE Electronics Letters*, vol. 34, pp. 942–943, May 1998.

[107] X. Wang and H.V. Poor, "Iterative (turbo) soft interference cancellation and decoding for coded CDMA," *IEEE Transactions on Communications*, vol. 47, pp. 1046–1061, July 1999.

[108] A. Sezgin, D. Wuebben and V. Kuehn, "Analysis of mapping strategies for turbo-coded space-time block codes," in *Proceedings of IEEE Information Theory Workshop*, (Paris, France), pp. 103–106, March/April 2003.

[109] C. Douillard, M. Jezequel, C. Berrou, A. Picart, P. Didier and A. Glavieux, "Iterative correction of intersymbol interference: turbo equalization," *European Transaction on Telecommunications*, vol. 6, pp. 507–511, September/October 1995.

[110] S. Benedetto, D. Divsalar, G. Montorsi and F. Pollara, "Serial concatenation of interleaved codes: performance analysis, design and iterative decoding," *IEEE Transactions on Information Theory*, vol. 44, pp. 909–926, May 1998.

[111] D. Divsalar, S. Dolinar and F. Pollara, "Low complexity turbo-like codes," in *2nd International Symposium on Turbo Codes and Related Topics*, (Brest, France), pp. 73–80, September 2000.

[112] D. Divsalar, S. Dolinar and F. Pollara, "Serial concatenated trellis coded modulation with rate-1 inner code," in *IEEE Global Telecommunications Conference (GLOBECOM)*, vol. 2, (San Francisco, CA), pp. 777–782, 2000.

[113] K.R. Narayanan, "Effect of precoding on the convergence of turbo equalization for partial response channels," *IEEE Journal on Selected Areas in Communications*, vol. 19, pp. 686–698, April 2001.

[114] I. Lee, "The effect of a precoder on serially concatenated coding systems with an ISI channel," *IEEE Transactions on Communications*, vol. 49, pp. 1168–1175, July 2001.

[115] L. Lifang, D. Divsalar and S. Dolinar, "Iterative demodulation, demapping and decoding of coded non-square QAM," in *IEEE Transactions on Communications*, vol. 53, pp. 16–19, January 2005.

[116] S. ten Brink, "Designing iterative decoding schemes with the extrinsic information transfer chart," *AEÜ International Journal of Electronics and Communications*, vol. 54, pp. 389–398, November 2000.

[117] S. ten Brink, "Convergence behavior of iteratively decoded parallel concatenated codes," *IEEE Transactions on Communications*, vol. 49, pp. 1727–1737, October 2001.

[118] M. Tüchler and J. Hagenauer, "EXIT charts of irregular codes," in *Conference on Information Science and Systems*, (Princtone, NJ), pp. 748–753, March 2002.

[119] J. Hagenauer, "The EXIT chart - Introduction to extrinsic information transfer in iterative processing," in *European Signal Processing Conference*, (Vienna, Austria), pp. 1541–1548, September 2004.

[120] S. ten Brink, "Convergence of multidimensional iterative decoding schemes," in *Conference Record of the Thirty-Fifth Asilomar Conference on Signals, Systems and Computers*, vol. 1, (Pacific Grove, CA, USA), pp. 270–274, 2001.

[121] M. Tüchler, "Convergence prediction for iterative decoding of threefold concatenated systems," in *IEEE Global Telecommunications Conference (GLOBECOM)*, vol. 2, (Taipei, Taiwan), pp. 1358–1362, November 2002.

[122] F. Brännström, L.K. Rasmussen and A.J. Grant, "Convergence analysis and optimal scheduling for multiple concatenated codes," *IEEE Transactions on Information Theory*, vol. 51, pp. 3354–3364, September 2005.

[123] O. F. Acikel and W. E. Ryan, "Punctured turbo-codes for BPSK/QPSK channels," *IEEE Transactions on Communications*, vol. 47, pp. 1315–1323, September 1999.

[124] H. El Gamal and A.R. Hammons, "Analyzing the turbo decoder using the Gaussian approximation," *IEEE Journal on Selected Areas in Communications*, vol. 47, pp. 671–686, February 2001.

[125] R. Ramamurthy and W.E. Ryan, "Convolutional double accumulate codes (or double turbo DPSK)," *IEEE Communications Letters*, vol. 5, pp. 157–159, April 2001.

[126] M. Tüchler, S. ten Brink and J. Hagenauer, "Measures for tracing convergence of iterative decoding algorithms," in *Proceedings of the 4th International ITG Conference on Source and Channel Coding*, (Berlin, Germany), pp. 53–60, January 2002.

[127] M. Tüchler, "Design of serially concatenated systems depending on the block length," *IEEE Transactions on Communications*, vol. 52, no. 2, pp. 209–218, 2004.

[128] Q. Luo and P. Sweeney, "Method to analyse convergence of turbo codes," *Electronics Letters*, vol. 41, pp. 757 – 758, June 2005.

[129] C. Douillard and C. Berrou, "Turbo codes with rate-m/(m+1) constituent convolutional codes," *IEEE Transactions on Communications*, vol. 53, pp. 1630 – 1638, October 2005.

[130] I. Chatzigeorgiou, M.R.D. Rodrigues, I.J. Wassell and R. Carrasco, "A novel technique to evaluate the transfer function of punctured turbo codes," in *IEEE International Conference on Communications, ICC '06.*, vol. 3, pp. 1166–1171, June 2006.

[131] W.R. Carson, I.J. Wassell and M. Rodrigues, "Optimal 8PSK mappings for BICM-ID over quasi-static fading channels," in *5th International Symposium on Turbo Codes and Related Topics*, pp. 128–133, September 2008.

[132] S.X. Ng, O.R. Alamri, Y. Li, J. Kliewer and L. Hanzo, "Near-capacity turbo trellis coded modulation design based on EXIT charts and union bounds," *IEEE Transactions on Communications*, vol. 56, pp. 2030–2039, December 2008.

[133] R.G. Maunder, J. Wang, S.X. Ng, L.-L. Yang and L. Hanzo, "On the performance and complexity of irregular variable length codes for near-capacity joint source and channel coding," *IEEE Transactions on Wireless Communications*, vol. 7, pp. 1338–1347, April 2008.

[134] C. Berrou, A. Graell i Amat, Y. Ould-Cheikh-Mouhamedou and Y. Saouter, "Improving the distance properties of turbo codes using a third component code: 3D turbo codes," *IEEE Transactions on Communications*, vol. 57, pp. 2505 – 2509, September 2009.

[135] A. Grant, "Convergence of non-binary iterative decoding," in *IEEE Global Telecommunications Conference*, vol. 2, (San Antonio, TX, USA), pp. 1058–1062, November 2001.

[136] H. Chen and A. Haimovich, "EXIT charts for turbo trellis-coded modulation," *IEEE Communications Letters*, vol. 8, pp. 668–670, November 2004.

[137] J. Kliewer, S.X. Ng and L. Hanzo, "Efficient computation of EXIT functions for non-binary iterative decoding," *IEEE Transactions on Communications*, vol. 54, pp. 2133–2136, December 2006.

[138] S. ten Brink, "Rate one-half code for approaching the Shannon limit by 0.1 dB," *Electronics Letters*, vol. 36, pp. 1293–1294, July 2000.

[139] D. Divsalar and M.K. Simon, "The design of trellis coded MPSK for fading channels: Set partitioning for optimum code design," *IEEE Transactions on Communications*, vol. 36, pp. 1013–1021, September 1988.

[140] D. Divsalar and M.K. Simon, "The design of trellis coded MPSK for fading channels: Performance criteria," *IEEE Transactions on Communications*, vol. 36, pp. 1004–1012, September 1988.

[141] A. Ashikhmin, G. Kramer and S. ten Brink, "Extrinsic information transfer functions: model and erasure channel properties," *IEEE Transactions on Information Theory*, vol. 50, no. 11, pp. 2657–2673, 2004.

[142] J. Kliewer, S.X. Ng and L. Hanzo, "On the computation of EXIT characteristics for symbol-based iterative decoding," in *4th International Symposium on Turbo Codes in connection with 6th International ITG-Conference on Source and Channel Coding*, (Munich, Germany), April 2006.

[143] S.X. Ng and L. Hanzo, "On the MIMO channel capacity of multidimensional signal sets," *IEEE Transactions on Vehicular Technology*, vol. 55, pp. 528–536, March 2006.

[144] S. Benedetto and G. Montorsi, "Unveiling turbo codes: Some results on parallel concatenated coding schemes," *IEEE Transactions on Information Theory*, vol. 42, pp. 409–428, March 1996.

[145] L.C. Perez, J. Seghers and D.J. Jr. Costello, "A distance spectrum interpretation of turbo codes," *IEEE Transactions on Information Theory*, vol. 42, pp. 1698–1709, November 1996.

[146] Garello, R. and Pierleoni, P. and Benedetto, S., "Computing the free distance of turbo codes and serially concatenated codes with interleavers: algorithms and applications," *IEEE Journal on Selected Areas in Communications*, vol. 19, pp. 800–812, May 2001.

[147] Y. Li and B. Vucetic, "Optimization of space-time block codes based on multidimensional super-set partitioning," *IEEE Signal Processing Letters*, vol. 12, pp. 317–320, April 2005.

[148] I. Chatzigeorgiou, M.R.D. Rodrigues, I.J. Wassell and R. Carrasco, "A union bound approximation for rapid performance evaluation of punctured turbo codes," in *41st Annual Conference on Information Sciences and Systems (CISS '07)*, pp. 474–479, March 2007.

[149] A. Graell i Amat, F. Brännström and L.K. Rasmussen, "On the design of rate-compatible serially concatenated convolutional codes," *European Transactions on Telecommunications*, vol. 18, pp. 519–527, 2007.

[150] K.T. Phan and C. Tellambura, "Receive antenna selection based on union-bound minimization using convex optimization," *IEEE Signal Processing Letters*, vol. 14, pp. 609–612, September 2007.

[151] S. ten Brink and G. Kramer, "Design of repeat-accumulate codes for iterative detection and decoding," *IEEE Transactions on Signal Processing*, vol. 51, pp. 2764–2772, November 2003.

[152] J. Hagenauer, "Rate-compatible punctured convolutional codes (RCPC codes) and their applications," *IEEE Transactions on Communications*, vol. 36, pp. 389–400, April 1988.

[153] B. Scanavino, G. Montorsi and S. Benedetto, "Convergence properties of iterative decoders working at bit and symbol level," in *IEEE Global Telecommunications Conference, 2001. GLOBECOM '01.*, vol. 2, (San Antonio, TX, USA), pp. 1037–1041, 2001.

[154] S.X. Ng, S. Das, J. Wang and L. Hanzo, "Near-capacity iteratively decoded space-time block coding," in *67th IEEE Vehicular Technology Conference, VTC-'08 Spring*, (Marina Bay, Singapore), May 2008.

[155] X. Li, A. Chindapol and J.A. Ritcey, "Bit-interleaved coded modulation with iterative decoding and 8PSK signaling," *IEEE Transactions on Communications*, vol. 50, pp. 1250–1257, August 2002.

[156] F. Schreckenbach, N. Görtz, J. Hagenauer and G. Bauch, "Optimization of symbol mappings for bit-interleaved coded Modulation with iterative decoding," *IEEE Communications Letters*, vol. 7, pp. 593–595, December 2003.

[157] N.H. Tran and H.H. Nguyen, "A novel multi-dimensional mapping of 8-PSK for BICM-ID," *IEEE Transactions on Wireless Communications*, vol. 6, pp. 1133–1142, March 2007.

[158] J. Wang, S. X. Ng, L. L. Yang and L. Hanzo, "Combined serially concatenated codes and MMSE equalization: An EXIT chart aided perspective," in *IEEE 64th Vehicular Technology Conference, VTC-'06 Fall*, pp. 1–5, September 2006.

[159] S.X. Ng, J. Wang, M. Tao, L.-L. Yang and L. Hanzo, "Iteratively decoded variable-length space-time coded modulation: code construction and convergence analysis," *IEEE Transactions on Wireless Communications*, vol. 6, pp. 1953–1963, May 2007.

[160] S.X. Ng, J. Wang and L. Hanzo, "Unveiling near-capacity code design: The realization of Shannon's communication theory for MIMO channels," in *IEEE International Conference on Communications, ICC '08*, pp. 1415–1419, May 2008.

[161] S.X. Ng and L. Hanzo, "On the MIMO channel capacity of multi-dimensional signal sets," in *IEEE Vehicular Technology Conference*, vol. 3, pp. 1594–1598, 2004.

[162] I. Land, P. Hoeher and S. Gligorević, "Computation of symbol-wise mutual information in transmission systems with logAPP decoders and application to EXIT charts," in *Proc. International ITG Conference on Source and Channel Coding (SCC)*, (Erlangen, Germany), pp. 195–202, January 2004.

[163] D. Divsalar and M.K. Simon, "Trellis coded modulation for 4800-9600 bits/s transmission over a fading mobile satellite channel," *IEEE Journal on Selected Areas in Communications*, vol. 5, pp. 162–175, February 1987.

[164] L.-L. Yang and L. Hanzo, "Adaptive rate DS-CDMA systems using variable spreading factors," *IEEE Transactions on Vehicular Technology*, vol. 53, no. 1, pp. 72–81, 2004.

[165] M. Z. Win and R. A. Scholtz, "Impulse radio: how it works," *IEEE Communications Letters*, vol. 2, pp. 36–38, Feb 1998.

[166] Federal Communications Commission, "Revision of Part 15 of the Commission's rules regarding ultra-wideband transmission systems, First Report and Order," *FCC*, April 2002.

[167] M. Oner, "On the spectral correlation of UWB impulse radio signals," *IEEE Communications Letters*, vol. 12, pp. 714–716, Oct 2008.

[168] M. Z. Win and R. A. Scholtz, "On the energy capture of ultrawide bandwidth signals in dense multipath environments," *IEEE Communications Letters*, vol. 2, pp. 245–247, Sep. 1998.

[169] L.A. De Rosa, "Random impulse system," *U.S. Patent 2,671,896*, Mar 1954.

[170] G.F. Ross, "A time domain criterion for the design of wideband radiating elements," *IEEE Transactions on Antennas and Wireless Propagation*, vol. 16, pp. 355–356, Nov 1968.

[171] G.F. Ross, "Transmission and reception system for generating and receiving base-band pulse signals for short base-band pulse communication system," *U.S. Patent 3,728,632*, Apr 1973.

[172] C.L. Bennett and G.F. Ross, "Time-domain electromagnetics and its applications," *Proceedings of the IEEE*, vol. 66, pp. 299–318, Mar 1978.

[173] H.F. Harmuth, "Synthetic aperture radar based on nonsinusoidal functions: VI-pulse position and pulse shape coding," *IEEE Transactions Electromagnetic Compatibility*, vol. 3, pp. 93–106, Apr 1980.

[174] C. Fowler, J. Entzminger and J. Corum, "Assessment of Ultra-Wideband (UWB) Technology," Summary Report of the DARPA/OSD Panel to examine stateof- the-art, benefits, and limitations of UWB Technology, 1990.

[175] R. Scholtz, "Multiple access with time-hopping impulse modulation," in *IEEE Military Communications Conference*, vol. 2, (Boston, MA), pp. 447–450, Oct 1993.

[176] R.J. Fontana and S.J. Gunderson, "Ultra-wideband precision asset location system," in *IEEE Conference on Ultra Wideband Systems and Technologies*, pp. 147–150, May 2002.

[177] S. Gezici, Z. Tian, G.B. Giannakis, H. Kobayashi, A.F. Molisch, H.V. Poor, Z. Sahinoglu, "Localization via ultra-wideband radios: a look at positioning aspects for future sensor networks," *IEEE Signal Processing Magazine*, vol. 22, pp. 70–84, July 2005.

[178] A.F. Molisch, D. Cassioli, C.-C. Chong, S. Emami, A. Fort, B. Kannan, J. Karedal, J. Kunisch, H.G. Schantz, K. Siwiak and M.Z. Win, "A comprehensive standardized model for ultrawideband propagation channels," *IEEE Transactions on Antennas and Propagation*, vol. 54, pp. 3151–3166, Nov 2006.

[179] G. Bacci, M. Luise, H.V. Poor and A.M. Tulino, "Energy efficient power control in impulse radio UWB wireless networks," *IEEE Journal of Selected Topics in Signal Processing*, vol. 1, pp. 508–520, Oct 2007.

[180] D. Dardari, A. Conti, U. Ferner, A. Giorgetti and M.Z. Win, "Ranging with ultrawide bandwidth signals in multipath environments," *Proceedings of the IEEE*, vol. 97, pp. 404–426, Feb 2009.

[181] M. Z. Win and R. A. Scholtz, "On the robustness of ultra-wide bandwidth signals in dense multipath environments," *IEEE Communications Letters*, vol. 2, pp. 51–53, Feb 1998.

[182] M. Hamalainen, V. Hovinen, R. Tesi, J.H.J. Iinatti and M. Latva-Aho, "On the UWB system coexistence with GSM 900, UMTS/WCDMA, and GPS," *IEEE Journal on Selected Areas in Communications*, vol. 20, pp. 1712–1721, Dec 2002.

[183] L. Hanzo, P.J. Cherriman and J. Streit, *Video Compression and Communications: From Basics to H.261, H.263, H.264, MPEG2, MPEG4 for DVB and HSDPA-Style Adaptive Turbo-Transceivers.* IEEE Press-John Wiley & Sons, September 2007.

[184] Nasruminallah and L. Hanzo, "EXIT-Chart optimised short block codes for iterative joint source and channel decoding in H.264 video telephony," *IEEE Transactions on Vehicular Technology*, vol. 58, pp. 4306–4315, October 2009.

[185] J. Ostermann, J. Bormans, P. List, D. Marpe, M. Narroschke, F. Pereira, T. Stockhammer and T. Wedi, "Video coding with H.264/AVC: tools, performance, and complexity," *IEEE Circuits and Systems Magazine*, vol. 4, pp. 7–28, First Quarter 2004.

[186] T. Stockhammer, M.M. Hannuksela and T. Wiegand, "H.264/AVC in wireless environments," *IEEE Transactions on Circuits and Systems for Video Technology*, vol. 13, pp. 657–673, Jul 2003.

[187] J. Liu, G. Tu, C. Zhang and Y. Yang, "Joint source and channel decoding for variable length encoded turbo codes," *EURASIP J. Adv. Signal Process*, vol. 2008, no. 1, pp. 1–10, 2008.

[188] M. Adrat, P. Vary and T. Clevorn, "Optimized bit rate allocation for iterative source-channel decoding and its extension towards multi-mode transmission," in *Proceedings of IST Mobile and Wireless Communications Summit (Dresden, Germany)*, pp. 1153–1157, Jun 2005.

[189] H. Sato and T. Ohtsuki, "Frequency domain channel estimation and equalisation for direct sequence ultra wideband DS-UWB system," *IEE Proceedings Communications*, vol. 153, pp. 93–98, Feb 2006.

[190] A.F. Molisch, "Ultrawideband propagation channels theory, measurement, and modeling," *IEEE Transactions on Vehicular Technology*, vol. 54, pp. 1528–1545, Sep 2005.

[191] M.D. Yacoub, J.E.V. Bautistu and L. Guedes, "On higher order statistics of the Nakagami-m distribution," *IEEE Transactions on Vehicular Technology*, vol. 48, pp. 790–794, May 1999.

[192] A. Klein, G. Kaleh and P. W. Baier, "Zero forcing and minimum mean-square-error equalization formultiuser detection in code-division multiple-access channels," *IEEE Transactions on Vehicular Technology*, vol. 45, pp. 276–287, May 1996.

[193] ITU-T: H.264 Recommendation , "H.264 : Advanced video coding for generic audiovisual services," (www.itu.int/rec/T-REC-H.264/en), p. 282, May 2003.

[194] P. Raibroycharoen, M.M. Ghandi, E.V. Jones and M. Ghanbari, "Performance analysis of H.264/AVC video transmission with unequal error protected turbo codes," *IEEE 61st Vehicular Technology Conference, VTC-'05 Spring*, vol. 3, pp. 1580–1584, May/Jun 2005.

[195] S. Wenger, "Video redundancy coding in H.263+," in *International Workshop on Audio-Visual Services over Packet Networks*, Sept 1997.

[196] T. Wiegand, G.J. Sullivan, G. Bjntegaard and A. Luthra, "Overview of the H.264/AVC video coding standard," *IEEE Transactions on Circuits and Systems for Video Technology*, vol. 13, pp. 560–576, Jul 2003.

[197] S. Wenger, "H.264/AVC over IP," *IEEE Transactions on Circuits and Systems for Video Technology*, vol. 13, pp. 645–656, Jul 2003.

[198] T. Stockhammer and M. Bystrom, "H.264/AVC data partitioning for mobile video communication," *ICIP '04. International Conference on Image Processing*, vol. 1, pp. 545–548, Oct 2004.

[199] D. Marpe, T. Wiegand and G.J. Sullivan, "The H.264/MPEG4 advanced video coding standard and its applications," *IEEE Communications Magazine*, vol. 44, pp. 134–143, Aug 2006.

[200] Y.C. Chang, S.W. Lee and R. Komiya, "A low-complexity unequal error protection of H.264/AVC video using adaptive hierarchical QAM," *IEEE Transactions on Consumer Electronics*, vol. 52, pp. 1153–1158, Nov 2006.

[201] G.J. Foschini, D. Chizhik, M.J. Gans, C. Papadias and R.A. Valenzuela, "Analysis and performance of some basic space-time architectures," *IEEE Journal on Selected Areas in Communications*, vol. 21, no. 3, pp. 303–320, 2003.

[202] V. Tarokh, N. Seshadri and A.R. Calderbank, "Space-time codes for high data rate wireless communication: performance criterion and code construction," *IEEE Transactions on Information Theory*, vol. 44, pp. 744–765, March 1998.

[203] G.J. Foschini and M.J. Gans, "On limits of wireless communications in a fading environment when using multiple antennas," *Kluwer Academic Publishers, Wireless Personal Communications*, vol. 6, pp. 311–335, March 1998.

[204] J. Abouei, H. Bagheri and A. Khandani, "An efficient adaptive distributed space-time coding scheme for cooperative relaying," *IEEE Transactions on Wireless Communications*, vol. 8, pp. 4957–4962, October 2009.

[205] J.N. Laneman, D.N. Tse and G.W. Wornell, "Cooperative diversity in wireless networks: Efficient protocols and outage behavior," *IEEE Transactions on Information Theory*, vol. 50, pp. 3062–3080, December 2004.

[206] T. Cover and A. El Gamal, "Capacity theorems for the relay channel," *IEEE Transactions on Information Theory*, vol. 25, no. 5, pp. 572–584, 1979.

[207] G. Kramer, M. Gastpar and P. Gupta, "Cooperative strategies and capacity theorems for relay networks," *IEEE Transactions on Information Theory*, vol. 51, pp. 3037–3063, September 2005.

[208] T.E. Hunter and A. Nosratinia, "Cooperation diversity through coding," in *IEEE International Symposium on Information Theory*, 2002.

[209] E. C. van der Meulen, "Three-terminal communication channels," *Advanced Applied Probability*, vol. 3, no. 1, pp. 120–154, 1971.

[210] E. C. van der Meulen, "A survey of multi-way channels in information theory: 1961-1976," *IEEE Transactions on Information Theory*, vol. 23, pp. 1–37, January 1977.

[211] A. Sendonaris, E. Erkip and B. Aazhang, "Increasing uplink capacity via user cooperation diversity," in *IEEE International Symposium on Information Theory*, (Cambridge, MA), August 1998.

[212] M. Dohler, E. Lefranc and H. Aghvami, "Space-time block codes for virtual antenna arrays," in *The 13th IEEE International Symposium on Personal, Indoor and Mobile Radio Communications*, vol. 1, pp. 414–417, September 2002.

[213] A. Sendonaris, E. Erkip and B. Aazhang, "User cooperation diversity part I: System description," *IEEE Transactions on Communications*, vol. 51, no. 11, pp. 1927–1938, 2003.

[214] A. Sendonaris, E. Erkip and B. Aazhang, "User cooperation diversity part II: Implementation aspects and performance analysis," *IEEE Transactions on Communications*, vol. 51, no. 11, pp. 1939–1948, 2003.

[215] J.N. Laneman and G.W. Wornell, "Distributed space-time-coded protocols for exploiting cooperative diversity in wireless networks," *IEEE Transactions on Information Theory*, vol. 49, no. 10, pp. 2415–2425, 2003.

[216] M.C. Valenti and B. Zhao, "Distributed turbo codes: towards the capacity of the relay channel," in *IEEE Vehicular Technology Conference, VTC-'03 Fall*, vol. 1, pp. 322–326, October 2003.

[217] B. Zhao and M.C. Valenti, "Distributed turbo coded diversity for relay channel," *IEE Electronics Letters*, vol. 39, pp. 786–787, May 2003.

[218] R.U. Nabar, H. Bolcskei and F.W. Kneubuhler, "Fading relay channels: performance limits and space-time signal design," *IEEE Journal on Selected Areas in Communications*, vol. 22, pp. 1099–1109, August 2004.

[219] A. Stefanov and E. Erkip, "Cooperative coding for wireless networks," *IEEE Transactions on Communications*, vol. 52, pp. 1470–1476, September 2004.

[220] K. Azarian, H. El Gamal and P. Schniter, "On the achievable diversity-multiplexing tradeoff in half-duplex cooperative channels," *IEEE Transactions on Information Theory*, vol. 51, pp. 4152–4172, December 2005.

[221] H.H. Sneessens and L. Vandendorpe, "Soft decode and forward improves cooperative communications," in *6th IEE International Conference on 3G and Beyond*, (Washington, DC), pp. 1–4, November 2005.

[222] R. Hu and J. Li, "Exploiting Slepian-Wolf codes in wireless user cooperation," in *IEEE 6th Workshop on Signal Processing Advances in Wireless Communications*, pp. 275–279, June 2005.

[223] M. Yu and J. Li, "Is amplify-and-forward practically better than decode-and-forward or vice versa?," in *IEEE International Conference on Acoustics, Speech and Signal Processing*, vol. 3, March 2005.

[224] T.E. Hunter and A. Nosratinia, "Diversity through coded cooperation," *IEEE Transactions on Wireless Communications*, vol. 5, pp. 283–289, February 2006.

[225] T.E. Hunter, S. Sanayei and A. Nosratinia, "Outage analysis of coded cooperation," *IEEE Transactions on Information Theory*, vol. 52, pp. 375–391, February 2006.

[226] Y. Li, B. Vucetic, T.F. Wong and M. Dohler, "Distributed turbo coding with soft information relaying in multihop relay networks," *IEEE Journal on Selected Areas in Communications*, vol. 24, pp. 2040–2050, November 2006.

[227] R. Hu and J. Li, "Practical compress-forward in user cooperation: Wyner-Ziv Cooperation," in *IEEE International Symposium on Information Theory*, (Seattle, WA), pp. 489–493, July 2006.

[228] A. Host-Madsen, "Capacity bounds for cooperative diversity," *IEEE Transactions on Information Theory*, vol. 52, pp. 1522–1544, April 2006.

[229] T. Bui and J. Yuan, "A decode and forward cooperation scheme with soft relaying in wireless communication," in *IEEE 8th Workshop on Signal Processing Advances in Wireless Communications (SPAWC)*, (Helsinki), pp. 1–5, June 2007.

[230] M.N. Khormuji and E.G. Larsson, "Improving collaborative transmit diversity by using constellation rearrangement," in *IEEE Wireless Communications and Networking Conference*, (Kowloon), pp. 803–807, March 2007.

[231] X. Bao and J. Li, "Efficient message relaying for wireless user cooperation: Decode-Amplify-Forward (DAF) and Hybrid DAF and coded-cooperation," *IEEE Transactions on Wireless Communications*, vol. 6, pp. 3975–3984, November 2007.

[232] L. Xiao, T. Fuja, J. Kliewer and D. Costello, "A network coding approach to cooperative diversity," *IEEE Transactions on Information Theory*, vol. 53, pp. 3714–3722, October 2007.

[233] G. Yue, X. Wang, Z. Yang and A. Host-Madsen, "Coding schemes for user cooperation in low-power regimes," *IEEE Transactions on Signal Processing*, vol. 56, pp. 2035–2049, May 2008.

[234] W. Zhang, Y. Li, X.-G. Xia, P.C. Ching and K.B. Letaief, "Distributed space-frequency coding for cooperative diversity in broadband wireless Ad Hoc networks," *IEEE Transactions on Wireless Communications*, vol. 7, pp. 995–1003, March 2008.

[235] T. Wang and G.B. Giannakis, "Complex field network coding for multiuser cooperative communications," *IEEE Journal on Selected Areas in Communications*, vol. 26, pp. 561–571, April 2008.

[236] E. Zimmermann, P. Herhold and G. Fettweis, "On the performance of cooperative relaying protocols in wireless networks," *European Transactions on Telecommunications*, vol. 16, no. 1, pp. 5–16, 2005.

[237] H. Ochiai, P. Mitran and V. Tarokh, "Design and analysis of collaborative diversity protocols for wireless sensor networks," in *IEEE Vehicular Technology Conference, VTC-'04 Fall*, (Los Angeles, USA), pp. 4645–4649, September 2004.

[238] P. Mitran, H. Ochiai and V. Tarokh, "Space-time diversity enhancements using collaborative communications," *IEEE Transactions on Information Theory*, vol. 51, pp. 2041–2057, June 2005.

[239] Y. Li, "Distributed coding for cooperative wireless networks: An overview and recent advances," *IEEE Communications Magazine*, vol. 47, pp. 71–77, August 2009.

[240] Z. Zhang and T.M. Duman, "Capacity-approaching turbo coding for half-duplex relaying," *IEEE Transactions on Communications*, vol. 55, pp. 1895–1906, October 2007.

[241] J. Hu and T. M. Duman, "Low density parity check codes over wireless relay channels," *IEEE Transactions on Wireless Communications*, vol. 6, pp. 3384–3394, September 2007.

[242] M. Elfituri, W. Hamouda and A. Ghrayeb, "A convolutional-based distributed coded cooperation scheme for relay channels," *IEEE Transactions on Vehicular Technology*, vol. 58, pp. 655–669, February 2009.

[243] A. Host-Madsen and J. Zhang, "Capacity bounds and power allocation for wireless relay channels," *IEEE Transactions on Information Theory*, vol. 51, pp. 2020–2040, June 2005.

[244] L. Hanzo and T. Keller, *OFDM and MC-CDMA: A primer.* IEEE Press-John Wiley & Sons, April 2006.

[245] T. Cover and J. Thomas, *Elements of information theory.* New York: Wiley, 2004.

[246] A.J. Goldsmith, *Wireless communication.* Cambridge University Press, 2005.

[247] N.C. Tse and P. Viswanath, *Fundamentals of wireless communication.* Cambridge University Press, 2005.

[248] A. Reznik, S. R. Kulkarni, and S. Verdu, "Capacity and optimal resource allocation in the degraded Gaussian relay channel with multiple relays," in *40th Allerton Conference on Communication, Control and Computing*, pp. 377–386, October 2002.

[249] B. Rankov and A. Wittneben, "Achievable rate regions for the two-way relay channel," in *IEEE International Symposium on Information Theory*, (Seattle, USA), pp. 1668–1672, July 2006.

[250] L. Kong, S. X. Ng, R. Y. S. Tee, R. G. Maunder and L. Hanzo, "Reduced-Complexity Near-Capacity Downlink Iteratively Decoded Generalized Multi-Layer Space-Time Coding Using Irregular Convolutional Codes," *IEEE Transactions on Wireless Communications*, vol. 9, pp. 1–12, Febuary 2010.

[251] C. Hausl and J. Hagenauer, "Iterative network and channel decoding for the two-way relay channel," in *Proceedings of IEEE ICC '06*, (Istanbul, Turkey), pp. 1568–1573, June 2006.

[252] C. Hausl and P. Dupraz, "Joint network-channel coding for the multiple-access relay channel," in *Proceedings of IEEE Sensor and Ad Hoc Communications*

and Networks (SECON) '06, (Hyatt Regency, USA), pp. 817–822, September 2006.

[253] N. Fawaz, D. Gesbert and M. Debbah, "When network coding and dirty paper coding meet in a cooperative ad hoc network," *IEEE Transactions on Wireless Communications*, vol. 7, pp. 1862–1867, May 2008.

[254] L. Xiao, T.E. Fuja, J. Kliewer and D.J. Costello, "A network coding approach to cooperative diversity," *IEEE Transactions on Information Theory*, vol. 53, pp. 3714–3722, October 2007.

[255] P. Bergmans and T. Cover, "Cooperative broadcasting," *IEEE Transactions on Information Theory*, vol. 20, pp. 317–324, May 1974.

[256] E.G. Larsson and B.R. Vojcic, "Cooperative transmit diversity based on superposition modulation," *IEEE Communications Letters*, vol. 9, pp. 778–780, September 2005.

[257] X. Ma and L. Ping, "Coded modulation using superimposed binary codes," *IEEE Transactions on Information Theory*, vol. 50, pp. 3331–3343, December 2004.

[258] G. Caire, S. Guemghar, A. Roumy and S. Verdu, "Maximizing the spectral efciency of coded CDMA under successive decoding," *IEEE Transactions on Information Theory*, vol. 50, pp. 152–164, January 2004.

[259] X.D. Wang and H.V. Poor, "Iterative (turbo) soft interference cancellation and decoding for coded CDMA," *IEEE Transactions on Communications*, vol. 47, pp. 1046–1061, July 1999.

[260] R. Zhang and L. Hanzo, "Superposition-coding aided multiplexed hybrid ARQ scheme for improved end-to-end transmission efficiency," *IEEE Transactions on Vehicular Technology*, vol. 58, pp. 4681–4686, Oct 2009.

[261] J.G. Proakis, *Digital communications*. New York: McGraw-Hill, 2001.

[262] J. C. MacKay, *Information theory, inference and learning algorithms*. Cambridge University Press, 2003.

[263] H. Imai and S. Hirakawa, "A new multilevel coding method using error-correcting codes," *IEEE Transaction on Information Theory*, vol. 23, pp. 371–377, May 1977.

[264] M. Costa, "Writing on dirty paper," *IEEE Transactions on Information Theory*, vol. 29, pp. 439–441, May 1983.

[265] R. Ahlswede, N. Cai, S.Y.R. Li and R.W. Yeung, "Network information flow," *IEEE Transactions on Information Theory*, vol. 4, pp. 1204–1216, July 2000.

[266] B. Hassibi and B.M. Hochwald, "High-rate codes that are linear in space and time," *IEEE Transactions on Information Theory*, vol. 48, pp. 1804–1824, June 2002.

[267] O. Shalvi, "Multiple source Cooperation diversity," *IEEE Communications Letters*, vol. 8, pp. 712–714, December 2004.

[268] H. Schoeneich and P.A. Hoeher, "Adaptive interleave-division multiple access-A potential air interference for 4G bearer services and wireless LANs," in *Proc. WOCN 04*, (Muscat, Oman), pp. 179–182, June 2004.

[269] P. Wang, J. Xiao and P. Li, "Comparison of orthogonal and non-orthogonal approaches to future wireless cellular systems," *IEEE Vehicular Technology Magazine*, vol. 1, pp. 4–11, September 2006.

[270] Y.D. Chen, S. Kishore and J. Li, "Wireless diversity through network coding," in *Proc. of IEEE WCNC '06*, (Las Vegas, USA), pp. 1681–1686, April 2006.

[271] R. Zhang and L. Hanzo, "Interleaved random space-time coding for multisource cooperations," *IEEE Transactions on Vehicular Technology*, vol. 58, pp. 2120–2125, May 2009.

[272] F. Brannstrom, T.M. Aulin and L.K. Rasmussen, "Iterative detectors for trellis-code multiple-access," *IEEE Transactions on Communications*, vol. 50, pp. 1478–1485, September 2002.

[273] F. Brannstrom, T.M. Aulin and L.K. Rasmussen, "Iterative multi-user detection of trellis code multiple access using a posteriori probabilities," in *Proc. of IEEE ICC '01*, vol. 1, (Helsinki, Finland), pp. 11–15, June 2001.

[274] P. Li, L.H. Liu, K.Y. Wu and W.K. Leung, "Interleave-division multiple-access," *IEEE Transactions on Wireless Communications*, vol. 5, pp. 938–947, April 2006.

[275] P. Frenger, P. Orten and T. Ottosson, "Code-spread CDMA using maximum free distance low-rate convolutional codes," *IEEE Transactions on Communications*, vol. 48, pp. 135–144, January 2000.

[276] A. Ribeiro, R.Q. Wang and G.B. Giannakis, "Multi-source cooperation with full-diversity spectral-efficiency and controllable-complexity," *IEEE Journal on Selected Areas in Communications*, vol. 25, pp. 415–425, February 2007.

[277] R. Zhang and L. Hanzo, "Coding schemes for energy efficient multi-source cooperation aided uplink transmission," *IEEE Signal Processing Letters*, vol. 16, pp. 438–441, May 2009.

[278] S. Verdu, *Multiuser detection.* Cambridge University Press, 1998.

[279] R. Lupas and S. Verdu, “Linear multiuser detectors for synchronous code-division multiple-access channels,” *IEEE Transactions on Information Theory*, vol. 35, pp. 123–136, January 1989.

[280] U. Madhow and M.L. Honig, “MMSE interference suppression for direct-sequence spread-spectrum CDMA,” *IEEE Transactions on Communications*, vol. 42, pp. 3178–3188, December 1994.

[281] L. Hanzo, M. Münster, B.J. Choi and T. Keller, *OFDM and MC-CDMA for broadband multi-user communications, WLANs and broadcasting.* Chichester, UK: Wiley, 2003.

[282] A. Duel-Hallen, J. Holtzman and Z. Zvonar, “Multiuser detection for CDMA systems,” *IEEE Personal Communications Magazine*, pp. 53–66, April 1995.

[283] M.K. Varanasi and B. Aazhang, “Multistage detection in asynchronous code-division multiple-access communications,” *IEEE Transactions on Communications*, vol. 38, pp. 509–519, April 1990.

[284] Y.C. Yoon, R. Kohno and H. Imai, “A spread-spectrum multiaccess system with cochannel interference cancellation for multipath fading channels,” *IEEE Journal on Selected Areas in Communications*, vol. 11, pp. 1067–1075, September 1993.

[285] P. Patel and J. Holtzman, “Analysis of a simple successive interference cancellation scheme in a DS/CDMA system,” *IEEE Journal on Selected Areas in Communications*, vol. 12, pp. 796–807, June 1994.

[286] Y. Li and R. Steele, “Serial interference cancellation method for CDMA,” *Electronics Letters*, vol. 30, pp. 1581–1583, September 1994.

[287] Y. Sanada and M. Nakagawa, “A multiuser interference cancellation technique utilizingconvolutional codes and orthogonal multicarrier modulation for wirelessindoor communications,” *IEEE Journal on Selected Areas in Communications*, vol. 14, pp. 1500–1509, October 1996.

[288] D. Divsalar, M.K. Simon and D. Raphaeli, “Improved parallel interference cancellation for CDMA,” *IEEE Transactions on Communications*, vol. 46, pp. 258–268, February 1998.

[289] A.L.C. Hui and K.B. Letaief, “Successive interference cancellation for multiuser asynchronous DS/CDMA detectors in multipath fading links,” *IEEE Transactions on Communications*, vol. 46, pp. 384–391, March 1998.

[290] A. Lampe and J.B. Huber, "On improved multiuser detection with iterated soft decision interference cancellation," in *Communication Theory Mini-Conference*, (Vancouver, BC), pp. 172–176, June 6–10 1999.

[291] M. Kobayashi, J. Boutros and G. Caire, "Successive interference cancellation with SISO decoding and EM channel estimation," *IEEE Journal On Selected Areas In Communications*, vol. 19, pp. 1450–1460, August 2001.

[292] H. V. Poor, "Turbo multiuser detection: A primer," *Jounal on Communications. Networks*, vol. 3, pp. 196–201, September 2001.

[293] G. Barriac and U. Madhow, "PASIC: A new paradigm for low-complexity multiuser detection," in *Conference on Information Sciences and Systems, Hopkins University*, (Baltimore, MD), 21-23 March 2001.

[294] Z.N. Shi and C.B. Schlegel, "Iterative multiuser detection and error control code decoding in random CDMA," *IEEE Transactions on Signal Processing*, vol. 54, pp. 1886– 1895, May 2006.

[295] A.S. Gupta and A. Singer, "Successive interference cancellation using constellation structure," *IEEE Transactions on Signal Processing*, vol. 55, pp. 5716–5730, December 2007.

[296] L. Song, R.C. de Lamare and A. G. Burr, "Successive Interference Cancellation Schemes for Time-Reversal Space-Time Block Codes," *IEEE Transactions on Vehicular Technology*, vol. 57, pp. 642–648, January 2008.

[297] Z. Shengli, S.-C. Liew and P.P.K. Lam, "Physical Layer Network Coding," *Computer Science - Information Theory*, April 2007.

[298] G. Caire, G. Taricco and E. Biglieri, "Bit-interleaved coded modulation," *IEEE Transactions on Information Theory*, vol. 44, pp. 927–946, May 1998.

[299] K. Wu and L. Ping, "Multilayer turbo space-time codes," *IEEE Communications Letters*, vol. 9, pp. 55–57, January 2005.

[300] L. Kong, S. X. Ng, R. G. Maunder and L. Hanzo, "Successive Relaying Aided Near-Capacity Irregular Distributed Space-Time Coding," in *IEEE Global Telecommunications Conference GLOBECOM*, (Honolulu, Hawaii), November 2009.

[301] L. Wang and L. Hanzo, "The Resource-Optimized Differentially Modulated Hybrid AF/DF Cooperative Cellular Uplink Using Multiple-Symbol Differential Sphere Detection," *IEEE Signal Processing Letters*, vol. 16, pp. 965–968, November 2009.

Index

Author Index

H

I

J

K

O

P

Q

R

T

U

V

Z